NASA Technical Memorandum 4679

Spaceborne Synthetic Aperture Radar: Current Status and Future Directions

A Report to the Committee on Earth Sciences

Space Studies Board
National Research Council

D. L. Evans, Editor
J. Apel
R. Arvidson
R. Bindschadler
F. Carsey
J. Dozier
K. Jezek
E. Kasischke
F. Li
J. Melack
B. Minster
P. Mouginis-Mark
J. van Zyl

National Aeronautics and
Space Administration

Scientific and Technical Information Office

1995

Acknowledgments

This publication was prepared by the Jet Propulsion Laboratory, California Institute of Technology, under a contract with the National Aeronautics and Space Administration. It contains material from contributors in United States government agencies, agencies of other governments, universities, and private industry.

Reference herein to any specific commercial product, process, or service by trade name, trademark, manufacturer, or otherwise, does not constitute or imply its endorsement by the United States Government, the National Aeronautics and Space Administration, or the Jet Propulsion Laboratory, California Institute of Technology.

ERS-1 data have been provided courtesy of the European Space Agency.

In addition to our many contributors, the Discipline Panel Chairmen and I wish to thank the dedicated team at JPL who were instrumental in producing this document.

Rich Benton
Roger Carlson
Charles Cordaro
Judi Dedmon
Robin Dumas
Terri Flynn
Mona Jasnow
Shannon McConnell
Ellen O'Leary
Joe Reymann
Annie Richardson
George Shultz
El Simpson
Jin Zhu

Diane Evans, Editor

Discipline Panel Chairmen

Ecology

Eric Kasischke, ERIM/Duke University
John Melack, University of California, Santa Barbara

Hydrology

Jeff Dozier, University of California, Santa Barbara
Jakob van Zyl, Jet Propulsion Laboratory

Marine Science and Applications

John Apel, Applied Physics Laboratory
Frank Carsey, Jet Propulsion Laboratory

Ice Sheets and Glaciers

Robert Bindschadler, Goddard Space Flight Center
Ken Jezek, Ohio State University

Solid Earth Science

Ray Arvidson, Washington University
Bernard Minster, University of California, San Diego
Pete Mouginis-Mark, University of Hawaii

Technology

Fuk Li, Jet Propulsion Laboratory
Merle Skolnik, Naval Research Laboratory

Interagency

Robert Winokur, NOAA/NESDIS

Preface

In June 1994 NASA's Office of Mission to Planet Earth (OMTPE) identified the need for a broadly scoped review of the nation's civilian spaceborne Synthetic Aperture Radar (SAR) program, and requested the Committee on Earth Studies (CES) of the Space Studies Board (SSB) of the National Research Council (NRC) to undertake such a review. The Board was charged with answering the following questions:

(1) Is multiparameter SAR the optimum spaceborne approach to characterize the critical geophysical parameters identified by the interdisciplinary Spaceborne Imaging Radar-C, X-Band Synthetic Aperture Radar (SIR-C/X-SAR) Earth science team, and if not, are the data products nevertheless of credible utility in Earth science? For example:

- How well can SAR be used to estimate biomass, characterize vegetation type, characterize forest stand maturity, clear-cut, or regrowth?
- How well can SAR be used to characterize snow-water equivalent, distinguish between new and refrozen ice, or estimate ice volume?
- How well can SAR characterize oceanographic features and parameters such as internal waves, oil slicks, wave direction, and air-sea interaction?
- How well can SAR characterize soil moisture?
- How well can SAR characterize geologic features such as rock type/composition, and surface texture?

(2) With respect to all of the above questions, how important are the multiple wavelength, multi-polarizing, variable-incidence angle capabilities to these characterizations?

(3) What is the potential of spaceborne radar interferometry in topographic mapping and surface change monitoring connected with natural hazards?

(4) What is the complementary nature of a spaceborne radar interferometry project to monitoring crustal strain and deploying dense arrays of Global Positioning System (GPS) receivers in selected areas of seismic hazard?

(5) What are the priorities in SAR technology development which are critical not only to NASA's maintaining leadership in spaceborne SAR technology, but to providing societally relevant geophysical parameters?

(6) What is the priority of SAR science in the context of the overall national and international Earth observing areas?

(7) With the answers to these questions as backdrop, how might the international space program community make the best use of its resources while satisfying individual programmatic requirements through joint planning and cooperation in future SAR flight projects?

(8) What would an appropriate role be for NASA in such an international SAR program? For example:

- What would an appropriate role be for the NASA Earth Observing System Data and Information System (EOSDIS) in such a program?

- How could the SIR-C/X-SAR or the EOS SAR Science Team expertise be used?

This report was prepared as background material through a series of discipline-oriented workshops held throughout the fall of 1994. Science Discipline Panel workshops and meetings, held in Late October and early November focused on Questions 1-4. The Technology Panel addressed Question 5 during two separate meetings on November 15 and 29. An Interagency panel formed to help address Questions 6-8 will report separately. The Chairmen of the Discipline Panels met on December 5, 1994 to discuss the report format and their key findings. Because of the broad interest in this subject, attempts have been made to solicit input and comments on this material from as broad a community as time allowed, including the international community. However, this should only be considered a "snap-shot" of a rapidly evolving field, as new results are reported on a continuing basis.

Contents

1—Executive Summary

INTRODUCTION

This report provides a context in which questions put forth by NASA' s Office of Mission to Planet Earth (OMTPE) regarding the next steps in spaceborne synthetic aperture radar (SAR) science and technology can be addressed. It summarizes the state-of-the-art in theory, experimental design, technology, data analysis and utilization of SAR data for studies of the Earth, and describes potential new applications.

This report is divided into five science chapters and a technology assessment. The science chapters are Ecology, Hydrology, Marine Science and Applications, Ice Sheets and Glaciers, and Solid Earth Sciences and Topography. Each Chapter outlines key science questions in the context of Mission to Planet Earth that can be addressed with SAR data. In addition, the chapters summarize the value of existing SAR data and currently planned SAR systems, and identify gaps in observational capabilities that need to be filled to address the scientific questions. Both demonstrated and potential capabilities are described, with appropriate references cited. Both NASA and non-NASA sources of SAR data are included, and the importance of multiple wavelengths, multiple polarizations, and variable incidence angles are substantiated for each measurement. A summary of sensors is included as an Appendix. Cases where SAR provides complementary data to other (non-SAR) measurement techniques are also described.

The chapter on technology assessment outlines SAR technology development which is critical not only to NASA's providing societally relevant geophysical parameters, but to maintaining competitiveness in SAR technology, and promoting economic development.

RECOMMENDATIONS

SAR data provide unique information about the health of the planet and its biodiversity, as well as critical data for natural hazards and resource assessments. Interferometric measurement capabilities uniquely provided by SAR are required to generate global topographic maps, to monitor surface topographic change, and to monitor glacier ice velocity and ocean features. Multiparameter SAR data are crucial for accurate land cover classification, measuring above-ground woody plant biomass, delineation of wetland inundation, measurement of snow and soil moisture, characterization of oil slicks, and monitoring of sea ice thickness.

The suite of spaceborne SAR systems and programs currently envisioned by the international community provides an important framework for addressing key science issues and applications. However, additional activities, and interferometric/multiparameter measurement capabilities are required for long-term environmental monitoring and commercial applications.

This report recommends NASA take an aggressive leadership role in an international SAR program to meet these needs. Specific near-term steps should be to:

(1) **Establish interagency and international SAR science teams.** These teams would be funded to exploit data from both NASA and non-NASA sources, and would be charged with development and testing/validation of new applications, both scientific and commercial in nature.

(2) **Initiate an advanced technology effort.** The initial focus of such a program should be on lowering the costs of the operational elements and exploiting the functionality of SAR. The NASA airborne radar (AIRSAR) which flies on the NASA DC-8 should be the focus of this activity.

(3) **Design an evolvable flight program.** The long-term objective of such a program is an operational interferometric, multiparameter spaceborne SAR for long-term environmental monitoring and commercial applications. Immediate steps toward this goal are to initiate an interferometric spaceborne mission, and to continue multiparameter measurements through additional flights of the Spaceborne Imaging Radar-C, X-Band Synthetic Aperture Radar (SIR-C/X-SAR) as a free-flyer or on the Space Shuttle.

2—Ecology

INTRODUCTION

The past five years have seen significant growth in research focused on developing approaches for using synthetic aperture radar (SAR) to study ecological processes. During this time, we have seen the development of a number of advanced airborne SAR systems, and the deployment of three spaceborne SAR systems: ERS-1, JERS-1, and SIR-C/X-SAR. Additional spaceborne SARs will be deployed through the remainder of this decade and into the next, including ERS-2, RADARSAT, and ASAR (see Appendix B).

The deployment of the multi-frequency, polarimetric SIR-C/X-SAR instruments on two Space Shuttle missions in April and October 1994 represents a milestone in the history of imaging radars. The data collected during these missions provide an important opportunity to further evaluate the utility of imaging radar data for examining surface characteristics important in a wide range of ecological processes.

Ecologists are generally aware of the utility of remote sensing data for studying processes at landscape scales. However, imaging radar data, such as that collected by synthetic aperture radars, have received less attention than optical data. Hindrances to use of SAR systems have included: (1) difficulty of understanding the information content of the complex phase and amplitude information recorded in multifrequency, polarimetric SAR data; (2) the lack of available, calibrated data over sites of interest; (3) the lack of accessible computer software to exploit the information present in the data; and (4) certain characteristics of SAR data, including relief displacement and image speckle. Computer software and hardware have developed to the point where most of the technological constraints of using SAR data have dissipated. In addition, a great deal of calibrated SAR imagery exists and is being collected by several airborne and satellite systems. This chapter focuses on our current understanding of the information content of SAR imagery with respect to ecological applications, based on recent research results.

In November 1994, a working group of scientists met on the campus of the University of California (Santa Barbara) to perform a critical review of the use of imaging radars to estimate surface characteristics important for the study of terrestrial ecosystem processes. The consensus of this group was that the ability of imaging radars to detect ecologically important characteristics of vegetated landscapes is well founded in both theory and observation. The working group felt the demonstrated capabilities of imaging radars for investigating terrestrial ecosystems could best be organized into four broad categories: (1) classification and detection of change in land cover; (2) estimation of woody plant biomass; (3) monitoring the extent and timing of inundation; and (4) monitoring other temporally dynamic processes, such as freeze/thaw status and soil moisture in fire-disturbed boreal forests.

This review is organized in the following manner: First, we present a brief review of the origins of the signatures recorded in a SAR image collected over a vegetated terrain. Then, we discuss each of the four topical areas, including an overview of the scientific importance or application of the topic area and a review of the demonstrated capabilities of SAR to provide information necessary to provide specific inputs. This is followed by a discussion of the optimal system configurations for specific ecological applications and an assessment of the capabilities of existing SAR systems (including SIR-C/X-SAR) and those scheduled for launch in the near future to provide information required for the application areas. Finally,

we present recommendations for future SAR programs within the Mission to Planet Earth (MTPE) and the U.S. Global Change Research Program.

BACKGROUND

Radar Sensing of Vegetated Landscapes: Physical Basis

Microwave backscatter is highly dependent on the orientation and size distribution of the scattering elements present within the region being imaged. Because of their high moisture content, individual components of forest canopies and other vegetative covers (e.g., leaves, branches, trunks) represent discrete scattering and absorbing elements to the microwave power transmitted by imaging radars. Variations in the microwave dielectric constant of vegetation elements or ground surface play a central role in determining the magnitude and phase of the microwave energy which is scattered from a vegetated surface and recorded and processed into a SAR image. Factors influencing the dielectric constant of vegetated surfaces include temperature of the scattering medium, relative moisture content of vegetation, soil, and snow cover, and the presence of water on vegetation.

Microwave scattering from land surfaces is strongly dependent on the size and orientation of the different elements comprising the vegetation. At longer radar wavelengths (P- and L-bands, 67 and 24 cm wavelengths), microwave scattering and absorption results from interactions with the tree boles and larger branches found within forests, as well as the ground surface. At these wavelengths, the smaller woody stems and the foliage act mainly as attenuators. At shorter radar wavelengths, (C- and X-bands, 6 and 3 cm wavelengths), microwave scattering and absorption results from interactions from smaller branches and leaves and needles in the canopy. The presence of a water-saturated or flooded surface leads to increased double-bounce scattering that enhances the strength of the ground-vegetation interaction term. Finally, the polarization combination of the received backscatter is dependent on the polarization of the transmitted microwave power and on the horizontal and/or vertical orientation of the scattering elements present in the vegetation.

Modeling clearly shows the differential dependence of microwave backscatter on the overall structure of vegetation canopies and on the variations in the characteristics of the ground layer. These models treat a forest stand either as a set of continuous horizontal layers (Richards et al., 1987; Durden et al., 1989; Sun and Simonett, 1990; Ulaby et al., 1990; Chauhan et al., 1991) or as a discontinuous layer with individual trees acting as distinct scattering centers (Sun et al., 1991; McDonald and Ulaby, 1993). Both model classes are similar in that they calculate the same major scattering terms: (1) volume scattering from the tree canopy (the branches and leaves/needles); (2) direct ground scattering; (3) ground-to-trunk scattering; (4) ground-to-crown scattering; and (5) ground-to-crown-to-ground scattering. (Figure 2-1 presents examples of outputs from the theoretical model of Ulaby et al., 1990). Most models use formulations which assume the tree trunks and branches can be modeled as lossy dielectric cylinders, and the leaves or needles as dielectric discs or cylinders, respectively.

A three-dimensional microwave backscatter model for forest canopies, which allows explicit spatial arrangement of scatterers, has been published (Sun and Ranson, 1995). Scattering models have been exercised and validated using SAR and scatterometer data collected over a wide range of vegetation canopies (Sun and Simonett, 1988; Chauhan et al., 1991; Durden et al., 1989; Lang et al., 1994; McDonald et al., 1990, 1991; Moghaddan et al., 1994; Way et al., 1994; Ranson and Sun, 1994; Wang et al., 1993a, 1993b, 1994a). Because of their complexity, however, these models have not proved invertible to allow estimation of surface and canopy characteristics needed to study specific ecological features or processes. The

value of these models lies in their utility in understanding the dependence of microwave backscatter on system and imaging parameters (frequency, polarization, and viewing geometry of the transmitted microwave radiation) and the basic geometric characteristics of the vegetated surface being studied (Figure 2-2). In addition, these models have also been useful in developing an understanding of the effects of temporally varying factors which influence microwave backscatter, including soil moisture (Wang et al., 1994b), air temperature (Rignot et al., 1994a), and flooding (Wang et al., 1995) (Figure 2-3). This understanding has proven critical in developing approaches to use SAR data in algorithms to estimate specific surface characteristics (see, e.g., Dobson et al., 1995c; Wang et al., 1994a; Kasischke et al., 1994a; and Rignot and Way, 1994).

ROLE OF SAR

Land Cover Classification

Ecologists use remote sensing technologies for two distinct purposes. The first addresses the fundamental ecological goal to understand relationships between organisms and their environments. To this end, remote sensing is used for interpretation of landscape patterns, examination of correlations among physical and biotic parameters, and extrapolation of known relationships to larger spatial scales. The second application involves using information derived from remote sensing systems in the study of specific ecosystem processes.

Vegetation classifications make possible studies of successional rates; landscape change; vegetation productivity and biomass; and effects of disturbances such as flooding, fires, disease, and harvesting or logging. These provide inputs for modeling of a variety of ecosystem processes, such as forest succession; vegetation/atmospheric exchanges of energy and water; and local, regional, and global-scale biogeochemical cycling.

Further terrestrial applications for remotely sensed data sets include inventory of forest resources, monitoring agricultural crops, locating vegetation containing particular species of interest, and monitoring land use and land-use change. Users of land cover classifications include plant and animal ecologists, modelers including those operating general circulation models (GCMs), land managers, government agencies, and economic forecasters. All applications require the classification of vegetation into types and the delineation of the structural and compositional boundaries of biotic communities.

For many ecological studies, there is a need for current information on the distribution and amount of vegetation. This need has not been fully addressed by a quarter century of spaceborne remote sensing systems operating in the visible and near-infrared region of the electromagnetic spectrum. Collection of visible/near-infrared imagery over ecologically important regions on a continuous basis is often limited by cloud cover, particularly in tropical and boreal biomes.

Image classification algorithms discriminate based on features extracted from the spectral, spatial, or temporal domains. Two general image classification approaches have been applied to SAR data: (1) maximum-likelihood classifiers including supervised and unsupervised cluster analysis and (2) knowledge-based techniques such as hierarchical decision trees and those based on determination of dominant scattering mechanisms from electromagnetic theory. A key issue for any of these approaches is how consistent or stable the classifier is when applied to new regions or the same region at different times.

A summary of the demonstrated capabilities of SAR-derived classification is given in Table 2-1 and Figure 2-4. This material is not intended to be all-inclusive, but draws examples from a number of ecosystems as recently reported in the literature. Manual classification of airborne SAR imagery provided the first comprehensive mapping of many tropical areas in the 1970's. The most notable of these was project RADAM in Brazil. Unsupervised classification of digital SAR imagery is a useful tool for characterizing landscapes without adequate vegetation maps (e.g., Pope et al., 1994). Most recent classification efforts have used supervised maximum likelihood approaches; these often lead to high classification accuracies for a given scene (de Grandi, et al., 1994; Lemoine, et al., 1994; Ranson and Sun, 1994; Rignot and Chellappa, 1992; Rignot et al., 1993). When applied to temporal sequences of images, this technique implicitly incorporates ancillary knowledge such as phenologic development or cropping calendars. The extendibility of supervised maximum likelihood techniques to regional or global scales is impaired by the need for local training. The knowledge-based techniques may overcome this limitation by first classifying on the basis of explicit relationships between radar backscatter and structural attributes (Dobson et al., 1995b; Pierce et al., 1994; van Zyl, 1989). These structural classes can then be relabelled locally on the basis of known linkages between structure and floristic community. At present, such classifiers have been successfully tested locally.

SAR can clearly (1) detect major hydrologic changes such as inundation (Figure 2-3, Ormsby et al., 1985; Morrissey et al., 1994, 1995; Hess et al., 1995), the presence of intercepted precipitation (Ulaby et al., 1983), and freeze/thaw status of vegetation (Rignot and Way, 1994; Way et al., 1994); (2) differentiate major structural differences in land-cover such as forest versus clear cuts or marshes versus flooded forests (Beaudoin et al., 1994; de Grandi et al., 1994; Dobson et al., 1995b; Drieman, 1994; Hess and Melack, 1994, Lopes et al., 1993; Lozano-Garcia and Hoffer, 1993; Pierce et al., 1994; Ranson and Sun, 1994), and (3) discriminate crop cover on the basis of structural attributes (Foody et al., 1994; Lemoine et al., 1994; van Zyl and Burnette, 1992). In addition, major height classes within a given vegetation type can be detected. Compositional variations within major vegetation types (physiognomic types) are not as readily distinguished, but can be separated with use of multitemporal, multifrequency and/or multipolarization imagery (Ahern et al., 1993; Drieman, 1994).

In regions characterized by persistent cloud-cover (e.g., boreal regions, tropical forest and much of Northern Europe), SAR may be the only viable alternative for classification of actual land-cover. In other regions, SAR is very useful as it provides information on structure and moisture status that is complementary to the information provided by optical sensing techniques (Lozano-Garcia and Hoffer, 1993). Moreover, SAR has a generic advantage over optical sensors because atmospheric correction is not needed. In addition, a number of studies have shown the power of multidate imagery for enhanced classification results (Ranson and Sun, 1994). Orbital SAR has proven itself to be very reliable for provision of multidate data because it is practically insensitive to local weather conditions. The calibration stability of existing satellite SARs makes it possible to incorporate time-dependent ancillary information, such as phenological development and cropping calendars, into classification.

A complication to SAR-derived land-cover classification is that imposed by topographic relief. In severe cases, the layover and shadowing produced by mountainous terrain makes classification inappropriate for these regions unless azimuth and viewing geometry have been carefully considered in the SAR sampling strategy. In less severe cases, the ancillary digital elevation data have been used to generate approximate corrections for terrain effects prior to classification. A second limitation is the spatial resolution of a given SAR. Landscape patches cannot be unambiguously discriminated and classified unless they are much greater

than the spatial resolution (for a single-look image). In general, classification of patch sizes <~2000 m^2 (i.e., ~45m x 45 m) is not practical from spaceborne SAR.

Measuring Above-Ground Woody Plant Biomass

The amount and distribution of biomass over the Earth's land surface is one of the major uncertainties in our ability to understand the global carbon cycle and how it may change in the future (Post, 1993). The living and dead biomass in both above and below-ground storage pools constitutes a major terrestrial store of carbon. Our knowledge of the biomass density within the Earth's terrestrial biomes is quite limited due to the difficulty of obtaining sufficient high quality observations that are representative of a region or ecosystem type (Smith et al., 1993; Dixon et al., 1994). Measurements on the ground are very time-consuming, labor-intensive and often constrained by lack of access. The physiological activity of living biomass and the fate of dead biomass determine the fluxes of carbon from the terrestrial biosphere to the atmosphere, and, thus, the accumulation or removal of important greenhouse gases (primarily carbon dioxide and methane) in the atmosphere. These processes are fairly dynamic and subject to change in response to a variety of environmental factors (e.g., temperature, moisture, nutrient availability) and patterns of disturbance, both natural (e.g., fire, windthrow, insect-induced mortality) and anthropogenic (deforestation, land degradation) (e.g., Solomon and Cramer, 1993).

Numerous studies have demonstrated that approaches using optical remotely sensed data do not work for most terrestrial biomass densities, because there is a saturation effect at very low levels of biomass. Currently, radar remote sensing appears to offer the greatest promise for obtaining estimates of biomass via remote sensing techniques.

The dependence of microwave backscatter on total above-ground biomass has been documented in monospecific pine forests found in the southeastern U.S. (Figure 2-5) and France (Dobson et al., 1992; Kasischke et al., 1994a; LeToan et al., 1992), mixed deciduous and coniferous forests of Maine, northern Michigan, and Alaska (Ranson et al., 1994; Dobson et al., 1994; Harrell et al., 1995; Rignot et al., 1994), and coniferous forests of the Pacific Northwest (Moghaddam et al., 1994). These studies all show the same results: (1) the sensitivity of microwave backscatter to biomass variations saturates after a certain level is reached; and (2) the biomass dependence of microwave backscatter varies as a function of radar wavelength and polarization (Figure 2-6). In summary, the saturation point is higher for longer wavelengths, and the HV polarization is most sensitive and VV the least.

A conclusion drawn by some scientists is these single-frequency saturation levels represent the upper limit of SAR's ability to monitor changes or differences in aboveground biomass in forests (Waring et al., 1994). However, this conclusion overlooks several important considerations. Microwave backscatter is correlated with total biomass and various components of biomass (e.g., branch biomass, needle biomass, bole biomass) or other physical characteristics (e.g., tree height, basal area) (Dobson et al., 1995c; Hussin et al., 1991; Kasischke et al., 1994a). This should not be surprising, since we know that different biomass components of trees are closely correlated. Since different radar frequencies and polarization combinations are sensitive to different layers of a forest canopy, it should be possible to use multiple channels of SAR data to estimate total above-ground biomass. Recent research supports this hypothesis.

Kasischke et al., (1994a) used a two-stage approach to estimate biomass of southern pine forests using JPL AIRSAR data. In step one, total branch biomass was estimated as a function of several different radar frequencies/polarizations. Total biomass was then

estimated from branch biomass based upon allometric equations, and resulted in a relative error on the order of 20% for biomass levels up to 400 t ha^{-1}. Ranson et al., (1994) used a ratio of P-band HV (PHV) and C-band HV (CHV) to estimate total biomass (up to 250 t ha^{-1}) in mixed coniferous/deciduous forests in Maine. This technique was applied to SIR-C/X-SAR LHV and CHV data to estimate boreal forest biomass up to 200 tons/ha within ±20 tons/ha (Ranson and Sun, 1995). Finally, Dobson et al., (1995c) used a multi-step, semi-empirical approach to estimate aboveground biomass from a combination of channels from SIR-C data collected over a mixed coniferous/deciduous forest in northern Michigan. In this approach, different SAR frequency/polarization combinations were used to estimate canopy-layer biomass, total height and total basal area, which were then used to estimate total biomass. Biomass estimates up to 250 t ha^{-1} with an uncertainty on the order of 16 t ha^{-1} were achieved (Figure 2-7).

Delineation of Wetland Inundation and Vegetative Cover

The availability of SAR data from airborne and satellite platforms has provided a unique opportunity to study dynamic wetland processes, information critical for the study of many ecosystem processes and applications. In this section, we discuss using SAR for several wetlands issues, including biogenic trace gas exchanges, monitoring the effects of rises in the average sea levels, and monitoring disease vectors.

In studies of biogenic trace gas exchange, remotely sensed data can provide unique information on the type and distribution of wetlands and on temporal distribution of inundation. Uncertainties in the spatial and seasonal extent of methane source and sink areas remain one of the greatest unknowns in the global methane budget (Bartlett and Harriss, 1993). Natural wetlands comprise the largest natural source of atmospheric methane (Aselmann and Crutzen, 1989; Fung et al., 1991). Hence, characterization of the areal and temporal extent of global wetlands would greatly extend our understanding of trace gas exchange from these ecosystems and of their significance to global processes.

Recent results using data from the TOPEX/POSEIDON radar altimeter has provided clear evidence that average sea levels are rising, at a rate of several millimeters per year (Nerem). These observations support evidence derived from tidal gages that sea levels have been rising over the past half century. The distribution of different vegetation species in coastal wetlands, especially estuaries, is highly sensitive to levels of tidal inundation. Monitoring changes in inundation and vegetation patterns in coastal wetlands will provide a key means to monitor the progression and effects of rises in sea level.

Finally, insect-borne organisms cause disease outbreaks throughout much of the developing world, particularly in the southern hemisphere. Many of these diseases are carried and transmitted by various species of mosquitoes. In regions with distinct wet and dry seasons, mosquito populations increase dramatically when breeding sites flood during prolonged episodes of high rainfall. Accurate maps of vegetation inundation are critical in identifying breeding grounds for disease vectors and in predicting and monitoring outbreaks of a variety of diseases.

For most scientific questions involving wetlands, it is necessary to distinguish not only flooded from non-flooded areas, but herbaceous from woody vegetation. For example, in floodplains of the central Amazon, methane generation rates from floating meadows are much higher than those from flooded forest. Delineation of both flooding status and vegetation, with accuracies greater than 90% for all categories, has been demonstrated using

multi-frequency, polarimetric SAR data sets for wetlands in the southeastern United States (JPL AIRSAR) and the central Amazon (SIR-C) (Melack et al., 1994; Hess et al., 1995).

The ability to penetrate the extensive cloud cover of northern and equatorial latitudes and to detect standing water beneath vegetation canopies is unique to SAR (Hess et al., 1990). In northern Alaska, for example, cloud cover and infrequent repeat cycles have limited the acquisition of optical satellite data (Landsat and SPOT) to a total of two scenes for the last 20 years. By comparison, ~50 scenes of ERS-1 SAR data have been acquired for Barrow over a two-year period, and RADARSAT will provide daily access. Similarly, in the equatorial regions of Manaus, Brazil, between 0 and 2 Landsat scenes are available each year.

SAR has proven useful in delineating inundation, a key indicator of the anaerobic conditions necessary for methane production. Backscatter from ERS-1 SAR acquired over Barrow, Alaska in 1991 is strongly related to the position of the local water table and thus to methane exchange rates (Figure 2-8; Morrissey et al., 1994). Backscatter from non-inundated sites was low, that from herbaceous inundated sites was high, and that from sites with the water table at the surface was intermediate, mirroring methane exchange rates for the region.

The capability to differentiate wetland source areas and non-wetlands with SAR is further enhanced by the availability of time series ERS-1 SAR data (Kasischke et al., 1995a). Seasonal changes in microwave backscatter for northern wetlands and non-wetlands are shown in Figure 2-9. Under an extended period of freezing temperatures in winter of 1992, radar returns for wetland and non-wetland did not differ significantly. Following snowmelt in the spring of 1992, backscatter for wetlands was consistently higher than that from non-wetlands. With the onset of colder temperatures and decreasing daylight in late summer, backscatter for both wetlands and non-wetlands decreased dramatically with freezing (Way and Rignot, 1994). These time series SAR data provide the only basis for an ongoing effort to map tundra wetlands on a global basis because cloud cover precludes using visible/near-IR channel imagery to monitor this biome on a continuing basis.

The sensitivity of microwave backscatter to vegetation and surface make SARs an attractive tool for characterizing wetland communities. While species composition per se usually cannot be detected with single-channel SAR, plant communities often can be, due to differences in vegetation height, density, or architecture. For example, a recent study using airborne SAR data collected over wetlands in Belize showed that a high degree of separability between the different vegetation communities could be achieved using a variety of indices based upon different radar frequencies and polarizations (Pope et al., 1994). Field studies of the same Belizean marsh communities demonstrate that vegetation species, composition, and biomass correlate well with salinity and nutrient gradients (Rejmankova et al., 1995). Given these relationships, the spatial distribution of wetland types and inundation patterns can be used to infer much about the chemistry and flow of surface and near-surface waters.

Studies by Tanis et al. (pri. comm., paper in review with *Rem. Sens. Environ.*) have shown that ERS-1 SAR imagery can discriminate between flooded and non-flooded areas in a coastal estuarine ecosystem along the Gulf Coast of Florida. Examination of tidal gage data revealed that the flooding detected on the ERS-1 imagery was due to variations in tidal stage. Techniques were developed to map the ranges of tidal flooding based on comparison of ERS-1 SAR imagery collected at high and low tides.

Another important issue in applied wetland ecology is the role of wetlands as breeding sites for mosquitoes that transmit a variety of diseases. Pope et al., (1992) used airborne X-, C- and L-band SAR data to examine flooding in sedge and grass-covered mosquito larval habitats in Kenya. LHH data provided the best flood detection in both wetland types, but

CHH and LVV also provided limited detection capability. The radar data (backscatter magnitude only) were not adequate for habitat mapping, which was accomplished with TM data. In contrast, the multifrequency, polarimetric airborne SAR data collected over the wetlands in Belize (Pope et al., 1994) were capable of mapping *Eleocharis* sp. dominated marshes, which have been shown to be important breeding habitats of the malaria vector *Anopheles albimanus* (Rejmankova et al., 1993). In summary, SAR data hold great promise for malaria risk assessment efforts in Belize and adjacent regions by providing spatial and temporal information on the distribution and flooding status of anopheline breeding sites.

Monitoring of Dynamic Processes in High-Latitude Ecosystems

The need to better quantify factors influencing the carbon cycle in northern biomes stems from several factors. First, based on current estimates of the present-day rates of increases in atmospheric carbon concentrations balanced against oceanic carbon uptake, Tans et al., (1990) concluded that a Northern Hemisphere terrestrial carbon sink on the order of 2.0 to 3.4 Gt C yr^{-1} is required to balance the global carbon budget. While Tans et al., (1990) associate this sink with temperate latitude forests, Bonan (1991a,b) suggests this sink may actually be a consequence of an imbalance in production and decomposition in high northern latitude ecosystems (the terrestrial biomes in high northern latitudes account for >40% of all carbon sequestered in living and dead biomass). Second, it is the consensus of most atmospheric general circulation models that significant warming of the northern-hemisphere, high latitudes will result from a doubling of atmospheric CO_2 concentrations (e.g., McFarlane et al., 1992). Given that the storage capacity of high northern latitudes is driven by the low rates of plant decomposition because of low annual temperatures, the projected temperature increases in this region will have profound influences on carbon cycling in its terrestrial biomes.

Uptake and release of CO_2 by the boreal forest may account for approximately 50% of the annual seasonal amplitude in atmospheric CO_2 at Point Barrow, Alaska, and ~30% of the seasonal amplitude at Mauna Loa (D'Arrigo et al., 1987). Data have shown that the seasonal amplitude of atmospheric CO_2 concentrations in northern latitudes has increased with time. This may reflect increased metabolic activity of ecosystems in northern latitudes due to warmer air temperatures and "CO_2 fertilization" (Bacastow et al., 1985; Houghton, 1987). Change to a warmer, drier climate may release more than 1 to 2 Gt C yr^{-1} to the atmosphere from boreal ecosystems due to a variety of feedbacks (Kasischke et al., 1995b). In addition to increasing metabolic activity, increased high latitude temperatures may also extend the growing season resulting in increased annual productivity, as well as periods of frost drought which may reduce annual productivity. Measurements of the length of the growing season may significantly improve current estimates of net annual CO_2 flux in the boreal regions (Way et al., 1994). For coniferous species, the summer frost-free period bounds the growing seasonal length.

Fires are an extremely important factor to a variety of processes which affect forest succession and biogeochemical cycles in boreal forests (Bonan and Shugart, 1989; Kasischke et al., 1995b; Viereck, 1983). Recent studies show that global warming may increase the frequency and intensity of fires in boreal forests and result in a significant release of carbon to the atmosphere (Kasischke et al., 1995b). Much of the carbon released will come from increased rates of decomposition in the ground layer. While global data sets are not available, records from North America show that an average of 2.5 million hectares have been affected annually by fire over the past decade. Fires in boreal forests tend to cover large areas, typically greater than 1,000 ha in size. Fires covering 50,000 to >1,000,000 ha are not

uncommon; thus, satellite remote sensors are an ideal tool for monitoring the locations and effects of fires in this region.

The ERS-1 SAR data collected at the Alaskan SAR Facility and Canadian and European receiving stations have provided a unique opportunity to study high-latitude terrestrial ecosystems found in North America. In addition to monitoring tundra biomes, ERS-1 SAR imagery was used to study boreal forests, focusing on issues related to the terrestrial carbon cycle. Specifically, this research studied the effects of changes in the length of growing season on net seasonal fluxes of CO_2 and the effects of fire on carbon cycling.

A number of remote sensing instruments may be used to estimate growing season length, and it is likely that a combination of sensors will provide the most accurate information (Way et al., 1994). The Advanced Very High Resolution Radiometer (AVHRR), for example, may provide good estimates of leaf-on period, thus bounding the growing season length for deciduous species. For coniferous species, growing season may be halted when air temperatures drop below –2° C. For closed canopy forests, canopy temperatures are within a few degrees of air temperatures (Luvall and Holbo, 1989), and can be estimated using thermal infrared emissions gathered by AVHRR. Access to these data is, however, limited by cloud cover. A third technique is to measure the length of the growing season by monitoring freeze/thaw transitions using imaging radar data (Figure 2-10) (Way et al., 1990; Way et al., 1994; Rignot et al., 1994; Rignot and Way, 1994). At microwave frequencies, freezing results in a large decrease of the dielectric constant of the dielectric constant of soil and vegetation because the crystal structure prevents the rotation of the polar water molecules contained within the soil and vegetation. This phase change results in a drop in radar backscatter of several dB.

Over the past several years, scientists have developed a greater understanding of the role of biomass burning in boreal forest in the global carbon cycle and the need to monitor these fires on a continuing basis. Because of their large sizes and remote locations, satellite sensing systems are now recognized as the only reliable means to annually locate and estimate the areal extent of fires in boreal forests (Kasischke and French, 1994). In 1990 and 1991, over 2 million ha of land surface were affected by fire in Alaska, with most (1.85 million ha) occurring in forested regions. Studies have shown that these recent fires resulted in characteristic signatures on ERS-1 SAR imagery (Kasischke et al., 1992; 1994c). Field research (Kasischke et al., 1995a) has shown that the spatial and temporal signatures present on the ERS-1 SAR imagery (Figure 2-11) are highly correlated with variations in the moisture found in the top 5 to 10 cm of the soil (Figure 2-12).

Schlenter and VanCleve (1985) have shown that rates of aerobic decomposition in black spruce forests are directly proportional to both temperature and soil moisture. Since soil temperatures increase significantly after fires in boreal forests, the rates of soil respiration in these fire-affected forests should also increase. Recent field measurements (Kasischke, pers. comm.) have shown this to be true in fire-disturbed black spruce forests in Alaska, where fluxes of CH_4 and CO_2 were greater within the burned sites than unburned sites. Areas which had high soil moistures also had significantly higher rates (by over an order of magnitude) of CH_4 and CO_2 fluxes than areas of low soil moisture. The ability of SAR data to monitor the spatial and temporal patterns of soil moisture therefore provides a means to more accurately quantify greenhouse gas emissions from fire-disturbed forests.

SAR SYSTEM CONSIDERATIONS

The wide range of applications discussed in this paper illustrates that there is probably no one ideal SAR system for ecological applications. For some applications, existing or planned

single-frequency/polarization systems may provide an adequate data set. For other applications these systems are inadequate.

To assess SAR system considerations for ecological applications we take the approach of first defining the system parameters for a specific list of applications. We then discuss the potential of existing or planned SAR systems for these applications.

Optimum System Parameters

The SAR parameters which define the utility of a specific system for ecological applications are its frequency, polarization, angle, resolution and sampling frequency. The common frequencies used today include P-band, L-band, S-band, C-band and X-band. (See Appendix B for details on SAR frequency bands and instruments used.) Radars typically transmit horizontally or vertically-polarized microwave energy and can receive either polarization, resulting in four linear polarizations - HH, HV, VH, and VV. Today's spaceborne SAR systems usually have a fixed center angle between 20° and 50° with images covering a few degrees from near edge to far edge. Future systems will operate in a SCANSAR mode, with image swaths covering a 20° to 50° range in angles. Today's spaceborne SARs have fairly fine resolution (20 to 40 m), narrow swath widths (60 to 100 km), and long sampling frequencies (20 to 40 days). SCANSAR systems will have the ability to cover wide areas at lower resolutions (up to 500-km swaths with 100 to 200 m resolution) and higher sampling frequencies (every 2 to 4 days).

Table 2-2 lists eight (8) ecological or land surface applications for imaging radar systems and summarizes the optimal SAR parameters for each application.

Utility of Existing/Planned SAR Systems

Three spaceborne imaging radar systems are now in operation or were deployed during the last year: ERS-1, JERS-1 and SIR-C/X-SAR. The ERS-1 SAR is a C-band VV (vertical transmit polarization/vertical receive polarization) launched in the summer of 1991. This system has a 25 m resolution and 100 km swath. The orbit of this system is tailored such that it has a 35-day exact repeat orbit during the northern hemisphere summer and fall (which means it can image the same ground location every 18 days or so), and a 3-day exact repeat orbit during the winter and spring in order to obtain frequent coverage of the polar ice cap. Coverage is limited to locations where ground receiving stations are installed. The JERS-1 SAR is an L-band HH system launched during the summer of 1992. It has a 40-m resolution and a 75-km swath. The exact repeat orbit on this system is 48 days. Onboard recording provides global access. The SIR-C/X-SAR system was flown onboard NASA's Space Shuttle on two ten day missions in April and October of 1994. This system consisted of a C- and L-band SAR system that was fully polarimetric (i.e., it collected HH, HV, VH, and VV imagery) and an X-band SAR which collected VV data. The resolution of this system ranged between 10 and 40 m, and it collected image swaths between 15 and 90 km wide. The ground coverage of this system was limited in order to image specific test sites during its two missions.

Three spaceborne SAR systems are planned for the future: ERS-2, RADARSAT, and ASAR. The ERS-2 SAR will be an exact duplicate of ERS-1, and is scheduled for launch in early 1995. The Canadian RADARSAT will consist of a C-band SAR with HH-polarization and has a variety of modes for resolution/swath width. The SCANSAR mode can yield swath widths up to 500 km with a spatial resolution of 100 m. This wide swath mode will allow imaging of the same geographic location once every 2 to 3 days. The ERS-2 follow-on,

known as Advanced SAR or ASAR, will be deployed on the planned European ENVISAT and consists of a dual-polarized C-band SAR. It will have both co-polarized channels (HH and VV), but not cross-polarized (HV). The planned "wide swath" mode has a 400-km swath width and 100-m resolution.

Table 2-3 summarizes the potential or demonstrated capabilities of these systems relative to the applications of ecological interest.

RECOMMENDATIONS

It is the consensus of the ecological working group that SAR data contain unique information that can be exploited by the terrestrial science community to study a wide range of physical, chemical and biological processes important to NASA's Mission to Planet Earth (MTPE), as well as the U.S. Global Change Research Program (GCRP). Over the past decade, NASA has taken the U.S. lead in development of the technological as well as the scientific research infrastructure related to airborne and spaceborne SAR systems. NASA initiatives in this area include: (1) development and operation of the JPL AIRSAR system; (2) development and deployment (with the German and Italian Space Agencies) of the SIR-C/X-SAR system; (3) establishment of the Alaska SAR Facility to receive SAR data from satellite systems such as ERS-1, JERS-1 and RADARSAT; and (4) sponsoring of extensive research programs to develop techniques to use information derived from these systems to study a wide range of oceanic and terrestrial processes. The size of NASA's investment in this area over the past decade has been significant.

These NASA-sponsored programs, as well as parallel programs in other countries, resulted in most of the research discussed in this paper. Based on these results, other U.S. government agencies are now beginning to recognize the utility of SAR data for monitoring terrestrial surfaces and processes, and are initiating research and development programs to exploit existing or future SAR systems. For example, the Environmental Protection Agency is sponsoring programs which will utilize SAR data as one component of a system to map and monitor variations in forest and vegetation cover in order to derive better estimates of the global terrestrial carbon budget. In another program, the U.S. Fish and Wildlife Service sponsored research to develop techniques to monitor tidal periods and vegetation cover in coastal estuaries.

It is the consensus of the ecology working group that the full utility of SAR for ecological applications is now only emerging and that this potential will not be fully realized within the MTPE and U.S. GCRP without a well-focused SAR R&D program within NASA. Fully exploiting the potential of imaging radars systems requires careful consideration of a number of sometimes conflicting factors, including:

(1) The need to conduct additional remote sensing science studies to understand the source of the different types of signatures present in radar imagery. This is particularly true in the multi-temporal data sets now being collected by existing satellite systems such as ERS-1 and JERS-1.

(2) Based on the results of recent studies using existing satellite SAR systems as well as recently collected SIR-C/X-SAR data, the need to conduct efforts to develop and validate algorithms which use radar data to estimate specific surface characteristics.

(3) The need to continue to develop new approaches to exploit the spatial and temporal information derived from radar imagery in ecosystem and process studies.

(4) The need to exploit the full breadth of the SIR-C/X-SAR data sets beyond the ~50 experiments presently being conducted. This need includes not only providing existing experiments with adequate resources to conclude their work, but also identification of additional research which could be carried out using this unique data set. We have not identified a compelling reason for a third flight that is an exact repeat of the first two flights, especially in light of the scale of effort required to analyze the existing data set and the fact that it is unlikely that sufficient resources will be provided to analyze these additional data.

(5) The need to develop and implement a coherent research plan within NASA's Mission to Planet Earth to fully exploit the SAR data sets being provided by existing and planned international SAR missions.

(6) To fully exploit the potential of SAR to meet the objectives of Mission to Planet Earth in the area of terrestrial ecosystem science, there is a need to develop a multi-frequency (with a minimum of two frequencies, C- and L-bands), polarimetric SAR system. In the development of such a system, the tradeoffs between resolution, swath width, and sampling frequency in terms of scientific requirements versus cost considerations must carefully be considered. However, if the cost of obtaining a multi-frequency, polarimetric spaceborne SAR is a reduction of spatial resolution, such a lower-resolution system would be quite suitable for many ecological applications.

The above needs, in essence, are the primary recommendations of the ecology working group. The working group realizes that it would be very difficult to encompass these recommendations in the context of existing programs within NASA, and that they are unlikely to be implemented unless a new program is started. Thus, we make the following summary recommendations:

(1) NASA should consider development of a new satellite remote sensing system which would contain a multi-frequency, polarimetric SAR.

(2) Even without the development of an advanced SAR system by NASA, the existing SAR data sets as well as those which will be collected by satellite SAR systems in the future do provide unique information for a variety of ecological processes. NASA should take a more proactive role in ensuring that these data are used in an effective manner within its Mission to Planet Earth.

(3) To achieve recommendation 2, NASA should create a multi-disciplinary SAR Facility Instrument Team. In addition to carrying out the recommendations outlined above, this team would also serve as the advisory board for development of the new SAR satellite system recommended above.

Table 2-1. Some recent examples of land cover classification approaches and findings using radar imagery.

Ecosystem	Purpose	Classifier	Data	Class No & Types	Accuracy	Parameters	Reference
Agricultural	Crop inventory	MLE Neural net	AIRSAR	9 C(5), H(4)	Med-High	CHH, CVV, CHV	Foody et al., 1994
Agricultural	Crop inventory	MLE Contrast	AIRSAR	9 B(2), C(7)	High	P, L	Lemoine et al., 1994
Tropical Floodplain forest	Map forest flooding	Decision tree	SIR-C	5 W, fH, H, F, fF	High	LHH, LHV, CHH	Hess et al., 1995
Subtropical Forest and wetland	Ecosystem mapping	MLE Cluster	AIRSAR	7 W, B, C, H, S, F(2)	Medium	P, L, C,	Pope et al., 1994
Temperate Floodplain Forest	Wildlife habitat mapping	Decision tree	AIRSAR	5 W,fH, H, fF, F	High	PHV, PHH, CHH, CHV	Hess and Melack, 1994
Temperate Conifer Forest	forest age class	MLE	AIRSAR	6 U, A, F(4)	Med-High	PHH, PVV, PHV	de Grandi et al., 1994
Boreal forest	Successional stage, biomass	MLE	AIRSAR	6 W, H, S, F(3)	High (low F)	P, L, C	Rignot et al., 1994

Classification approaches: Maximum Likelihood Estimators (MLE) including Maximum Contrast Classifiers, Cluster analysis (Unsupervised classification), Decision tree, Neural network

Land cover classes: Agriculture(A), Water(W), Bare soil(B), Crops(C), Urban(U), Herbaceous(H), Shrubs(S), Forest(F), flooded(f). Number of types in a cover class is indicated by the number in parentheses.

Table 2-2. Optimal SAR Parameters for Land Surface Applications

APPLICATION AREA	*PARAMETER*				
	RADAR FREQUENCY	*POLARIZATION*	*INCIDENCE ANGLE*	*RESOLUTION*	*SAMPLING FREQUENCY*
Vegetation Mapping	best results achieved if multiple frequencies are available; as a minumum, need two frequencies, one high and one low, e.g., L and C-band	important parameter in classification especially for single frequency systems	both low (20° to 40°) and high (40° to 60°) are desired	high resolutions are desirable for mapping smaller sampling units	higher sampling frequencies (greater than once every 2 weeks) not required for mapping purposes when multiple-channels are available, may improve classification for single-channel systems
Crop Monitoring	multiple frequencies are not always required, especially if multi-date data are used in classification	important parameter in classification especially for single frequency systems, not always necessary	lower angles (20° to 40°) are desired	higher resolutions are required for discrimination of small fields	higher sampling frequencies (greater than once per week) important for monitoring crop phenology and status and for improving classification accuracies
Biomass Estimation	L- or P-band are required but multiple frequencies are needed to develop best algorithms; as a minimum, L- and C-band are required	cross polarization data have most sensitivity to biomass variations; multi-polarization systems improve biomass algorithms	lower angles (20° to 35°) are required	for studying biomass dynamics in small forest stands, finer resolutions are required; for large area study, coarser resolutions can be used	high sampling frequencies are not required; sampling at proper phenologic stage and under optimum weather conditions is important
Monitoring Flooded Forests	L- and P-band are optimum, but some sensitivity at C-band if few leaves are present and HH polarization used	polarization very important for community discrimination; HH polarization most sensitive, HV and VV polarization can be important	lower angles (20° to 40°) are needed for maximum sensitivity to flooding	higher resolutions may not be as important as a high sampling frequency, but are important for mapping narrow features	high sampling frequencies usually important

Table 2-2 (continued). Optimal SAR Parameters for Land Surface Applications (continued)

APPLICATION AREA	*PARAMETER*				
	RADAR FREQUENCY	*POLARIZATION*	*INCIDENCE ANGLE*	*RESOLUTION*	*SAMPLING FREQUENCY*
Monitoring Coastal/ Low Stature Wetlands	X and C-band are required	for discrimination of different vegetation types, multiple polarizations are required; use HH or VV for monitoring inundation	intermediate angles (30° to 40°) are desired	high resolution is required in some cases	higher sampling frequencies are required for monitoring flooding dynamics; multi-temporal data can improve classification accuracy
Monitoring Tundra Inundation	X and C-band are required	for discrimination of different vegetation types, multiple polarizations are required; use HH or VV for monitoring inundation	lower angles (20° to 40°) are desired	high resolution is required in some cases	higher sampling frequencies required for monitoring flooding dynamics; multi-temporal data improves classification accuracy
Monitoring Fire-Disturbed Boreal Forests	X and C-band are optimum, multiple frequencies improve monitoring of burn severity	polarization not important for relative soil moisture monitoring, but very important in moisture estimation and monitoring severity of burns	lower angles desired (20° to 40°) but may not be necessary	high resolution is not required	high sampling frequencies required for monitoring seasonal variations in soil moisture
Detection of Frozen/Thawed Vegetation	can be detected at both low and high radar frequencies; L-band data may be more effective; multiple-frequencies may be required to differentiate vegetation thawing from variations in surface moisture	polarization may be important to differentiate vegetation thawing from variations in surface moisture	incidence angle not a critical parameter	high resolution is not required if high resolution vegetation map available	high sampling frequencies required

Table 2-3. Potential or Demonstrated Capabilities of Spaceborne SARs for Ecology

APPLICATION AREA	*SPACECRAFT CAPABILITIES*				
	ERS-1/ERS-2	***JERS-1***	***Radarsat***	***ENVISAT***	***SIR-C/X-SAR***
Vegetation Mapping	Poor overall, improvement with multitemporal data	Somewhat better than ERS-1, but still poor overall, multitemporal may improve, but has low sampling frequency	probably poor without using multi-temporal data	better than single polarization systems, but still not optimum; multi-temporal data needed	near optimum configuration
Crop Monitoring	good results achieved using multi-temporal data	poor overall, sampling frequency too low	good potential with multi-temporal sampling	improvement over single-channel systems	near optimum for single-date classification
Biomass Estimation	poor except for low biomasses	good for lower biomass, but still limited	poor except for very low biomass	some improvement over ERS-1/Radarsat, but still poor	near optimum configuration, but lower frequency (P-band) still optimum system
Monitoring Flooded Forests	poor except when few leaves are present	a good system for flood detection, but poor for monitoring because of low sampling frequency	will be better than ERS-1, but limited to leaf off conditions or low density stands	will be better than ERS-1, but limited to leaf off conditions or low density stands	near optimum in terms of frequency/ polarization, poor in terms of repeat frequency
Monitoring Coastal/ Low Stature Wetlands	adequate in some situations	poor	better than ERS-1 because of higher repeat frequency and HH polarization	good overall - better than ERS-1/ Radarsat because of multiple-polarizations and high repeat frequency	near optimum in terms of frequency/ polarization, poor in terms of repeat frequency

Table 2-3 (continued). Potential or Demonstrated Capabilities of Spaceborne SARs for Ecology

Monitoring Tundra Inundation	very good	poor, frequency too low	potential high, especially with wide-swath mode	potential excellent with dual polarizations and wide swath mode	orbital ephemeris does not reach high latitudes, data not applicable
Monitoring Fire-Disturbed Boreal Forests	very good	poor, sensitivity to variations in soil moisture low	potential high, especially with wide-swath mode	potential excellent with dual polarizations and wide swath mode	excellent potential for lower-latitude boreal forests
Detection of Frozen/ Thawed Vegetation	fair for this application, repeat frequency limits system somewhat	poor, repeat frequency too low	potential high, especially with wide-swath mode	potential excellent with dual polarizations and wide swath mode	can study processes on a limited basis with existing data

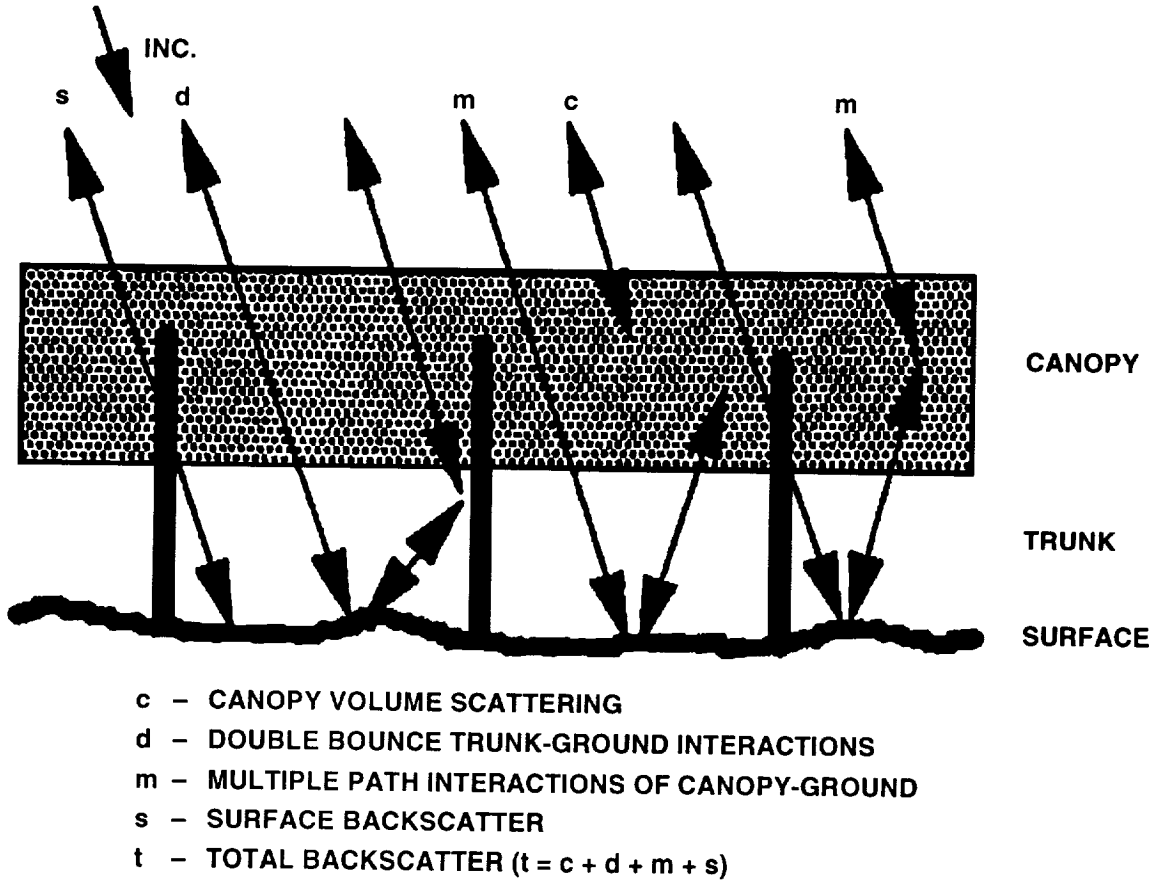

Figure 2-1. Schematic diagram of major scattering terms in microwave modeling of forest canopies (after Wang et al 1993c).

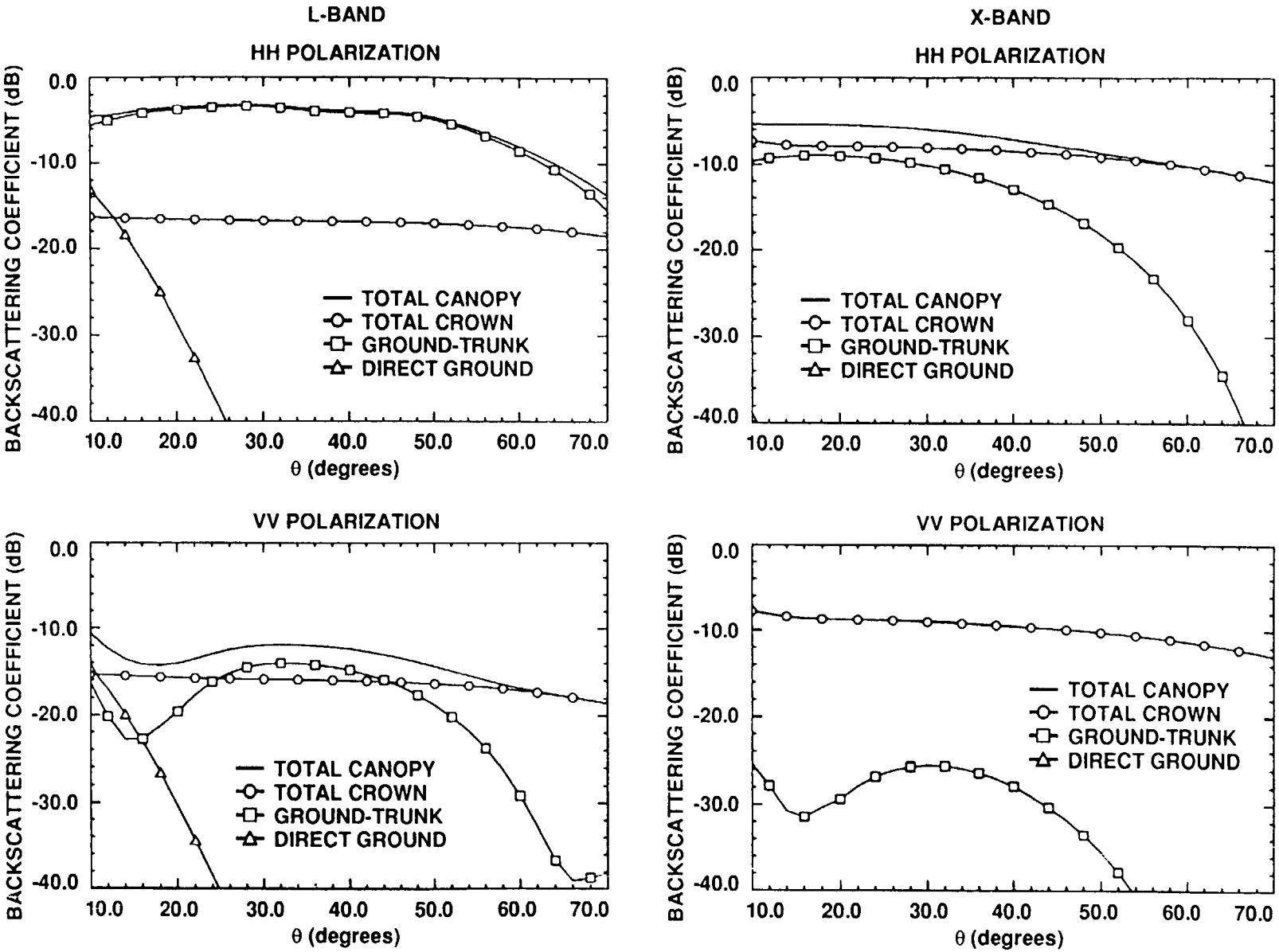

Figure 2-2. a) Use of theoretical models to understand radar scattering from vegetated surfaces. Model predicted microwave scattering from a trembling aspen stand as a function of radar frequency and incidence angle (after Ulaby et al., 1990). Note how the dominant scattering term varies as a function of frequency, polarization and incidence angle. At X-VV, total canopy scattering is equal to the total crown scattering.

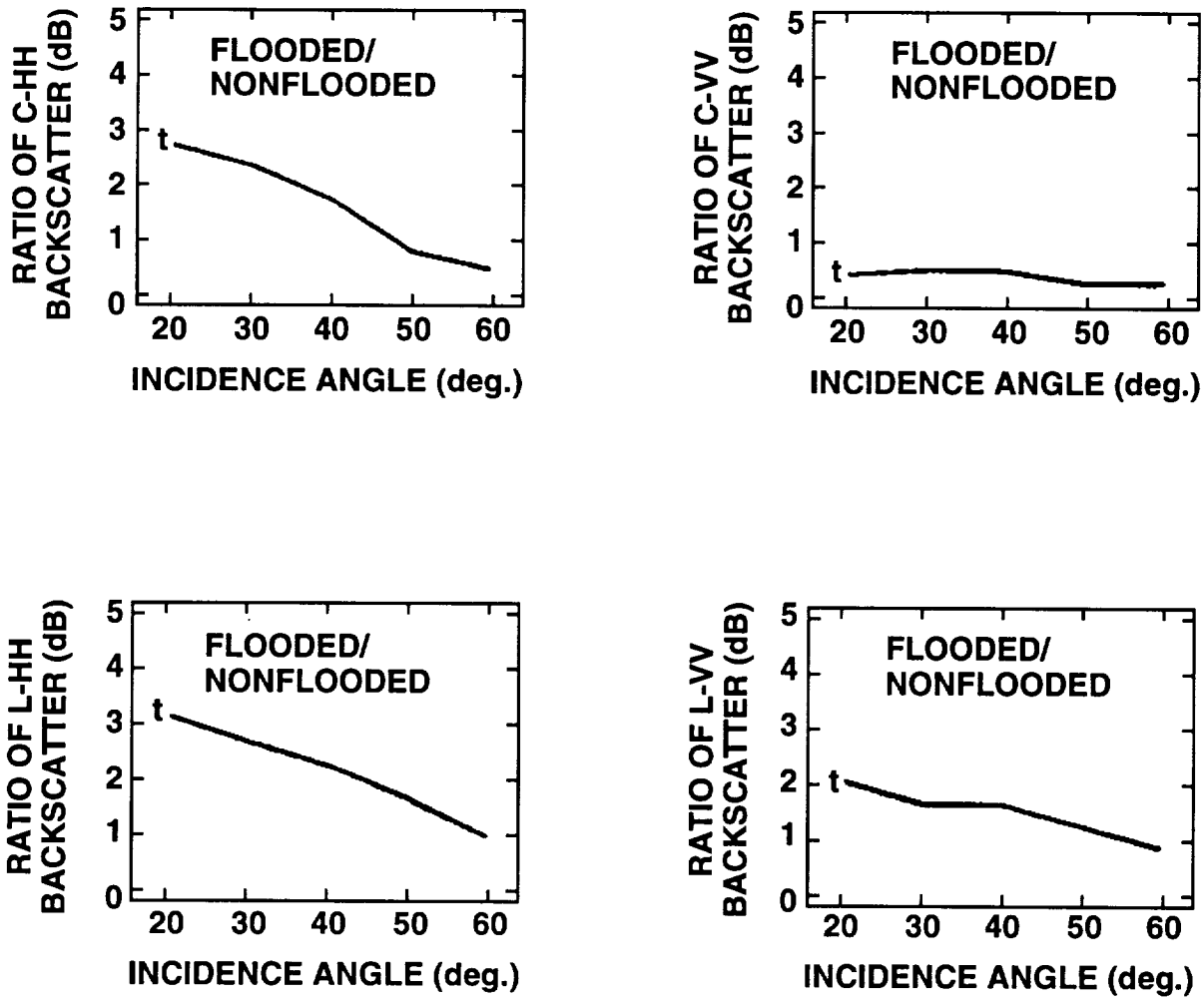

Figure 2-3. Use of theoretical models to understand radar scattering from vegetated surfaces. Model-predicted microwave scattering from a flooded forest on the floodplain of the Amazon River as a function of radar frequency and incidence angle (after Wang et al., 1995). "t" indicates total backscatter as shown in Figure 2-1.

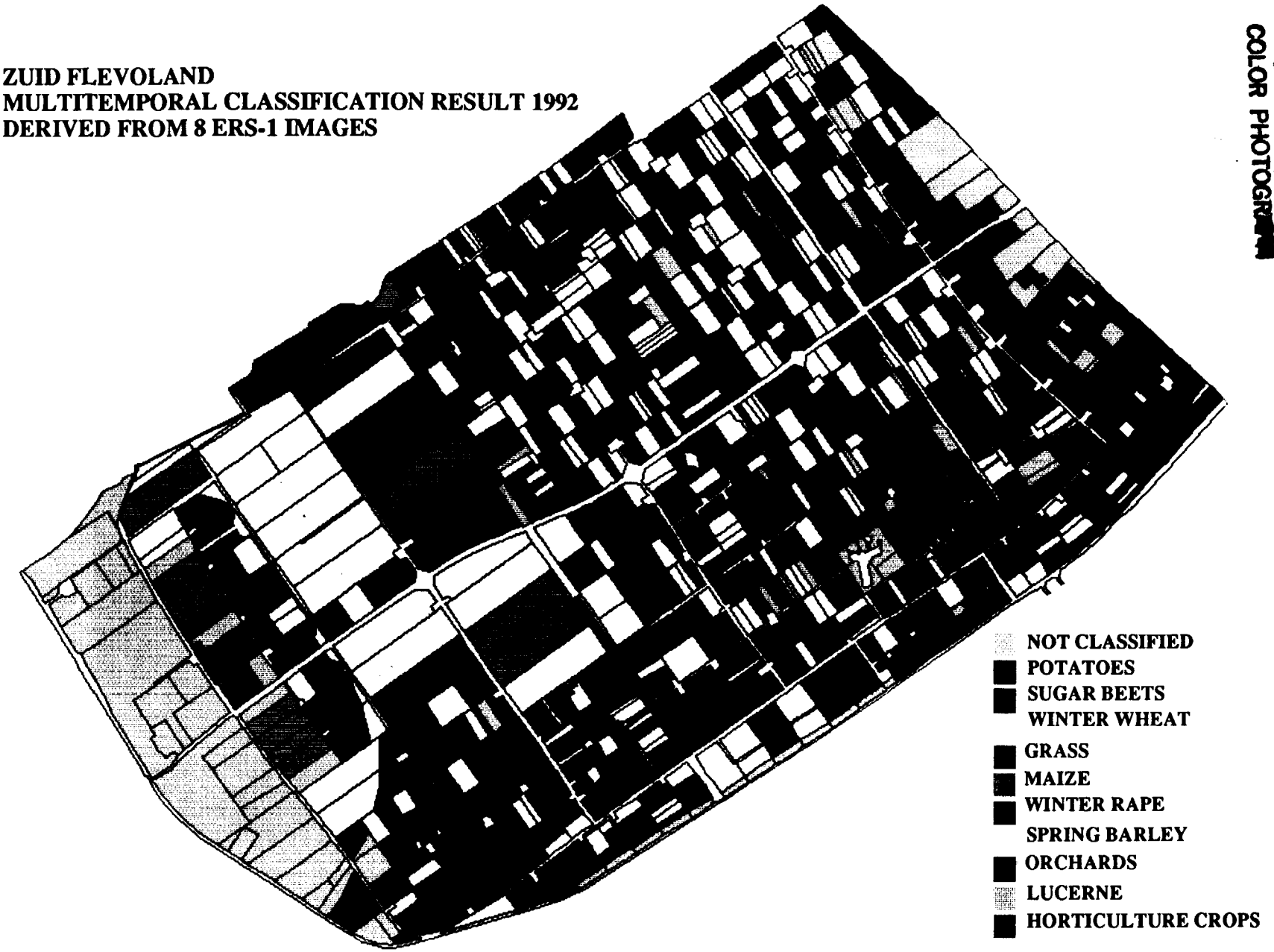

Figure 2-4. a) Image of crop classification derived from multi-temporal ERS-1 SAR imagery collected over Flevoland, The Netherlands (after Schotten et al., 1995).

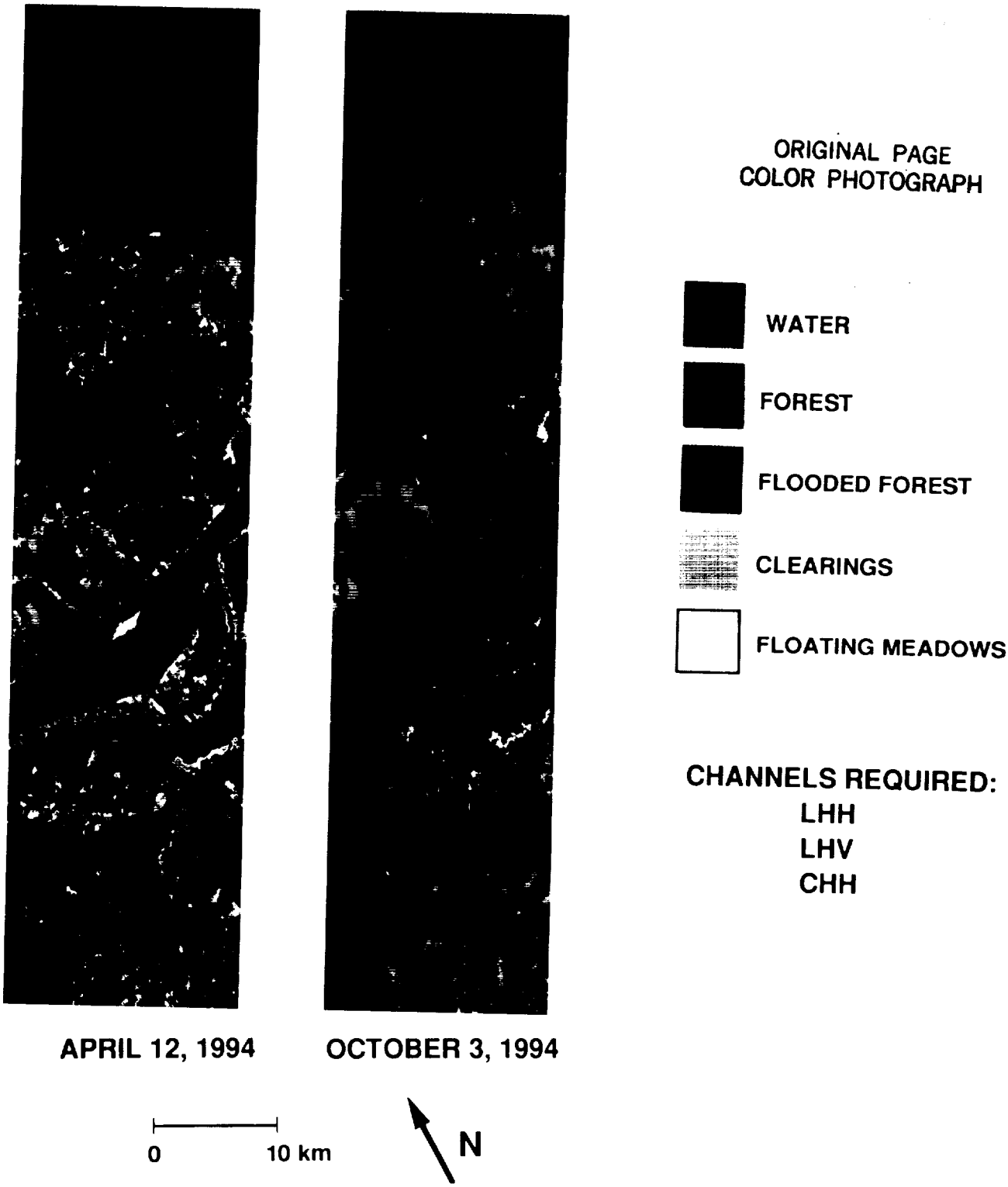

Figure 2-4. b) Maps of the flooding and land cover from data obtained by the SRL-1 on April 12, 1994 (left) and SRL-2 on October 3, 1994 (right). The rivers extending across the scenes are the Rio Negro (top) and Rio Solimoes (Center). Classification was prepared using L-band HH and HV polarizations, and C-band HH polarization. Field studies by boat, on foot, and in low flying aircraft done by UCSB in collaboration with Brazil's INPA and INPE during the SRL-1 and SRL-2 missions have validated the interpretation of the radar images (Hess, Melack, Filoso, and Wang, 1995).

ORIGINAL PAGE
COLOR PHOTOGRAPH

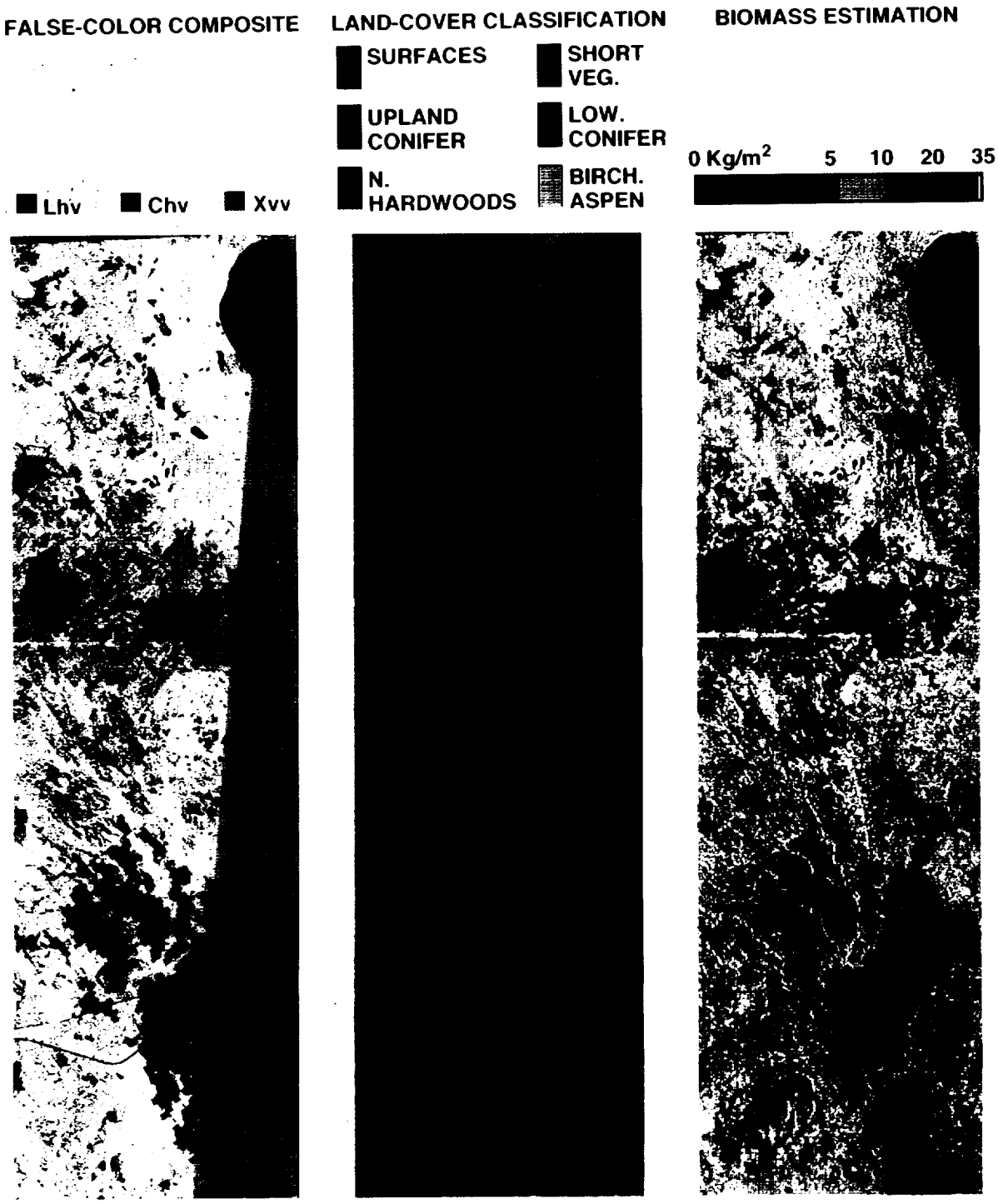

Figure 2-4. c) Images showing classification of natural vegetation/landcover and biomass estimation derived from SIR-C/X-SAR data from Northern, Michigan forests (Dobson et al., 1995c).

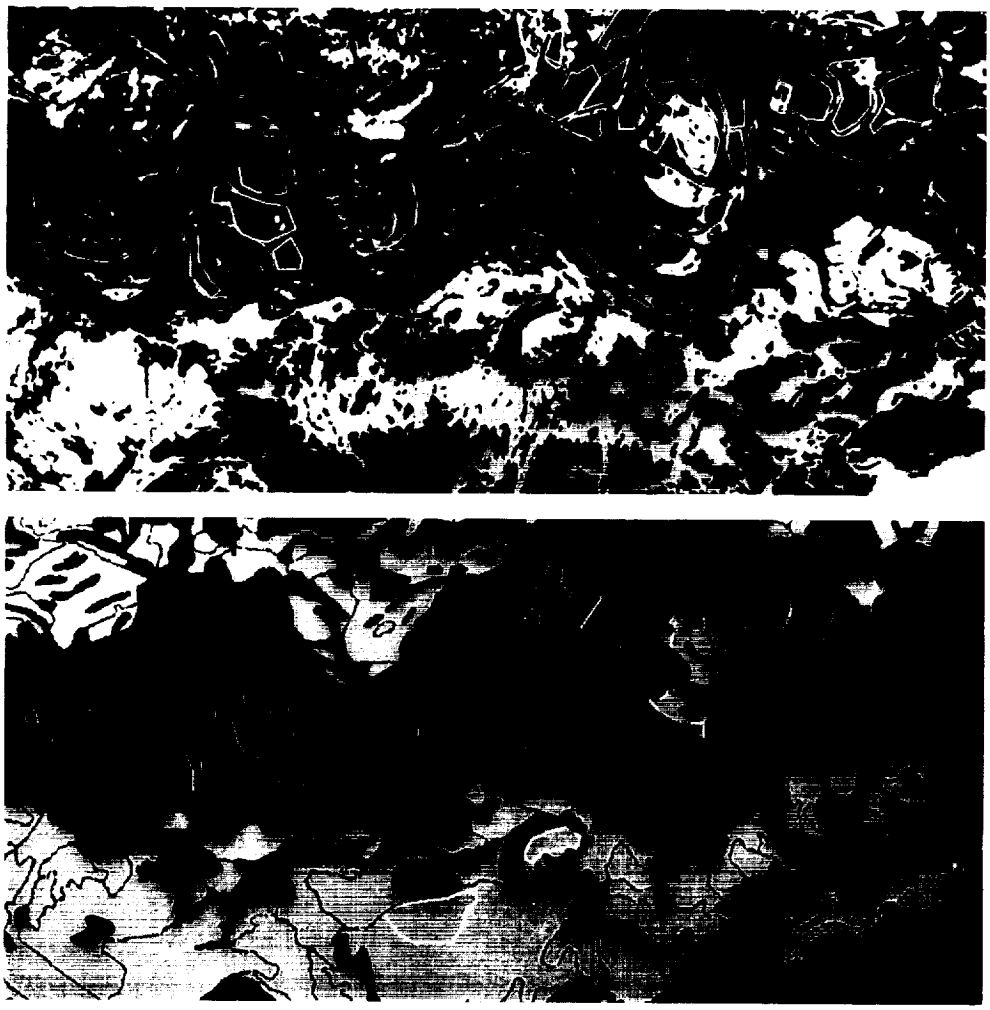

Figure 2-4. d) Images showing classification of natural vegetation/ landcover (top) based on AIRSAR data of Bonanza Creek, Alaska and vegetation map (bottom) (Rignot and Way, 1994).

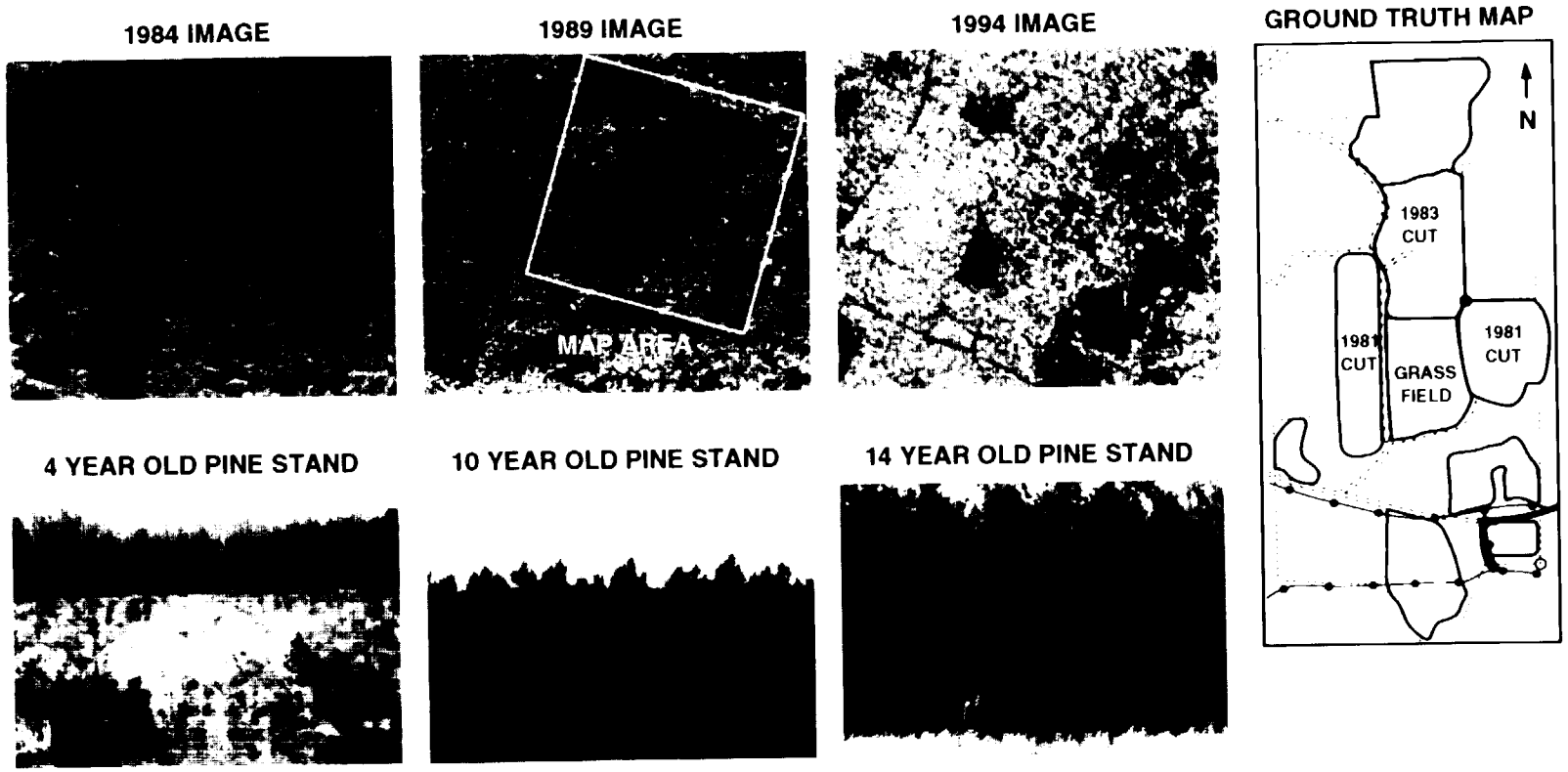

Figure 2-5. Airborne and SIR-C L-band (VV) SAR imagery collected over Duke Forest, North Carolina. Figure presents SAR data collected over the same study site in approximately five-year intervals since 1984, including airborne (1984 and 1989) and SIR-C L-band (1994), VV SAR imagery collected over a series of young pine stands which were seeded in 1981 and 1983. The surface photographs are of the pine stand reseeded in 1981 to the west of the grass field in the center of the study area.

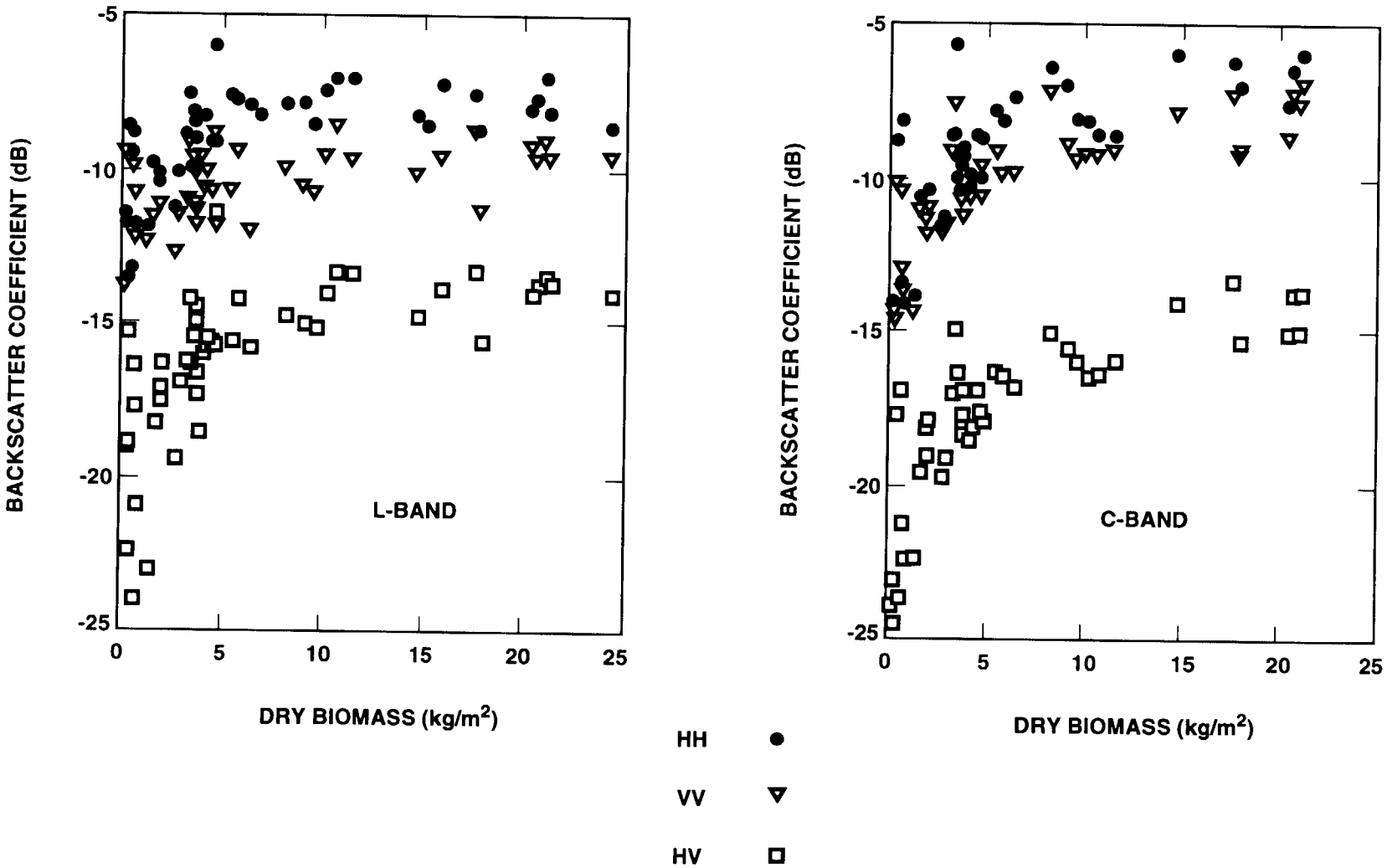

Figure 2-6. Dependence of L- and C-band SAR backscatter on aboveground biomass (from Dobson et al., 1995c).

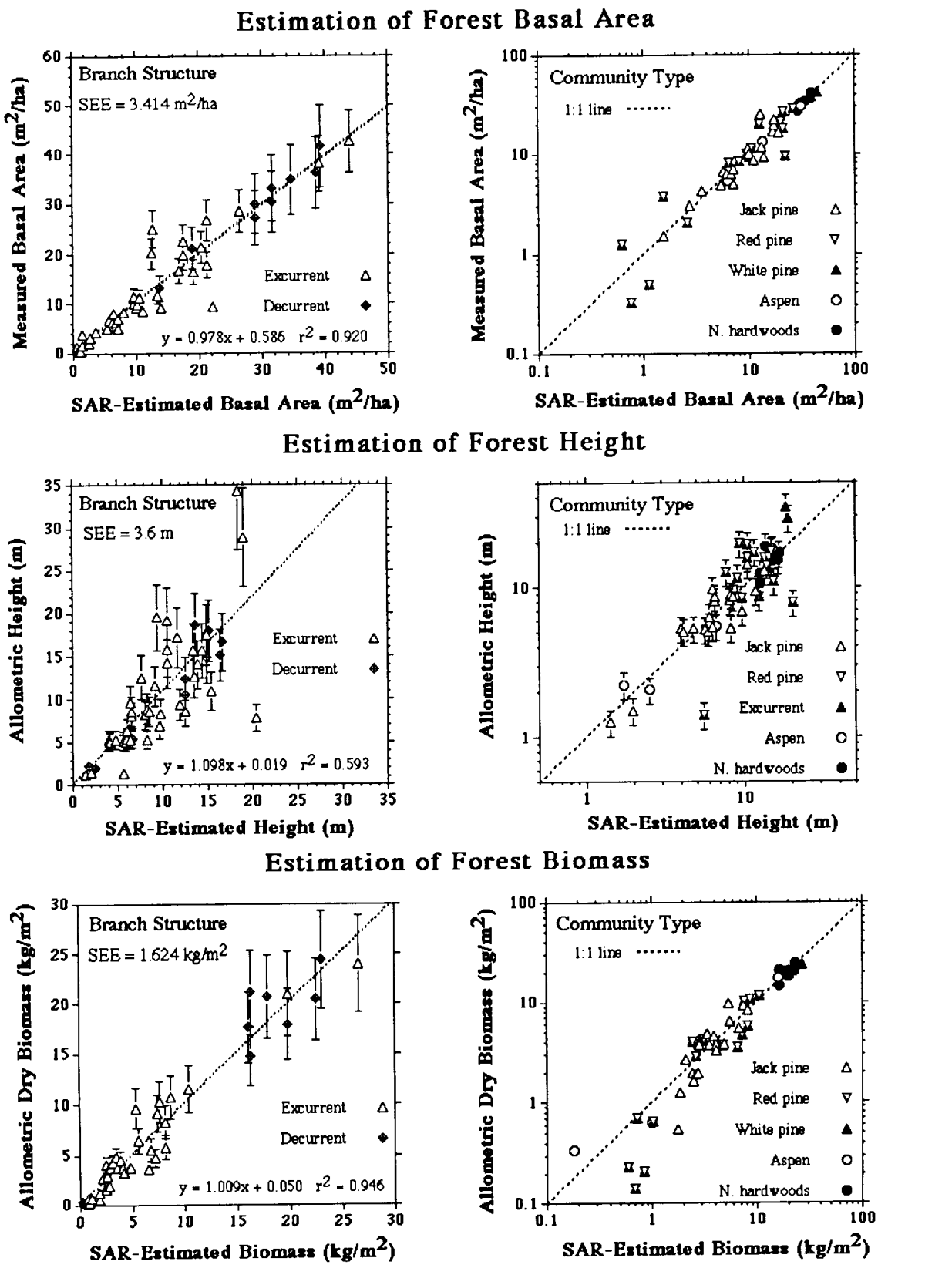

Figure 2-7. Predicted versus actual basal area, height and biomass using semi-empirical approach (from Dobson et al., 1995c).

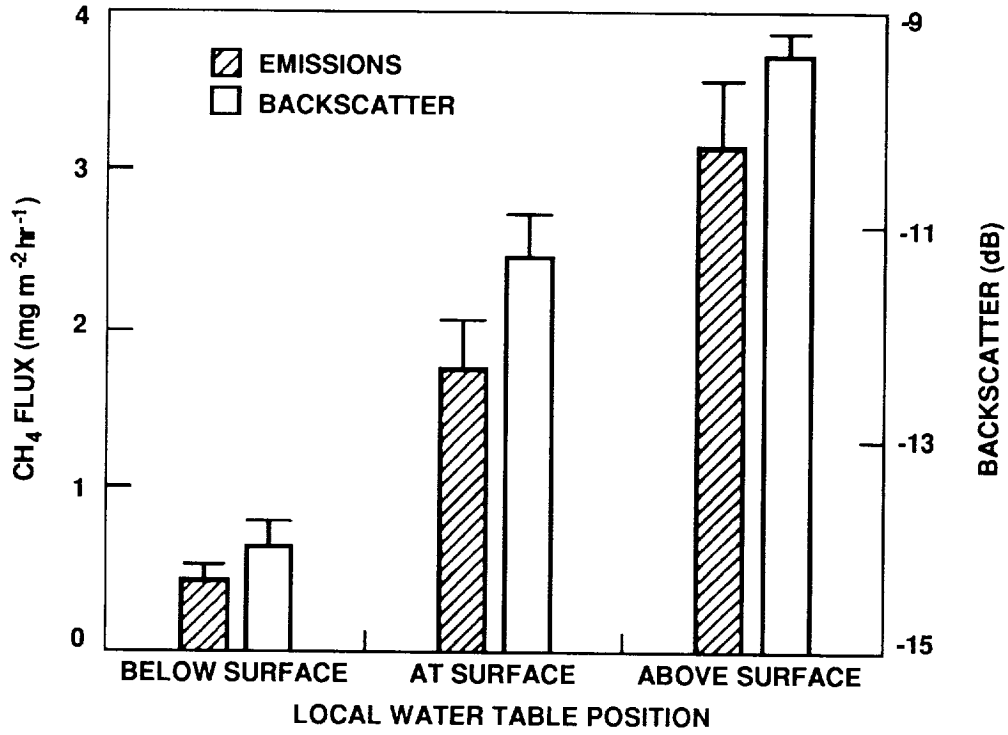

Figure 2-8. Methane emissions and ERS-1 SAR backscatter related to the position of the local water table for herbaceous sites at Barrow, Alaska, mean +- standard error.

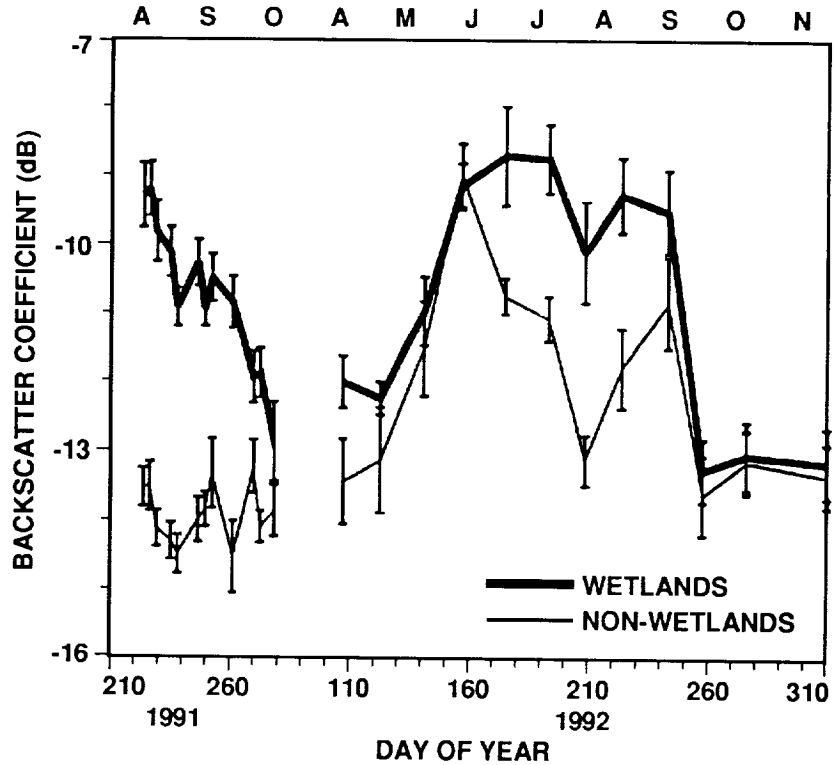

Figure 2-9. Seasonal variation in ERS-1 SAR backscatter for wetlands ("flooded") and non-wetlands ("moist/dry") for data collected over Barrow, Alaska (mean +- standard error) (from Kasischke et al., 1995a).

COLOR PHOTOGRAPH

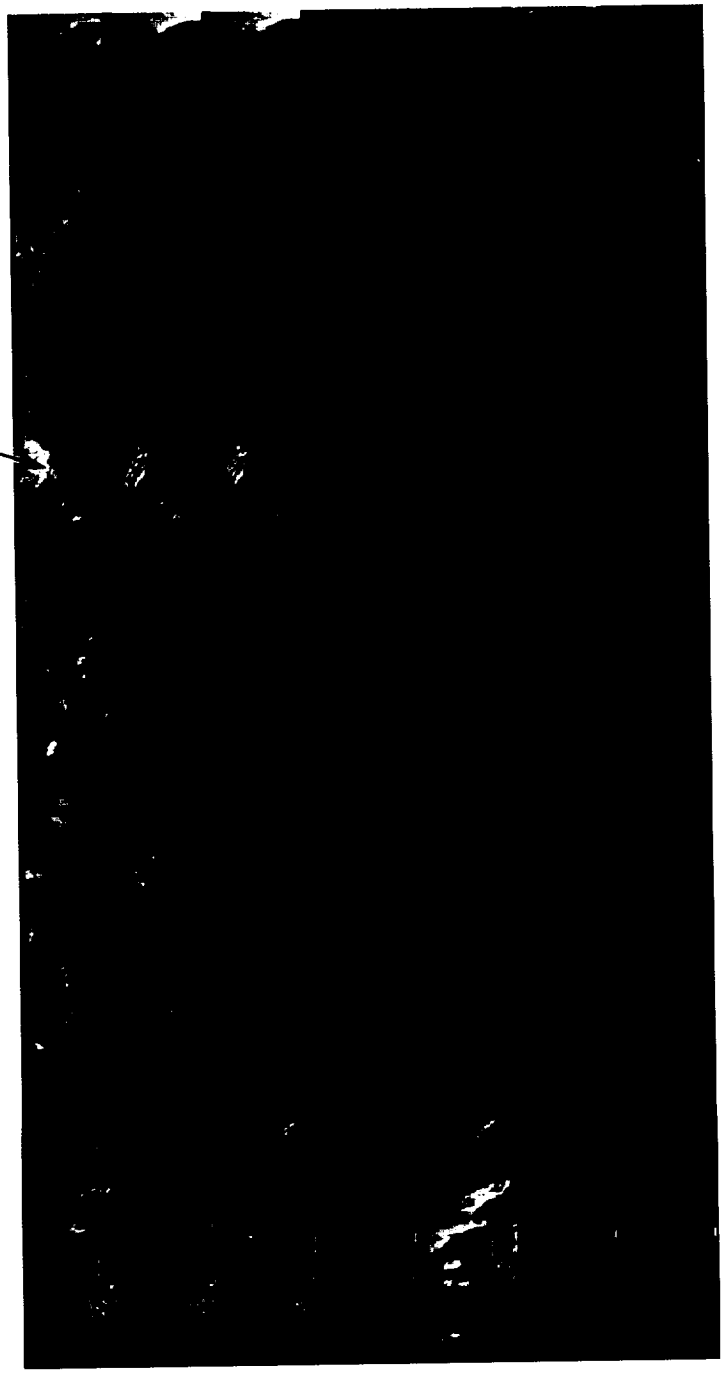

Figure 2-10. North-south transects across Alaska acquired by ERS-1 SAR during the 1991 Commissioning Phase. ERS-1 is passing from north (top) to south and looking to its right. Each transect is 100 km wide by 1400 km in length with 200 m resolution on the ground. The radar backscatter is represented in gray tone. Areas of pronounced textural variations correspond to mountainous regions of the Brooks Range to the north and the Alaska Range to the south. From left to right, Rev #384, DOY 224 is the reference transect used to compute changes in radar backscatter relative to a thawed state of the landscape. This pass is followed by Rev #814 (DOY 24), 1072 (DOY 272), 1201 (DOY 281), 1330 (DOY 290), 1502 (DOY 302) and 1760 (DOY 320). Areas which show a decrease in backscatter larger than 3 dB are colored blue with an intensity modulation determined by the amplitude of the signal. (after Rignot and Way, 1994)

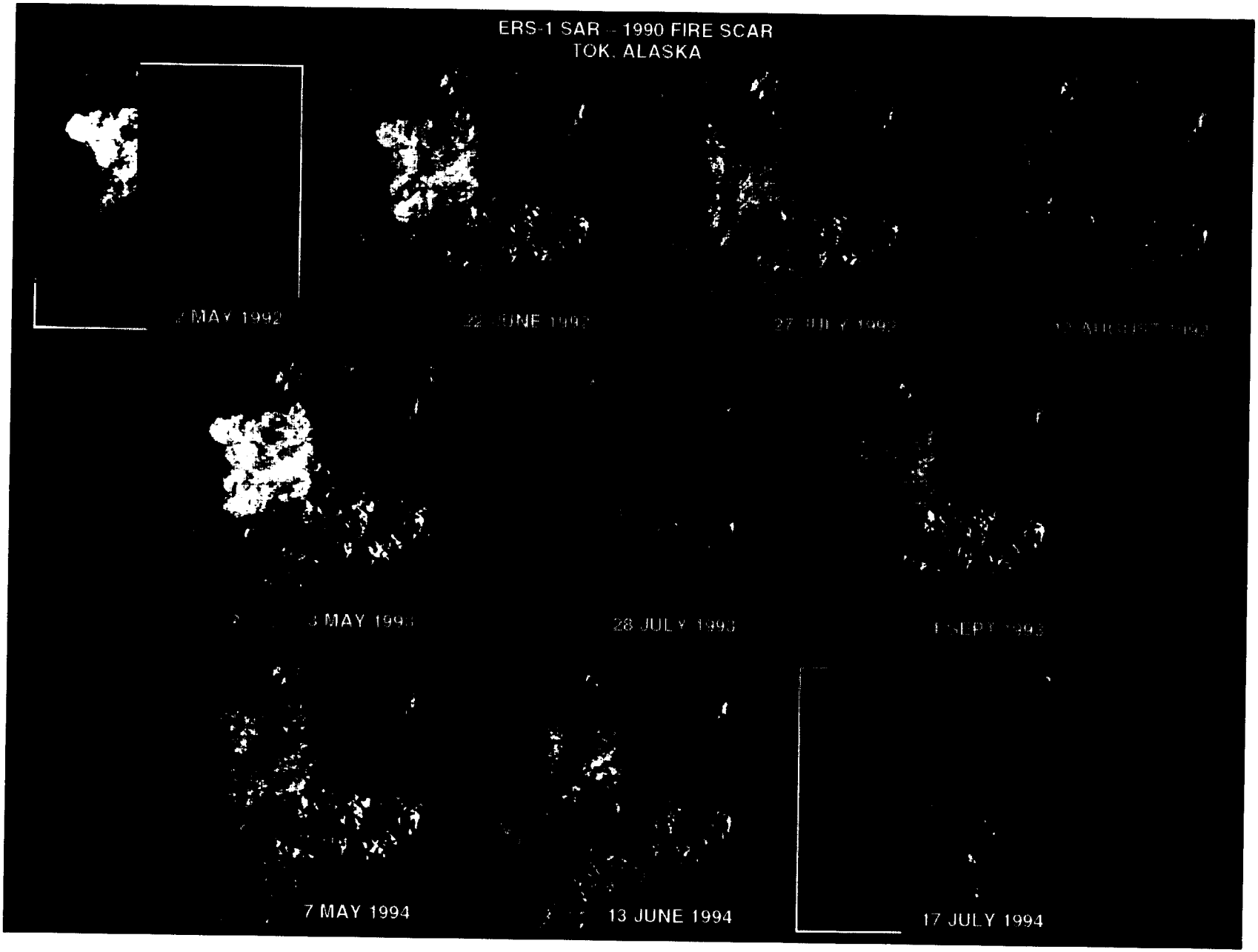

Figure 2-11. ERS-1 SAR images collected in 1992 to 1994 over a fire-disturbed spruce forest near Tok, Alaska (from Kasischke et al., 1995a).

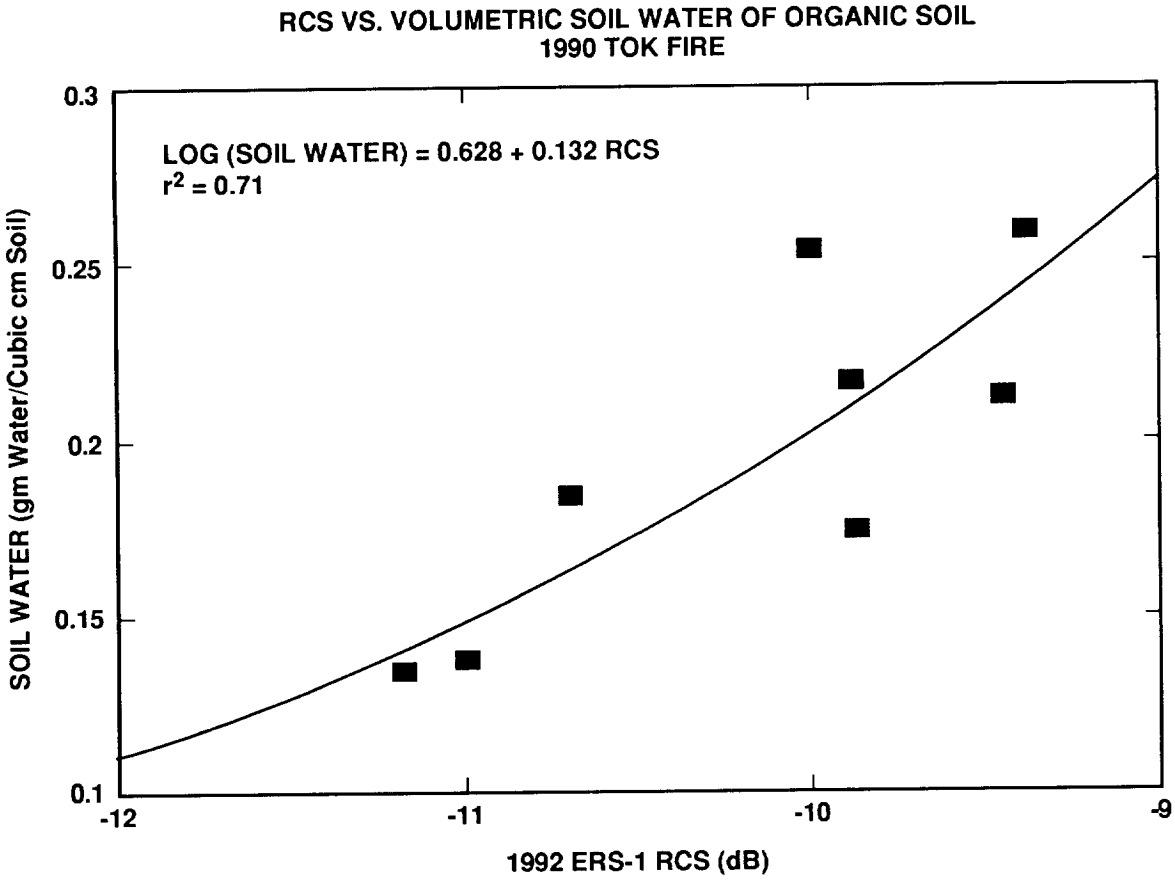

Figure 2-12. Relationship between ERS-1 SAR radar cross section and volumetric soil moisture from test sites in the 1990 Tok forest fire site (from Kasischke et al., 1995a).

3—Hydrology

INTRODUCTION

The cryosphere is a major component of the hydrosphere and interacts significantly with the global climate system, the geosphere, and the biosphere. Over 30 percent of the Earth's land surface is covered seasonally by snow, and about 10 percent is covered permanently with snow or ice.

Snow and ice play important interactive roles in regional climates, because snow has a higher albedo than any other natural surface. The earliest signs of global climate change are likely in the polar regions and in the seasonal snow cover and alpine glaciers. For investigations in hydrology and land-surface climatology, seasonal snow cover and alpine glaciers are critical to the radiation and water balances. Over major portions of the middle and high latitudes, and at high elevations in the tropical latitudes, snow and alpine glaciers are the largest contributors to runoff in rivers and to ground-water recharge. The dual problems of estimating both the quantity of water held by seasonal snow packs and timing of snowmelt confront snow hydrologists. Understanding the processes in the seasonal snow cover is also important for studies of the chemical balance of alpine drainage basins, because of translocation of anions and cations within the snow pack and possible concentrated release in the first phases of the melt season.

Soil moisture is an environmental descriptor that integrates much of the land surface hydrology and is the interface for interaction between the solid Earth surface and life. As central as this seems to man's existence and biogeochemical cycles, it is a descriptor that has not had wide spread application as a variable in any land process models. There are two primary reasons for this. It is a difficult variable to measure, not at one point in time, but in a consistent and spatially comprehensive basis. Also, it exhibits very large spatial and temporal variability; thus point measurements have had very little meaning. The practical result of this is that soil moisture has not been used as measurable variable in any of our current hydrologic, climatic, agricultural, or biogeochemical models.

Both passive microwave and active microwave (SAR) techniques have provided solid theoretical and experimental results that the top five cm of soil moisture can be measured from aircraft and space platforms under a variety of environmental conditions and through a moderate vegetation cover (Figures 3-1, 3-2). This section will define the science issues and application opportunities that can be addressed by microwave remote sensing of soil moisture and snow water equivalence, describe the capabilities and limitations of the passive and SAR systems, describe the progress to date and document the research still needed to take this technology to an operational status.

BACKGROUND

The scientific objectives related to snow and ice identified by the National Research Council are:

- To study the global hydrologic cycle to determine the distributions, dimensions, properties, and relevant dynamics of snow, sea and lake ice, ice sheets and shelves.
- To determine and understand the mechanisms for the transfers of water between the major global reservoirs (glacier flow, melting, and freezing).

- To predict on appropriate time scales the distributions, volumes, and fluxes associated with snow cover, sea ice, ice sheets and shelves, ground ice, and permafrost.

Although snow and ice phenomena play important roles in global processes, difficult access hampers data collection, and conventional studies of snow and ice cannot address the correct scales of most phenomena. In situ sampling methods have limited utility for capturing the spatial and temporal variability of snow and ice processes. Operational hydrology and climatology require timely measurement of snow-pack parameters.

The redistribution of solar energy over the globe is central to studies in climate. Water serves a fundamental role in this redistribution through the energy associated with evapotranspiration, the transport of atmospheric water vapor, and precipitation. Residence time for atmospheric water is on the order of a week, and for soil moisture, from a couple of days to months, which emphasize the active nature of the hydrologic cycle. Understanding the importance of the land-surface hydrology to climate has emerged as an important research area since the mid 1960s when researchers at the Geophysical Fluid Dynamics Laboratory placed a land hydrology component into their general circulation model (GCM) (see Manabe et al., 1965; Manabe, 1969).

As the sophistication of GCMs has increased, the role of the land surface component has become more and more important. However, a major weakness in the current GCMs is, according to the CES-89 report, "the adequate parameterization of variables representing the terrestrial phase of the hydrologic cycle..., which is primarily the result of totally inadequate information concerning the degree of spatial variability of precipitation, evapotranspiration, and other components of hydrology." This report goes further to say "the lack of regional-scale measurements introduces a severe shortcoming in the testing of GCM output."

Perhaps the most important role that the land surface component of a GCM performs is the partitioning of incoming radiative energy into sensible and latent heat fluxes. The major factor involved in determining the relative proportions of the two heat fluxes is the availability of water, generally in the form of soil moisture. A number of modeling studies have demonstrated the sensitivity of soil moisture anomalies to climate (Walker and Rowntree, 1977, Rowntree and Bolton, 1983, Rind, 1982, Shukla and Mintz, 1982, Delworth and Manabe, 1989). Researchers have reported, for instance, that soil moisture is the second most important forcing function, second only to the sea surface temperature in the mid latitudes, and it becomes the most important forcing function in the summer months.

The role of soil moisture is equally important at smaller scales. Recent studies with mesoscale atmospheric models have similarly demonstrated a sensitivity to spatial gradients of soil moisture. For example, Fast and McCorcle (1991) have shown that soil moisture gradients can induce thermally induced circulations similar to sea breezes. Chang and Wetzel (1991) have concluded that the spatial variations of vegetation and soil moisture affect the surface baroclinic structures through differential heating, which in turn indicate the location and intensity of surface dynamic and thermodynamic discontinuities necessary to develop severe storms. In yet another study, Lanicci et al., (1987) have shown that dry soil conditions over northern Mexico and variable soil moisture conditions over the southern Great Plains can dynamically interact to alter prestorm conditions and subsequent convective rainfall patterns.

It is still unclear whether the spatial distribution of soil moisture collected at regional scales is useful for GCM and mesoscale modeling. One indication in favor is the recent study by Betts et al., (1994) showing that initialization of ECMWF weather predictions on current soil moisture (during the summer of 1993 in the US Great Plains region) can lead to improved

rainfall predictions. The extreme wetness conditions, in comparison to climatological average soil moisture, clearly was a factor in the effect. For more normal conditions, soil moisture anomalies will vary with the spatial and temporal scales of rain events--scales that may be meaningful to 4-dimensional data assimilations (4DDA) and mesoscale modeling.

Based on these studies and scales ranging from GCM to mesoscale, it appears that soil moisture will be an important hydrologic variable for hydrometeorological modeling and validation studies. Because of the ubiquitous nature of soil moisture in many disciplines, there are numerous potential science applications for frequent and spatially comprehensive measurements of soil moisture. However, most of these will fit under the umbrella of the following four science issues which are the highest priority:

- To understand the role of surface soil moisture in the partitioning of incoming radiant energy into latent and sensible heat fluxes at a variety of scales from mesoscale to GCM scale.

- To understand the relationship between the surface 5 cm of soil moisture observable by microwave techniques and the total profile (1 m or more) soil moisture that is accessible to plants and transpiration to the atmosphere.

- To understand how spatial and temporal patterns of soil moisture are related to the physical and hydrologic properties of soils.

- To understand how the spatial and temporal patterns of soil moisture can be used to improve our ability to model runoff at a variety of scales and adapt hydrologic models to areas of differing climate, biomes and soils, and geology.

With the potential for measuring soil moisture having been demonstrated, the obvious question to ask is how might society use such soil moisture measurements? As in the science issues, there are four general areas in which routine measurements of soil moisture could have major impacts on our day-to-day lives:

- Improvements in medium range weather forecasting by incorporating measured soil moisture on a 30-km grid on a daily basis.

- Agricultural applications would include on-farm uses for improving irrigation scheduling and efficiencies, to improving crop yield modeling for both domestic and foreign areas. The scales of interest here would be 100 m to 1 km and three to seven days.

- Water management applications require better quantification of water uses, storages and runoff to monitor existing resources and to assist decision makers in allocation of limited resources or coordination of relief efforts in times of flooding. The scales of interest here would also be 100 m to 1 km and three to seven days.

- Climate models, particularly for annual and inter annual variability, need to be able to represent the land surface hydrologic processes accurately. Measured soil moisture can be used as a state variable and as a validity measure for GCMs. The scales of interest here are 1 to 10 km and 7 to 30 days.

ROLE OF SAR

Satellite remote sensing has become increasingly important to hydrologists and climatologists because the data provide information on the spatial and temporal distributions

of parameters of climatic and hydrologic importance: snow covered area, surface albedo, snow water equivalence, and snow wetness (liquid water content). For the seasonal snow cover, remote sensing improves the monitoring of existing conditions and has been incorporated into several runoff-forecasting and management systems. Visible and near-infrared sensors have been used extensively to measure snow-covered area. While the signal in this portion of the electromagnetic spectrum is sensitive to snow grain size and impurities, it is not sensitive to wetness and is sensitive to water equivalence only for shallow snow packs. In addition, cloud cover hampers data collection from these sensors, so the opportunities for obtaining suitable data can be infrequent. In addition to accurate measurements of snow extent and albedo, forecasting of melt (at both continental and drainage-basin scales) requires information about spatial and temporal distributions of snow water equivalence and free liquid-water content.

Passive microwave signals are sensitive to snow properties of hydrologic interest. However, the spatial resolution of spaceborne passive microwave sensors is much coarser than the natural scale of variation in mountainous areas. Active microwave remote sensing has long promised the advantages of: (1) all-weather day or night imaging capabilities; (2) high resolution suitable for alpine regions; (3) sensitivity to most snow properties of interest to snow hydrologists and climatologists. Over the last decade, major improvements in technology from data acquisition and processing to quantitative interpretation have put capabilities for advanced snow and ice measurements at our doorstep.

For snow, recent studies (using SIR-C/X-SAR, AIRSAR, and ERS-1 data) have shown a significant improvement in understanding and modeling the backscattering and polarization properties as a function of snow-pack parameters. An accurate algorithm to retrieve snow wetness, which indicates where and at what rate snow is melting, has been developed and tested using C-band SIR C and JPL AIRSAR data (Figures 3-3a, 3-3b). Thus, accurate information about the spatial and temporal distributions and melting status of snow cover can be provided for hydrological and climatic investigations and operations. Maps of snow-covered area derived from SIR-C/X-SAR and AIRSAR now compare reasonably well (85-90% accuracy) with those derived from visible imagery, which require clear weather and daylight.

For soil moisture, recent advances in remote sensing technology have demonstrated that soil moisture can be measured by a variety of techniques. However, only microwave technology has the ability to quantitatively measure soil moisture under a variety of topographic and vegetation cover conditions, so potentially it could be extended to routine measurements from a satellite system. A number of experiments using sensors mounted in trucks, aircraft, and spacecraft have shown that the moisture within a thin layer of soil, on the order of 5 cm, can be accurately measured for bare soil and thinly vegetated surfaces.

Soil Moisture Remote Sensing

There are two basic microwave approaches that are typically used to measure soil moisture. One is passive (which is based on radiometry) and the other is active and uses radar. Both approaches utilize the large contrast between the dielectric constant of dry soil and water. At L-band, the dielectric constant can vary from about 3 for dry soil to about 20 for wet soil, which can result in a change in emissivity for passive systems from about 0.95 to 0.6 or lower and an increase in the radar backscatter approaching 10 dB. There are also major differences between the two systems in spatial resolution, swath width, data rate, and power requirements. However, almost without exception, the two systems are complementary; that is, strengths in one are matched by weaknesses in the other, and vice versa. The advantages of passive microwave systems include frequent coverage, low data rates, and (relative to active microwave) simpler data processing. The disadvantages include poor resolution. In the

case of the active microwave systems, the advantages include high resolution, but this comes at the expense of higher data rates and more complex processing.

Measurements show that the estimated soil moisture for L-band frequencies correlate best with soil moistures in the top 5 cm of the soil. The sensitivity of active microwave sensors to soil moisture was demonstrated with many ground, airborne, and even some spaceborne experiments (Ulaby and Batlivala, 1976; Ulaby, et al., 1978; Chang et al., 1980; Jackson et al., 1981; Wang et al., 1986; Dobson and Ulaby, 1986; Lin et al., 1994a, b). Even though these experiments have documented the sensitivity of the radar signal to soil moisture, algorithms to invert radar measurements to infer soil moisture (Oh et al., 1992; Dubois et al., 1994) must still be further evaluated over a broader range of conditions.

Difficulties in Soil Moisture Remote Sensing

A significant difficulty in remotely sensing soil moisture, either with active and passive systems, is the effect of target characteristics other than the soil moisture; for example surface roughness, vegetation, and topography. The two most important target properties are surface roughness and those related to the vegetation canopy. Applying a backscattering model, Lin et al., (1994) have studied the sensitivity of radar signals to various land surface parameters; specifically for L-band (1.25 GHz) over a short grass canopy they found that the most important parameter appears to be the surface roughness. In most natural settings, the effect of roughness may be equal or greater than the effect of soil moisture on the radar backscatter. Thus, the soil moisture problem becomes one of determining the roughness effect independently so that a model can be inverted to yield a soil moisture estimate.

Surface Roughness Effects: Improved understanding of surface scattering processes is needed to further our understanding of the role of surface roughness in soil moisture estimation. Thus, theoretical surface backscattering models have been developed for this purpose; namely, the small perturbation model (SPM), the physical optics model (POM) and geometrical optics model (GOM). In a broad sense, the geometrical optics model is best suited for very rough surface, the physical optics model is suitable for surfaces with intermediate scales of roughness, and the small perturbation model is suitable for smooth surfaces. In general, these models have not provided good predictive values in field-scale observed soil moisture, and more research is needed into surface scattering models. Examples of recent work are Fung et al. (1992) and Oh et al. (1992).

The approach adopted by Oh et al. (1992) is based on scattering behavior in limiting cases and on experimental data. They have developed an empirical model in terms of the root mean square (rms) roughness height, the wave number, and the relative dielectric constant. By using this model with multipolarized radar data, the soil moisture content and the surface roughness can be determined. The key to this approach is that the co-polarization ratios (HH/VV) and cross-polarization ratios (HV/VV) which are given explicitly in terms of the roughness and the soil dielectric constant. In more recent work (Dubois et al., 1995), an algorithm was derived that uses L-band HH and VV radar cross sections only to estimate surface roughness and soil moisture. In this case, the algorithm was tested with both airborne and spaceborne SAR data and accuracies of 3–4% absolute was found for surfaces with vegetation that has a normalized difference vegetation index (NDVI) < 0.4. Thus, initial results look promising when applied to bare soil and sparse vegetation. But, current SAR satellite sensors (ERS-1/2 and RADARSAT) are both single-polarization instruments (C-VV and C-HH, respectively), and even when used together cannot provide cross-polarization ratios.

Vegetation Effects: The effect of vegetation is to attenuate the microwave emission from the soil; it also adds to the total radiative flux with its own emission. The degree to which vegetation affects the determination of soil moisture depends upon the wavelength, the mass and water content of vegetation, and the vegetation's structural characteristics as it influences its scattering properties. Thus, with radar the effect of the vegetation canopy adds more complexity to the problem. To infer soil moisture, one must determine the soil roughness effects and the effects of the vegetation canopy, which is a complex inference problem and may not be unique without high temporal resolution data in which only soil moisture is changing. As with the roughness case, the effect of vegetation on the active microwave sensing of soil moisture is greatly dependent upon the instrument incidence angle, frequency, and polarization. The vegetation contains water along and has plant structure. Radar backscatter is sensitive to both of these characteristics (Lin et al., 1994a). Therefore, the radar backscatter from a vegetated surface will have the integrated effect of the vegetation and underlying soil.

Two general approaches have been used to model the volume scattering, the wave approach and the intensity (or radiative transfer) approach. Both approaches have their constraints, especially in dealing with complex vegetation structures. Several groups are involved in research in the area of estimating soil moisture from active microwave data in the presence of vegetation. Few results have been presented or published, however. Saatchi et al. (1994) showed that by using C-band and L-band data, the canopy water content of grasses in the Konza Prairie could be estimated with an accuracy of about 20%, while Lin et al. (1994) reported an accuracy of about 6% when estimating soil moisture over grass covered areas in England.

Assuming that the effects of vegetation could be accounted for in the case of active microwave sensors, and given the fact that the best resolution than could be expected from a spaceborne low frequency radiometer is on the order of tens of kilometers, it is clear that SAR can play an important role in providing remotely sensed surface soil moisture maps. The optimum radar parameters based on the demonstrated algorithms would be a polarimetric L-band radar system with a resolution on the order of 100 m. There is evidence that suggests that inferring soil moisture in vegetated areas would require some higher frequency SAR data, either C-band or X-band. Continued research is needed to help resolve the effectiveness of radar data for soil moisture under different vegetation types and densities. One approach is using multi-temporal data from a satellite platform, which may provide the long term data sets necessary to isolate the fast-changing soil moisture effects from the slowly changing vegetation and roughness effects. Another promising approach is combining the SAR radar measurements with a distributed hydrologic models to infer soil moisture (for example Lin et al., 1994b).

Field Measurements of Soil Moisture

When deciding the usefulness of the remote sensing instruments and the inferred soil moisture estimates, one has to take into account the natural spatial variability of soil moisture. Thus, when estimating the accuracy of a technique, estimated and in situ measured values are typically compared. In this way, areal averages from the remotely sensed data are compared to point measurements, and the natural variation in the measured quantity becomes a very important factor in judging the performance of a given technique.

In most countries, there are a number of in-situ soil moisture measurements taken in support of operational activities related to agriculture. Two examples of such measurements programs are the Illinois State (U.S.) Soil Moisture Program, an 18-site measurement network in operation since 1981; and the long term soil moisture measurements in the former Soviet Union and reported by Vinnikov and Yeserkepova (1991). Typically these measurements are

taken using a neutron probe, Time Domain Reflectivity (TD) instrument, or through labor-intensive techniques such as gravimetric measurements. Also, typically these are made on a three-day, weekly, or longer basis and in some cases (for agricultural experiments) only during the growing season. For example the current Illinois network makes biweekly samples during the growing season and monthly samples at other times; the data reported by Vinnikov and Yeserkepova (1991) were sampled at a monthly time interval.

The in-situ measurements generally provide good definition with depth, usually consisting of measurements every 5 or 10 cm throughout the root zone to depths of one to two meters. Thus, the profile is well defined but there is usually not an extensive spatial sampling to detect soil moisture gradients in the horizontal plane. A number of investigators have looked into the spatial variability of soil properties. Rogowski (1972) found that over a range of soils that the coefficient of variation in the distribution of water content at 15 bars was in the range of 15 to 35%; and for experimental hydraulic conductivity was 5 to 68%. Hawley et al., (1982) investigated the effect of sample volume on estimated soil moisture content. Using a 2m square plot and 10 samples, the estimated CV was in the range of 5% for the three different soil moisture conditions investigated; implying a CV of 15–20% for a single sample, which is consistent with the other similar studies. In addition, they concluded that samples greater than 200g (50 cc) are needed for accurate estimates.

Field scale variability (16 ha, > 40 acres) was evaluated by Bell et al., (1980) using data collected in 57 fields in Arizona, Kansas, and South Dakota. The nominal standard deviation of all the data analyzed was between 2 and 3%, soil moisture. For remote sensing studies, this means that perfect correlations to ground observations are unlikely and that the inherent error due to field-scale variability is of the same order of magnitude as the demonstrated accuracies of the inversion results for both active and passive microwave instruments.

While there are direct uses for the surface soil moistures, a much wider range of research and applications would benefit from an estimate of the profile soil moisture. Although there is still much work to be done in this area, some basic concepts have been proven. Kostov and Jackson (Kostov, 1993) have identified four general approaches: statistical, knowledge-based (a priori information), radiometric inversion, and soil water modeling. Regional profile mapping using a straightforward regression approach was demonstrated in Jackson et al., (1987). Knowledge-based approaches have been used extensively by Reutov and Shutko (1986 and 1990) and also by Jackson (1980). Recent research has focused on a combination of the inversion and modeling approaches (Entekhabi et al., 1994). Each of these approaches needs to be considered in the development of large scale mapping programs because any one in particular may not be compatible due to limitations caused by ancillary data requirements or the temporal and spatial sampling.

Radar Observations for Soil Moisture

SAR satellites offer perhaps the best opportunity to measure soil moisture routinely at regional scales. Currently, the ERS-1 C-band (VV) and JERS-1 L-band SARs are operating, and the Canadian RADARSAT, also C-band (HH), will be launched in mid-1995. Although it is believed that an L-band polarimetric system would be optimal for soil moisture, the preliminary results from the ERS-1 demonstrate its capability as a soil moisture instrument under ideal conditions: bare soil, near saturation, constant roughness. The main drawback to the SAR systems is the lack of existing algorithms for the routine determination of soil moisture. However, through airborne and SIR-C remote sensing experiments, field observations are accumulating for a diverse set of sites. It is hoped that these data are sufficient for developing suitable algorithms. It is critical that these diverse data sets be brought together in a SAR soil moisture data base.

Experimental data sets can be grouped into three classes, of which only one is discussed in this report. These classes are: (i) In-situ operational soil moisture data sets, taken by water resources and agricultural agencies for a variety of reasons. Even though these data sets are important for hydrological research, the lack of simultaneous remote sensing data make these soil moisture measurements of limited value for the development of soil moisture remote sensing algorithms. (ii) Remote sensing experiments with passive microwave sensors. Examples of these include HAPEX-MOBILHY (Hydrologic Atmospheric Pilot Experiment and Modelisation du Bilan Hydrique) program in southern France in 1985; HAPEX-SAHEL in Niger (West Africa) in 1992; and the First ISLSCP Field Experiment (FIFE) in Kansas in 1987. (iii) Remote sensing experiments with SAR and in some cases passive microwave sensors. These experiments include:

Mac-Hydro-90 in the Mahantango catchment (central Pennsylvania) in 1990 which was a multi-sensor campaign (using the DC-8 with the three frequency polarimetric Synthetic Aperture Radar (SAR) ,and the C-130 carrying the PBMR L-band radiometer and the NS001 thematic mapper simulator.

Washita-92, conducted over the Little Washita catchment in Oklahoma in 1992, was another multi-sensor campaign (using the DC-8 with the three frequency polarimetric Synthetic Aperture Radar (SAR), and the C-130 carrying the NS001 thematic mapper simulator, the Thermal Imaging Mapper, the Electronically Steered Thinned Array Radiometer (ESTAR), a 37-GHz radiometer, and a USDA laser profiler.)

Mac-Europe-91, a multi-aircraft campaign DC-8 and EU-2 for remote sensing in Europe during 1991. Soil moisture data were collected at a number of sites including Slapton Wood, Devon, England; Montespertoli, Tuscony, Italy; EFEDA experiment in Spain.

Shuttle Imaging Radar, SIR-C, flights in April and October 1994. There were a number of sites for which radar data were collected for soil moisture studies. These sites included the Little Washita (OK, USA), Mahantango catchment (PA, USA), Alcona (Manitoba, Canada), Zwalm catchment (Belgium), and Montespertoli (Italy).

It is critical that these data be made available to provide algorithm developers a broader range of soil moisture data.

CURRENT AND PLANNED SAR ASSETS AND THEIR USE

Several methods for mapping melting snow-covered regions have been developed and tested using AIRSAR and ERS-1 imagery. Mapping wet snow and glaciers in remote alpine regions using a conventional single-pass, single-polarization SAR imagery requires an accurate Digital Elevation Model (DEM), but analysis of time-series ERS-1 data sets showed significant improvement in mapping accuracy and corresponding decrease in the need for a DEM. However, the capability of a single-polarization SAR to study alpine snow is limited to map wet snow cover only. Furthermore, multi-frequency, multi-polarization SAR can effectively map the extent of wet-snow regions without requiring any topographic information. Numerical simulations show that a similar technique could map dry snow cover; verification is ongoing. Thus, a multi-frequency, polarized SAR provides snow mapping capability from small to large scales. SIR-C/X-SAR also can map firn regions, which indicates the regions of annual snow accumulation or of glacier growth. This capability provides an important tool for mass-balance studies of glaciers.

The most fundamental snow cover property, in terms of water supply forecasting, is the snow-water equivalence: the total amount of water the snow would yield at a point if it

melted. This variable has been traditionally measured at several hundred snow courses throughout the mountainous regions of the western U.S. How to extrapolate these widely dispersed measurements remains a fundamental problem in estimating the total water volume in the mountains. Numerical simulations with multi-frequency, dual-polarization SAR have shown it can monitor the spatial and temporal distributions of snow-water equivalence. Data analysis with SIR-C/X-SAR is ongoing. With accurate estimates of snow-covered area, detection of melting snow, and the measurement of the spatial distribution of snow water equivalence, we will better understand the most fundamental problems in snow hydrology: the spatial and temporal distributions of snow properties in alpine regions.

To derive the maximum benefit in terms of research or application out of remotely sensed soil moisture, the remote sensing data must be integrated into a geographic information system and analyzed taking into account the soil properties and land characteristics. Therefore, the required resolution of the remotely sensed soil moisture data is related to the intended usage and the ancillary data bases available for interpretation. It makes little sense to collect data globally at a resolution much higher than that of the ancillary data. It therefore appears that based on the range of projected applications and the available ancillary data bases that a spatial resolution on the order of 100 m to 200 m may be advantageous for processing and interpretation. It is true that the detail offered in higher resolution SAR data is interesting, however, it does not seem to be really needed except for mapping and other less time critical analyses.

The timing and frequency of observation are very important in the valuation of the remote sensing data for application and analysis. Surface soil moisture is diurnal in nature, generally decreasing during the day and rising slightly at night (in the absence of precipitation). The time of the observation will most certainly be considered in its use. Certain times of the day may offer certain advantages. For instance, to extrapolate a surface observation to the profile using a physically based approach, Jackson (1980) has shown that a predawn observation is advantageous. In fact, late afternoon observations of surface soil moisture using shorter wavelengths may provide little to no information. An improvement in this single observation could be made by utilizing diurnal changes, an a.m. and a p.m. observation. For bare soils this could provide a good estimate of the total surface flux during the day. Frequency of coverage is a much more difficult subject. Of course, this too is dependent on the application. It seems that daily coverage would be of greatest value for all regions. There is a significant sacrifice in increasing this, however, the next plateau would be three days. Observations at lower frequencies might only be of selected value.

Given this sampling requirement and the previous experimental results, it is clear that the currently planned international SARs can provide little beyond change detection for changing moisture conditions and mapping of wet alpine snow cover only.

RECOMMENDATIONS

The recent results indicating that soil moisture and snow water equivalence could indeed be measured accurately with spaceborne multiparameter SARs bring the remote sensing one step closer to providing some important variables to help understand and routinely monitor the hydrologic cycle. However, even though the status of SAR for measuring these quantities is very promising, it is recognized that there are a number of logical steps to be taken in order for the general scientific and public communities to benefit from this research.

Given the previous experimental results, and the recent algorithms derived to infer soil moisture and snow water equivalence, it is clear that single frequency SARs can provide little beyond change detection for changing moisture conditions. It is highly doubtful whether

even the magnitude of the change in the soil moisture could be quantified from these types of single parameter SAR measurements without a significant number of risky assumptions. Therefore, the logical conclusion is that the ultimate goal should certainly be an operational spaceborne multiparameter SAR for routine soil moisture and snow water equivalence mapping. Recognizing that this is not likely to happen soon, we therefore urge the continued support of the NASA multiparameter airborne SAR program as a vehicle to continue the development and validation of soil moisture, snow wetness, and snow water equivalence algorithms in the short term with the long term goal the definition and launch of an operational SAR to monitor these important variables of the hydrologic cycle. Below we outline a few steps we consider necessary to achieve this goal:

(1) Combine all data collected during AIRSAR and SIR-C/X-SAR campaigns and analyze their ability to determine soil moisture empirically (sigma 0 vs. measured soil moisture) and using all available algorithms. Develop statistics to define how large the errors are, what type of errors, and what conditions the analysis or algorithms work or do not work well. Using both US and foreign campaigns should provide data from more than twenty sites and numerous conditions.

(2) Continue a vigorous research program to extend current algorithms to infer soil moisture from vegetated surfaces and to refine the snow water equivalence algorithms. The emphasis should be on well coordinated campaigns involving both active and passive microwave instruments over a variety of different terrain types.

(3) Examine the relationship between surface measurements and profile measurements of soil moisture to evaluate the severity of the problem, if it exists. Data exist to address the following question: How well can the profile moisture be modeled if the surface 5 cm of soil moisture can be measured every 3 days at a precision of $\pm 4\%$ by volume? What are the performances of various models including simple regression models?

(4) Encourage land process modelers (mesoscale, GCM and runoff) to attempt to use measured soil moisture and snow water equivalence from SIR-C/X and AIRSAR campaigns in their modeling.

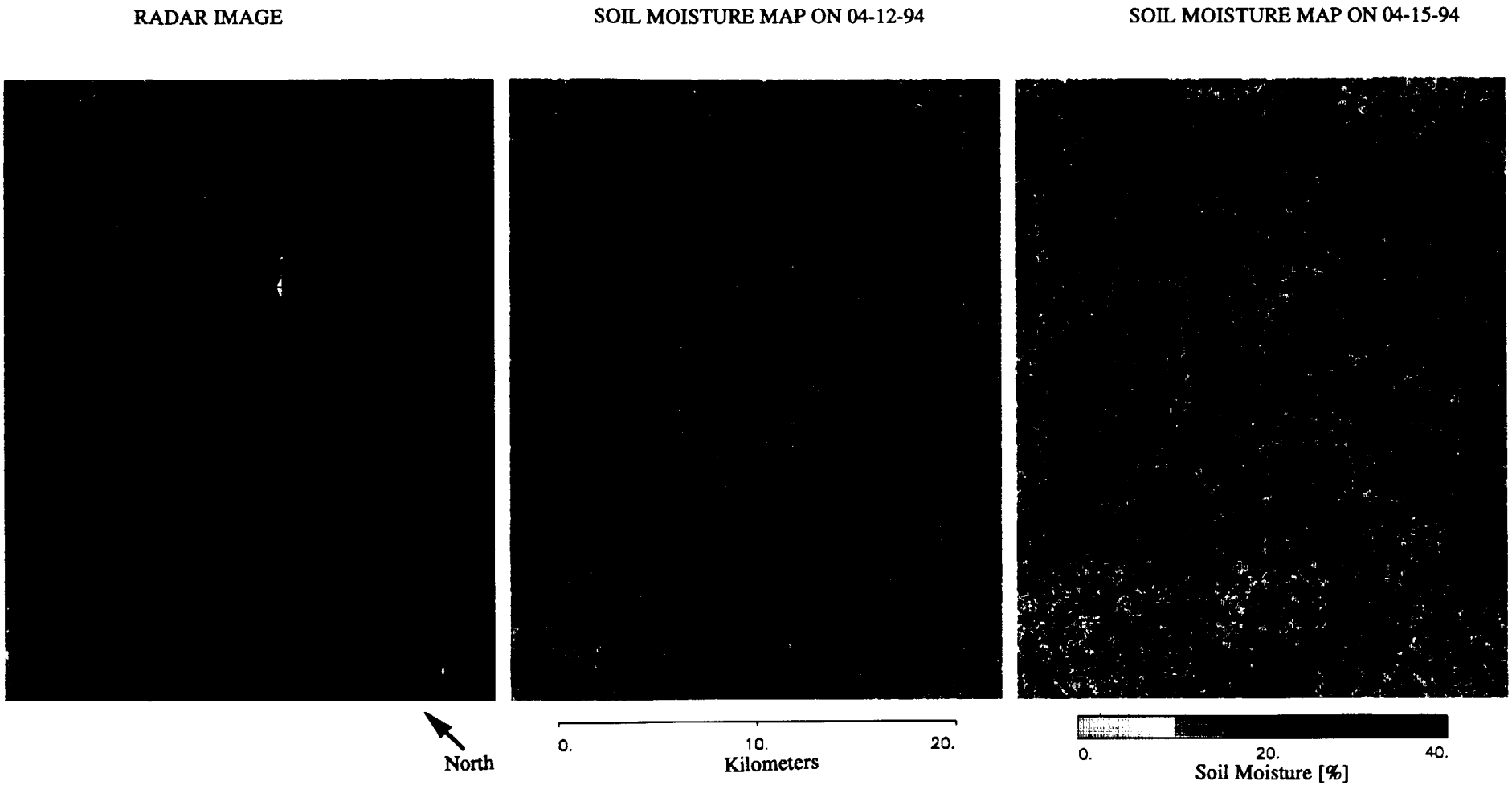

Figure 3-1. L-Band HH image and two soil moisture maps of Chickasha, Oklahoma derived from SIR-C data for April 12, 1994 and April 15, 1994. The first day was extremely wet and the second day was drier (from Dubois et al., 1995).

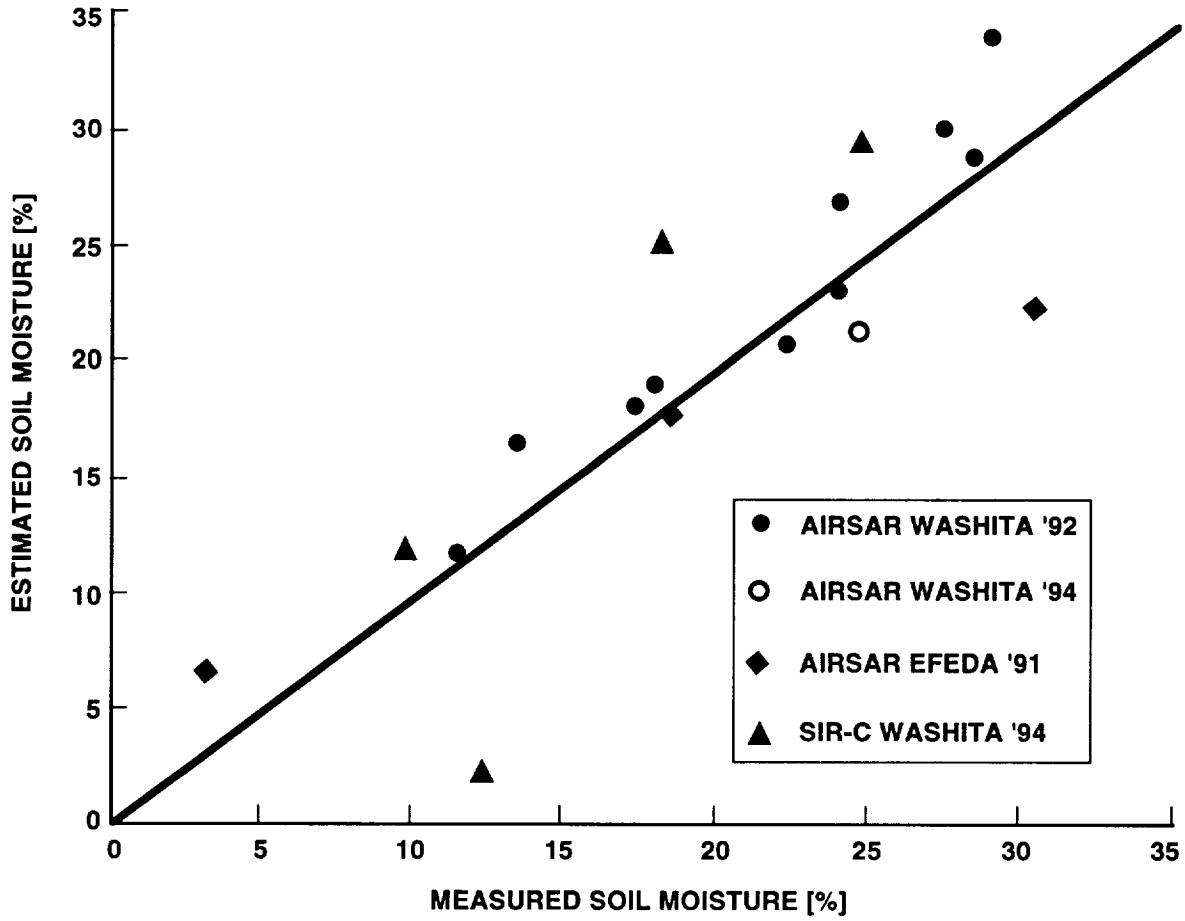

Figure 3-2. Radar estimated soil moisture versus measured soil moisture for the different active microwave data sets where both radar data and in-situ soil moisture measurements were available. The overall RMS error is 3.5% (from Dubois et al., 1995).

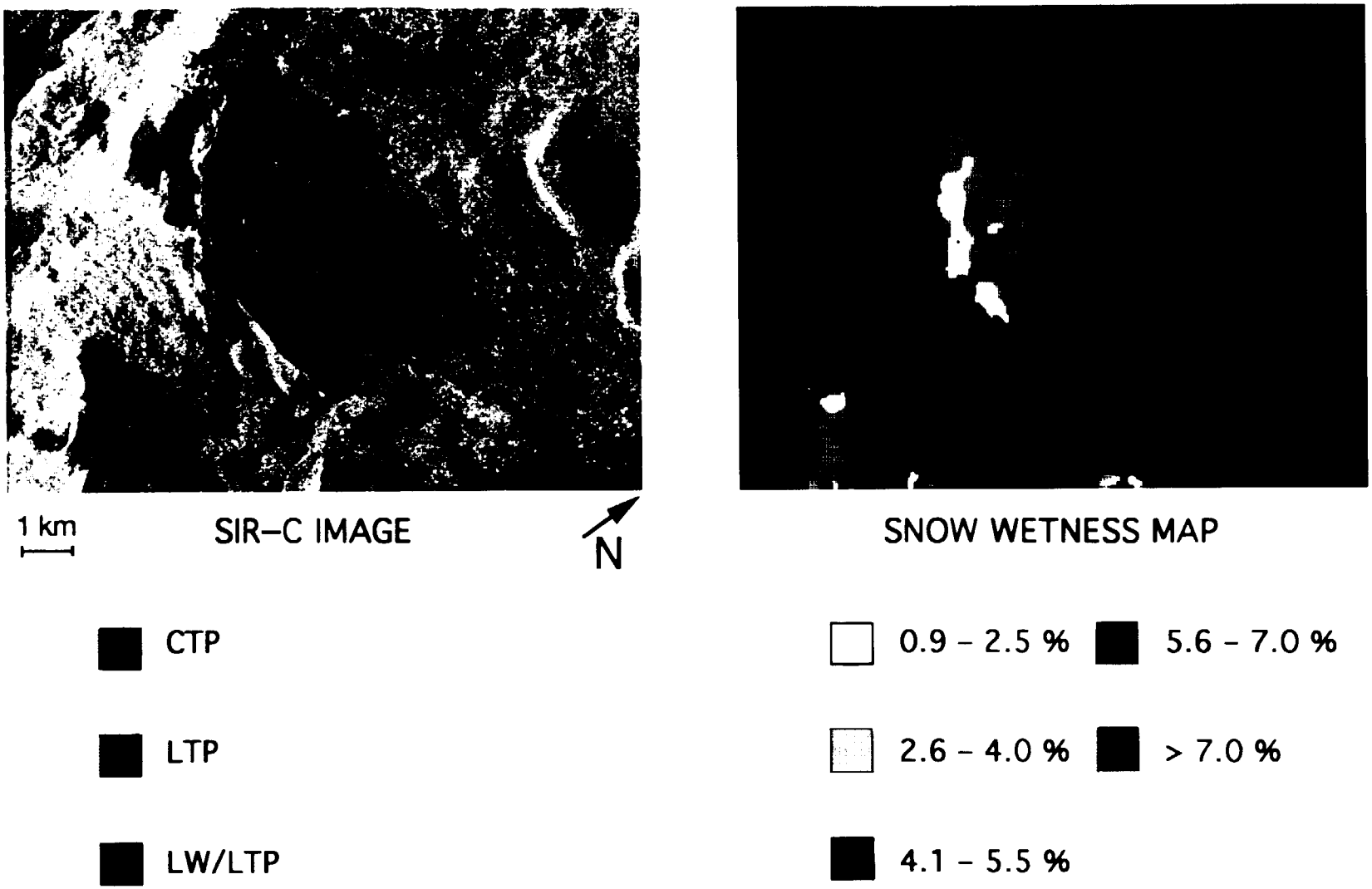

Figure 3-3. a) SIR-C C-band image of Mammoth Mountain, California taken on April 11, 1994 and snow wetness map derived from the data Image is 23 kilometers by 45 kilometers (from Shi and Dozier, 1995).

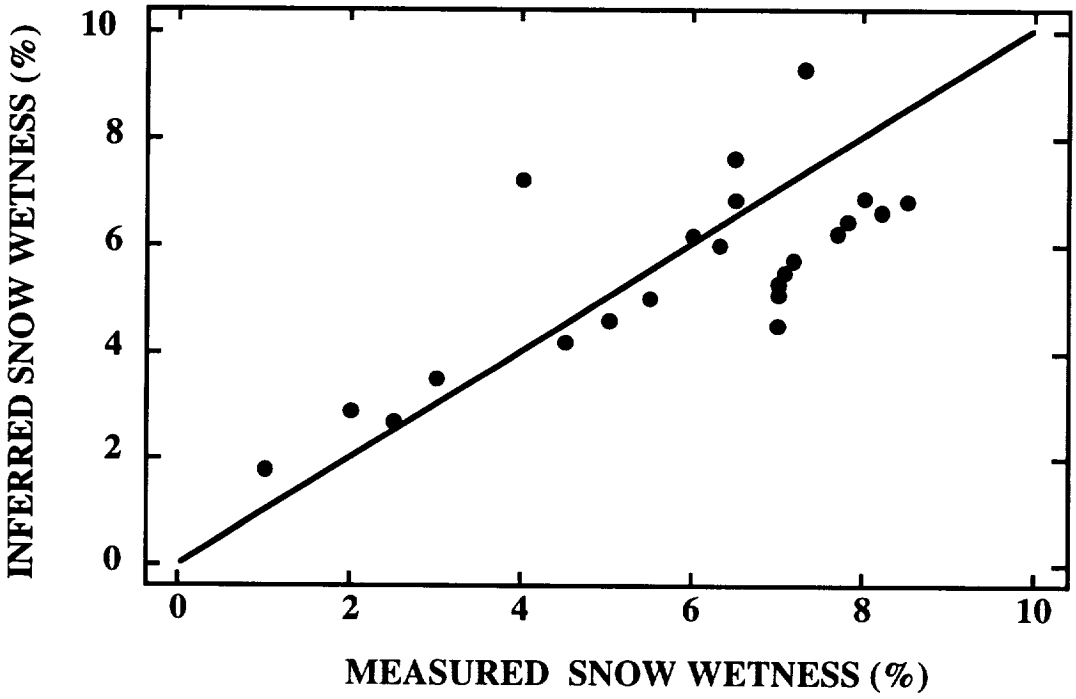

Figure 3-3. b) Comparison of ground measurements with SAR-derived snow wetness (from Shi and Dozier, 1995).

4—Marine Science and Applications

INTRODUCTION

Synthetic aperture radar images of the ocean surface very often reveal a remarkable range of signatures inscribed on the uppermost layers of the sea. These telltale variations in surface roughness can be interpreted in terms of geophysical and geochemical processes occurring on or near the surface of the sea. When used collectively with (a) adequate theories of radar surface scattering, and (b) an understanding of the underlying hydrospheric, atmospheric or cryospheric dynamics, these images offer unparalleled and indeed otherwise unattainable quantitative data on the marine environment, data that are relevant to important questions in Earth science and marine operations.

This chapter presents a summary of scientific achievements in ocean and ice research, and lays out the potential for further advances based on research to date. It develops a rationale for a vigorous, continuing program that is firmly grounded in past achievements and in new, interesting, and relevant developments in SAR technology, hydrodynamics and scattering theory. The chapter develops the scientific basis for an ongoing NASA SAR program during the next decade, and sets forth a prioritized sequence of space flights with advanced instruments, along with a program of supporting research utilizing data from space-based and aircraft-based SARs. The program keeps governmental agency requirements for space-based data firmly in view.

BACKGROUND

Synthetic aperture radar was first flown on Seasat; launched in 1978, it carried among other sensors an L-band SAR that yielded stunning day/night, all-weather views of the Earth, its oceans and its ice cover. This mission set into motion a number of follow-on spaceflight programs by the former USSR, the European Space Agency, Japan, and Canada, as well as secondary efforts in airborne SAR by several other nations; in addition, the US has flown short, widely spaced flights of Shuttle Imaging Radars A, B, and C in addition to airborne systems.

These data have resulted in a series of quantitative scientific findings and theoretical advances in upper-ocean and lower atmosphere dynamics and in polar ice studies. Many papers have been published in the scientific and engineering literature, references to the most seminal of which are cited here as examples of the progress. New findings that derive from the ongoing space-based SARs continue to be reported, especially from ERS-1, which provides unparalleled global, continuing data coverage.

The strong view of the scientific community working on these problems is that current single-channel, space-based SARs are yielding only a fraction of the information available from more advanced multifrequency, multipolarization, and multi-aperture configurations. Fascinating glimpses of this have been provided by the SIR-C/X SAR, as well as from aircraft instruments, especially the AIRSAR on the NASA DC-8. An example of prime importance is the potential for measuring ocean surface current velocities on scales ranging from estuarine/coastal to the ocean basins, using the along-track interferometric mode of SAR - the ATISAR. Such a capability would represent a revolutionary advance in the understanding of ocean dynamics, and would provide the missing dimension to large-scale currents derived from radar altimeter measurements.

If properly enhanced capabilities can be realized in a spaced-based configuration, the data on wind stress, current velocities, mesoscale current distributions, sea-ice thickness, air-sea interchange, and similar phenomena entering into the coupled ocean/atmosphere/ice system will be extremely valuable in meeting objectives of Mission to Planet Earth. The data must be blended with other space and surface-derived information and assimilated into numerical models or used to understand physical and chemical processes that can be parametrically incorporated into such models.

Scientific Objectives

A national SAR program for oceans and ice can be formulated considering the concerns of present-day ocean and atmospheric science, the history of past achievements in SAR ocean observations, the state of development of ocean backscatter and hydrodynamic theory, and the recent instrument advances in SAR engineering. The prime objective of a SAR program for the ocean is the determination of surface currents for information on mesoscale phenomena as related to climate modeling, surfactant dispersal and transport, coastal dynamics, marine biology, and lateral fluxes at the ice margin. As will be discussed below, this capability of surface-current determination is still the subject of intense development and experimentation. Secondary objectives for SAR applications include improved surface fluxes of ice-covered seas, determination of fine-scale wind fields (especially in the coastal regime), surveillance of surface films and slicks, and monitoring of surface and internal gravity waves. In the operational community, SAR data over the coastal ocean are additionally seen as a crucially needed tool in three general areas: regulatory functions (compliance monitoring and enforcement); warning of potential threats to life, environmental quality, property and commercial operations; and post-event measurement of impact and responses. The primary applications include search and rescue, fisheries management, monitoring of coastline and bathymetry changes, and ship detection and routing. In most of these areas of science and operations, further development is called for prior to the routine generation of data products.

Observational Results

In some senses, the fractal-like surface of the sea and its overlying cover of ice are simple, especially in terms of topography, composition, and texture. Because of this, it has been possible to arrive at a reasonable understanding of several important oceanic processes, notably internal wave dynamics, surfactant properties, and wave spectra, by using SAR imagery in conjunction with in-situ data and theoretical hydrodynamics. In many cases, considerable success has been achieved; in others, provocative but incomplete results have been obtained; more work is clearly called for.

Beyond the microphysical level, however, SAR has made significant contributions to the disciplines of open-sea and coastal oceanography, marine boundary layer meteorology, and sea ice dynamics. The morphology of the patterns, together with an understanding of backscatter variations, allow one to deduce information on a wide range of oceanic and cryospheric phenomena. For example, extremely valuable data have been obtained on surface and internal waves, fronts, eddies, variations in bottom topography/bathymetry, upwellings, small-scale and mesoscale currents, rainfall variations, surface wind speed and stress, atmospheric convection, sea ice motions, marginal ice-zone processes, ice age, leads, polynyas, vessel wakes, surfactant/oil distributions, and a variety of other processes that give rise to subtle variations in surface roughness detectable by SAR. There are consequent polarization, frequency, and incidence angle sensitivities that must be considered in assessing the specific oceanographic value of SAR data.

Theoretical Developments

Theoretical approaches to SAR interpretation use quantitative analysis from electromagnetics, liquid-state physics, hydrodynamics, scattering from random media, and signal processing to interpret the imagery as two-dimensional field measurements, not simply as patterns on the surface of the sea or the ice. A few examples of theoretical developments will illustrate the advance of oceanographic SAR technology beyond simple geographical image analysis. The transmitted radar signal is characterized by its amplitude, frequency, phase, polarization, and incidence angle, and the received signal will contain information on the properties of the scattering target that are sensitive to those quantities and their modulations or variations. Initially, through the stimulus of surface wave imaging, polarimetric radar scattering theory advanced significantly; early views were that specular-point scatter governs at small incidence angles, while Bragg scatter is the mechanism of scatter at larger angles. Now more complete (but yet not adequate) theories suggest a mixture of both processes occurs. Such studies, together with observational results, suggest that SAR can observe changes in the ocean wave spectrum at the Bragg wavelength as small as a few percent. SAR imaging theory has thus helped to clarify the virtues and shortcomings of SAR as a surface wave spectrum analyzer. Detailed studies have been performed of the SAR Doppler spectrum of waves and the potential of along-track interferometry for measuring surface currents. In surface hydrodynamics, the influences of currents and their gradients on the surface waves have been advanced, as have theories for surface wave/wave interactions and surface wave/internal wave interactions. Models of nonlinear soliton dynamics have been applied to internal solitary waves in the sea with good agreement obtained between theory and data from SAR images and in-situ observations. In ice studies, the application of ice dynamics, rheological theory, and models of multicomponent dielectrics to ice detection and motion have aided the understanding of sea ice.

ROLE OF SAR

From the previous discussions, it is clear that SAR has significant capability for observing ocean processes. We will indicate the types of observations that can be made by dividing the discussion along the lines of: Open Ocean, Coastal Ocean and Marine Operations, Marine Boundary Layer Meteorology, and Polar Oceans, together with added comments on Applications. Examples of SAR imagery and analysis are presented to illustrate results; these images are only representative and are not necessarily major developments in and by themselves. The priorities of the NASA Mission to Planet Earth are implicitly assumed here, for which issues of Global and Regional Change are paramount. Many of these relate directly to climate change, since the ocean is a major component of the climate engine.

Open Ocean

(1) **Surface Waves.** The open ocean process that has been best studied by SAR are long surface waves, their spatial spectra, and their refraction patterns (Pierson, 1965). The SAR image fidelity depends on the altitude and velocity of the platform. A low-altitude spacecraft (300 km or less) such as SIR-C/X-SAR allows direct computation of wave spectra, including those traveling in the direction of spacecraft velocity (Beal et al., 1983; 1986). At altitudes of typical polar-orbiters (such as ERS-1), sophisticated corrections are needed. Wave observations in the Southern Oceans from SIR-C/X-SAR are shown in Figure 4-1, along with a comparison of their speed and direction obtained from (a) an on-board processor/spectrum analyzer, and (b) the US Navy's Wave

Analysis Model (WAM) (Monaldo and Beal, 1994). Satisfactory agreement is obtained in most cases, and the remaining differences are likely more due to forecast error than to SAR errors. Long-term observations of ocean wave spectra could allow studies of exchange of momentum between atmosphere and ocean, especially during storm conditions. In addition, wave refraction by large-scale current systems such as the Gulf Stream is readily observed in high-resolution images, and provides estimates of the current speed under some conditions. In the future, a dedicated, low-drag, low-flying SAR could be implemented that would yield valuable operational information on long-wave spectra to forecasting agencies. Such a system is a candidate for a small spacecraft (MacArthur, 1987).

(2) **Mesoscale Currents.** At the scale of the internal Rossby radius of deformation, 10-40 km, the ocean mesoscale, important interactions between the planetary boundary layer, the ocean mixed layer and quasi-geostrophic oceanic dynamics occur. These interactions control meridional fluxes of heat, global circulation, internal variations in ocean-atmosphere, and other critical processes. The boundaries of oceanic mesoscale systems are imaged by SAR as discontinuities at the current boundaries and as streak lines within the current system. When used in conjunction with infrared imagers such as AVHRR, a synergism is realized that increases the mapping capabilities of both sensors. Mesoscale features include western and eastern boundary currents, rings, eddies, fronts, equatorial waves, upwellings, and similar features. These fluctuations, e.g., Gulf Stream rings, transport large amounts of heat and momentum, and as such are important processes in the general circulation of the ocean. They are also key links of biological ocean processes (Schumacher et al, 1991). Figure 4-2 shows multifrequency AIRSAR images of the California Current, a typical mesoscale boundary current along the eastern edge of the Pacific Ocean. The three images were made at P, L, and C-bands and show significantly different information. As in other applications, the SARs all-weather capability is a major asset in observing regions of the sea covered by persistent clouds or fog, as is often the case in this region of California. The deployment of an along-track interferometric SAR would make possible line-of-sight surface current velocities which will be exceedingly valuable in understanding these phenomena. Such measurements strongly complement and augment the radar altimeter's measurements (e.g., TOPEX/POSEIDON) of time-varying geostrophic currents by providing a quantitative determination of the surface current, not just the geostrophic portion; these current measurements would also resolve small-scale processes as they would operate at much higher resolution than the altimeter. An example is shown on the left of Figure 4-3, which illustrates two SAR current-velocity maps of the Gulf Stream made from the NASA AIRSAR operating in its along-track interferometric mode, taken during the recent ONR High-Res Experiment (Thompson et al., 1994) and color coded as to east (upper) and north (lower) components of velocity. Superimposed on these are red current vectors determined by a Doppler hf radar system on shore. A comparison of the current-velocities measured by the well-established Doppler hf system and the SAR velocities (scatter diagrams on the right side of Figure 4-3), argues that the SAR is measuring open-ocean surface currents with good fidelity, although problems remain with establishing the zeroes of Doppler shift (Thompson and Jensen, 1993). In the deep sea, much spatial and temporal averaging is possible, which would enhance the accuracy of the data. Assuming that open-ocean surface current velocities can ultimately be determined satisfactorily from space-based SAR, the combination of SAR and IR imagers, radar altimeters, and in-situ observations beneath the surface will allow the oceanic component of fluxes of heat and momentum and their variations to be well determined. Such measurements would contribute strongly to the objectives of Mission to Planet Earth.

(3) **Surface Wind Speed/Stress.** The SAR is actually an imaging scatterometer, and one that is radiometrically calibrated can be used to determine scalar wind speed via absolute backscatter measurements. However, such measurements are contaminated by surfactants, upwellings, etc., (as are wind-scatterometer measurements) so that ancillary information is required. Surface wind stress, waves, and surface currents are related, but in a complicated, nonlocal fashion. Low resolution and wide swath observations, similar to those for currents in the open ocean, are required for the winds, with the required resolutions being finer than the scales of frontal systems and storm gradients at sea. These would complement the coarse-scale winds (10–50 km) obtained from wind scatterometers.

(4) **Open-Ocean Internal Waves.** Large solitary waves are generated by flows over topographic features, generally but not exclusively near shore, and are known to propagate for hundreds of kilometers in the open ocean. They contribute unknown amounts to the global internal wave spectrum. High-resolution SAR images of such waves in the deep sea have been obtained, but are rare, and more data are needed for survey purposes (Rufenach et al., 1985). If the ATISAR is implemented in a high-resolution mode, the surface currents can be used in a model to obtain the underwater amplitude and current fields. In addition, deep bathymetric features such as mid-ocean ridges and seamounts are suspected to be sources of open-ocean signatures, including internal waves. Russian work suggests that topography as deep as 5000 m may have surface expression through formation of a "Taylor-cone;" similar features are speculated to occur in convective regions of the ocean (Carsey and Garwood, 1993)

Coastal Oceans and Marine Operations

Although coastal oceans and estuaries comprise about 10% of the Earth's surface, they produce about 25% of global biomass production. In the coming decades, the effects of global change and human activities will be especially pronounced in the coastal zone "where measurements are difficult to make and processes difficult to model because of the many more factors that influence the system, compared to the open ocean." (OSB, 1992, p.107), and cross-shelf exchange processes are poorly understood. Here the spatial scales vary from tens of meters to kilometers and temporal scales from tens of minutes to a few days (Liu et al., 1994a). Surface forcing by winds and waves drive vertical mixing throughout much of the water column, depending on season and geography, and ice can play a unique role (Liu et al., 1994b). High-resolution surface current and wind speed observations from the ATISAR would be especially valuable here; in a recent review (Flemming, 1995) operational users listed surface currents and sea surface temperature fields to be the two most valuable ocean data products of those discussed for development. Figures 4-4 (a) and 4-4 (b) respectively show a Seasat L-band SAR scene taken southeast of Nantucket, Mass., in July 1978, and a Skylab Ektachrome photograph of the same region taken several years earlier; both of these display many signatures of features that typify those in coastal oceans; the image will be used as an example for this discussion.

(1) **Underwater Topography.** The medium and fine-scale bathymetry of the region is mirrored in surface roughness variations caused by tidal flow and associated wave spectral changes over shallow areas. A comparison of the lighter patterns from bottom-reflected light in the photograph with the roughness variations in the SAR image demonstrates that underwater shoals having depths from perhaps 5 to 50 m are imaged with SAR via surface roughness and radar backscatter variations. There is a successful quantitative theory for this process that uses a Boltzmann-like equation to describe the changes to the surface wave spectrum that lead to the signatures.

(2) **Upwelling and Air-Sea Interaction.** The pumping up of colder subsurface water to the surface shows up in this image as a smoother (lower backscatter) area east of Nantucket, the "Nantucket Upwelling," well known to local fishermen and sailors. Reduced sensible and latent fluxes over the colder water because of lowered air-sea temperature differences is accompanied by reduced atmospheric turbulence levels, and thus less roughness in the regions of the cooler ocean contacting the atmosphere. In VV polarization, such a pattern would appear similar to this HH-image under stable air/sea conditions; however, under unstable conditions, the polarizations would differ significantly, thereby identifying areas of strong evaporation.

(3) **Internal Waves.** To the east of Nantucket is a region of quasiperiodic oscillations that are surface signatures of internal waves, or propagating underwater motions supported by density gradients. They are generated by tidal flow over Georges Bank to the east through complex nonlinear processes. Such a phenomenon is better illustrated by Figure 4-5, which is an ERS-1 C-band/VV SAR image of the ocean near the Hudson Canyon southeast of New York; the bathymetric contours are shown in red. The packets of quasiperiodic oscillations are internal solitary waves, or solitons, generated by tidal flow near the edge of the continental shelf break (the region of highest gradient of bathymetry). Each semidiurnal tidal cycle (approximately 12 h) during the spring, summer, and fall, the tidal currents flowing offshore produce a depression of the upper layers of the sea that quickly develop into nonlinear oscillations. As these solitons propagate, the larger waves travel faster than the smaller ones, and there is a sorting of the waves by amplitude and hence wavelength. Figure 4-5 presents a history of seven packets generated by the previous 3 days of tidal action. The lifetimes of the solitons are of order 1 to 2 days. When they break inshore, they resuspend bottom sediments, thus adding nutrients to the water column, greatly enhancing biological productivity, and altering the optical opacity of the water column significantly.

(4) **Soloy.** This Russian word describes combined upwelling and mixing caused by flow against a topographic feature. Figure 4-6 (a) is an S-band/HH image from the Russian spacecraft Almaz-1, made on July 5, 1991 off the west coast of Ireland. The soloy is occurring at an indentation in the continental shelf and is the source of internal waves seen at the upper left. Figure 4-6 (b) is a simultaneous NASA/AIRSAR image at P, L, and C-bands/VV, taken along the swath shown in Figure 4-6 (a); the lowest frame is a color-composite of the three frequencies.

(5) **Coastal Wave Refraction.** Surface waves in water of approximately one-half their wavelength feel the effects of the bottom and undergo refraction, focusing/ amplification, and defocusing/diminution. For example, in the New York Bight, storm waves arriving from the east impact the shorelines of New Jersey and Long Island quite differently. The wave refraction patterns must be observed during the storm in order to understand the effects correctly, and this only can be provided by SAR on aircraft or spacecraft.

(6) **Shoreline Changes.** Storm damage to coastlines and loss of land due to sea level rise are significant issues in a milieu of global change. The SARs ability to image through clouds and storms makes it a valuable instrument for observations during storms (Zhang et al., 1994).

(7) **Coastal Watch.** Repeated SAR observations on the scale of Figures 4-4 a and 4-5 will allow monitoring of coastal and estuarine waters for a variety of information. Essentially any process leading to a change in radar backscatter of a few percent can be observed under normal wind conditions. Here multiparameter SARs may be of even more importance for detecting subtle changes in the coastal environment.

(8) **Surfactant Monitoring.** Detection of natural and man-made slicks on the sea is crucial to the protection of the environment and the enforcement of regulations. In order to demonstrate the signatures of various types of oils and other surfactants such as oleic acids, a controlled release of oils and surfactants in the North Sea was made recently by German scientists and imaged by SIR-C/X; the slicks are readily detectable and appear as regions of variously reduced backscatter (Wahl et al., 1993; True et al., 1994; Wismann et al., 1993).

(9) **Monitoring of Shipping and Search and Rescue.** Ships and ship wakes are often detectable in SAR images (Griffin et al, 1992; Fu and Holt, 1992), and the line-of-sight velocity of the vessels can be estimated from their Doppler shifts. Wakes include both the invariant 39° Kelvin wake, and in stratified water, occasionally an internal wave wake. Figure 4-7 is a summertime ERS-1 image of a large vessel in the Skagaarak off Sweden, and shows a long, asymmetrical internal wave wake. Monitoring of vessels in the US Exclusive Economic Zone (EEZ) via hard echoes and wake detection is a possibility, although 100% detection probability is not assured. Similarly, support of search-and-rescue operations is feasible via SAR or real-aperture radar (RAR) on aircraft.

(10) **Fisheries Support.** Wind-driven offshore transport and turbulent mixing have important effects on the larval survival and subsequent recruitment of many fish species (Bakun and Parish, 1982). Space-based SAR can locate current boundaries, fronts (Grabak et al., 1994), convergence zones, eddies, and ice fields, all of which influence commercially-important fish populations (Burns et al., 1981).

The addition of a current-measuring mode to a future SAR system would enlarge the suite of environmental data significantly and greatly enhance the information available for change management and regulatory enforcement as well as an increased value to science. Prediction of coastal currents via numerical models that are tuned and initialized by current measurements of all types (especially including SAR) is a capability that is highly desirable. Obtaining a two-dimensional realization of surface current velocities would add greatly to the efficacy of marine forecasts, fish stock assessment (Fiedler et al., 1984), vessel drift, search-and-rescue, and similar items requiring a knowledge of surface drifts.

Information from the combination of an advanced SAR, an ocean color scanner, and a thermal-infrared scanner will be of much relevance to science and applications in coastal waters. There, spatial scales vary from tens of meters to tens of kilometers, and, in shallow depths, the surface signatures visible in imaging devices are connected more closely with subsurface conditions than is the case in the deep ocean. Thus the SAR for coastal oceanography needs high resolution (25 m) and a narrower swath (100 km) than its open-ocean equivalent. It also needs more frequent revisit times. These requirements argue for a US receiving station in the contiguous 48 states having real-time processing and analysis capabilities for the present-day SAR systems.

Marine Boundary Layer Meteorology

In both the open and coastal oceans, various atmospheric signatures, usually due to wind stress and its gradients, are seen with varying sensitivities. It should be cautioned that these investigations are recent and are not yet fully established capabilities. The realization that SAR shows atmospheric effects is only now being appreciated and still ill-understood. The subject is an important area of investigation in the SAR program proposed ahead.

(1) **Surface Wind Stress.** One prospect is the quantitative measurement of surface wind stress by the SAR (see Gerling, 1986; Shuchman et al., 1994; Wackerman et al., 1994), where backscatter observations may be interpreted as with a wind scatterometer. The development of a scatterometric SAR is in its infancy but the promise clearly exists. An example of such effects is shown in Figure 4-8 (Alpers, pri. comm., 1994), which is an ERS-1 C-band image of the Straits of Messina between Italy and Sicily made late at night. One observes katabatic or drainage winds flowing down mountain valleys and out to the sea. Also visible are long, periodic signatures paralleling the coast that are thought to be eddies, internal waves, and atmospheric roll vortices of some type. These atmospheric processes are being imaged via differential roughness at the short Bragg wavelengths of the ocean surface wave spectrum. A number of similar atmospheric processes have been investigated in SAR data (Vachon, 1994; Pri. Comm., W. Alpers and G. Stilke paper submitted to *J. Geophys. Res.*, "Observation of an undular bore in the marine atmosphere by the synthetic aperture radar aboard the ERS-1 satellite.")

(2) **Atmospheric Convection.** In real aperture radar (RAR) imagery taken at Ku/VV (15 GHz) frequencies, atmospheric convective cells are made manifest via the variations of surface wind stress that they cause at the surface. Figure 4-9 shows simultaneous HH (Panels 1 and 3) and VV (Panels 2 and 4) RAR images from the Russian Toros aircraft radar; vertically polarized images show atmospheric stress variations due to the convective cells, while horizontally polarized images show internal wave strain rates. Larger incidence angles favor the imaging of such features. The differences between such dual polarized images allow one to identify regions of atmospheric convection over the ocean. It may even be possible, using data from multiparameter SARs, to make estimates of the evaporative flux occurring in such unstable regions. Such measurements would be of first-order importance to atmospheric dynamics on the time scales of both weather and climate. Direct space-derived estimates of evaporative flux observations are not currently part of Mission to Planet Earth.

(3) **Rain Rates.** The X-band system on the SIR-C/X-SAR radar has recently observed what appear to be rainfall patterns. While not yet quantified, the promise of high-resolution measurement of tropical rain rates is clear. In studies of the ENSO (El Niño-Southern Oscillation) phenomenon and short-term climate variability, the determination of realistic rainfall rates (which are measures of the release of the latent heat of evaporation to the atmosphere) is paramount to the parameterization of numerical models of the coupled ocean-atmosphere system. Cloudiness and rain in the tropics are sub-grid processes about which much remains unknown. Their importance was reaffirmed in the recent Tropical Ocean Global Atmosphere/Coupled Ocean-Atmosphere Response Experiment (TOGA/COARE) campaign.

(4) **Rain Patterns.** In addition to rain rate measurements, it is known that SAR can image rainfall patterns on the sea surface via (a) damping of Bragg scatterers in the region of heavy rain, which leads to a "rain-free hole" and (b) the increased stress of atmospheric winds in the region of downdrafts and outflows from local rain storms, which shows up as a larger area of increased backscatter. It is possible that local wind speeds can also be inferred from the backscatter variations within the storm footprint. Again, these observations are of small scale but of large importance to climate studies.

The realization that SAR shows atmospheric effects is recent and still not well-understood. The area is an important one to investigate in future SAR programs.

Polar Oceans

In the polar oceans, the fluxes of heat, momentum, mass, and salt that result from air-sea-ice interactions play fundamental roles in the global climate system (Aagaard and Carmack, 1995; Maykut, 1986; Stouffer et al., 1989). The dynamics and thickness of the sea ice cover are the key elements of these fluxes. Ice motion controls the distribution of thin ice and therefore surface exchange processes dependent on ice thickness, including heat flux to the atmosphere, ice production, and the associated salinity production in the polar oceans. As ice thickens by growth and deformation, the turbulent heat exchange between the ice-covered ocean and the atmosphere is reduced. Detailed time-series measurements of ice motion and thickness from satellite sensors are essential in providing estimates of these fluxes.

(1) **Fluxes.** At present, heat and salt fluxes may be estimated using repeated SAR data for ice motion, radiative fluxes estimated by other means, and modeled air temperatures and winds. These approaches parameterize ice thickness changes, which are notoriously difficult to measure (Bourke and McLaren, 1992) and essentially assume that the sea is at its freezing temperature. While such an assumption is valid in the wintertime Arctic, it is known to be significantly in error in the marginal seas and in much of the Southern Ocean surrounding Antarctica. The estimation of surface fluxes and the response of the upper ocean is also important at the ice margin (Carsey and Roach, 1994)

For areas in which there are significant oceanic fluxes, a direct measurement of ice thickness over time is the optimal approach for deriving heat and salinity transport. There are good indications that ice thicknesses of less than 100 cm can be estimated using the like-channels (HH and VV) of a polarimetric L-Band SAR (see Drinkwater et al., 1992), as shown in Figure 4-10 (Winebrenner et al., 1995). Copolar phases ranging from -50° to $+30^\circ$ have been observed in ice of differing apparent thickness; such values span both lower-than-expected values for thick ice and higher-than-expected values for open water. A model has been developed that explains these variations, and it has considerable potential for robustly estimating sea ice thickness using magnitudes and phases of SAR data; cross-polarized data are not required. Field validation and time-series data are needed to diagnose both the polarimetric and the ice growth models, in order to estimate ice growth over time. This work is of great importance for accurate estimates of surface fluxes in polar regions, where intermediate and deep water-mass formation takes place. For the short-term, surface fluxes relying on repeated coverage of single-channel SAR is the only solution; in future, a polarimetric L-band SAR system to directly measure ice thickness changes is highly desirable.

(3) **Ice Dynamics.** Ice motion is a key variable for predicting ocean-ice fluxes. During the last several years, maps of the vector motions of Arctic sea ice have been automatically generated from SAR data by the ASF (Kwok et al., 1992; Holt et al., 1992). The ice-motion algorithm identifies the same sea ice features seen in pairs of SAR images taken three or more days apart and then derives their absolute motion relative to a fixed geographical grid. Ice motion vector maps have been made of several regions of the Arctic and Antarctic Oceans, with the densest coverage being over the Beaufort/Chukchi Seas extending over a period of greater than two years. Ice motion maps have been used to examine lead dynamics (Stern et al., 1994), oceanic circulation in the Arctic Ocean and the Weddell Sea (Kwok and Colony, 1994), and ice fluxes through the Fram Strait (Schweiger and Rothrock, 1994). The RADARSAT Geophysical Processor System (RGPS) is being developed to monitor ice motion, to determine ice age, and to infer ice growth rates and surface fluxes for the Arctic Ocean, the marginal ice zone, and its adjoining seas (Kwok et al., 1994). This technology is

useful and well-developed, and should be continued and enhanced with SAR data to come.

(5) **Monitoring and Prediction of Iceberg Motion.** Airborne and spaceborne SAR systems are useful for monitoring icebergs, but the detectability of icebergs depends on many factors such as the SAR system characteristics (e.g., frequency, signal-to-noise ratio, incidence angle, and polarization), as well as the physical characteristics of the iceberg (i.e., size and shape) and environmental characteristics (e.g., sea state). Studies have shown that higher-frequency SAR instruments provide greater radar return from icebergs. Additionally, a cross-polarized SAR system can be used to enhance the contrast between icebergs and the oceanic background.

(6) **Sea and Lake Ice Coverage.** Experience with ERS-1 has demonstrated the utility of SAR for analysis and forecasting of sea and lake ice. Ice parameters obtainable from this SAR include concentration, age, location of leads and polynyas, and ridge location and density. Research into SAR imaging suggests that in the future, multipolarization/ multifrequency SAR measurements will allow acquisition of (1) improved ice-type and ice concentration data during the spring, when melt processes complicate the interpretation of simple SAR imagery (Onstott, 1992; Fetterer et al., 1994), and (2) improved discrimination between open water, new ice, and first-year ice (Steffen and Heinrichs, 1994).

CURRENT AND PLANNED SAR ASSETS AND THEIR USE

From the viewpoint of either a research or an operational program, the existence of ongoing, continuous flights is essential. However, the other side of such a commitment is that technical capabilities, especially sensors, advance only slowly in such programs. Almost all of the SARs on recent spacecraft (excepting SIR and the two Russian SARs) are single polarization, single channel devices. Therefore the opportunity to perform the kinds of sophisticated analyses of SAR imagery that have been suggested above will be quite limited. Thus, while the extra-U.S. programs will provide useful, continuing data, the diversity of the channels, and hence the information derivable from them, is quite limited. Repeat data at 3 to 5-day intervals from near-term systems are required to track and monitor ocean mesoscale and ice features for operational programs such as Coastal Watch, for tracking of storms and icebergs, and for fisheries monitoring.

The analysis of SAR capabilities and ongoing programs above clearly points to an important role that NASA should play in the future—as developer and operator of advanced, multiparameter synthetic aperture radars that use the data as measurements, rather than just as backscatter maps of the oceans and sea ice. Furthermore, it will be important for both oceanic and polar science to have the sensors in high-inclination orbits, preferably near-polar, so that high-latitude processes may be observed. The orbit should be prograde so as to precess through the day/night cycle as rapidly as possible, to avoid aliasing diurnal effects into seasonal ones.

A review of the requirements given earlier suggest that the following future SAR configurations would serve a large percentage of the research and operational needs of the Nation (Table 4-1).

Thus this future program posits two distinct types of missions, one having modes with both high and low resolution, each with an along-track interferometric SAR capability; and one with a single channel looking both left and right.

A significant amount of research and development needs to be undertaken before the ATISAR can be exploited with confidence; on the other hand, the SpectraSat technology has been proven, and a program could be launched with little further development.

RECOMMENDATIONS

It is clear from the above discussion that SAR observations are highly valuable to the ocean and ice sciences, as well as serving numerous operational requirements. Very good data have been obtained on surface and internal waves, coastal ocean processes, variations in bottom topography/bathymetry, upwellings, small-scale and mesoscale currents, rainfall variations, surface wind speed and stress, atmospheric convection, sea ice cover, marginal ice-zone processes, ice age, leads, polynyas, vessel wakes, surfactant/oil distributions, and a variety of other processes leading to subtle variations in surface roughness. Many of these observations are unique to SAR; others take advantage of the operation of SAR under conditions of cloud cover and nighttime. SAR data to support scientific analysis, algorithm development, and process modeling are now acquired from international satellites, airborne systems, and SIR-C/X-SAR. However, additional exciting scientific prospects are in the early stages of development; of special scientific and applications interest is the determination of surface currents in the open sea and in the coastal zone using along-track interferometry. Such a capability would be of utmost importance in understanding ocean circulation. Commercial and applications interests that may be served include: wave and marine weather forecasting, Gulf Stream nowcasting, ship routing, ship and surfactant and slick surveillance in the EEZ, fish stock assessment, coastal monitoring, iceberg warning, and sea ice cover.

Specific recommendations are:

(1) Continue with and significantly strengthen the U.S. research and development program in SAR oceanic/atmospheric/polar science and applications. The promise of SAR in these areas is considerable and needs proper support to yield a return to the nation that is appropriate to its investment in SAR programs to date. A vigorous airborne SAR program with the AIRSAR is needed to support multiparameter SAR sensor development investigations using multifrequency, polarimetric, interferometric data, and to serve as a test-bed for advanced concepts in SAR observations.

(2) Undertake a three-satellite program with a polar orbiting ATISAR, a SIR-C/X-SAR free-flyer, and a SpectraSat being the major program elements. The AIRSAR is needed throughout the program as a developmental platform and as a source of scientific verification and studies. These programs will ultimately produce along-track interferometric data over the oceans of first-order importance to Mission to Planet Earth, to Global Change objectives, and to operational agencies.

(3) Provide improved access by U.S. scientists to the SAR available from international programs. These data sets are known to be quite good in topics such as sea ice and mesoscale features. In addition, cooperation with foreign space agencies in science activities and even in joint flight programs should be sought; for example, Russian Federation boosters are capable of injecting the SIR-C/X-SAR free-flyer into the medium altitude polar orbit desired.

(4) Maintain close cooperation with NASA and other government agencies having appreciable marine responsibilities. These include NOAA, Navy, NSF, USGS, EPA, Coast Guard, and Army Corps of Engineers. Other-agency support was highly valuable during the evolution of Landsat and Seasat.

(5) Develop, in concert with a larger community of scientists, a more detailed scientific program plan for use of SAR, in a fashion similar to the NASA space physics and astronomy/astrophysics programs several years ago.

(6) Blend the requirements for use of SAR in oceans/atmospheres/ice with those from the other Earth science disciplines to arrive at a specification for a spacecraft program that serves a broad range of needs in Earth science and applications. Reports to date show significant commonality of both sensors and spacecraft.

Table 4-1. Future SAR Configurations for Ocean and Ice

1. ATISAR: Ocean Currents, Winds, Features, Sea Ice Thickness, Coastal Processes	
Frequency/polarization:	L- and C-bands, simultaneous HH and VV
Incidence angle:	20-45°
Modes:	(a) high-resolution (20 m), narrow swath (100 km), interferometric (b) low-resolution (500–1000 m), wide swath (500 km), interferometric
Interferometer characteristics:	two along-track antennas on one C-band channel, separated by < 50 m; fore-and-aft looks for vector currents; a coarse resolution, wide swath mode using data averaging for open-ocean currents, fine resolution, narrow swath mode for coastal oceans
Orbit:	low-Earth, near 90°, non-sun-synchronous, prograde
2. SpectraSat: Ocean Wave Spectrometer	
Frequency/polarization:	C, HH
Incidence Angle:	±25°
Mode:	left and right looking antennas; small-scene sampling, highest resolution, on-board spectral analysis
Orbit:	275 km, near 60°, sun-synchronous, prograde; orbit maintenance needed.

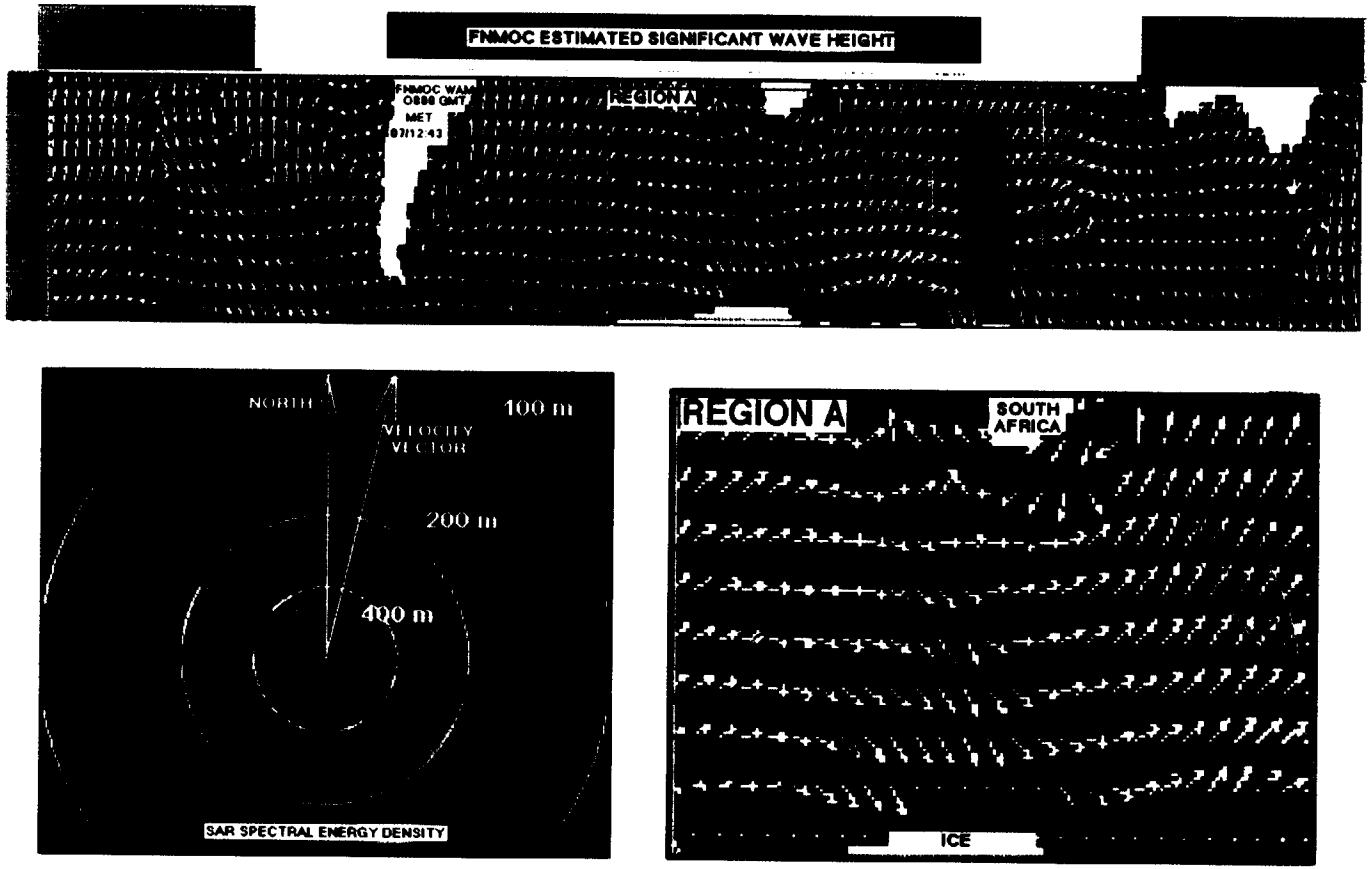

Figure 4-1. Upper panel: SIR-C/X ocean surface wave vectors (orange arrows) derived from the on-board real-time processor for the Southern Oceans from 30° S to 60° S, compared with wave vectors (white arrows) and wave heights (color codes) from the U.S. Navey Wave Analysis Model; continents are in white. Lower right panel: Detail of region between Africa and Antartica. Lower left panel: Wave vector spectrum at geographical point shown. Good agreement is obtained between SAR waves and the numerical forecast (Robert Beal).

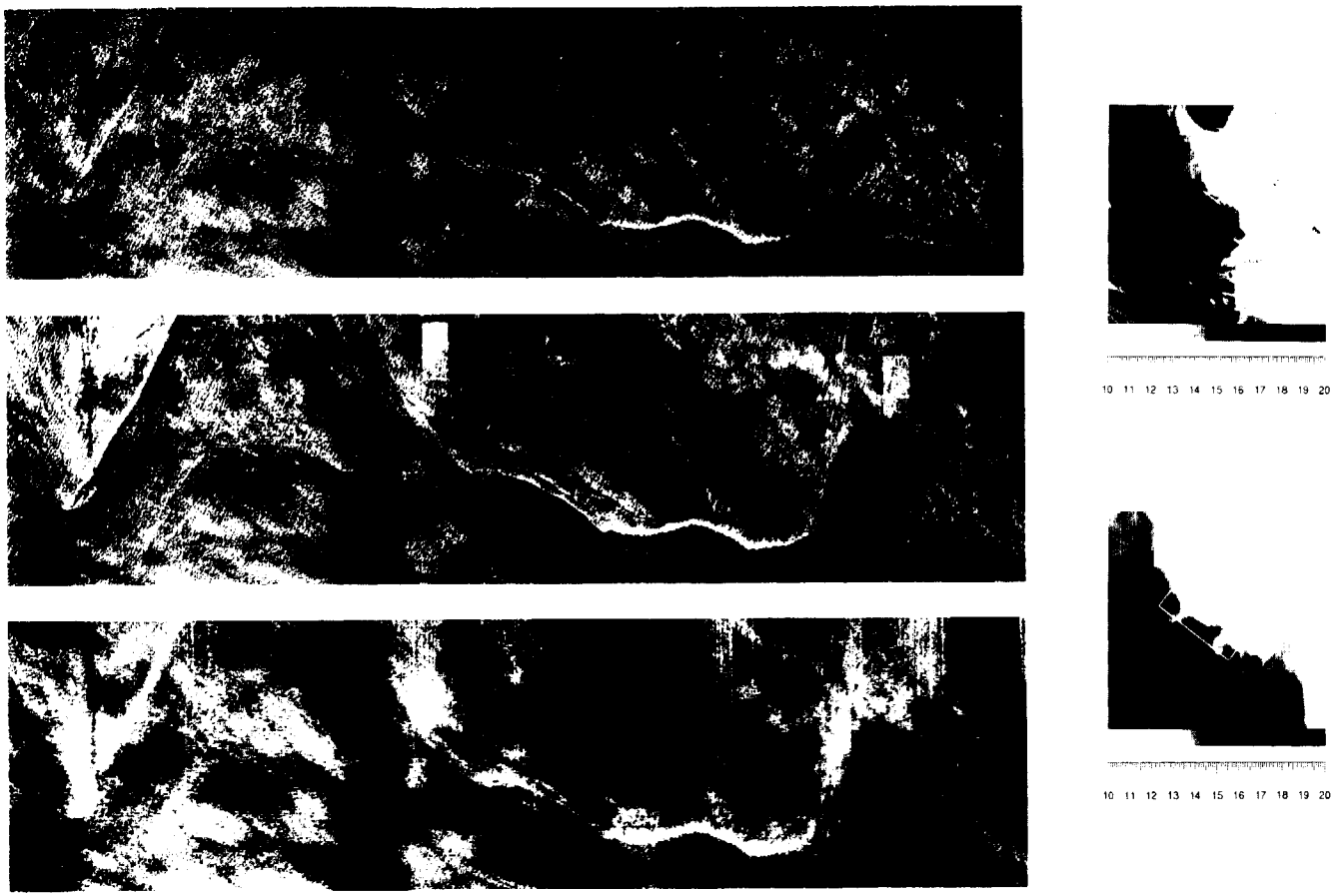

Figure 4-2. These images of the California Current were acquired on September 8, 1989 at about 1900 UTC by the AIRSAR aboard NASA's DC-8 aircraft at C-band (top), L-band (middle), and P-band (bottom). The aircraft was heading towards 128°, from left to right on the images, at an altitude of 8300 m. The area shown, centered near 40°N and 126°W, is approximately 4 km with a resolution of 6 m. In summer, the California Current is characterized by intense jets carrying cold water from nearshore upwelling towards offshore; they appear as cold filaments in the AVHRR image of sea surface temperature taken on 7 September at 1330 UTC (top right panel). These jets are delimited by sharp thermal and velocity fronts, which are often convergent, and are subject to small scale instabilities, as seen in the enlarged infrared image (bottom right panel). The signatures of the fronts are seen as dark and bright delineations in the radar images. The fronts are visible when wind waves and swell are undergoing refraction by the current shear, (resulting in increased amplitude), and when the waves are damped by the biological films concentrated in the convergence zones. The distribution of delineations gives information on the dynamics of the upwelling jets not obtainable by other means. Note the differences in returns for each SAR wavelength, due to the varying length scales of the frequency - dependent scattering.

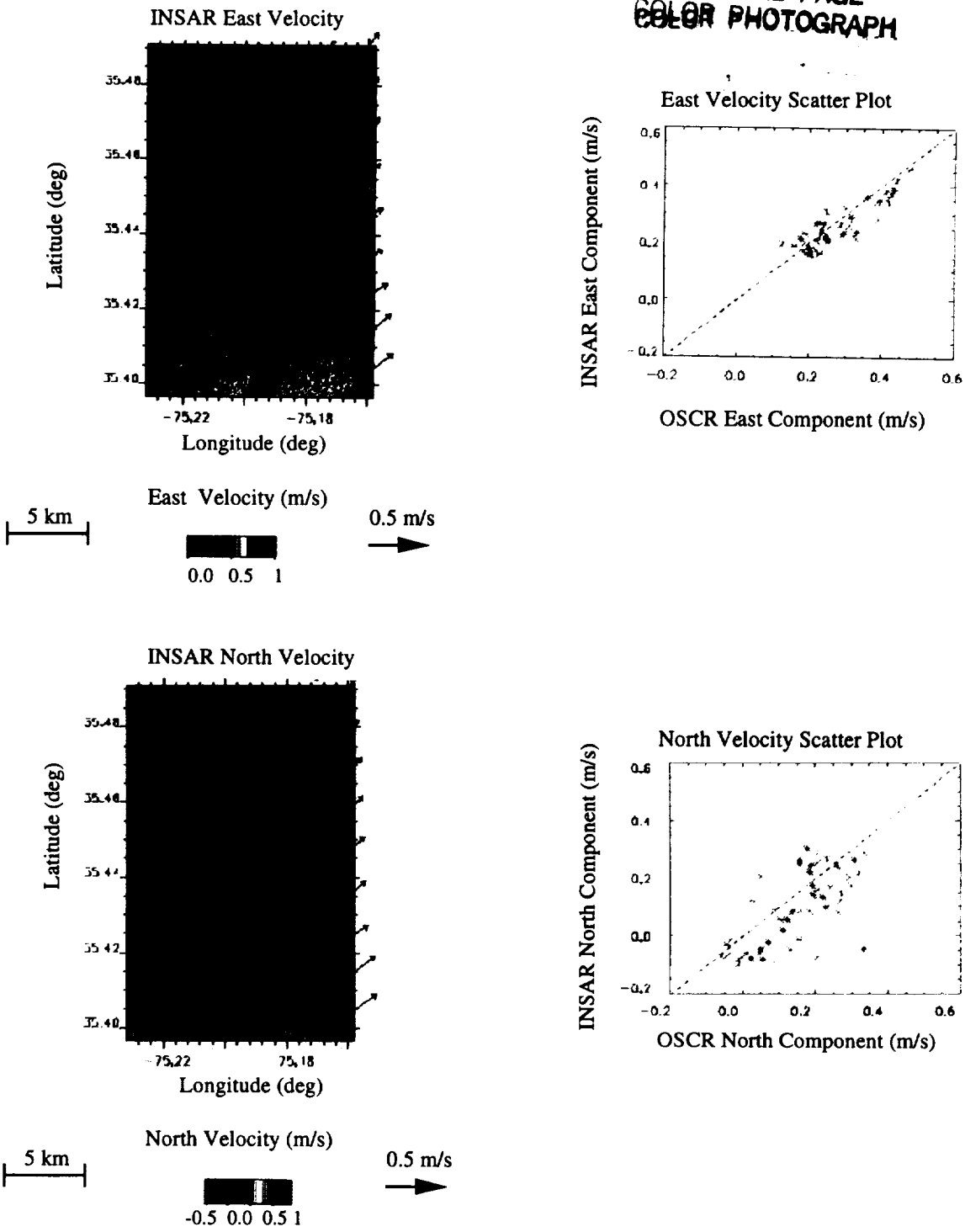

Figure 4-3. The color images at the top and bottom of the figure show, respectively, the east and north velocity components inferred from AIRSAR measurements off Cape Hatteras near the Gulf Stream. These measurements were collected from the NASA DC-8 AIRSAR during the ONR High-Res experiment, on June 20, 1993, and are separated in time by about 35 minutes. The red arrows in the images show the surface velocity fields as measured by an HF radar system operated during High-Res by the University of Miami. The scatter plots to the right of each image show a comparison of the HF current components with those from the corresponding AIRSAR measurements smoothed over roughly 1 km to match the resolution of the HF radar system.

Figure 4-4. a) *Seasat* L-band SAR image of the ocean near Nantucket Island, showing bathymetric signatures, upwelling, and internal waves (John Apel).

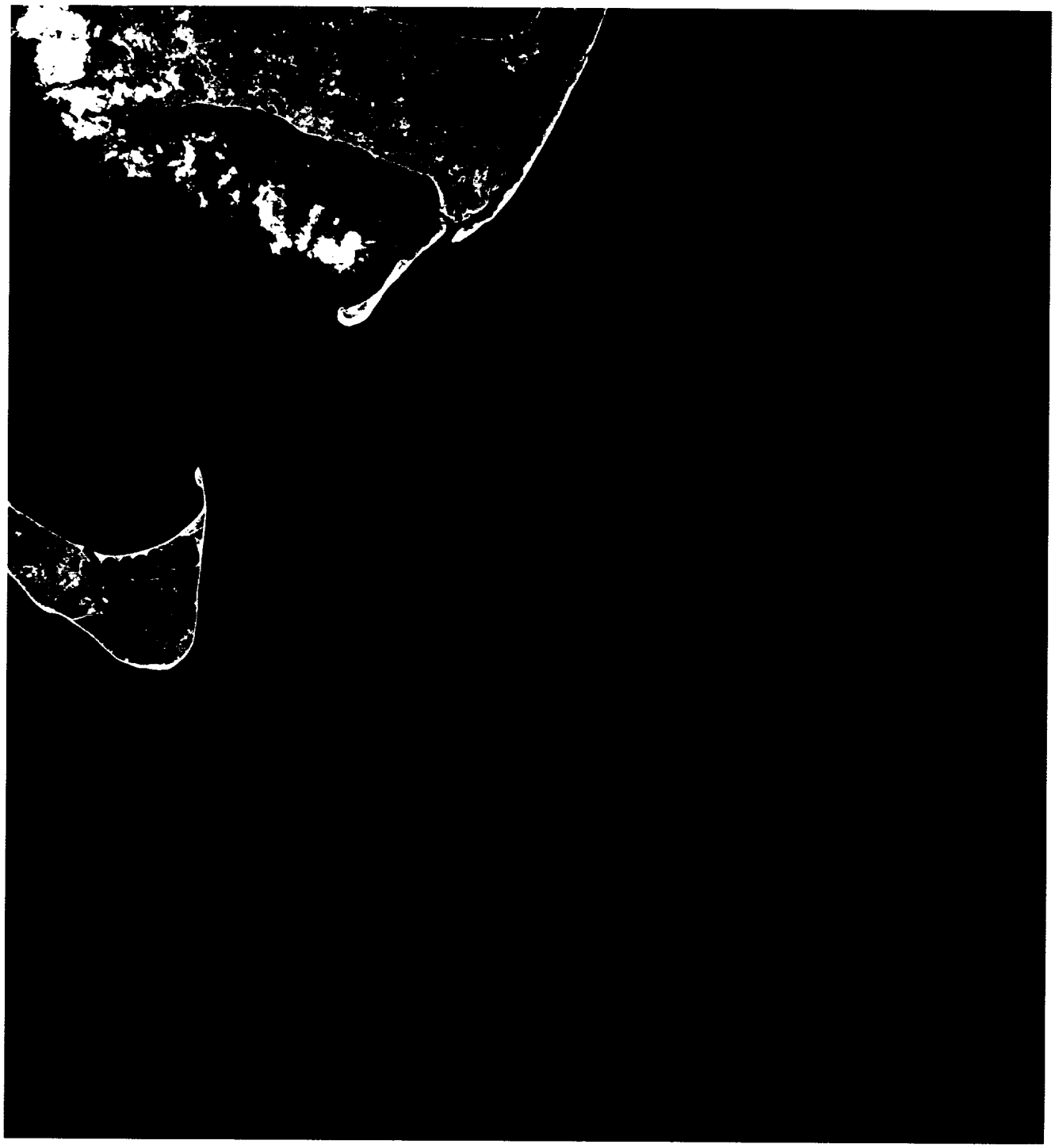

Figure 4-4. b) Skylab image of the same region made several years before 4-4 (a), showing white shoal regions that match the bathymetry and SAR backscatter variations very accurately (John Apel).

ERS-1 SAR ORBIT 5266-3 18 JULY 1992 15:34:35 DEPTH CONTOURS - METERS

Figure 4-5. ERS-1 C-band image of solitary waves generated by tidal flow against the continental shelf, with bathymetry shown in red; the deep indentation is the Hudson Canyon. Region shown is approximately 50 n mi (93 km) on a side (Ricky Chapman).

Figure 4-6. a) Image of the ocean west of Ireland made by the Soviet spacecraft *Almaz-1* with its S-band/HH SAR on July 5, 1991, showing a region of tidally induced updwelling and internal wave generation at the edge of the continental shelf. The dark regions are thought to be cool, stable areas of upwelled water, called in Russion "Soloy." Horizontal strip was simultaneously underflown by the NASA/JPL *AIRSAR* (Valentin Etkin).

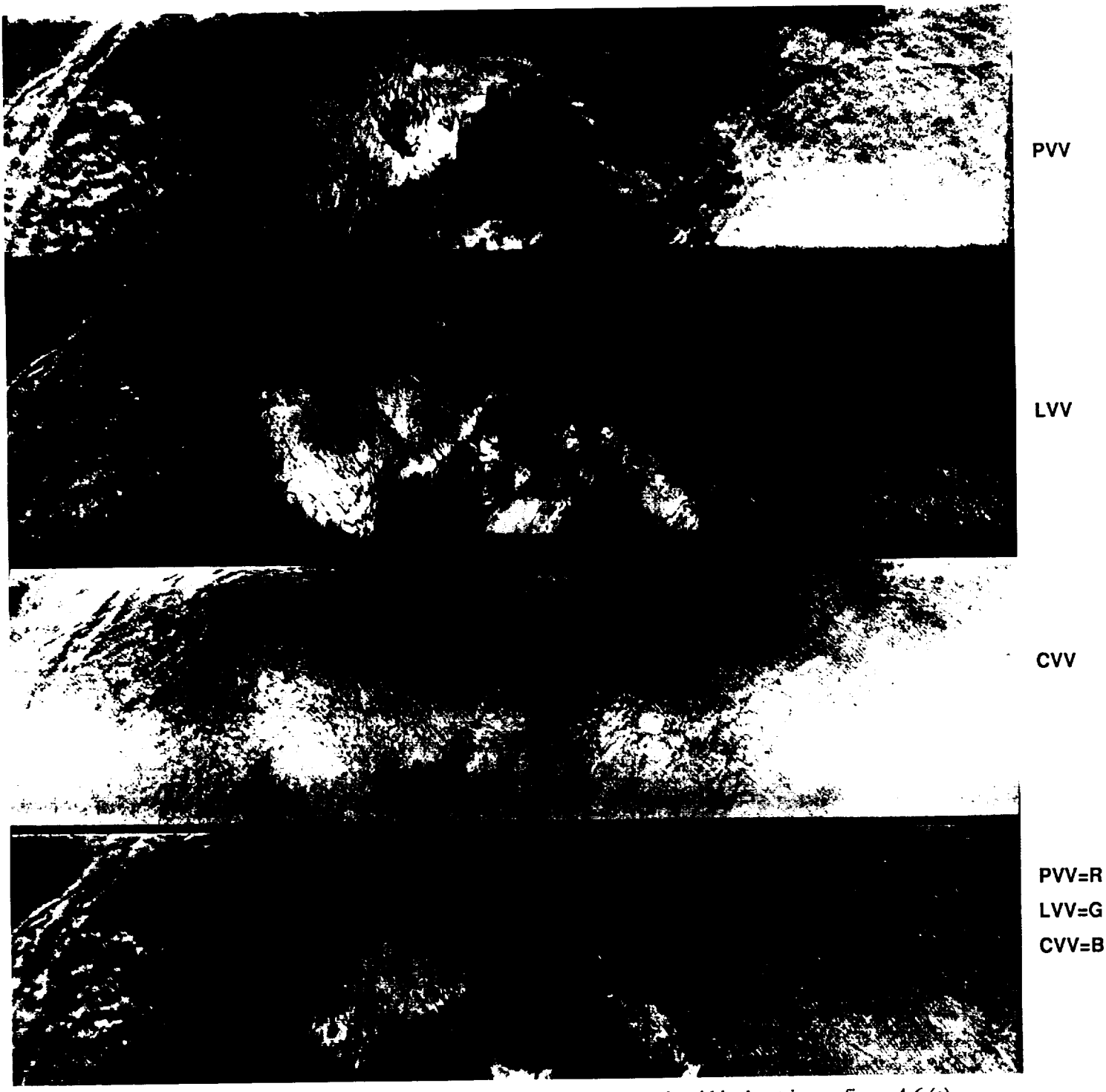

Figure 4-6. b) AIRSAR images at P, L, and C-bands/VV of the area made within the stripe on figure 4-6 (a). Significant differences exist between the AIRSAR images that relate to the surface roughness variations over the upwelling; these occur because what is "rough" at a short radar wavelength is often "smooth" at longer lengths -- the Rayleigh criterion for a rough surface. Radar crossection reduction at C-band is in excess of 7 dB. The surface wind speed was uniformly 5 m/s throughout the entire region shown, thus illustrating the effects of air-sea interation on radar backscatter (Richard Carande). PVV = Red, LVV = Green, CVV = Blue.

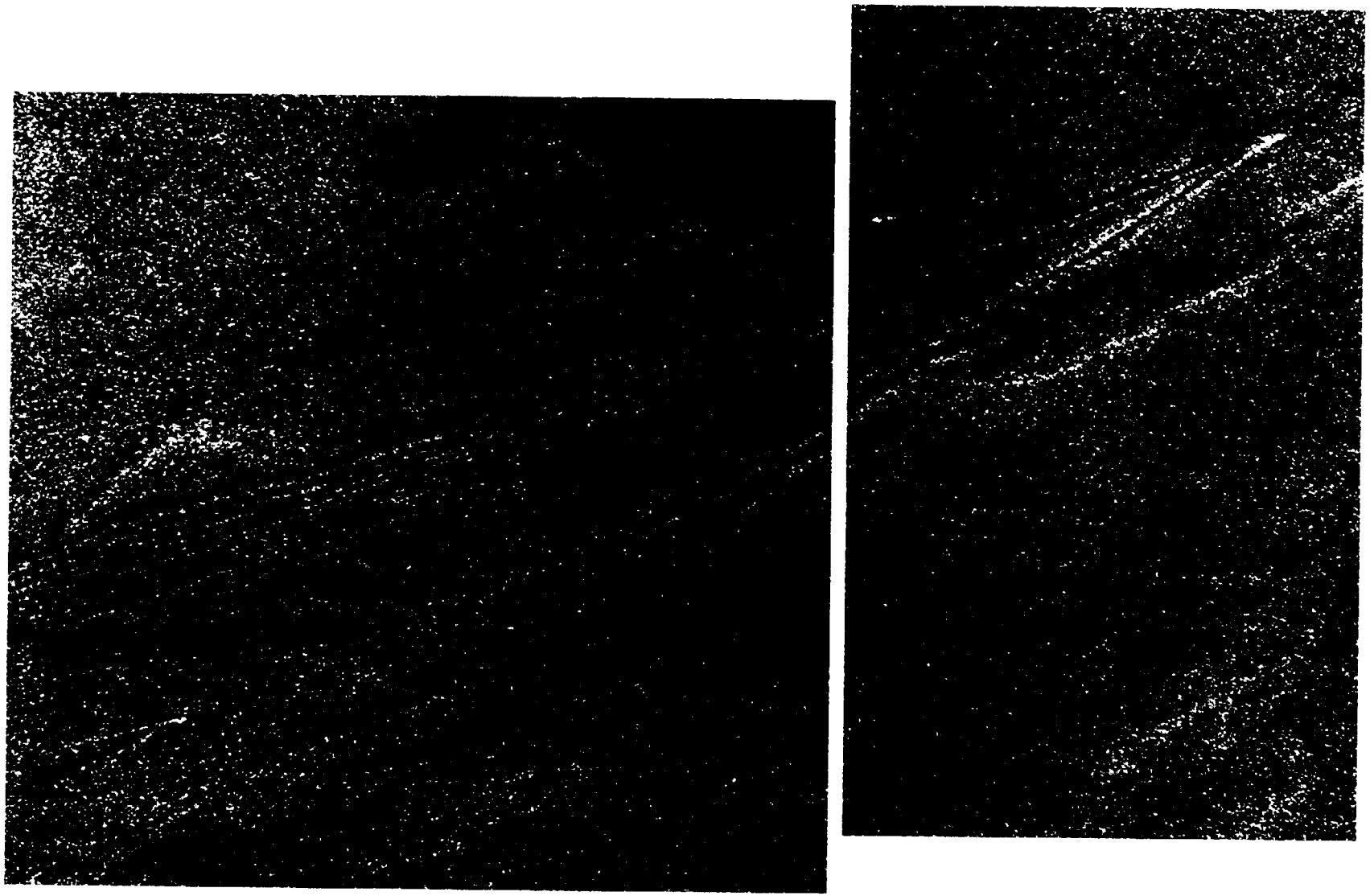

Figure 4-7. *ERS-1* C-band image of a large vessel in the Skagerrak off Sweden, made on 5 August 1991, and showing an internal wave wake over 40 km long. The narrow vee differentiates the internal wake from the 39° surface Kelvin wake (figure courtesy of Norwegian Defense Research Establishment; © ESA/EURIMAGE/TSS/Spacetec, 1991).

Figure 4-8. *ERS-1* C-band/VV image of the Straits of Messina between Italy and Sicily made during the late night. Katabatic or drainage winds are observed flowing down mountain valleys and out to the sea. Also visible are long, periodic signatures that are thought to be eddies, internal waves, and atmospheric roll vortices of some type. These atmospheric processes are being imaged via differential roughness at the short Bragg wavelengths of the ocean surface wave spectrum (Werner Alpers).

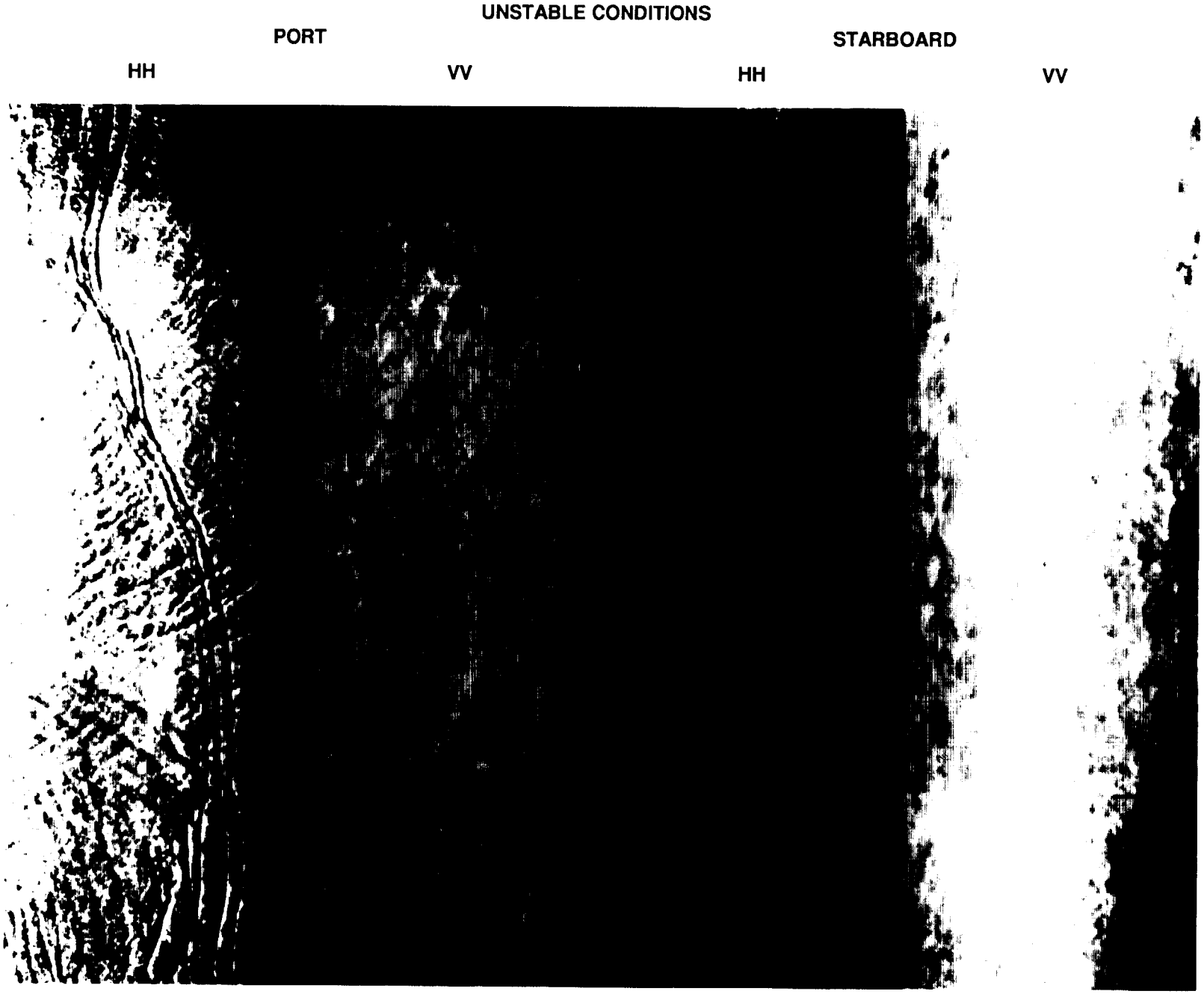

Figure 4-9. Simultaneous images of the ocean surface from a Russian *Toros* real aperture radar operating at 15 GHz near 60° incidence angle; port and starboard pairs of images are shown. For port side: Leftmost image is at HH-polarization, next is VV. For starboard side: third is HH; rightmost is VV. Strongly unstable air-sea conditions existed (Valentin Etkin).

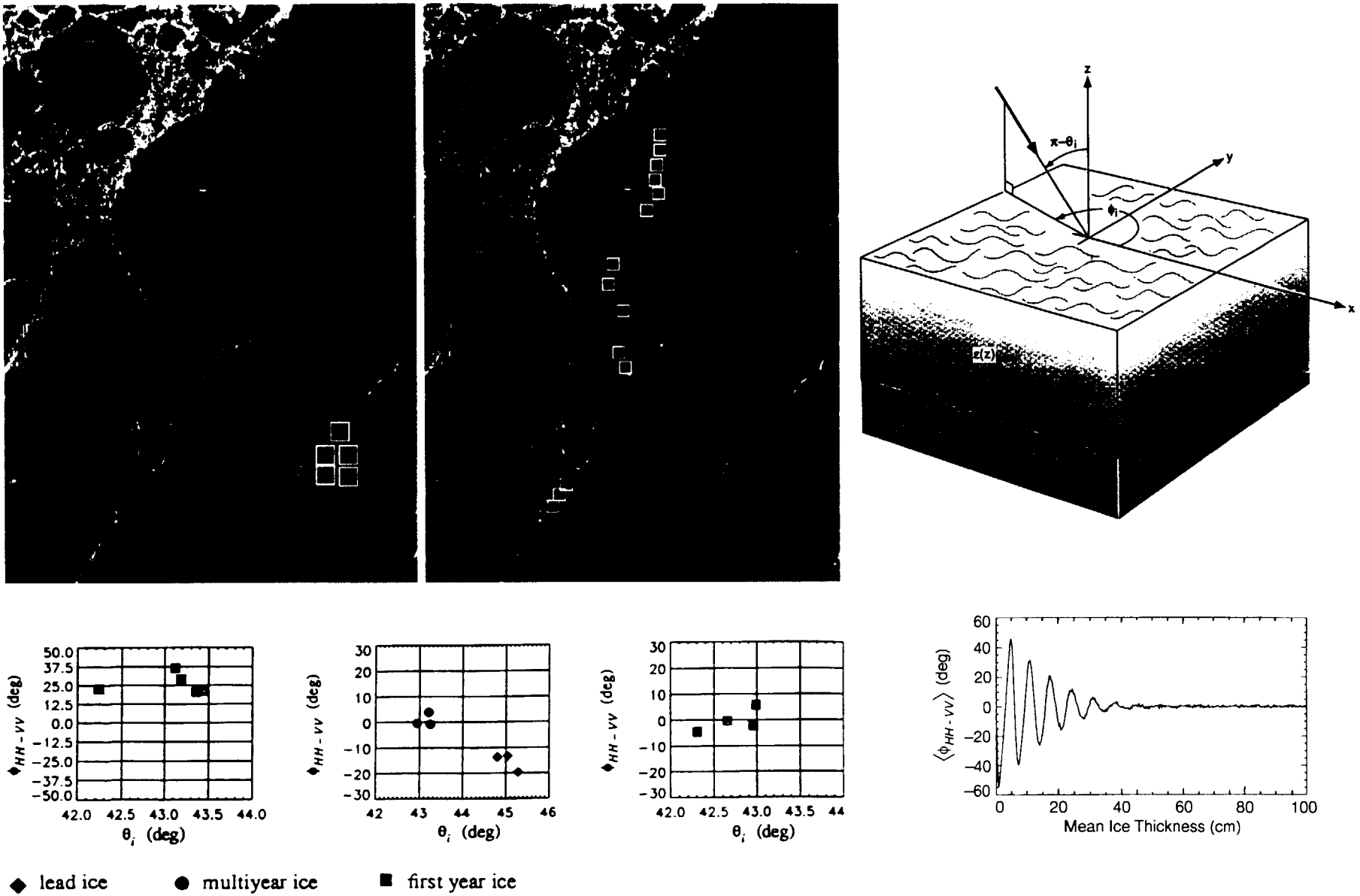

Figure 4-10. Winter sea ice data displays showing estimates of thickness from SAR polarimetry: upper left, a 3-frequency color AIRSAR data image (boxes typical of studied subregions); Lower left, copolar phase plots extracted from representative areas visually identified in SAR and passive microwave imagery; upper right, theoretical geometry; lower right, theoretical dependence of copolar phase with thin-ice thickness. Values consistent with those in lower right, but they cannot be validated with data now in hand (Winebrenner, in press).

5—Ice Sheets and Glaciers

INTRODUCTION

Ice sheets and glaciers form the largest component of perennial ice on this planet. Over 75% of the world's fresh water is presently locked up in these frozen reservoirs. Their extents, however, undergo considerable fluctuations. The expansion and reduction of ice sheets and glaciers from glacial periods to interglacial periods has been one of the most dramatic climatic signals in Earth history. Even on short time scales of a few years, changes in ice volume have modulated and continue to modulate, sea level. This has never been more important than it is today, given the increase in economic development of coastal areas. Recent evidence of the rapidity with which sea level has changed due to rapid changes in ice-sheet discharge has heightened our awareness of the dynamic nature of this icy component of our climate. While it is certain that small glaciers are experiencing broad retreat and contributing to sea level rise by increased melting, the contributions of the two largest ice sheets in Greenland and Antarctica, which contain over 98% of the world's ice, remain unknown.

Ice sheets, by their very presence, affect global climate. Greenland and Antarctica both are dominated by large cold ice sheets that rise to high elevations and are among the highest albedo objects on Earth. Despite these similar characteristics, their effects on the climate have important differences. Antarctica has a nearly circular symmetry which encourages the development of strong zonal circulations of the atmosphere and ocean around it. On the other hand, Greenland sits as an obstacle to zonal circulations, deflecting the flow of the jet stream and preventing the establishment of strong zonal circulation.

Understanding these roles of ice sheets and glaciers in climate has been the focus of a small group of scientists for a relatively short period of time. The size of the community and the relative "newness" of glaciology are due, in part, to the remoteness and harsh climate of glacierized regions. These facts are juxtaposed with the climatic importance of ice sheets. Satellite remote sensing has revolutionized this branch of climate science by empowering glaciologists with instruments capable of collecting spatially extensive, yet detailed, data sets of critical parameters. SAR, with its ability to collect ice-sheet data through cloud and throughout the extended polar night has already demonstrated unique capabilities that make it an indispensable new tool for the glaciologist. This is only the beginning: more recent techniques, such as interferometry, have expanded the uses of SAR in glacier and ice-sheet research even farther, and promise glaciologists increased capabilities to collect critical data.

KEY QUESTIONS

There are a number of key questions being addressed by glaciologists to which SAR data can make substantial contributions.

Are glaciers and ice sheets useful indicators of current climate change?

Glaciers and ice sheets most commonly occur at high elevations and in remote areas difficult to access. Such areas are typically not included in climate monitoring networks. If ways can be found to extract useful climatic parameters from observations of the ice, then ice sheets and glaciers provide valuable extensions of more traditional climate monitoring networks.

The interplay of annual cycles of snow accumulation and melting generates a succession of snow facies that serve as valuable indicators of the climatic regime characteristic of any point on an ice sheet or glacier (Williams et al., 1991). Figure 5-1 illustrates the essential subsurface stratigraphic characteristics. Beginning with the highest elevations, areas that experience no melt comprise the dry-snow facies. At lower elevations, melt-water percolates into the underlying, sub-freezing snow pack as a network of vertical ice pipes and horizontal ice lenses, forming the percolation facies. The amount of melt tends to increase at lower elevations. Eventually, melt is extensive enough that the latent heat released by the internal refreezing process warms the snow pack to the melting temperature throughout, and a fraction of additional melt water is retained within the snow pack in liquid form (the remainder leaves the ice mass as runoff). This situation characterizes the soaked-snow facies. At the lowest elevations is the bare-ice facies, formed when all surface snow is removed by ablation. The upper edge of the bare ice facies marks the snow-line at the end of the mass balance year.

As climatic conditions change, so will the positions of these boundaries. Conveniently, the low surface slopes of glaciers (typically 10^{-2}) and even lower surface slopes of ice sheets (typically 10^{-3}) transform subtle shifts of only a few meters in the elevations of these boundaries to large horizontal shifts on the order of a few kilometers. In addition to indicating the altitudinal extent and intensity of melt, these facies differ in spectral albedo. Thus, as facies extents change, so does the net radiation balance of the ice sheets.

Glacier length is the glaciological parameter with the longest history of observation. While glacier-length changes clearly illustrate that climate has changed, glaciers (and especially ice sheets) are one of the most sluggish climate components. Thus, the inverse problem of detecting or inferring climate change from measurements of ice extent is very difficult. This general view does not hold, however, on smaller, steeper mountain glaciers whose response times are of the order of years to decades.

How do the ice sheets affect atmospheric and oceanic circulations?

The general effects of ice sheets on the atmosphere and oceans were discussed above. Clearly, changes in either the albedo of the surface (through a change in snow facies extents), or changes in the geometric shapes of the ice sheets will alter their climatic effect and perturb the global climate system. Usually these changes are discussed in the extreme cases of glacial periods, when surface temperatures in central North America or Europe fell an average of 10 to 12 degrees Celsius, but smaller changes in ice sheets will also perturb the climate (Dawson, 1992). The relationship is probably highly non-linear; the climate record from Greenland ice cores shows that dramatic climate changes can occur in much less than a decade (Alley et al., 1993).

Remnants of vast armadas of icebergs have been detected in the western North Atlantic, well beyond the reach of ice sheets (Heinrich, 1988). It has been suggested that the melting of these icebergs would introduce a sufficient quantity of fresh water into the North Atlantic to completely transform the global pattern of oceanic circulation, altering the climate in every corner of the world (Broecker and Denton, 1989).

What is the current mass balance of ice sheets and glaciers?

Ice-sheet or glacier mass balance is defined as the annual difference between mass gain and mass loss. It is important globally because it has a dominant effect on sea-level change.

During the last glacial maximum, global sea level was approximately 125 meters lower, the water being locked up primarily in the now-extinct Laurentide and Fennoscandian ice sheets of the Northern Hemisphere and an expanded Antarctic ice sheet (Shackleton, 1987; Denton and Hughes, 1981). Present ice volume, which is contained mostly in the Antarctic and Greenland ice sheets, is sufficient to raise sea level approximately 80 meters (Bader, 1961, Drewry et al., 1982).

By comparison, the annual turnover in ice-sheet mass is modest. Annual snow accumulation over the Antarctic and Greenland ice sheets is equivalent to an ocean layer only 6 mm thick (Bentley and Giovenetto, 1991; Ohmura and Reeh, 1991). A nearly equivalent amount of ice is returned to the oceans through melting and iceberg discharge. Estimates of present mass balance are poorly constrained: the Greenland ice sheet appears relatively stable, the Antarctic ice sheet seems to be growing slowly and the remaining small glaciers and ice caps are wasting away rapidly (Meier, 1993). Oddly enough, this range of behaviors may be due to the same phenomenon: global warming. Warmer summer temperatures enhance ice melting but also increase the frequency of precipitation events, which could result in growth of ice sheets and glaciers. In Antarctica almost no summer melt occurs except on the Antarctic Peninsula so the increased snowfall would enlarge the ice sheet. Mountain glaciers experience a net reduction in mass at low elevations due to the warmer summer temperatures, but, in some cases, may be growing at higher elevations. In Greenland, the two opposing effects appear to be roughly balanced.

These conclusions are based on sparse data. A notable weakness in one or more of these present estimates of mass balance is that they fail to add up to the present rate of sea-level change, even when liberal error estimates and other contributing effects are included (Meier, 1993). Confidence in predictions of future sea-level change must be tempered until we better understand the current mass balance of the existing ice.

What are the controls on ice flow and are there inherent instabilities in ice flow that could lead to dramatic changes in the dynamics of ice sheets or glaciers?

The subject of ice dynamics ranges from deformation and recrystalization of individual crystals, to surge-type glaciers, to the flow of the Antarctic ice sheet. Most of the controlling processes lie hidden within or underneath the ice, but the effects are clearly evidenced by deformation and flow of the ice. This topic is relevant to global climate because of the effect altered ice flow has on ice volume and, therefore, on sea level.

The ice-sheet environment determines the magnitudes of both snow accumulation and melting, but ice dynamics determines the rate at which ice is delivered to the oceans or to ablation areas. Thus, ice dynamics is a major component of the mass balance. This becomes obvious when examining the record of sea level since the last glacial maximum 20,000 years ago (Figure 5-2). During this period, sea level rose episodically in a series of brief jumps rather than smoothly. Geologic evidence confirms that these jumps correspond to the partial or complete collapses of marine-based ice sheets. Such behavior apparently caused sea level to rise at rates of at least 35 mm/yr, more than twenty times the present rate of rise. Although no such collapses have occurred for the last 4000 years, the West Antarctic ice sheet is the last marine-based ice sheet on the planet, and it contains enough ice to raise sea level more than five meters (Drewry et al., 1982). There is a pressing need to determine if, when, and how rapidly this ice sheet may collapse.

How much of the heat absorbed by the surface snow pack is retained by the ice mass and how much escapes as meltwater?

Warm temperatures melt surface snow, and the resulting meltwater most often drains into the underlying snow pack. Residual colder winter temperatures in this snowpack conduct heat away from the meltwater. If the residence time of the meltwater is sufficiently long, or if the snow pack is sufficiently cold, the meltwater refreezes. In this case, melting recorded at the surface does not represent mass that leaves the glacier; rather, this mass is captured at depth within the snow pack. On the other hand, if a system of snow-pack drainage is well developed with surface streams and moulins (vertical cavities) that quickly transport water through the glacier or ice sheet, not only can the initial quantity of meltwater leave the glacier, but additional melting can occur at the interface between rushing water and the surrounding ice.

The importance of these two extreme cases is apparent when viewed from the perspective of mass balance (Pfeffer et al., 1991). In one case none of the surface meltwater actually leaves the glacier, while in the other case the mass lost from the glacier is actually more than the amount of meltwater produced at the surface. The relevance of this effect to climate change lies in the fact that different snow facies respond differently to changing temperatures. For example, a formerly dry-snow area that begins to experience melt will retain most of the meltwater for many years as the system of internal drainage (comprised of vertical ice pipes and horizontal ice lenses) develops. However, a percolation facies that warms will be less effective at retaining increased amounts of meltwater, possibly delaying its eventual transformation to a soaked-snow facies.

ROLE OF SAR IN ANSWERING THESE QUESTIONS

SAR provides the obvious benefits of a weather-independent, day-night imaging system. These advantages are particularly crucial in the ice-sheet and glacier environments where persistent clouds continue to hamper data acquisitions by visible imagers and where the polar night imposes a prolonged period of darkness. In addition, unlike visible imagers, radar penetrates the snow surface, which provides glaciologists with a tool capable of sensing internal properties of the ice sheet or glacier.

Before ERS-1 was launched, limited SAR data of ice sheets only hinted at the potential glaciological uses of SAR. ERS-1 data have allowed full demonstration of many of these uses and have expanded the glaciological applications of SAR to even broader horizons.

The list that follows identifies the key parameters of ice sheets and glaciers that can be measured with SAR, and describes how glaciologists will be able to use this information to answer the key questions identified above.

Snow Facies

Radar penetrates the snow surface, so the measured backscatter is a combination of surface and volume scattering. This characteristic enables SAR to discriminate clearly between all the snow facies described above using backscatter amplitude data alone. This discrimination is most effective during middle to late winter when surface water is absent. Dry snow appears dark in SAR because both surface scattering and volume scattering are low. At lower elevations, in the percolation facies, backscatter rises dramatically due to volume scattering from the network of subsurface ice bodies. The soaked-snow facies is composed of larger snow grains than the dry-snow facies because both melt-water and warmer temperatures serve to accelerate grain growth. Thus, the soaked-snow facies is radar dark when water is present, but in winter the backscatter increases to a level intermediate to the

radar-dark dry-snow facies and radar-bright percolation facies. Finally, the bare-ice facies is radar dark due to strong specular surface scattering. Figure 5-3 clearly shows these different snow facies in a SAR-image mosaic of the Greenland ice sheet. The northeast portion of the dry-snow facies is slightly brighter than the rest of this facies. This is believed to be due to a decrease in the accumulation rate in this region (Jezek, 1993; Ohmura and Reeh, 1991). Figure 5-4 shows that the facies correlate closely with surface elevation. The ability to discriminate all the snow facies, which is impossible with visible imagery, establishes the unique use of SAR in a monitoring program of ice sheets for indications of climate change over their broad expanses. SIR-C/X-SAR data of the Patagonian ice fields indicate that facies discrimination is also possible using multifrequency data (Forster and Isacks, 1994).

Seasonal Melt

Water is strongly radar-absorptive. This permits the use of SAR for monitoring of the summer melt season on ice sheets and glaciers. Time-series SAR data of Greenland have demonstrated that the gradual refreezing of free water at depth can be detected and have shown that this free-water component exists for a surprisingly long time after the snow surface has cooled below freezing (Figure 5-5).

Radar at lower frequencies penetrates more deeply into snow. Thus, multi-frequency data permit a depth-variable view of the snowpack. This has been most clearly demonstrated by SIR-C/X-SAR data of the Patagonian ice fields (Figure 5-6). While a capability does not yet exist to quantify either the amount of melting or refreezing, the multi-frequency SARs sensitivity to conditions at different depths is already useful in monitoring the thermal and hydrologic evolution of ice sheets as climate changes. Future development of this capability will increase SARs utility in this area even further.

Icebergs

Mass loss by iceberg calving exceeds mass loss by melting for the Antarctic ice sheet and is approximately equal to the amount of surface melting for the Greenland ice sheet (Bader, 1961). Thus, this is a critical term in determining ice-sheet mass balance (although it does not directly affect sea level). Icebergs are visible in cloud-free visible imagery, but the requirements of a monitoring program include routine and dependable acquisition of high-resolution imagery, even during the extended polar night. These requirements match the capabilities of SAR and make it the preferred instrument for this activity. Figure 5-7 shows that icebergs as easily identified in SAR imagery.

Surface Morphology

Most surface morphological features are seen by either SAR or a visible imaging system. SAR holds the dual advantages of its all-weather, day-night capability while visible imagers avoid image degradation caused by speckle. Specific features that can be identified include streams and lakes, flowbands (linear forms stretched longitudinally in the direction of motion), ice edge, moraines and crevasses (Figure 5-8). The ability to identify such features opens the door to monitoring their evolution.

Lakes can be an especially good indicator of surface hydrologic activity. They tend to form in the same surface depressions each summer (locations fixed in space by the flow of ice over bed undulations), and their size and numbers are indications of the intensity of melt. Thus, they serve as ancillary data to the climate monitoring activity already described.

Ice margins are important because they change in response to changes in the flow of the ice. The radar contrast at many ice margins is less distinct than the contrast in visible imagery. However, there are many situations where this generality does not hold. These include areas where persistent cloud cover impedes collection of visible data, where fresh snow has covered the visible contrast between ice and adjacent terrain, and where ice near the edge is covered by rock or other debris. In the last case, differences in the polarization signatures of the moraine-covered ice and ice-free debris may permit identification of the ice margin.

Crevasses present serious hazards to field personnel but are one of the most useful natural features for glaciological study. Their orientations provide information on the state of stress within the ice. A more quantitative use is the measurement of ice motion accomplished by following unique crevasses or crevasse patterns over time (see next section). Additionally, SAR has demonstrated an ability to detect crevasse fields where visible imagery cannot (Hartl et al., 1994; Vaughan et al., 1994). This is due to either the detection of micro-cracks, below the resolution of the visible imagery, or from detection of buried crevasses by penetrating through the surface layers of the snow.

Ice Velocity

Ice velocity is one of the most fundamental parameters in the study of ice dynamics. The proven ability to obtain this information from time-sequential imagery using a cross-correlation technique significantly expanded the amount and density of such data available to glaciologists (Bindschadler and Scambos, 1991). This technique tracks patches of the surface containing crevasses and other surface features from one image to another by searching for the matching pattern of surface features in a second image. Displacements can be measured to sub-pixel accuracy, but typical displacements should be at least a few pixels to minimize the impact of systematic errors in coregistration of images (typically 1 to 2 pixels) (Scambos et al., 1992). Although developed initially for visible imagery, this technique also has been shown to work with SAR imagery (see Figure 5-9) (Fahnestock et al., 1993). A requirement of this technique is that the same sets of surface features be resolvable in both images. This requirement is not met over most of the ice sheets, but is usually met in the most active flow regions.

The application of interferometric techniques using SAR data holds the potential of obtaining ice velocity data from any ice sheet region. The technique utilizes the phase measurement of the backscattered radar pulse from every ground pixel to make a sub-wavelength scale measurement of displacement (usually a few millimeters) at every pixel (Goldstein et al., 1993). In the ideal case, the two images would be collected from the same point in space (zero-baseline). In practice, however, the baseline between observation points is finite so the interferogram contains a combination of motion and topographic information. Images must be coregistered to sub-pixel accuracy and the backscatter signatures from the same pixel in each image must be correlated for the phase difference to have a physically meaningful interpretation. Either a different viewing geometry or metamorphic changes in the surface or subsurface of a target pixel can destroy the phase correlation for a particular pixel.

Successful ice-sheet interferograms have typically used time separations of only a few days (Goldstein et al., 1993, Rignot et al., in press, Joughin et al., in press). Figure 5-10 shows an example of an interferogram from the Bagley Icefield in Alaska. Interferometrically measured displacements are in the direction of view, which for satellite SARs is in the range of 20 to 40 degrees from vertical. If the general direction of flow is known (along the regional surface gradient), one velocity component is sufficient to estimate the total velocity. Greater precision in velocity requires that a second interferogram be obtained from a

different viewing angle. This can usually be accomplished by acquiring image pairs from both ascending and descending orbits.

Because interferograms contain no absolute displacement information, only velocity differences are obtained. Nevertheless, velocity gradient data (strain rates) are highly useful. To obtain absolute velocities, a theoretical minimum of two control values are needed to provide a datum and to correct for along-track variations in baseline. In practice, more control is desirable and may be necessary.

Surface Topography

As mentioned above, interferometry with a non-zero baseline includes both topographic and motion information because the measured range difference (in units of phase) is the result of both surface movement and topography-induced parallax. This mixture of topographic and motion information requires that the topography be known with sufficient accuracy to remove its effects from the interferometrically-determined phase differences, in order to extract ice displacements. Fortunately, by using a third SAR image, an extremely clean separation of the topographic and velocity signals is possible if the velocity and topography are constant over the interval spanned by the three images (Kwok and Fahnestock, in press). Figure 5-11 shows an example of this separation.

As with the interferometric velocity output, the extracted topographic output is relative elevation, rather than absolute elevation. In principle, a single absolute elevation is sufficient to provide the datum for an entire interferogram but, again, insufficient knowledge of the precise baselines for each interferogram require that more elevation control points be used. The range of elevations spanned by a two-pi cycle of phase difference depends upon the baseline. For topographic relief of a particular scale, there is an optimal range of baselines between the undesirable extremes of too short a baseline, where insufficient parallax is achieved to resolve elevation variations, and too long a baseline where phases decorrelate. The accuracy of the derived elevations also is dependent upon the baselines of the interferograms. In one study area, shown in Figure 5-12, relative elevation accuracies of less than 2 meters were obtained with ERS-1 data having an effective baseline of 520 meters (Joughin et al., 1994). Eventually, the flow of ice is expected to be well enough understood that it will be possible to invert topographic and surface motion data to obtain basal topography and basal shear stress, which are additional parameters needed for ice-dynamics studies.

POSSIBLE ADDITIONAL USES OF SAR DATA

The ability to make the measurements described above with SAR data was demonstrated only after the collection of a substantial amount of ice-sheet data by ERS-1. The list is probably complete for the C-band, single polarization SAR carried by ERS-1. Before these data were available to demonstrate these techniques, limited Seasat and airborne data could only suggest the potentials that awaited glaciologists. In the case of interferometry, no mention of this now-proven technique was ever made in the pre-ERS-1 ice-sheet community. To extend this analogy, then, it probably is impossible to predict accurately the future uses of a SAR enhanced with additional polarizations and frequencies because multiple-frequency and multiple-polarization data sets of ice sheets from which to extrapolate remain very sparse.

Therefore, additional necessary work is posed in the form of questions that still need to be answered. In the process of answering these questions, new potential uses of SAR are likely to be discovered.

Is there a "best" SAR frequency for ice sheets and glaciers?

It is known that single-band data (C-band) permit almost all the analyses summarized above because a wealth of such data has been collected, from which these techniques have been developed. Seasat provided a limited amount of L-band data that confirmed it also can be used for snow facies, icebergs, and surface morphology research (Bindschadler et al., 1987). Limited airborne P-band and X-band data have hinted that these frequencies may also be used (Jezek et al., 1993). Recently, Space-Shuttle-based multi-frequency (L- and C-band), multi-polarimetric data have been added to the data pool.

What has been missing is a methodical comparison of data of the same ice-sheet areas using different frequencies and including complex data so interferometric products can be examined. L-band and P-band penetrate deeper than C-band, but the quantitative advantages and disadvantages of sensing deeper, older snow have not been established. A more diffuse volume-scattering component might provide a more temporally stable signature of the various snow facies. Airborne data have highlighted major differences in backscatter signatures when the frequency shifts from P-band to C-band (with the intermediate L-band being more like P-band) (Jezek et al., 1993). Similar backscatter variations have been seen in SIR-C/X-SAR data (cf. Figure 5-5) (Forster and Isacks, 1994). These differences could lead to techniques to derive a number of important variables including: grain-size versus depth distributions (critical for the quantification of accumulation rates from passive microwave data); meltwater production; and the amount of free water retained by the snow pack (by following the depth of the winter freezing wave as it penetrates the snow pack).

Interferometric applications might be aided by lower frequencies that permit longer baselines and have a relatively greater and more temporally stable volume-scattering component, making them less sensitive to meteorological events on the surface that decorrelate successive images. However, the increased contribution of the deeper volume scattering component could lead to an enhanced geometric decorrelation sensitivity or lower signal-to-noise, thus restricting available interferometric image pairs.

P-band radar might even penetrate the full depth of some glaciers. This would make it possible to map subglacial topography using interferometric techniques. Obtaining both surface and bed topography leads directly to ice volume--one of the critical climatic parameters discussed at the outset of this chapter. If successful, this would substantially improve all existing ice-volume estimates because existing data have been collected along linear ground tracks or flight lines, so the resulting ice-thickness maps have been produced by spatial interpolation.

Can useful scientific information be obtained by studying polarization effects?

Limited polarization data have been used to determine the dielectric constant and to extract the small-scale surface roughness of portions of the Greenland ice sheet (Jezek et al., 1993). The dielectric constant can be used to derive, albeit indirectly, surface albedo. Albedo has obvious importance in the energy balance of the ice sheet. Surface roughness is also a necessary consideration in exchange of energy because it affects the near-surface wind profile. Field measurements of surface roughness suffer from sampling sparseness but would be a necessary component of surface-truth experiments designed to develop the ability to

remotely determine surface roughness. Given that different radar frequencies are sensitive to surface roughness on different scales, a wide spectrum of surface roughness may be obtainable.

In winter, the percolation zone displays anomalous backscatter polarization behavior. Similar behavior has been observed elsewhere in the solar system, ranging from icy Jovian moons to the Martian polar cap to, perhaps, a polar cap on Mercury. The common denominator seems to be ice, though not necessarily water ice. Anomalously polarized backscatter is, however, otherwise very rare in the solar system. Theoretical explanations of this are speculative, but all bear on the depth distribution of volume scattering. In the case of the percolation zone in Greenland, this depth distribution is linked to the redistributions of melt water and heat. This is of considerable interest because melting is one of the major mass-loss mechanisms of the Greenland ice sheet and could affect the salinity balance of the North Atlantic. Understanding and using anomalously polarized backscatter as a remote-sensing tool could lead to a unique probe of physical properties of both terrestrial and extraterrestrial icy regions.

What are the physical processes that cause target decorrelation and what are their relative effects?

It has been hypothesized that the occurrence of windstorms, snowfall, surface- and depth-hoar formation, melting, and refreezing between the epochs of two SAR images are meteorological events that can alter the backscatter signature from the target sufficiently to decorrelate the phase data and prevent the generation of interference fringes. Few studies have been done to actually quantify the effects of any of these events on the correlation of successive images. Jezek and Rignot (1994) hypothesized that spatial patterns of decorrelation in one ERS-1 image pair of Greenland may actually be due to variations in the distribution of snow deposited between the images. At C-band, 10 cm of fresh snow adds one additional wavelength (or fringe) to the round-trip radar distance.

More studies are necessary and will lead not only to guidelines for improving the likelihood of collecting correlated image pairs from which interferometric products can be produced, but also will produce meteorologically meaningful data over a spatially broad scale as compared with local data provided by sparsely distributed ice-sheet meteorological stations. Independent views afforded by interferometric SAR could prove valuable in interpreting the data sets provided by passive microwave sensors or radar altimeters, both of which also derive some of their signal from the sub-surface snow pack.

WHAT MUST BE DONE TO CONFIRM THESE POTENTIALS?

Most of the SAR technique-development investigations for ice-sheet and glacier research require data at frequencies other than C-band. Now that the C-band data set is extensive enough over the ice covered areas, more limited coverage at other frequencies can be placed into a meaningful context. This research is a necessary prerequisite to the development of a satellite SAR mission at any frequency other than the proven C-band. The fidelity and sparseness of JERS-1 L-band data of ice sheets has failed to provide a data set capable of verifying the utility of L-band data for glaciological studies.

A critical component of the collection of data at frequencies other than C-band is the collection of interferometric pairs spaced in time so that motion information as well as topographic information are included in the phase differences. A particularly useful data set

would be the collection of interferometric triplets of a moving ice sheet in at least C-band and L-band.

Ground truth is a mandatory part in the development of any new remote sensing application. This is certainly true with SAR data of ice sheets where volume scattering is often the dominant backscatter component. Field measurements are the only certain means of documenting specific physical properties of the snow pack and the temporal changes in these properties between remote data collections. To the extent possible, these measurements should be contemporaneous with airborne or satellite SAR acquisitions. Scattering measurements made with ground-based radar systems provide a data set for comparison with the remote measurements. Standard techniques allow surface parties to collect depth profiles of density, water content, grain size, conductivity, permittivity, temperature, and icy inclusions. These persons also can record surface meteorological conditions and help optimize the collection of SAR data from remote platforms.

CURRENT SAR ASSETS AND THEIR USE

ERS-1 has provided an invaluable SAR data set which has been used to establish the scientific utility of SAR for ice-sheet and glacier research. A few interferometric pairs await analysis, but for the purposes of developing or demonstrating new techniques, the use of this data set is virtually complete. No plans exist to place ERS-1 into a short repeat cycle orbit so that interferometric opportunities from this single satellite have probably ceased. The continuation of the ERS series with ERS-2 and ENVISAT will allow monitoring of the Greenland ice sheet snow facies to proceed.

JERS-1 carries an L-band SAR. It promised the same capabilities as ERS-1, but damage caused by a faulty antenna deployment has compromised the quality of the data. Thus, it has not provided an adequate opportunity to assess the merits of L-band data of ice sheets and glaciers relative to C-band.

The AIRSAR facility (C-, L- and P-band antennas on a DC-8 aircraft) provides the best existing means to collect the multi-frequency and multi-polarization data sets needed to assess the relative merits of these different windows of the electromagnetic spectrum. Multiple antennas have the obvious advantage of collecting simultaneous and coincident data. From knowledge of the positions of snow facies and surface features gleaned from the ERS-1 data set, aircraft missions can be planned in a manner that optimizes the utility of the collected data.

A critical augmentation to AIRSAR is the ability to collect interferometric data by navigating the aircraft with GPS real-time corrections. This capability will be crucial in investigations of the frequency-specific characteristics of interferometric data. The missions should be flown at various times of the year during periods when particular meteorological events (i.e., onset of melting and freezing, snowfall, high surface winds, etc.) are most likely.

PLANNED FUTURE MISSIONS

ERS-2, when launched, will continue the capability of the ERS-1 SAR. An exciting prospect is an ERS-1/ERS-2 tandem mission for the collection of interferometric data.

RADARSAT, carrying another C-band SAR, is planned for launch in 1995. After an extended initial operational period, a scheduled orbit maneuver will afford RADARSAT the first SAR-view of most of the Antarctic ice sheet, including the regions south of latitude

78°S. The primary goal of this maneuver is to map the Antarctic ice sheet with SAR. It will take approximately two weeks, less than one orbit cycle, after which time RADARSAT will return to the nominal north-looking configuration. No possibilities exist for interferometric data collection during this short period. A second mapping may occur later in an extended RADARSAT mission. This mapping is exploratory, and it remains tantalizingly impossible to predict all that may be discovered with these data.

RECOMMENDATIONS

SAR remains a technology that is grossly underutilized in proportion to its proven capability to assist glaciologists in answering some of the most pressing questions in their discipline. These questions have direct relevance to global climate and future sea-level change.

SAR interferometry can provide data sets whose regional collection was never before feasible, yet are crucial to glaciological studies. A mission designed to produce complete interferometric coverage of permanently ice-covered areas promises extraordinary glaciological returns.

The omission of large portions of the polar regions by virtually every satellite mission to date continues a long, but undesirable, tradition that restricts the glaciological utility of satellite data. At present more than 2/3 of the Earth's permanent ice cover cannot be viewed by existing spaceborne SARs. Modern awareness of the climatic importance of the polar regions must be expressed in the ability of new sensors to extend their view to the poles. As in the case of RADARSAT, this polar view need not be available continuously, but, unlike RADARSAT, when available, it should be for a number of repeat cycles so that the enormous utility of SAR interferometry can be applied to the glaciological problems of global significance.

This chapter closes with the following specific recommendations:

(1) An interferometric mission at C-band should be conducted that includes multiple-image views of all ice sheets and glaciers sufficient to yield detailed surface topography and surface-velocity data sets.

(2) Future SAR missions should include maneuvering and data collection capability sufficient to monitor all permanently ice-covered areas at least once per year.

(3) Airborne and surface measurements should be carried out to assess the relative merits of different frequencies and combinations of frequencies and polarizations in deriving parameters needed to answer pressing glaciological questions relevant to the global climate.

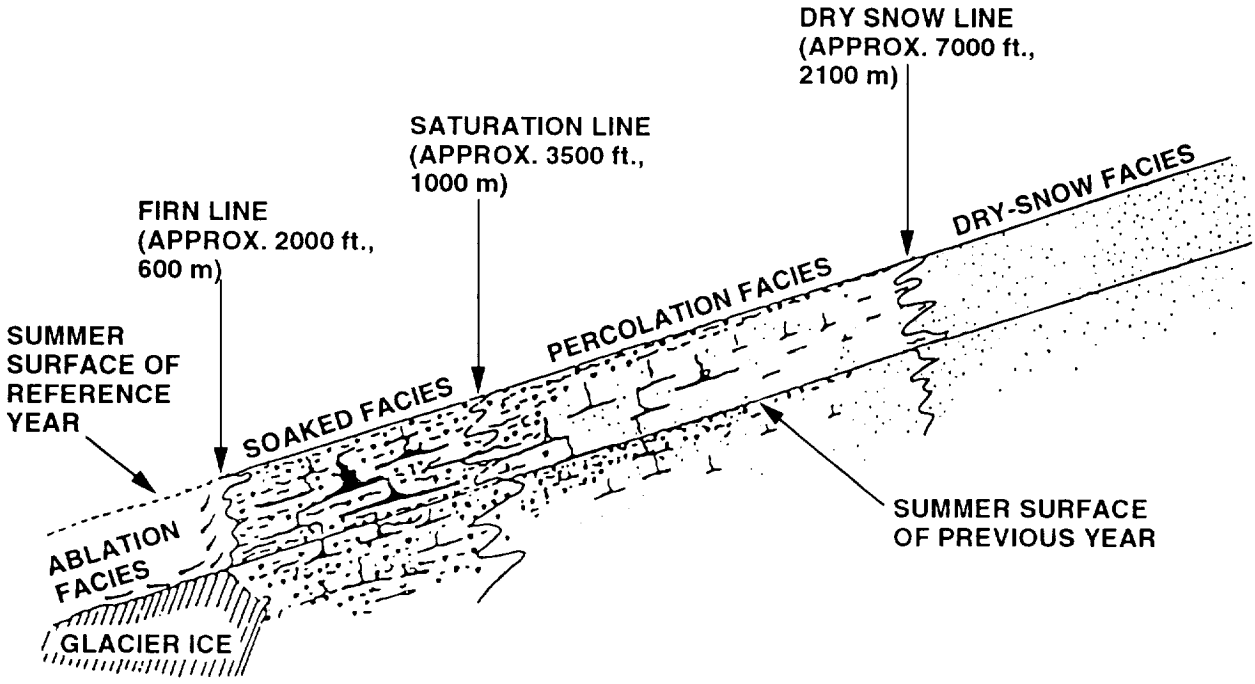

Figure 5-1. Schematic crossection of snowpack (Benson, 1963).

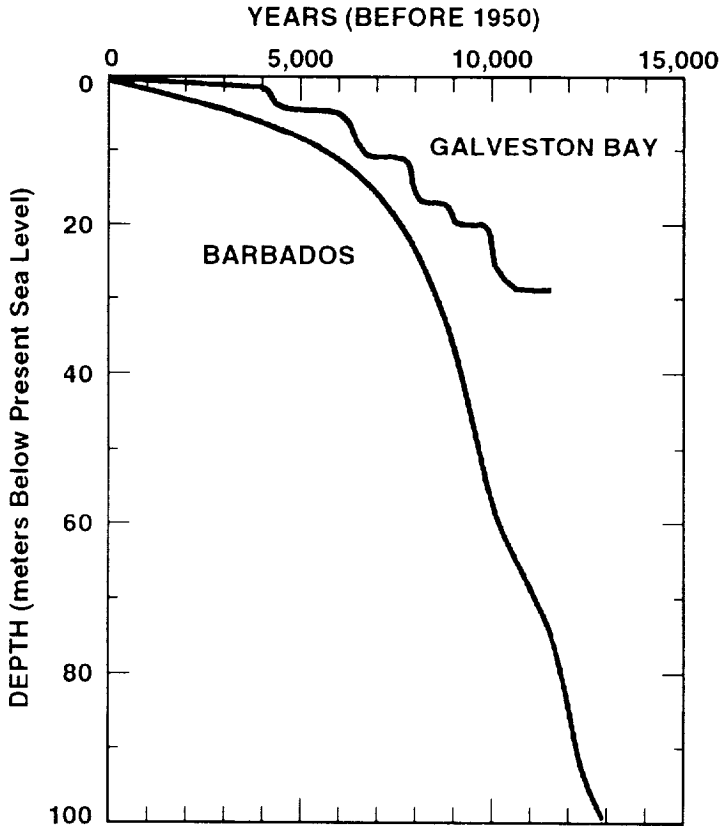

Figure 5-2. Sea-level history from Barbados and Galveston Bay (Anderson, pers. comm).

Figure 5-3. Greenland SAR mosaic (Fahnestock et al., 1993).

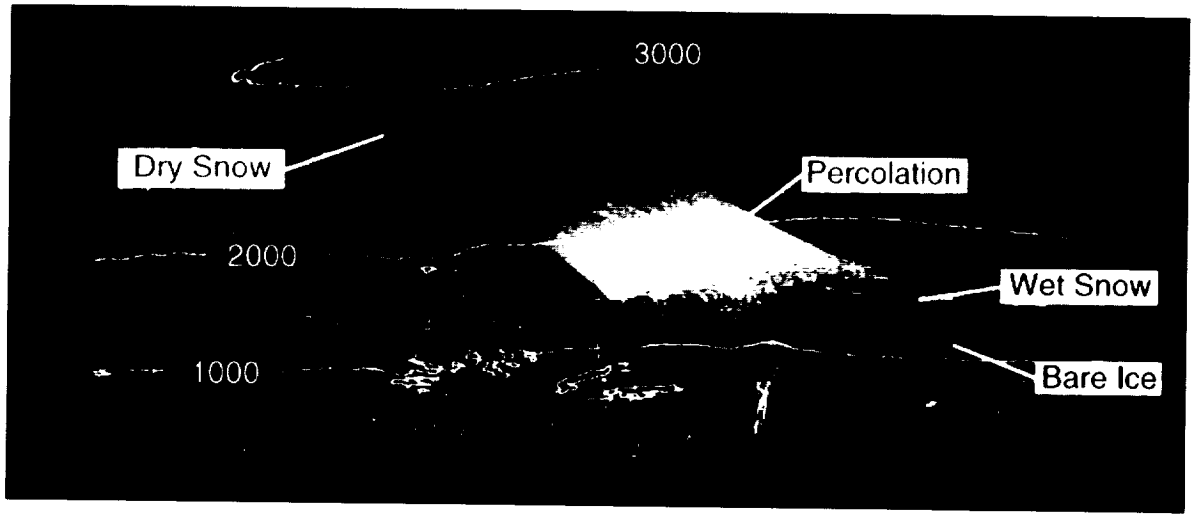

Figure 5-4. Side-looking perspective of snow facies in western Greenland (Fahnestock and others, 1993), (elevation lines of 1000, 2000, and 3000 meters, roughly 3300, 6600 9800 ft.).

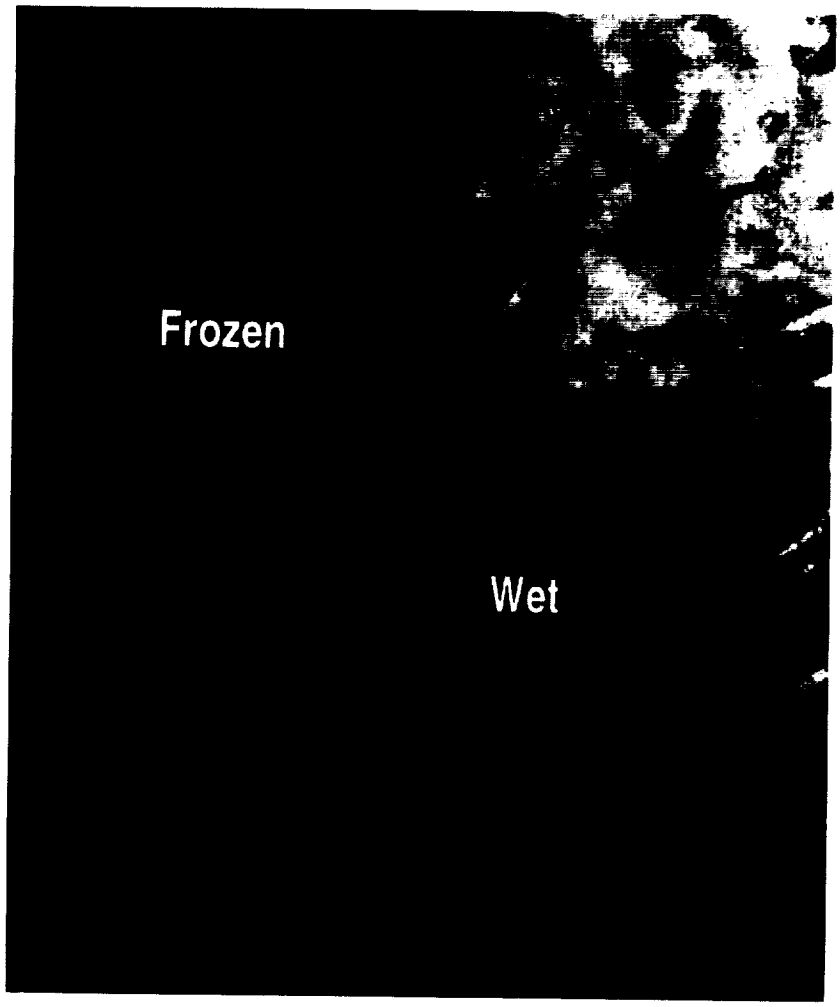

Figure 5-5. Two views of a portion of Greenland ice sheet showing contrast in radar backscatter between wet and frozen conditions.

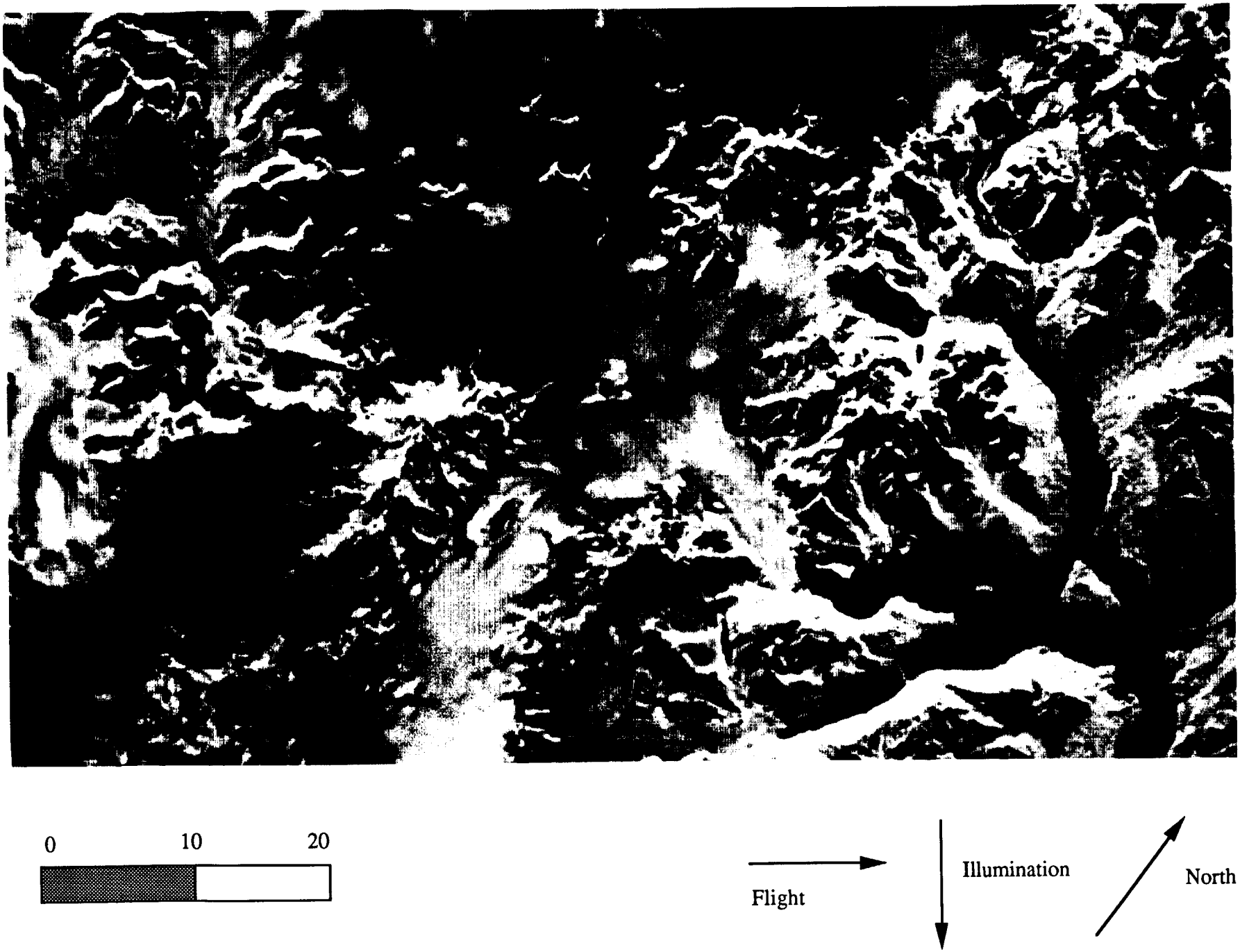

Figure 5-6. SIR-C Image of the South Patagonian Icefield (red=CHH, green=LHH, blue=LHV).

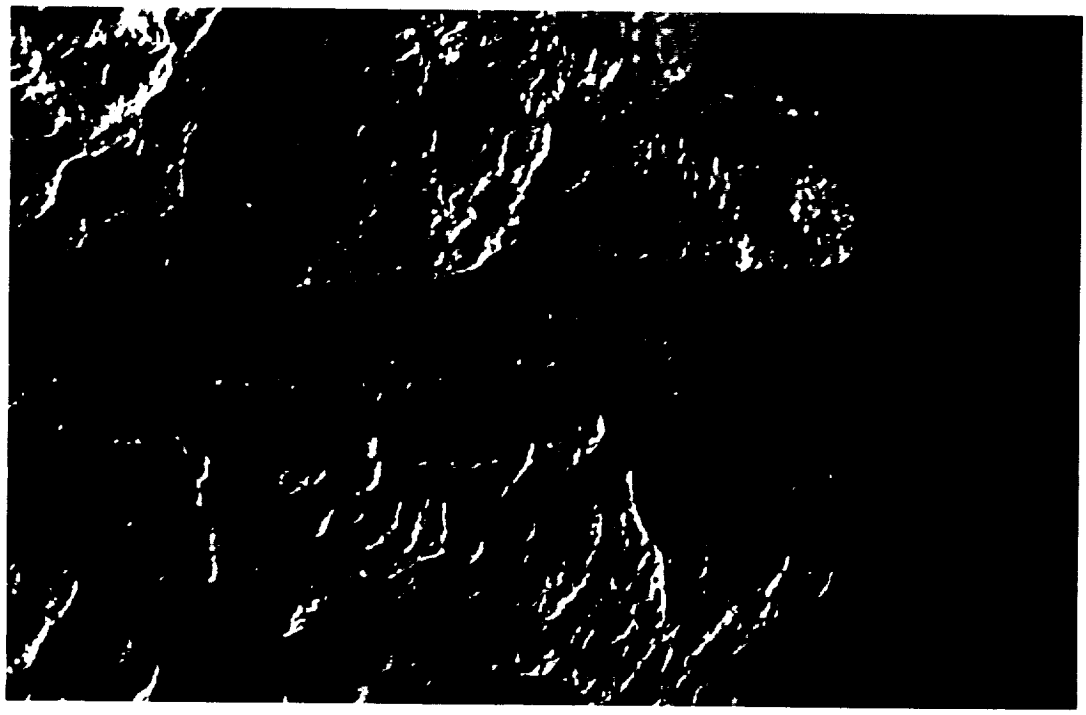

Figure 5-7. Icebergs in Jakobshavns Fiord.

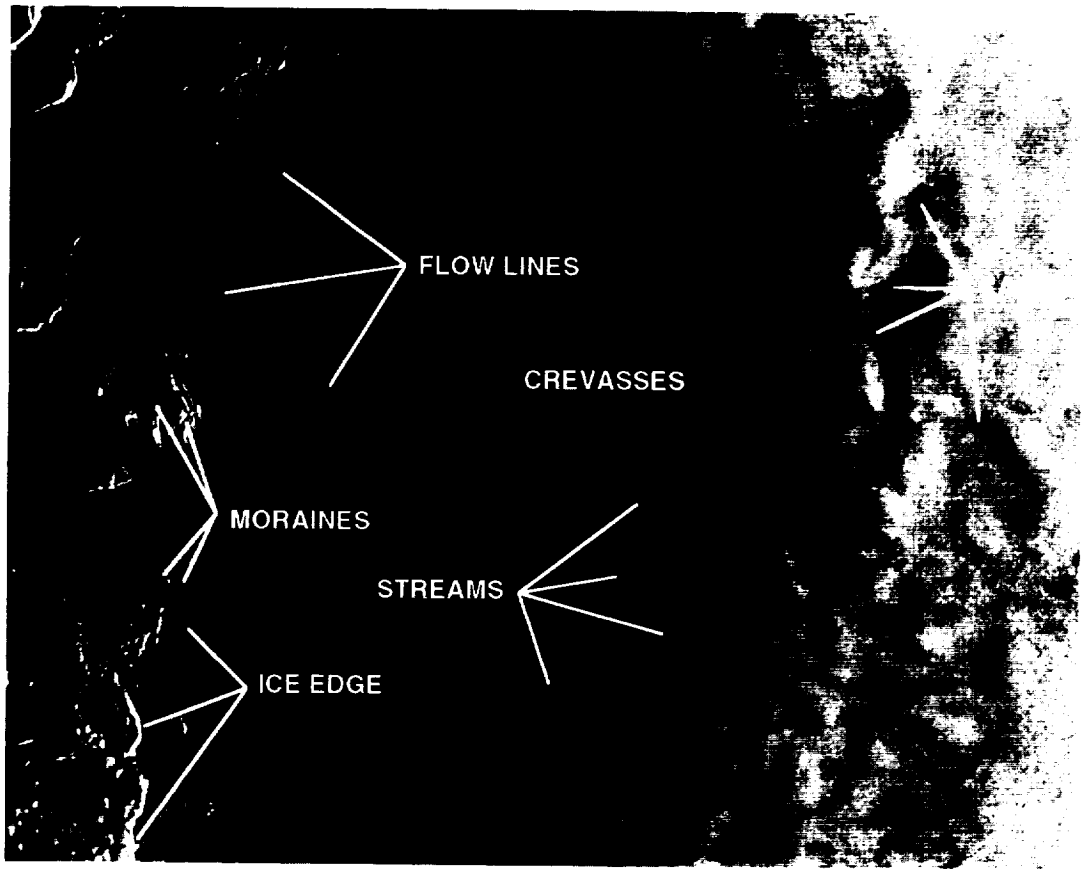

Figure 5-8. SAR image of western Greenland showing crevasses, lakes, streams, flow lines, moraines and ice edge.

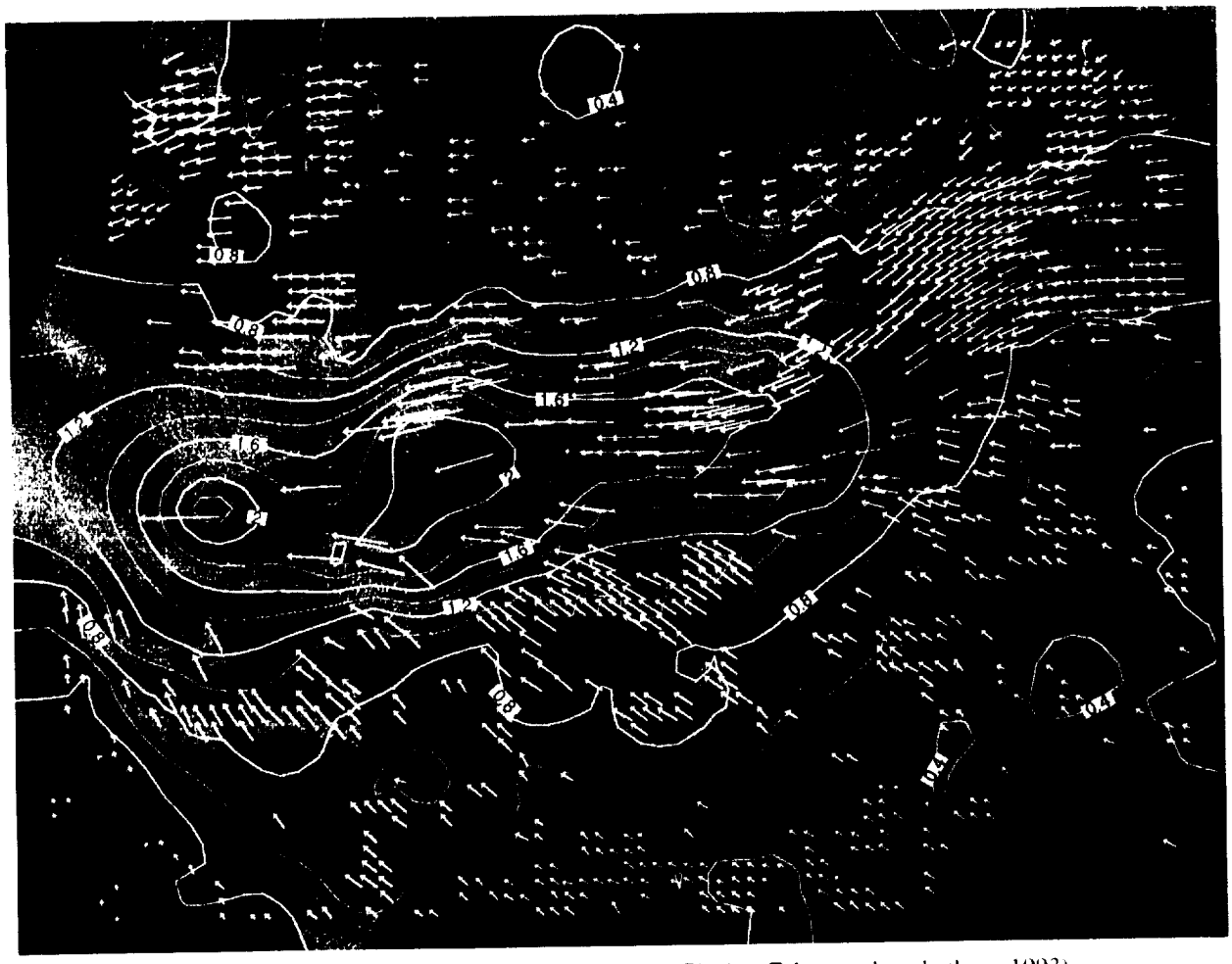

Figure 5-9. Surface velocity field of Jakobshavns Glacier (Fahnestock and others, 1993).

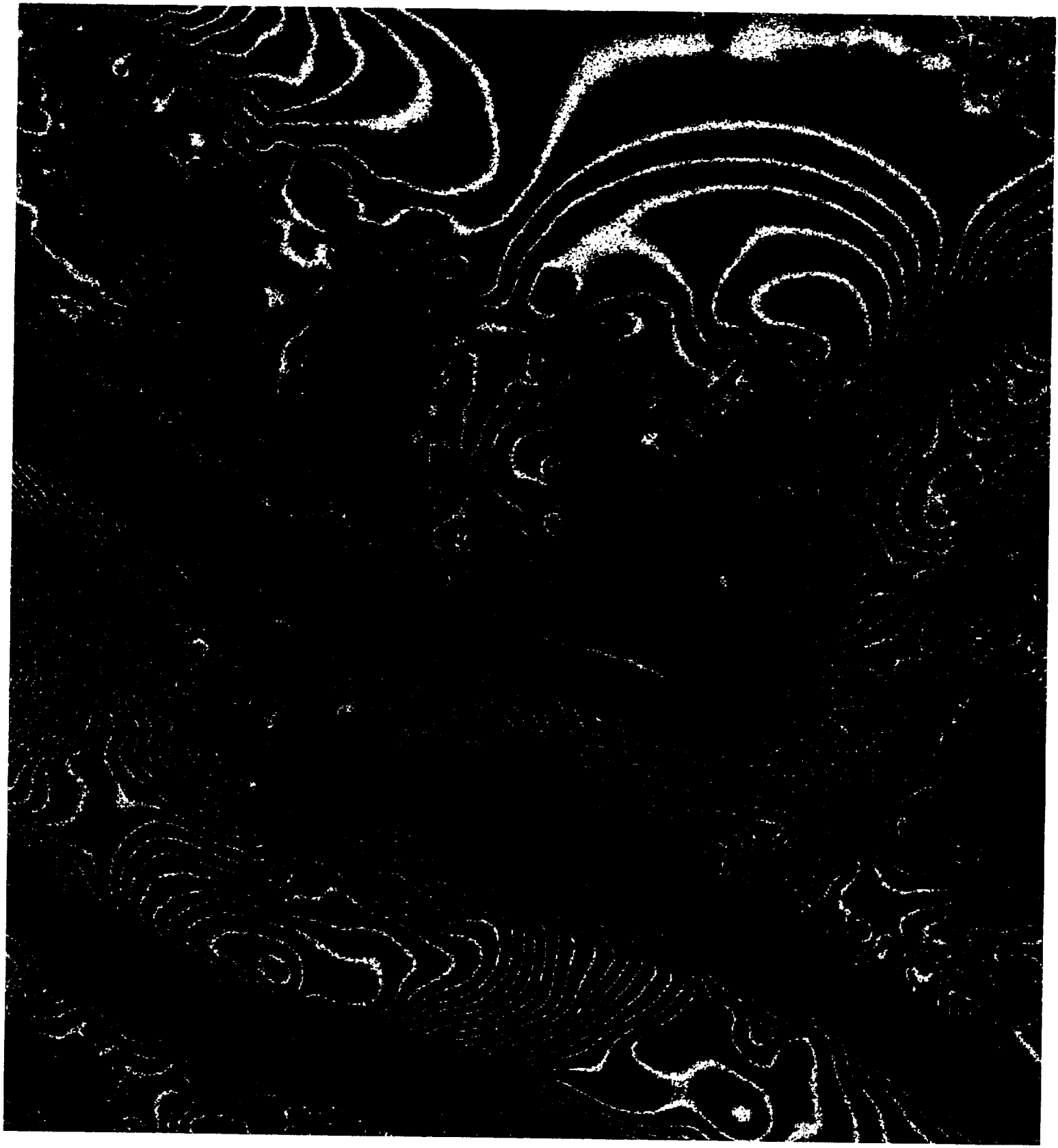

Figure 5-10. Interferogram of Bagley Icefield, Alaska, and tributaries during surge of Bering Glacier (Fatland and Lingle, 1994).

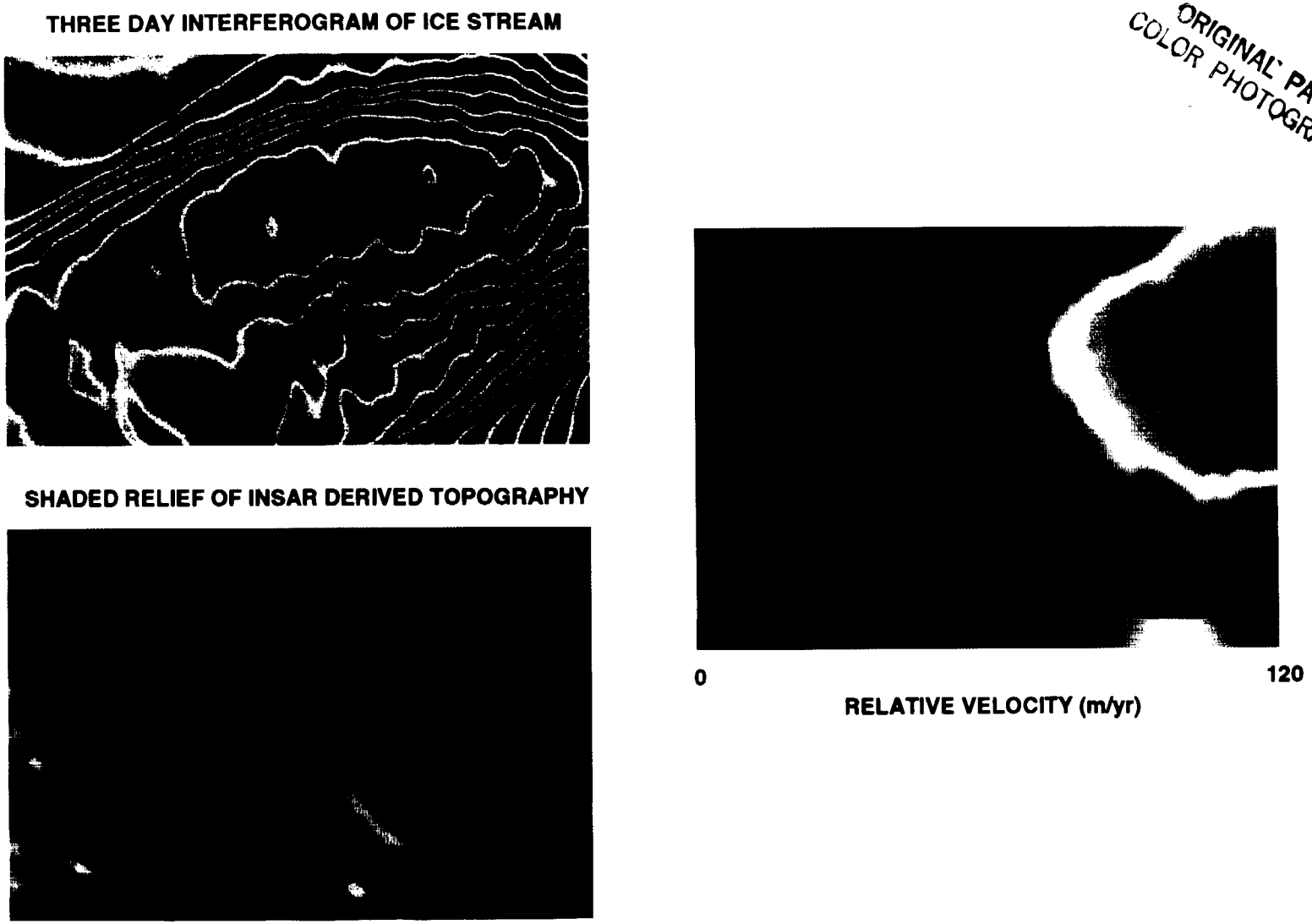

Figure 5-11. Interferogram of 50 km x 50 km area in northeast Greenland with surface topography and velocity components separated (Kwok and Fahnestock, in press).

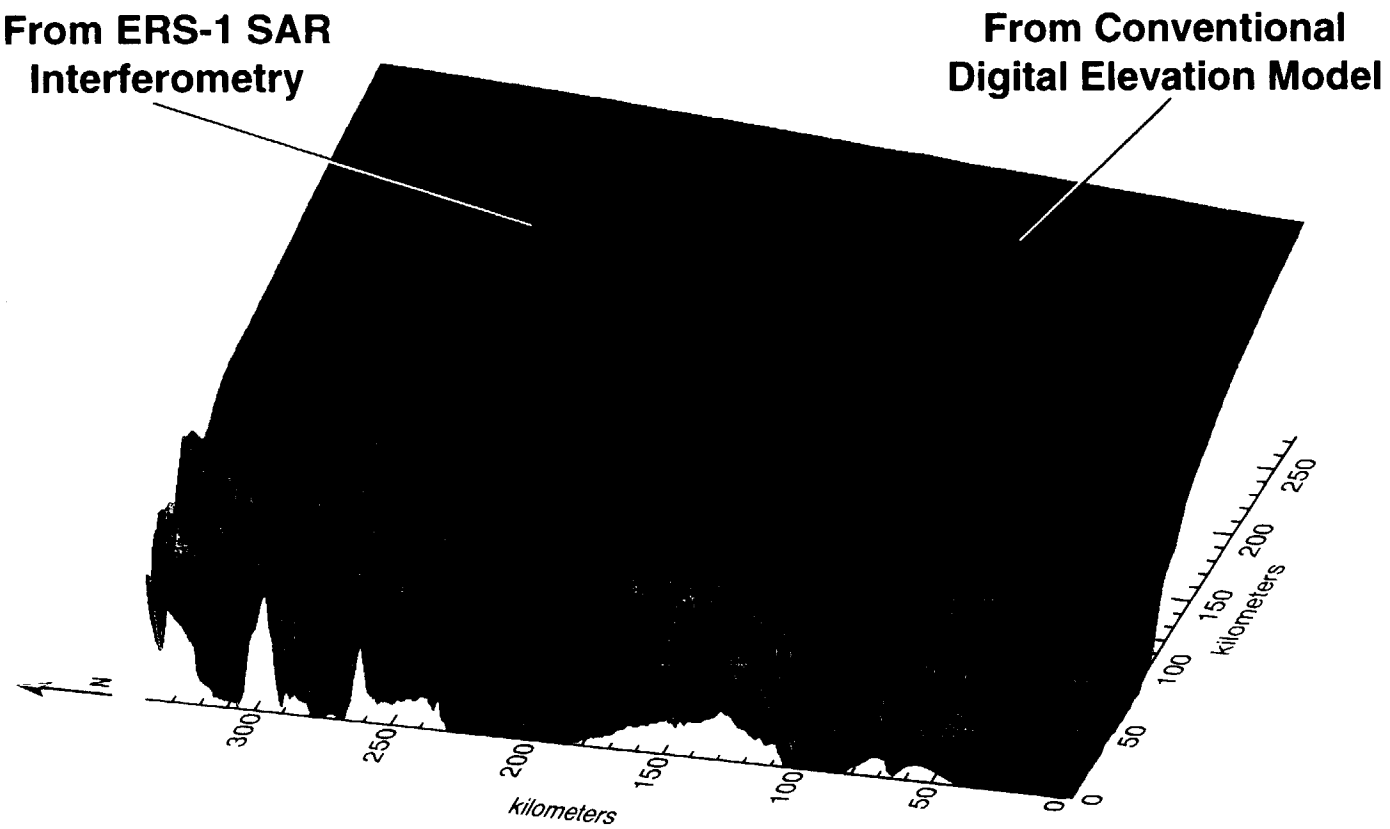

Figure 5-12. Surface topography of western Greenland derived from satellite radar altimetry and SAR interferometry (Joughin et al., 1994).

6—Solid Earth Sciences and Topography

INTRODUCTION

The purpose of this chapter is to delineate key science objectives in the solid Earth sciences for future NASA orbital radar observations. In order to identify a future role for U.S. radars, it is necessary to specify the types of data that are most needed by the community to answer current geological and geodynamics questions, and to describe the surface phenomena that are best studied using radar. In each instance, it is pertinent to lay out a program of radar observations and analyses that would maximize science returns at reasonable cost. The context for this chapter is to identify NASA's future role in orbital radar systems following the successful completion of the SRL-1 and SRL-2 Shuttle Radar SIR-C/X-SAR experiments. In particular, the relative merits of potential U.S. radars compared to the current and future radar systems to be flown by foreign agencies are addressed.

BACKGROUND

Research and discoveries in the solid Earth sciences over the past few decades have revolutionized our understanding of the Earth. For example, we now realize that sea floor spreading and associated continental assembly and breakup are primary modes by which the Earth releases internal heat. These processes also control the locations and nature of volcanism and earthquakes. Study of deep sea sediment cores shows that variations in solar insolation related to changes in Earth's orbit caused Pleistocene glacial epochs. The role of these variations on modulation of the long term changes in Earth's climate remains a hotly debated topic. Research has also suggested long term coupling between tectonics and climate, e.g., the emergence of the Tibetan Plateau modified atmospheric circulation in ways that led to enhanced Indian Ocean monsoons. These enhanced monsoons caused increased weathering on the Plateau, leading to increased consumption of carbon dioxide, and a Cenozoic cooldown of the Earth.

NASA's programs in geology and geodynamics have added significant results to our increased understanding of Earth. For example, GPS and VLBI measurements of the velocities of lithospheric plates are consistent with ages inferred from magnetic striping and geochronologies of oceanic crust. Recently, coseismic vertical displacements of centimeters have been measured using radar interferometry (Massonnet et al., 1993, 1994; Zebker et al., 1994). With regard to continental assembly and break up, 23 digital Landsat scenes were mosaicked, and field and isotopic data were used by Sultan et al. (1992) to reconstruct the Nubian and Arabian Shields before opening of the Red Sea. Results show that the great late-Proterozoic Najd transcurrent fault in fact extends into the Nubian Shield and that the Red Sea opening was accomplished with minimal crustal thinning.

Studies of the solid Earth have also contributed in the area of global climatic change and Earth systems science. For example, Arvidson et al. (1994), using SPOT stereogrammetric analyses, field work, and isotopic measurements, were able to model the evolution of the interbedded Quaternary deposits in the Eastern Desert, Egypt, and to show how eustatic sea level, tectonic uplift, and climate affected landforms and deposits. Brakenridge et al. (1994) have used ERS-1 radar as an all-weather system to monitor flood water levels for the great midwestern U.S. floods of 1993.

Lacking in many of these studies of the solid Earth is a detailed knowledge of the topography of the landscape, or the rate of deformation of the surface due, for instance, to earthquakes or

active volcanism. It is with this background of solid Earth sciences that measurement objectives for SAR are delineated in the following sections. Because of the increasing national relevance of natural hazards, we also include objectives related to predicting and observing hazards and monitoring their aftermath.

CONTEXT FOR U.S. RADAR MEASUREMENTS

The U.S. Global Change Research Program (GCRP) identified several key solid Earth processes that have a bearing on Global Change. These topics include several that can be investigated with orbital radars: coastal erosion, volcanic processes, surficial processes, and crustal motions and sea level change. The radar systems on board ERS-1, JERS-1 and, in the future RADARSAT and ERS-2, are generally adequate for mapping these phenomena over large regions of the Earth on a routine basis. Where an image in a timely manner is all that is required, these single-wavelength, single-polarization radars can be successfully employed for a wide variety of solid Earth applications, including mapping river flooding (Brakenridge 1994), mapping remote volcanoes that are frequently masked by clouds and long polar nights (Rowland et al., 1994), and paleo-drainage features in deserts (McCauley et al., 1982).

Almost all solid Earth sciences studies benefit from knowledge of topography, where the required resolution depends on the specific study, but generally in the range of 25–30 m spatial and 2–5 m vertical (Figure 6-1). The measurement of topography and topographic change with orbital radars has been demonstrated in a few limited cases (Figure 6-2), but in general this technique is still in its infancy and only limited research has been done on the validation of the data sets. With the exception of a one year time-series for the Landers earthquake in California (Massonnet et al., 1994), no long-term studies of ground deformation have been done with radar interferometry. However, we know from GPS measurements made at permanent sites (e.g., Figure 6-3) that surface displacements at rates of ~3 cm/yr. can occur in volcanic and tectonic environments. Topographic data can be used to calculate local slopes (Figure 6-4), the volumes of landforms (e.g., volcanic cones, river valleys, or sand dunes). Surface displacement may take place due to the rupture of a fault line or the growth of a volcano. In Solid Earth science it is the measurement of topography and topographic change that we consider to be NASA's role in imaging radars; these topics are the most innovative and technologically challenging, while at the same time they also offer the greatest scientific advances.

Radar also offers geologic information on surface properties through the strength of the back scattered radiation at whatever combination is used of frequency, incidence angle, and polarization state. The greatest degree of information is obtained with multiple frequencies, incidence angles, and the full Stokes scattering matrix (van Zyl, 1989). This extensive information is important in studies of surficial deposits and materials because it allows characterization of the scattering process and separation of dielectric constant from textural parameters. The multi-frequency component of radar studies in deserts is important because the different wavelengths penetrate to different depths beneath the surface, thereby providing a crude 3-D view of buried drainage basins in areas such as the Sahara Desert.

Scattering information is important in studies of surficial materials and processes in vegetated areas, e.g., recovery of scoured and sand-covered areas from the 1993 midwestern U.S. floods. In this latter case, herbaceous grasses are encroaching on the affected areas, as are stands of cottonwoods. Multi-temporal polarimetric SAR at C, L, and P bands allow mapping of the vegetation density and character, and show how the underlying surfaces are changing by wind and water-related processes (see Chapter 2-Ecology).

SCIENCE THEMES

Topographic Mapping and Crustal Motions

Considerable excitement has been generated by interferometric SAR investigations of the 1992 Landers earthquake in California (e.g., Massonnet et al., 1993; Zebker et al., 1994). Indeed the detection and quantitative investigation of ground deformations resulting from an earthquake or a volcano holds great promise for the Earth science community (Mouginis-Mark, 1994). The ability to use orbital radars for topographic mapping and topographic change detection is viewed as the single most important role that a new U.S. radar mission could play, not withstanding other important contributions that the data from such a system could provide for regional mapping and quantitative studies of surface backscatter characteristics.

Topographic data have been generated by combining data for Long Valley, California, from the SRL-1 and SRL-2 missions (Figure 6-2). In this instance, the radar interferometric data can be used to aid in the visualization of geologic features such as mountain ranges and fault zones. The topographic data derived by radar interferometry are also inherently more useful than data derived from stereo air photography because the derived digital elevation model (DEM) is self-consistent. Moreover, the interferometry technique works well in areas of low topographic relief where classical stereo methods tend to fail because tie points cannot be identified.

To develop topographic change maps requires an additional level of knowledge of the surface and local meteorology. A preliminary comparison of SRL-1 and SRL-2 data at the Kilauea, Hawaii volcano area (obtained in April and October 1994) shows variations in phase at a scale of 20–50 km (Figure 6-5) that are currently interpreted as anomalies due to the local weather. This effect is more clearly seen in data collected during the last four days of the SRL-2 mission. Here, phase variations equivalent to surface displacement of a few centimeters appear on successive days, but are absent when data two or three days apart are viewed (Figure 6-6). Although parts of the surface can be seen to be entirely decorrelated due to the eruption of new lava flows (Figure 6-7), the regional trends in phase shift (Figure 6-6) have the morphology and size that are typical of rain cells in this area. Thus, local meteorology may have an important influence on the analysis of radar interferometry data. Such effects cannot be avoided, but they can be quantified by the use of a GPS array on the ground to provide the wet atmosphere delay, or by the inter-comparison of several radar scenes collected in a period of about 1 week.

An important difference in approach to the exploitation of the radar interferometry method for studying ground deformation exists within the Solid Earth Panel. For dry environments, it is clear that the 3-day repeat orbit of ERS-1 was very useful as a demonstration of radar interferometry over arid areas and dry glaciers. This very short time meant that radar data could be correlated even in vegetated regions. In regions where fast growing vegetation is found, a time gap of 8 days appears to be the longest interval between observations that can be tolerated. However, unpublished work by Zebker et al. (1993) with ERS-1 data for volcanoes in Alaska has failed to produce the radar correlation even using 3-day repeat coverage. Snow and ice, and potentially wind disturbing the surface, conspire to prevent ERS-1 data being used in this setting. In addition, the 23° incidence angle produces severe lay-over on steep topography. In arid zones, however, the 35-day repeat period (achieved during the non-ice mapping phase of the ERS-1 mission) and much longer repeat cycles are tolerable for interferometry. An ERS-1 quality radar is adequate to detect such movements, provided that before- and after-event images are available. Furthermore, while the 3-day

repeat of ERS-1 is useful for interferometry experiments, this mode of operation is a compromise concerning coverage and repetition. Only a small percentage of the Earth is covered in the 3-day repeat mode (~10% coverage compared to that achieved with the 35-day repeat). In addition, the "ice mapping phases" of ERS-1 have been limited to the period between January and March, so that the interferometry coverage available for other parts of the world may not have the appropriate temporal coverage. The ability to collect topographic data from radar interferometry in one pass using a pair of antennas (which is the method used in the TOPSAR airborne system) is an excellent way to avoid the problems of temporal decorrelation of the surface: the interferogram is constructed from data collected in a single pass. There are exciting possibilities in using a boom-mounted second antenna on the Space Shuttle to collect near-global topography during a single mission (SRL-3). This technique is described in more detail below.

Numerous issues remain regarding the type of radar observations that are needed to enable radar interferometry experiments to be successful. Unless a two-antenna interferometer is flown, the temporal frequency of the repeat-pass, the errors due to ionospheric perturbations and atmospheric water vapor, and the surface characteristics are all believed to be important. None of these issues have been rigorously investigated. We can draw on the experience with the ERS-1 and SIR-C/X-SAR missions to make some recommendations for the use of future radars, including the possible reflight of SIR-C/X-SAR as SRL-3. However, it is clear that a combination of orbital radar observations and GPS measurements in the field are both required for geodynamics and topographic analyses for two reasons. First, as was demonstrated with the analysis of the Landers earthquake data (Zebker et al., 1994), the radar-derived deformation map provides only line-of-sight changes with poor temporal resolution. GPS data from well monumented sites are needed to provide the 3-axis ground movement and to provide a continuous record of ground deformation against which the radar data can compared. Second, the neutral atmosphere will have a significant effect on the radar interferometry because the moisture in the atmosphere can induce a time delay equivalent to ground movement up to ~30 cm, which is far in excess of the ground movement that is typically expected along fault lines (except during catastrophic rupture) or dormant volcanoes. New techniques have been developed that use the time delay information contained within the GPS signal to determine the water vapor content of the atmosphere (Bevis and Bussinger, 1994 unpublished data). If such measurements were to be obtained concurrent with imaging radar data for an interferometry experiment, it would be possible to remove this uncertainty in the resultant radar deformation map.

Regional Mapping

There is considerable interest in the geology community for a radar mission that is devoted to mapping as much of the Earth's surface as possible. Radar's ability to penetrate thin sand layers in desert environments has been known since the first Shuttle radar experiment (SIR-A) back in 1981. In desert environments, the applications of a radar (whether multi-wavelength and polarization or single wavelength and polarization) are numerous, and include ground water hydrology (both its development and remediation), mineral exploration (including deposits of economic value such as gravels and clays), paleo-drainage mapping that can serve as indicators of climate change, and archeological research (Figure 6-8). In many other types of geologic settings, comparable mapping mode radar data would also serve to characterize the Earth's environment for comparison with future radar and (in areas that are not frequently cloud covered) Landsat data. In this way, a radar data base would be established that is equivalent to the 20-year record of Landsat images, except that many new areas, such as Indonesia, West Africa, and the Kurile/Aleutian Arc would be imaged.

This approach could be particularly beneficial for inter-disciplinary studies related to glaciers and the hydrologic cycle. Preliminary results for the two SIR-C/X-SAR experiments have shown that numerous features associated with glaciers in the Andes can all be mapped. Through the identification of moraines, pressure ridges, outflow channels, and the snouts of the ice sheets as a function of time, the water balance of the glacier can be determined. This in turn helps in the analysis of the hydrology of the region and has importance for the analysis of climate change, since the glaciers are sensitive indicators of the net loss or build-up of ice due to changes in the local climate.

In each of these instances, it is hard to argue for the need for a new U.S. radar. The issue is really one of regional data coverage, rather than the specific attributes of a SIR-C/X-SAR class radar. Many parts of the world have not been imaged by radar because the ERS-1 spacecraft lacks a tape recorder, and so has to rely on a series of ground stations for direct broadcast of the data. With the advent of RADARSAT in 1995, such a limitation will disappear. In addition, it would be far more economically practical, if the community were to rely on ERS-1 and its successor ERS-2, to establish new ground stations (which cost <1% of a new satellite) to capture additional data over parts of the world where radar data are currently lacking.

Quantitative Lithologic Mapping with SAR

The effects of long- and short-term geologic processes on the Earth's surface are expressed as gross compositional (lithological) differences between rock types, as more subtle within-lithology variation (sedimentary facies, sedimentary structures, facies migration, igneous phases, and hydrothermal alteration), as weathering products and soils, and ultimately as differences in the geomorphic configuration of the land surface (Sparks, 1971). Lithologic mapping potentially can provide information crucial to diverse issues such as desertification, natural resources (oil and gas, minerals, and water); and natural hazards such as volcanoes, earthquakes, and environmental contamination.

Traditionally, optical remote sensing has been used to directly characterize lithology on the basis of composition. There are numerous successful case studies in the published literature. Most of these studies, however, only consider composition at the molecular level, and do not take into account the gross geomorphology of the surfaces being studied. In addition, single-frequency SAR data has long contributed to structural and geomorphic mapping (see Sabins, 1987, for examples). Approaches for the extraction of lithological information usually consist of photo interpretation (including stereoscopic viewing when available). While lithology typically can not be mapped directly without additional information, photogeologic methods still present one of the most valuable approaches towards extracting geologic information from radar data.

The new generation of polarimetric, multi-frequency SARs such as the JPL AIRSAR and SIR-C/X-SAR systems, provide more powerful tools for extracting lithologic information from radar data and for supplementing optical remote sensing determinations of lithology. Because SAR systems interact with the Earth's surface on the 1 to 100+ cm scale, rather than the molecular scale, direct mapping of lithology based on composition is not possible (Elachi, 1987). Radar return is primarily controlled by the relationship between the radar wavelength and the scale of surface roughness with respect to the radar signal (cm-scale relief). Fortunately, the surface morphology of geologic materials is often related to the composition and weathering characteristics of the materials forming the surface. Figure 6-9 shows an example of this, where the roughness of alluvial fan surfaces may be related to the parent materials and the climatic conditions under which the fans formed. If a fan has an average vertical relief of 6 cm, then it might appear smooth (dark) to an L-Band radar system or

rough (bright) to an X-band system. Additionally, the multi-frequency nature of these systems allows for theoretical modeling and extraction of quantitative surface roughness based on inversion of the models. Several investigators have used AIRSAR data and model inversions to identify areas with varying surface roughness (van Zyl, 1989; van Zyl et al., 1991; Evans et al., 1992; Kierein-Young, 1993; Kierein-Young and Kruse, 1992). The multiple wavelengths acquired by the AIRSAR and SIR-C/X-SAR systems are critical to successful lithologic mapping using surface roughness parameters, and such an analysis would not be possible with any of the current or planned foreign radar systems.

Analysis of Geomorphic Processes

Quad-pol radar data are also needed to investigate the relationship between radar backscatter and aerodynamic roughness. Although the original motivation for this study was the analysis of sand and dust transport (still valid), the method can also be extended to include climate modeling. In particular, general circulation models (GCMs) currently use only 2 or 3 (e.g., land and ocean) values of aerodynamic roughness, simply because there have been no easy means for getting good values. Yet Sud et al. (1988) have shown that by adding more values (e.g., land, ocean, and desert), GCM predictions change drastically in terms of precipitation, wind regime, etc. Consequently, the work of Greeley and coworkers holds promise as a technique for mapping large areas to derive aerodynamic roughness values for input to the next generation of general circulation models.

The ability of wind to initiate dust and sand storms is dependent on the roughness of the surface at the sub-meter scale, measured by the aerodynamic roughness (Z_0). This parameter is a measure of the drag imposed by the surface on the wind and is therefore important also in general circulation models (GCMs). For dry, unvegetated and relatively flat surfaces, the radar backscatter coefficient (sigma-0) is a function of surface roughness at a scale comparable to the radar wavelength. Studies by Greeley et al. (1988, 1991) and Blumberg and Greeley (1993) have shown that there is a correlation between sigma-0 and Z_0. Blumberg and Greeley (1993) developed a model to estimate Z_0 from radar backscatter coefficients using AIRSAR data and found that the best correlation is with L-Band cross-polarized data. Concurrent measurements with specialized micro-meteorology masts (Figure 6-10) to measure the wind speed, wind direction, and temperature through the lower portion of the atmospheric boundary-layer, calibrated data from SRL-1 for Stovepipe Wells, Death Valley, were analyzed. These models were then applied to SRL-1 data, and an estimate of Z_0 was computed. Results show that the models could predict Z_0 very closely when using calibrated data (Figure 6-11).

These observations are important because they demonstrate the importance of obtaining calibrated, multi-wavelength and multi-polarization radar data. Use of ERS-1 or RADARSAT data (both C-Band single polarization systems) would not have enabled the same degree of characterization of the eolian roughness of the surface to have been determined.

Orbital radars have also been used to map river flooding and have been recently demonstrated by Brakenridge et al. (1994). In late spring and summer of 1993, the Upper Mississippi River experienced record-setting heavy rainfall. Wisconsin, Iowa, and Illinois experienced the wettest June–July period on record since 1895. In Iowa, measurable rainfall fell somewhere in the state for 33 consecutive days from June 22–July 25. Unusually heavy rains occurred in July, a month that is more commonly characterized by regional moisture deficits.

The radar was used to delineate the flooded agricultural fields along the valley floor and areas of unflooded agricultural land and flooded riverine forest. However, the flood stages determined from ERS-1 scenes lack close-interval sampling in time, and they are not as accurate as in-situ recording gages. The satellite data nevertheless offer an important spatial perspective for particular moments in time. Instead of a continuous local record of rising or falling stage, a single ERS-1 image is a time-instantaneous, spatially continuous portrait of flood stage along as much as 100 km of valley reach. Given favorable flood plain morphology for measuring flood stage, longitudinal profiles of the instantaneous flood surface can be constructed. For this type of investigation, short repeat-time coverage is crucial. This coverage might be achieved using different satellites (e.g., ERS-2 and RADARSAT) or a spacecraft in a short-repeat orbit (although the 3-day repeat of ERS-1 will leave many geographic areas out of the field of view for this part of the mission). RADARSAT could also provide rapid site-revisit capability, provided that the selection of identical viewing geometries is not a requirement.

HOW COULD A NEW U.S. SAR CONTRIBUTE TO ANSWERING THESE SCIENCE QUESTIONS?

Capabilities of Current Radars

For many aspects of the Solid Earth research, mapping from single radar images is adequate for the identification of spatial information and general lithologic characteristics. Given the continuing series of radars that will be launched through 2002 (i.e., ERS-2, RADARSAT, ENVISAT ASAR, and ALOS), it does not appear to be cost effective for NASA to fly a comparable radar system. Increasingly, it is appropriate for U.S. scientists to draw upon international partners to provide these imaging radar data sets.

However, these foreign radars have limited capabilities; this means that they are not ideal for making interferometric measurements for three main reasons:

(1) The orbital characteristics of these radars are not optimized for the collection of interferometric data. No foreign radar is planned that would perform the single-pass interferometry for topographic mapping (comparable to the ideas for SRL-3 described below), so that exact-repeat orbits would have to be used. In this case, the exact-repeat frequency varies from 3 days (for selected areas) with the ice-mapping phase of ERS-1 to 24 days for RADARSAT and 35 days for the mapping phase of ERS-1. In the short-term (for about one year), this situation will improve because of the tandem flight of ERS-1 and ERS-2. Exact-repeat coverage will be achieved within one day, but the site-revisit time, within which a second set of measurements can be made, will still be either 3 days (limited areas) or 35 days (global coverage). These long-repeat times mean that surface decorrelation may take place between observations (precluding topographic or ground deformation mapping) and that transient events may be missed entirely. A further issue is that the orbit of the spacecraft may not be known to sufficient detail that the baseline distance between successive orbits can be calculated for the interferometry experiments.

(2) Single wavelength/single polarization radars (including all the planned foreign radars) cannot be used to routinely determine surface topography and topographic change due to the unknown influence of the ionosphere on the time-delay of the radar signal. As is the case with VLBI measurements, the ionospheric delay can be uniquely resolved with two wavelengths. This effect can be reduced by collecting the radar data at night, but this would limit the coverage and site-revisit frequency. In addition, multi-wavelength measurements enhance the probability that radar interferometry experiments can be

conducted because they allow a wider range of baseline distances to be considered (X-band measurements require a separation of a few tens of meters, C-band a few hundred meters, and L-band about 1 km).

(3) From the analysis of the SIR-C/X-SAR data, it is clear that for many parts of the world the cross-pol radar data (at both C-Band and L-Band) are much more useful for the analysis of the surface morphology than like-pol (HH or VV) data. No foreign radar has this cross-pol capability, so that lithologic mapping with ERS-1, RADARSAT, or JERS-1 is more difficult than with SIR-C/X-SAR.

It is in this context, where no foreign radar is ideal for interferometric studies, that the idea of flying SRL-3 with an attached boom to conduct single-pass interferometry is so exciting. Indeed it is believed that flying this mission concept would dramatically advance the Earth Science Community's understanding of the planet. While the details of the capabilities of a boom-mounted system are still being investigated, the inherent height accuracy of the proposed X-SAR radar interferometer would be better than 5 m vertical at a spatial resolution of 25 m/pixel. What is truly exciting is the opportunity to collect an almost global (equatorward of 62°) topographic map using the wide-swath (SCANSAR) mode, which provides 50 m/pixel resolution and a height accuracy better than 20 m. In addition, a complete radar image of the world between 62°N–62°S would also be obtained, thereby providing a benchmark data set against which future global change could be measured. The combined use of X-band at high spatial resolution and C-band in SCANSAR mode would enable the quality of the two DEMs to be tested against each other, as well as provide the regional framework (SIR-C) for detailed local (X-SAR) studies.

A major advantage of the SRL-3 topographic mission is that all of the topographic data would be referenced to a single topographic datum. Until now, the reference surface for maps from one continent do not match the datum for another continent (Figure 6-12). Particularly for long-wavelength (>1,000 km) studies of the gravity field and structure of the Earth, it is crucial to use a common datum (typically the geoid). The SRL-3 data would naturally be referenced to the Earth's geoid. Thus, a whole new range of geophysical and geodynamics studies would be possible that currently cannot be rigorously attempted.

It is our opinion that there is a major leadership role that NASA can play by flying the SRL-3 mission using a second boom-mounted antenna to perform single-pass interferometry. The data set so collected could be one of the most valuable and widely used data sets NASA has ever collected, and would serve as a benchmark data sets for decades to come. In particular, this data set would meet and exceed NASA's commitment to provide a global digital topographic data base in support of the Earth Observing System (EOS) with the added bonus that these data could be made available to the community prior to the launch of the EOS A.M.-1 platform. Synergism between the topographic data set and other information (e.g., Landsat, MODIS, ASTER images) would greatly facilitate studies dedicated to hydrology, ecology and land use.

Development of a New U.S. Radar Satellite

Development of the future U.S. radar system should be seen as incremental in implementation, starting from the existing aircraft TOPSAR system and the SRL-2 interferometry experiments, and ultimately leading to a long-duration free-flyer. Logical steps to achieve this goal are:

(1) Continue the experimental studies of radar interferometry for topographic mapping using the aircraft TOPSAR system. Much remains to be understood about the accuracy

of topographic measurements at the meter to tens of meter scale, and the effects of different ground covers (e.g., vegetation vs. bare rock) and regional slopes. A comparison between the topography determined at more than one wavelength (including the effects of atmospheric water vapor on the time delay of the signal) can best be investigated under the controlled conditions of the TOPSAR experiments. In addition, the science community needs a short-term data source to develop expertise in the analysis of high spatial resolution topographic data sets.

(2) The use of a boom-mounted antenna on the SRL-3 Shuttle mission. As described above, this new technology provides the capability to map the Earth's topography (and provide an image) for all the land between 62°N and 62°S using single-pass interferometry.

(3) A free-flying radar could be constructed from the existing SIR-C/X-SAR hardware, and placed into orbit by the Shuttle for a 1–2 year mission. This mission concept has the advantage that most of the radar technology has already been developed, but the disadvantages are that the orbital inclination will be 57° due to the Shuttle launch, and the altitude will be relatively low (resulting in a short-duration mission). However, this orbit enables the ascending and descending orbits of the Shuttle to observe the same point on the ground from almost orthogonal aspect angles. The complete 3-D topography could therefore be mapped: Slopes will be well determined in at least one of the two pairs of scenes. This capability will not be available through the ERS-1 and ERS-2 spacecraft because the near-polar orbits means that the ascending and descending ground tracks intersect at narrow angles.

(4) The ultimate goal should be to launch a free-flying radar into a near polar (for global coverage) with a short (<3 day) exact repeat orbit for rapid site-revisit capability. This system would augment the data base collected by the SRL-3 mission or, alternatively, if SRL-3 is not flown, would establish a baseline topographic data set in its own right. The key difference would be that the coverage would be global as the spacecraft would be placed in a polar orbit, and that the spatial resolution would be uniformly high (as opposed to some areas having the 50 m/pixel coverage provided by SIR-C operating in SCANSAR mode).

In order to avoid surface decorrelation, this free-flying radar should have two antennas so that single-pass interferometry can be achieved. The parameters of this radar should include at least two different wavelengths (to compensate for the ionosphere) and have a variable incidence angle (to permit rapid retargeting of the antenna, as well as reduce lay-over in areas of high topography). Mission duration should be at least 3 years to enable the derivation of a global topographic map followed by monitoring for ground deformation at selected sites.

This mission concept, with two antennas flying on co-orbital platforms, has a great advantage. Interferometry experiments can be conducted for the Solid Earth investigations, and the same spacecraft can also be flown to conduct along-track interferometry that will be of great value for the analysis of ocean surface phenomena. We therefore see strong synergism between the Solid Earth Sciences/Topography and Marine Applications recommendations.

RECOMMENDATIONS

(1) Flying SRL-3 with a boom-mounted second antenna to perform single-pass topographic mapping would not only produce a quantum leap in our understanding of the world's topography, but would also represent a significant technological challenge in radar

interferometry. To have the greatest value, SRL-3 should include both X-band and C-band interferometers to collect high and low resolution data, respectively. It is clear that the imaging data will also have great long-term value for global change studies, independent of the topographic mapping. This mission concept offers outstanding possibilities for enhancing NASA's standing in the international radar community at relatively low cost and in a short time frame (the SRL-3 mission could fly within two years).

(2) Continue to fly the NASA airborne TOPSAR/AIRSAR. This airborne system is crucial for continued interferometry algorithm development; the TOPSAR hardware is seen as the vital test-bed to develop new interferometric techniques that ultimately will be tried on spaceborne systems.

(3) NASA needs to support a vigorous data analysis program using the SRL-2 exact-repeat data set. Data obtained during the last four days of the mission will enable proof-of-concept studies in interferometry over an adequate variety of targets. More importantly, different radar baselines and the effects of local meteorology on the phase data can be investigated with this short-repeat coverage.

(4) Utilize data from non-US radar systems to pursue science objectives to the extent that these systems acquire relevant measurements, cause they will be there and we can do some good science. This capability would be significantly enhanced if there are additional ground stations established around the world to take advantage of the tandem mission of ERS-1 and ERS-2. A crucial component of this work with foreign radars is the need for a U.S. investigator team to be funded to work with the data.

(5) NASA should begin to build a free-flyer satellite with interferometric capability and cross-polarization and multiple incidence angle (nominally 20–45°) capabilities, to maintain U.S. involvement in unique and important ways. Results from this type of experiment promise to revolutionize several fields of study related to topography and topographic change. Single-pass interferometry is seen as the only way to avoid meteorological errors in the phase data, and a two wavelength SAR is needed to remove ionospheric effects. This same instrument has a very high probability of making quantum leaps in our understanding of Solid Earth and Oceanography sciences, as well as serving as an excellent tool for hazard mitigation studies.

Part of such a mission should have strong international participation so that more than one spacecraft could be used to reduce the time interval between observations. A significant component of such a mission could be dedicated to disaster-monitoring once a baseline data set has been constructed. The ability of the radar to have a wide swath width (up to 500 km at degraded spatial resolution) and the capability to image any point on the Earth's surface through the use of a steerable antenna enhances the possibility of imaging the surface during the event (such as river flooding), rather than just obtaining data once the physical process is over.

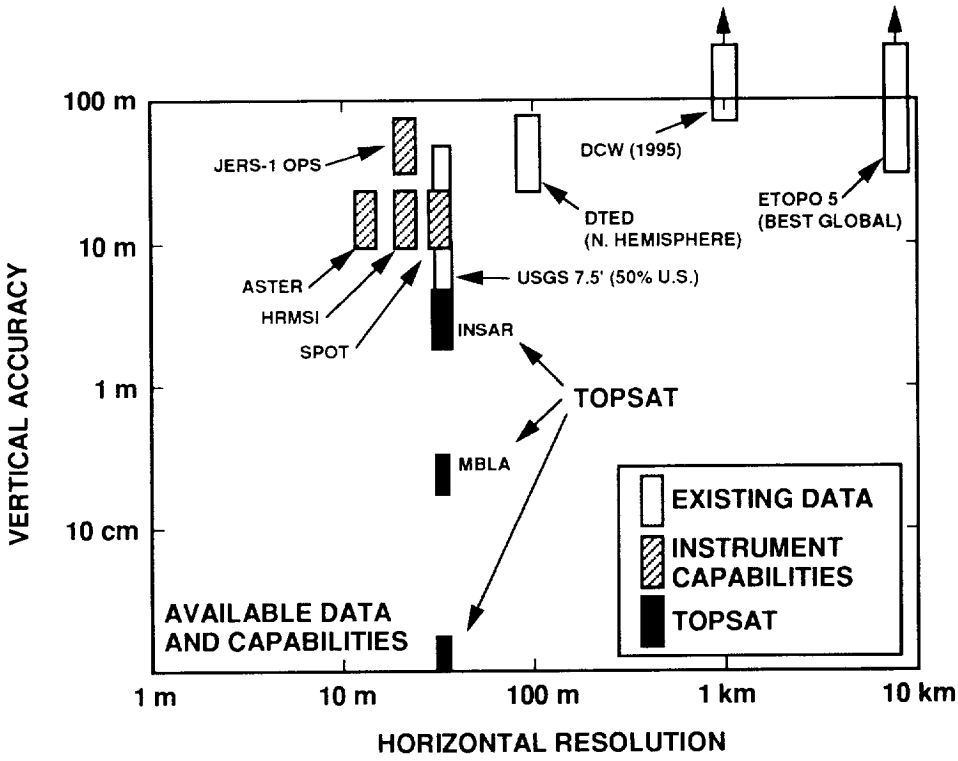

Figure 6-1. a) Summary of the spatial and vertical accuracy of topographic data that are required for various solid Earth science investigations.

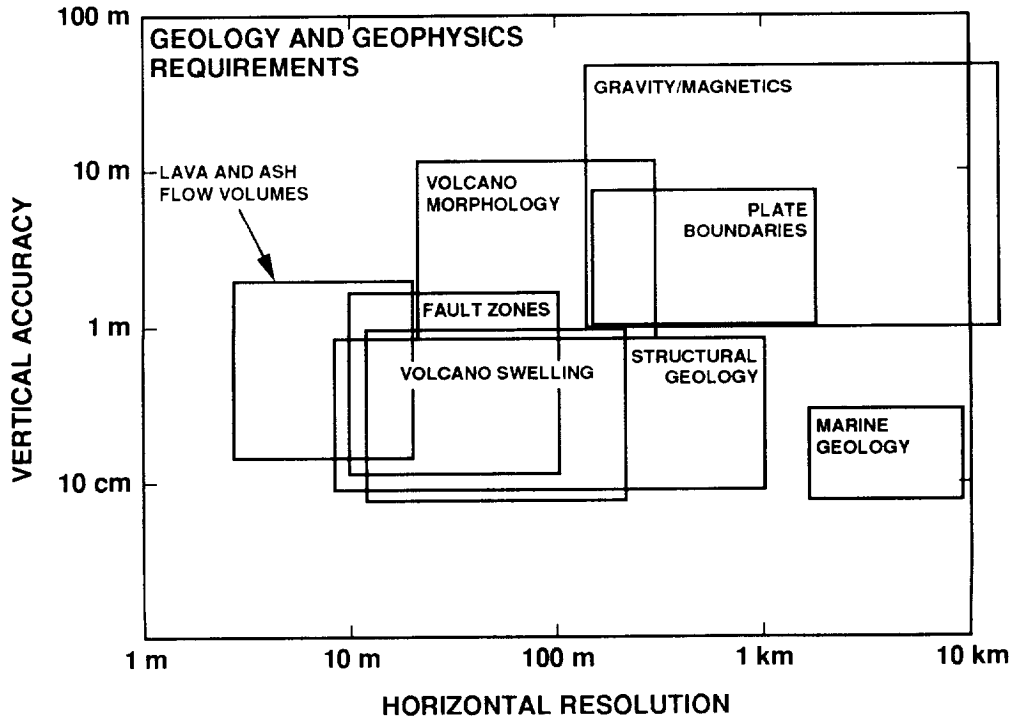

Figure 6-1. b) Summary of the availability of topographic data at various horizontal resolutions and vertical accuracies, as will be measured by various future spacecraft and conventional topographic data bases.

ORIGINAL PAGE
COLOR PHOTOGRAPH

Figure 6-2. Long Valley region of east-central California acquired by SIR-C/X-SAR interferometer.

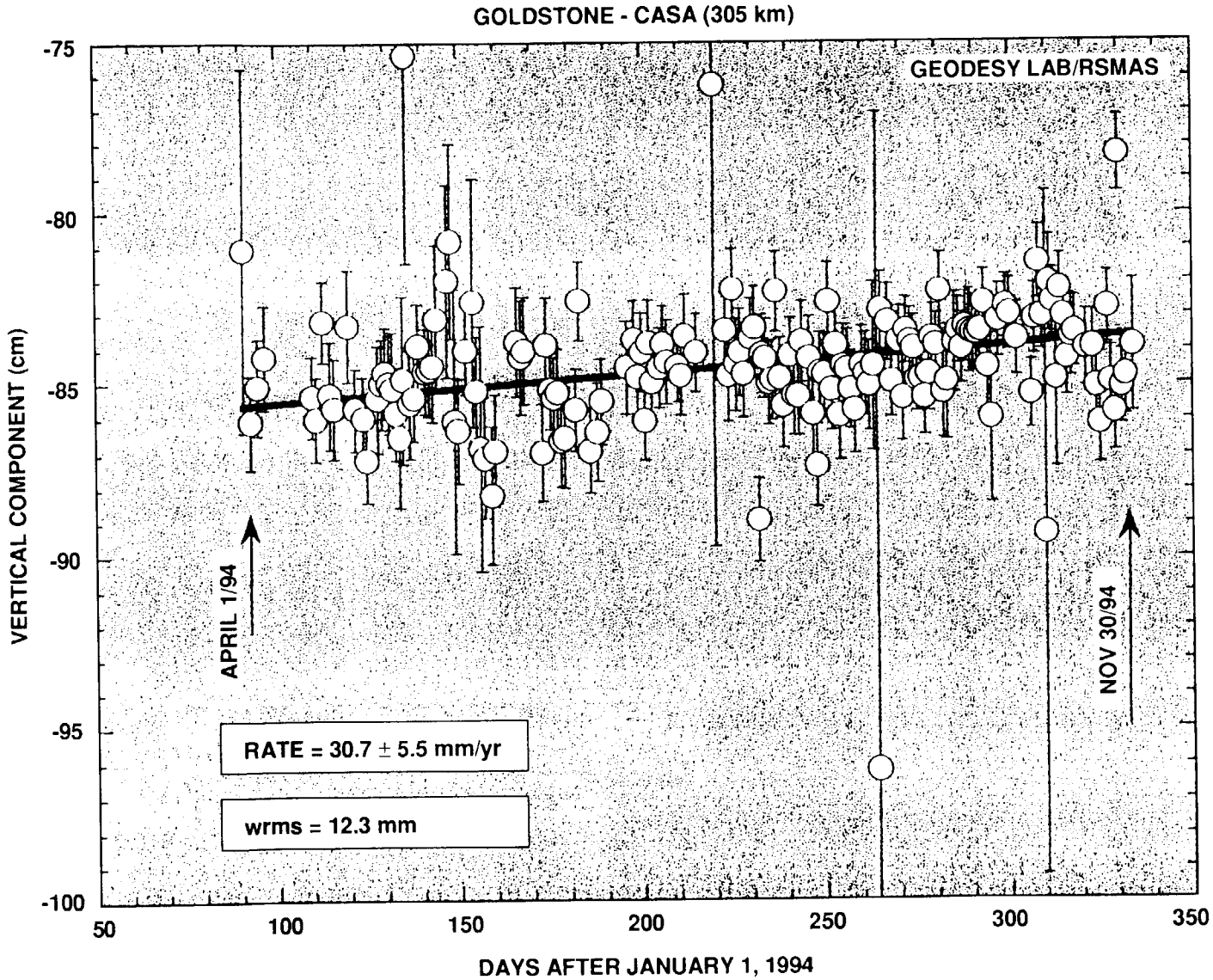

Figure 6-3. Vertical deformation at Long Valley, CA, as recorded by a permanent GPS station. Vertical movements of this magnitude are the type that need to be measured by any technique (such as radar interferometry) in order to understand the geologic process and mitigate natural hazards. Unpublished data from T. Dixon, 1994.

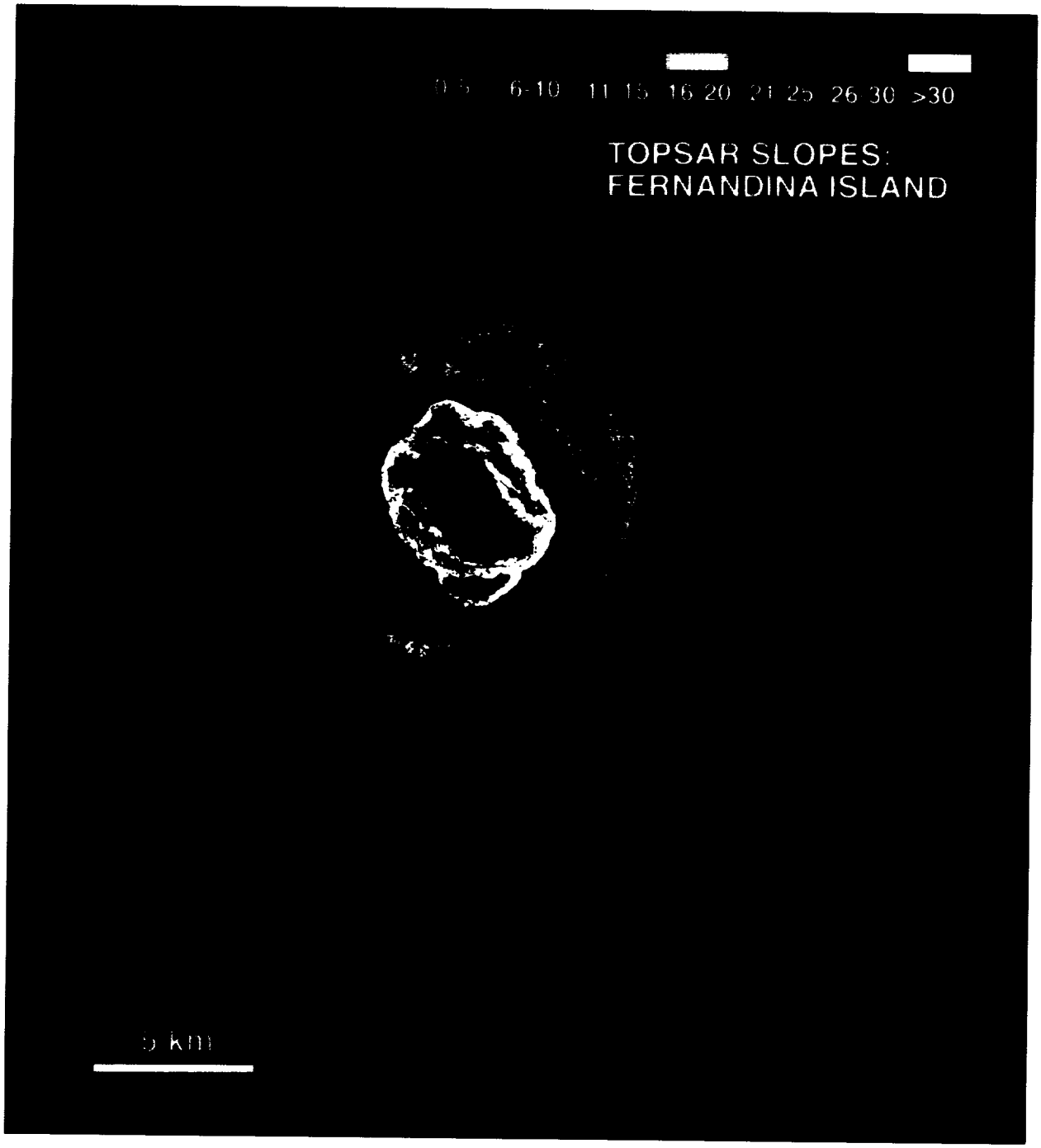

Figure 6-4. This map was prepared from TOPSAR airborne interferometry data obtained over the basaltic shield volcano Fernandina in the W. Galapagos Islands. The first derivative of the digital topographic data (obtained at 10 m/pixel resolution) has been calculated for an area 30 x 30 m in size so that the variation in slopes on the volcano can be identified. Here we see that the upper slopes on the outside of the caldera can exceed 30°, while the flanks near the coast all have slopes less than 5°. This type of analysis lends itself very well to many types of geomorphic studies (including an analysis of drainage basins, mountain ranges, and volcanoes), and is well suited to the regional view of topography that would be provided by an orbital radar interferometer.

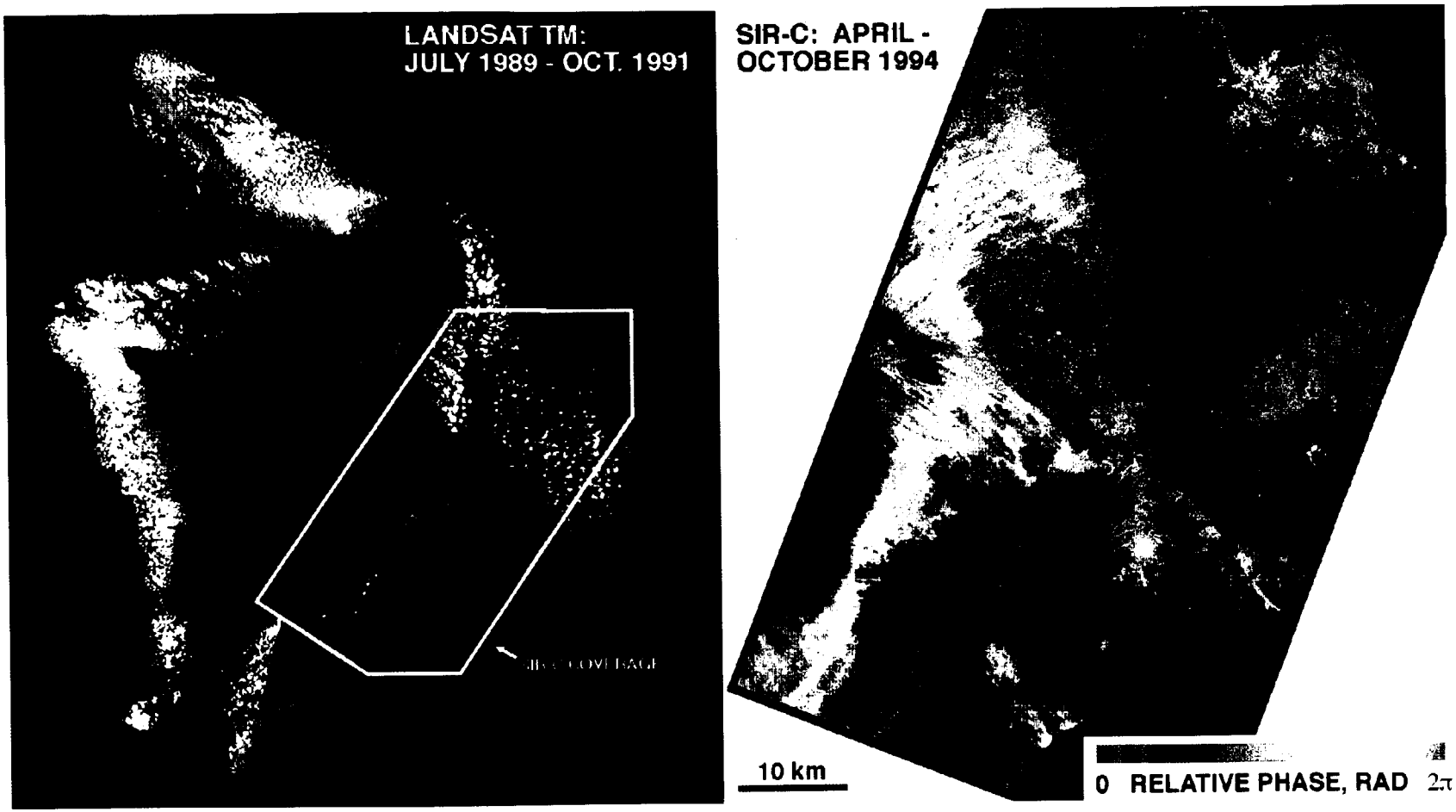

Figure 6-5. A comparison of radar phase data collected over Kilauea volcano, Hawaii, between the SRL-1 (April 1994) and SRL-2 (October 1994) missions illustrates some of the problems in using this technique in tropical settings. At left is a Landsat Thematic Mapper image of the Big Island of Hawaii showing the location of the SIR-C/X-SAR data. At right is the L-band (24 cm) phase data collected on single orbits (Data Takes 68.0) between the two missions. Notice the broad (10-20 km) variations in phase that are probably due to meteorological effects. Without additional knowledge, these variations could be interpreted as real changes in surface topography. Note that this regional-scale anomaly could be quantified with the use of a GPS array that measures the water vapor in the atmosphere. Black area shows where no correlation could be achieved due to changes on the surface.

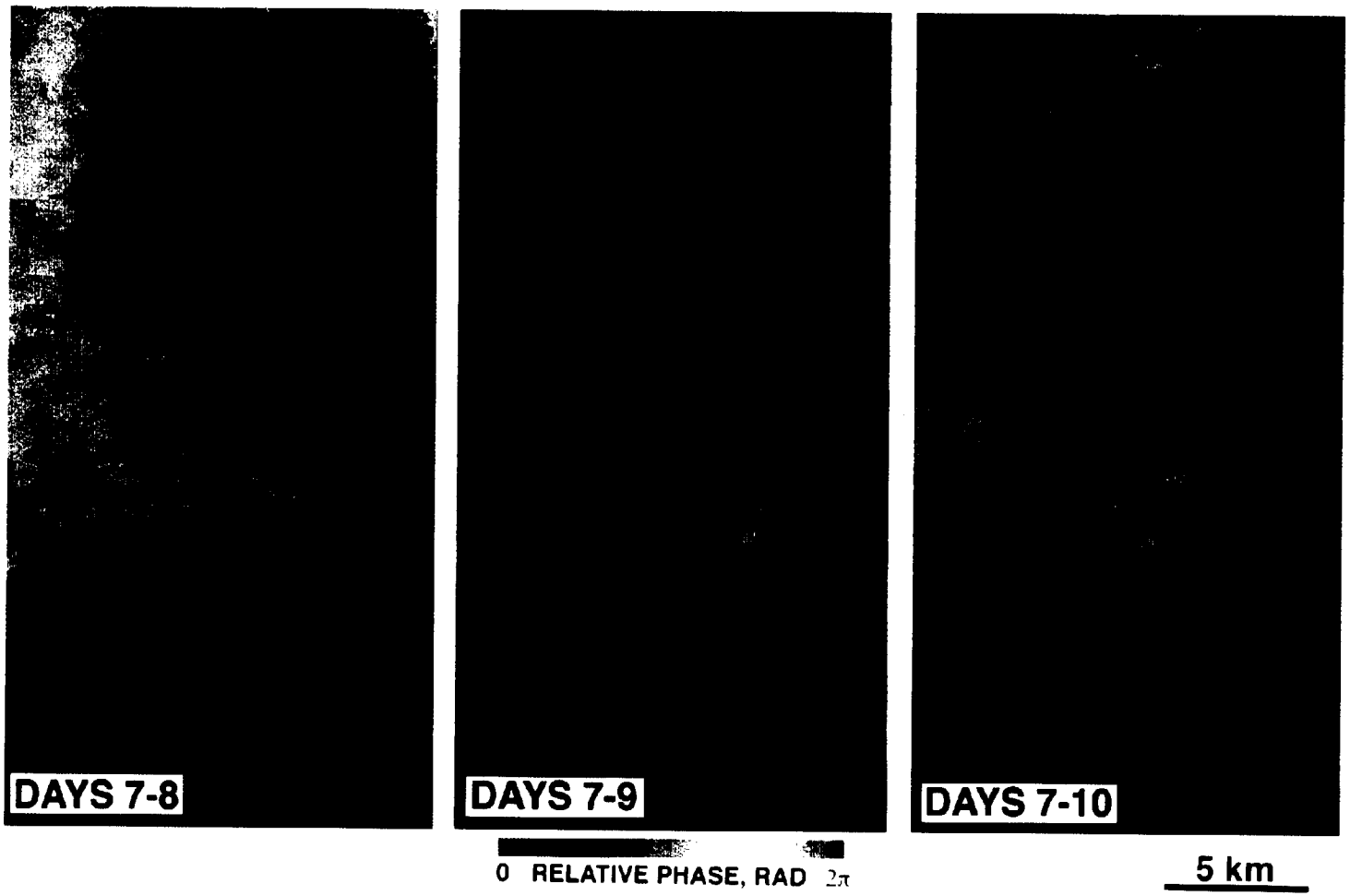

Figure 6-6. Comparison of the phase data collected over the Pu'u O'o eruption site of Kilauea volcano, Hawaii, on days 7 to 10 of the SRL-2 mission (October 7th-10th, 1994). The three images compare the phase data for October 7th with October 8th (left), 9th (center), and 10th (right). Particularly relevant are the patches of purple phase anomalies ~15-20 km inland (towards the top of the image). These anomalies are transient on a daily basis, and are interpreted to be due to the presence of rain cells at the time of data collection. They indicate that interferometric data needs to be collected frequently so that local atmospheric errors can be eliminated by excluding the worst scenes from the deformation comparisons.

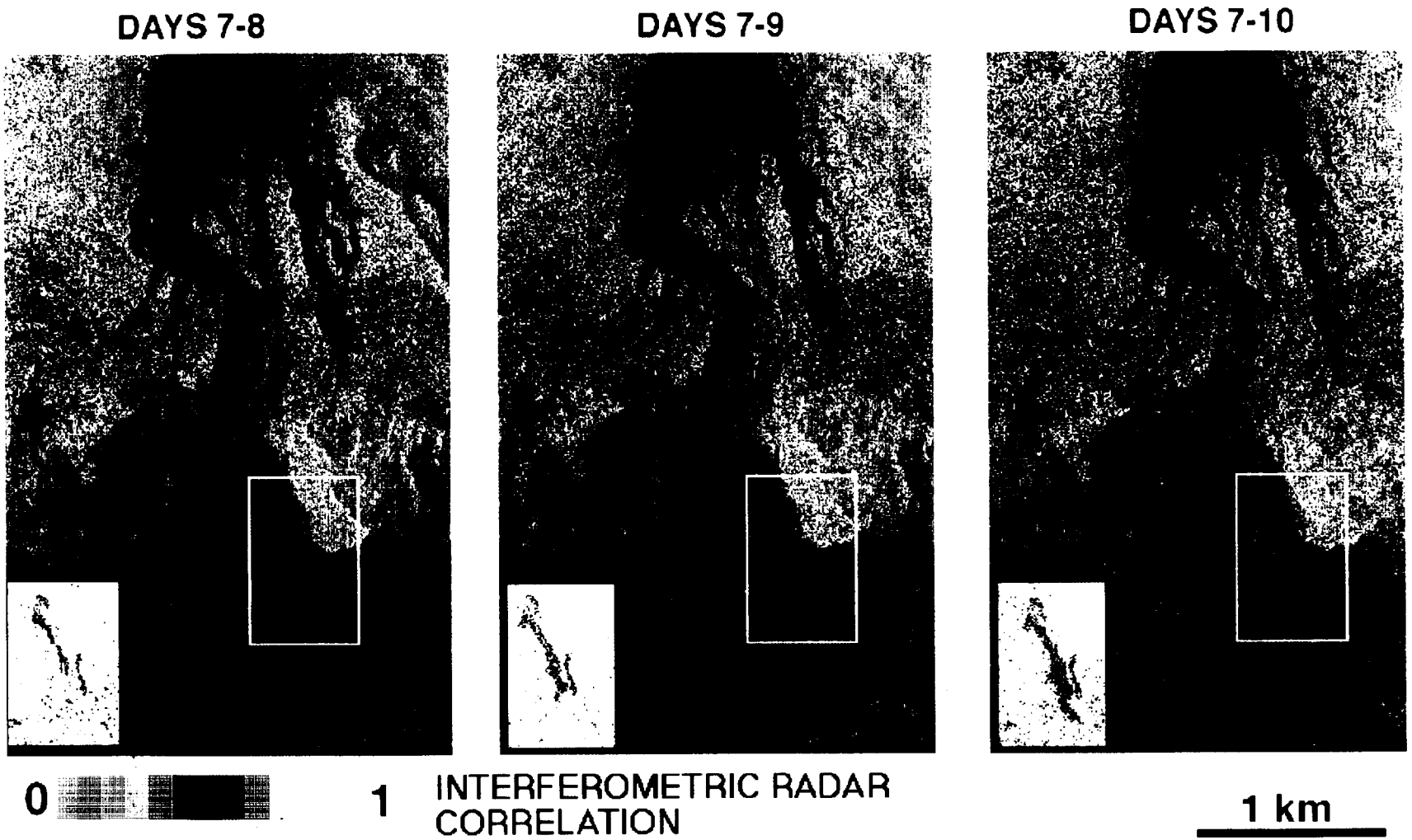

Figure 6-7. Comparison of surface changes detected by SRL-2 interferometry over the Pu'u O'o lava flow field, Kilauea, Hawaii, between October 7th-10th, 1994. Inserts show enhancements of the changes in the location of an active lava flow which was growing from the top of the image towards the bottom. The light purple areas across the center of the image are heavily forested areas, and the dark area at the bottom is the ocean.

Figure 6-8. This SIR-C image shows the region around the site of the lost city of Ubar in southern Oman, on the Arabian Peninsula. The ancient city was discovered in 1992 with the aid of remote sensing data. Archeologists believe Ubar existed from about 2800 B.C. to about 300 A.D. and was a remote desert outpost where caravans were assembled for the transport of frankincense across the desert.

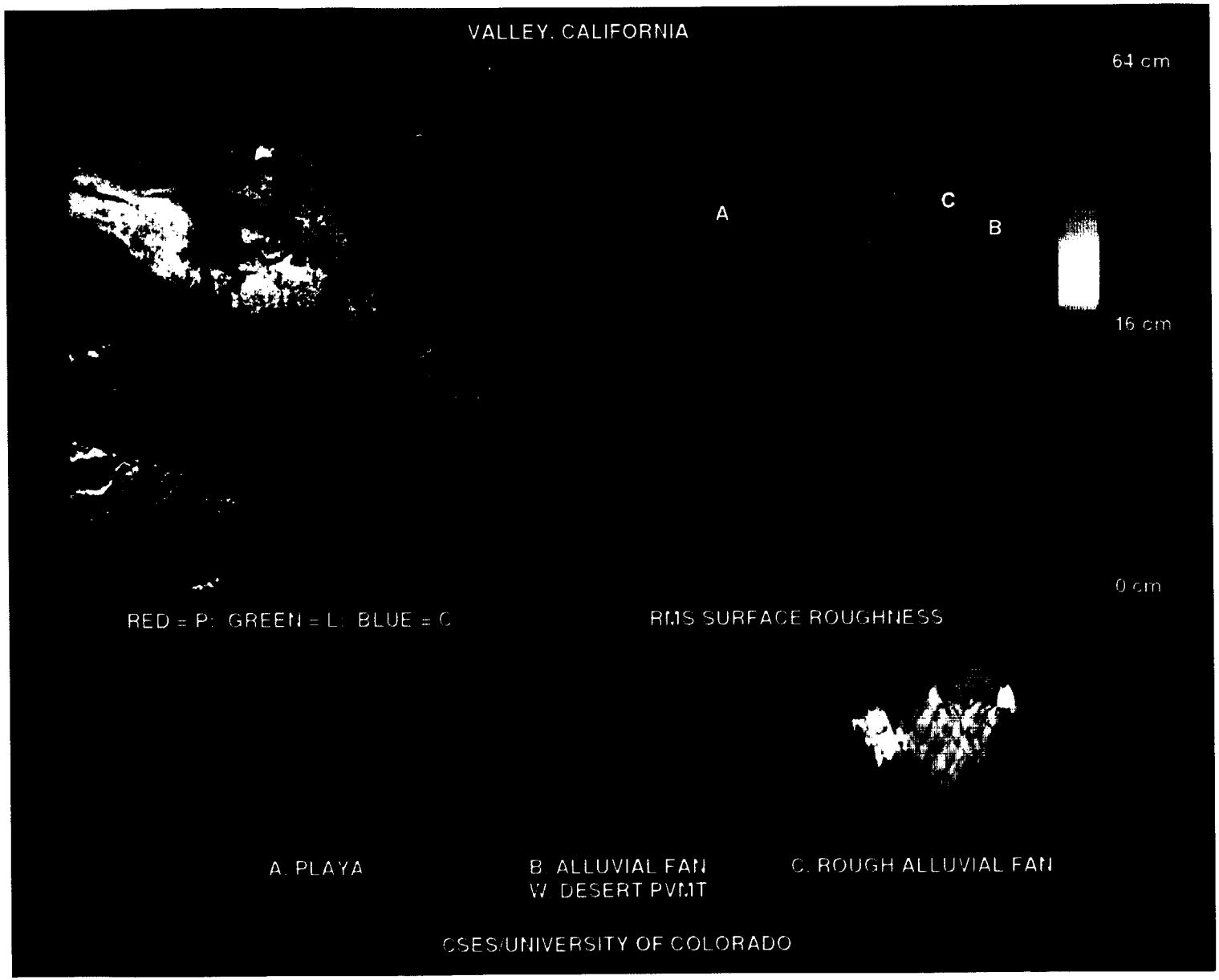

Figure 6-9. These images of Trail Canyon alluvial fan, Death Valley, California show the capability of polarimetric multifrequency radar to discriminate lithologies based on quantitative surface roughness.

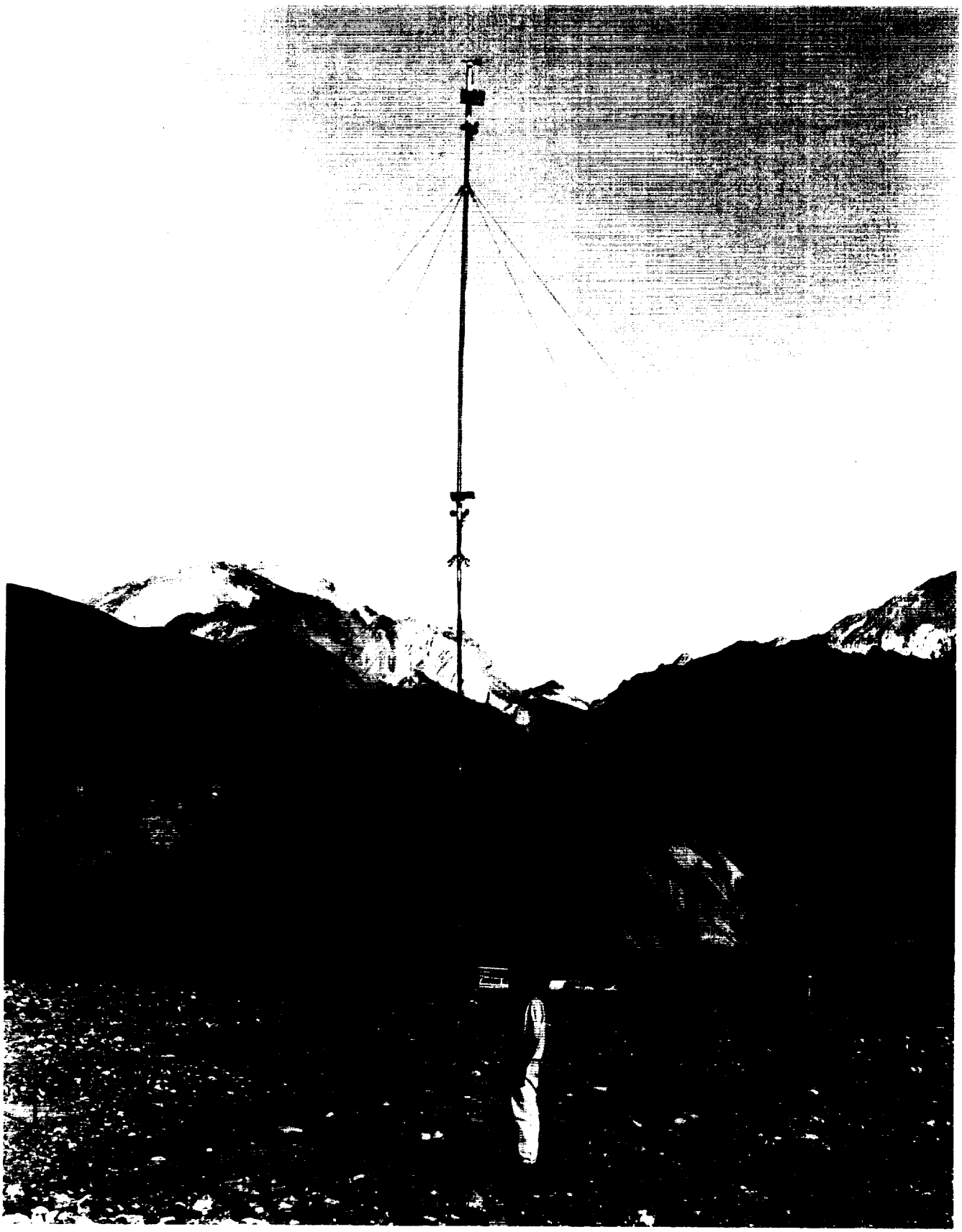

Figure 6-10. Photograph of the 9.8 meter mast deployed at Death Valley, California that was used to collect wind speed and temperature data within the surface boundary layer.

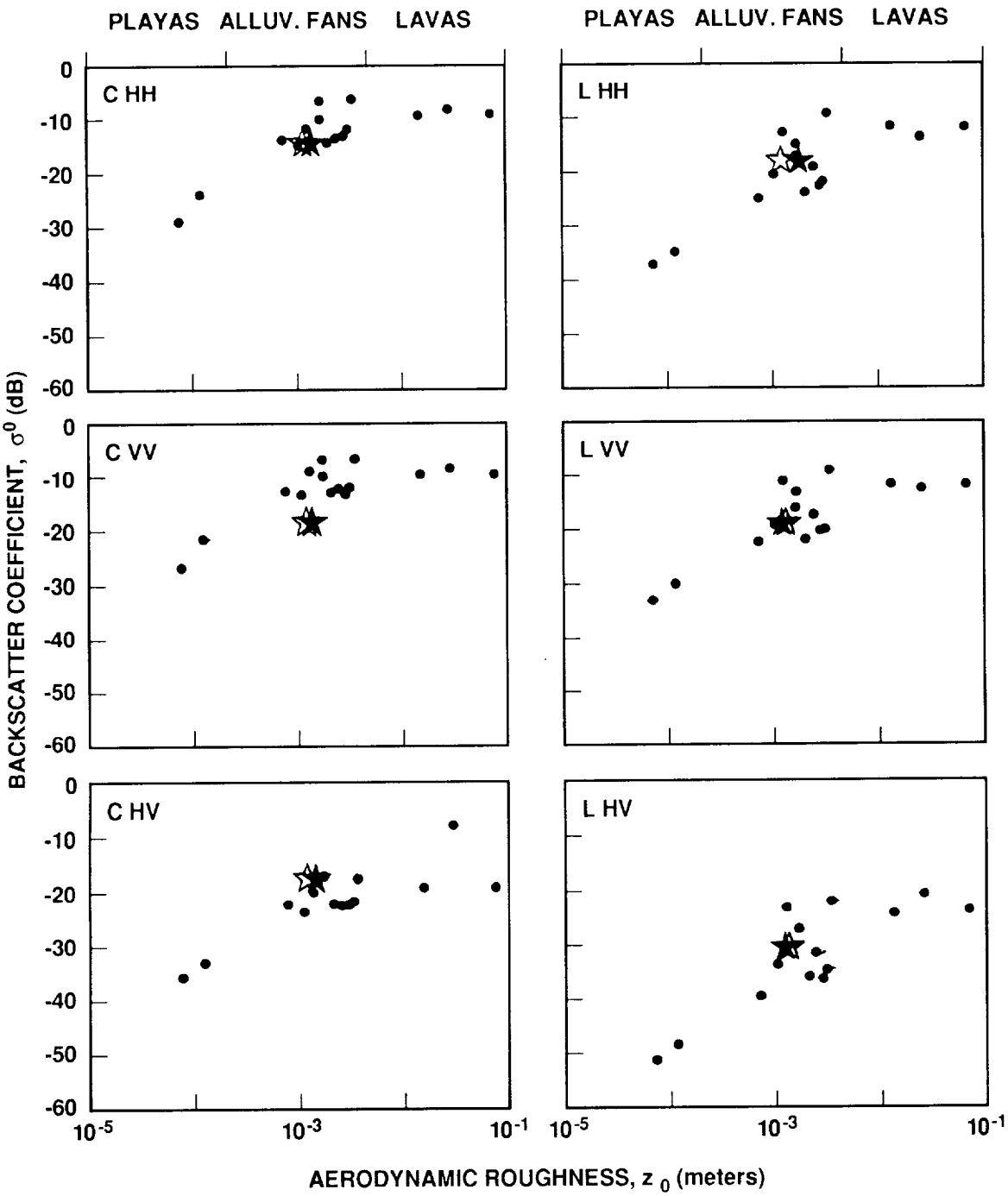

Figure 6-11. Radar backscatter observations of the SRL-1 super site at Stovepipe Wells, Death Valley, have been used to calculate aerodynamic roughness. The solid circles are from AIRSAR campaigns. Black star denotes prediction of Z_0 for the site. The models were based on AIRSAR data, the backscatter values were derived from SRL-1 data. The open star denotes the measured Z_0 value based on wind and temperature data collected in the field.

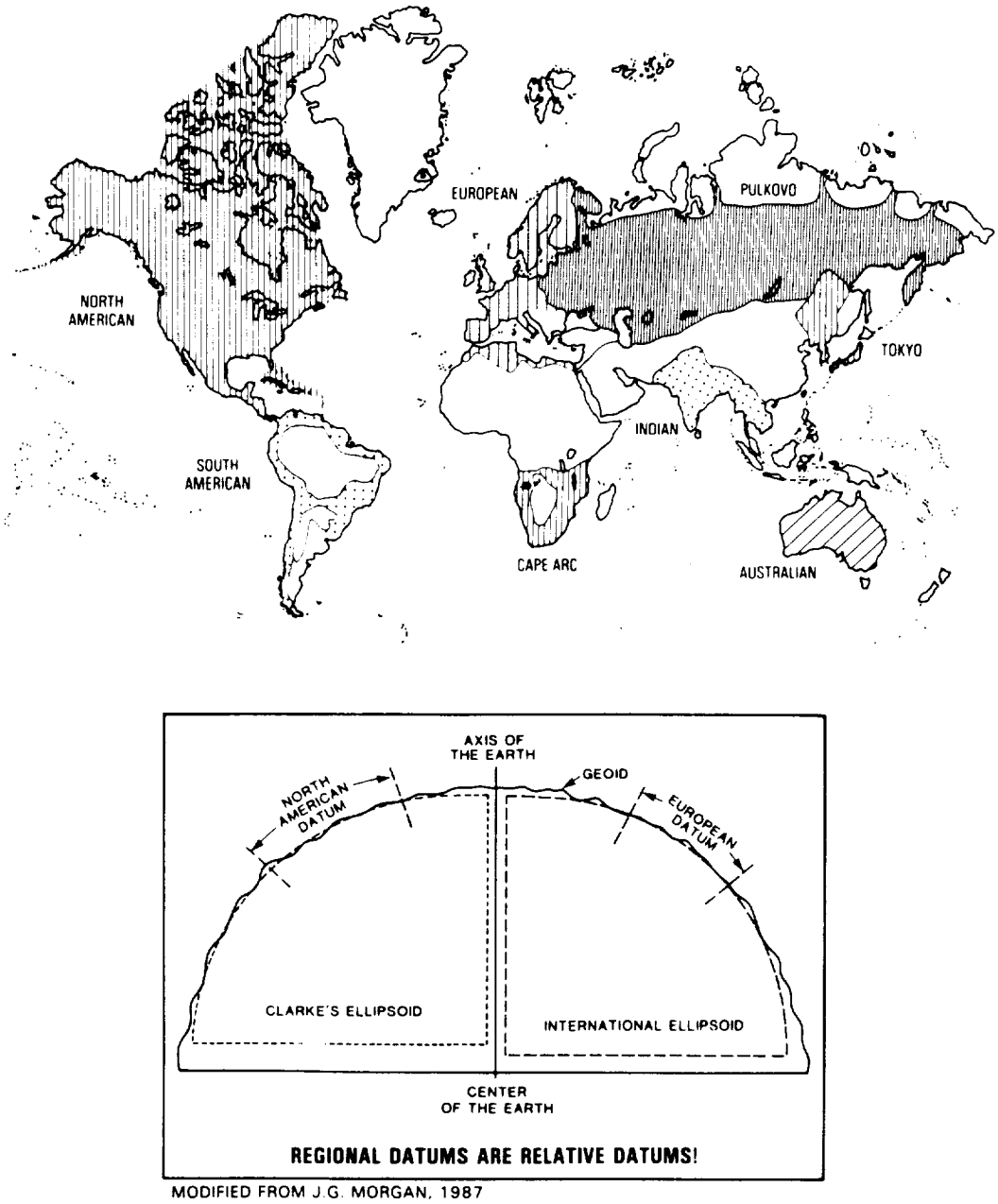

Figure 6-12 a). No single reference datum is presently in use throughout the world. This figure shows major datum blocks currently in use and illustrates how reference ellipsoids differ. A coherent topographic data set referrable to a single reference surface can only be readily obtained from satellite measurements (from Burke and Dixon, 1988).

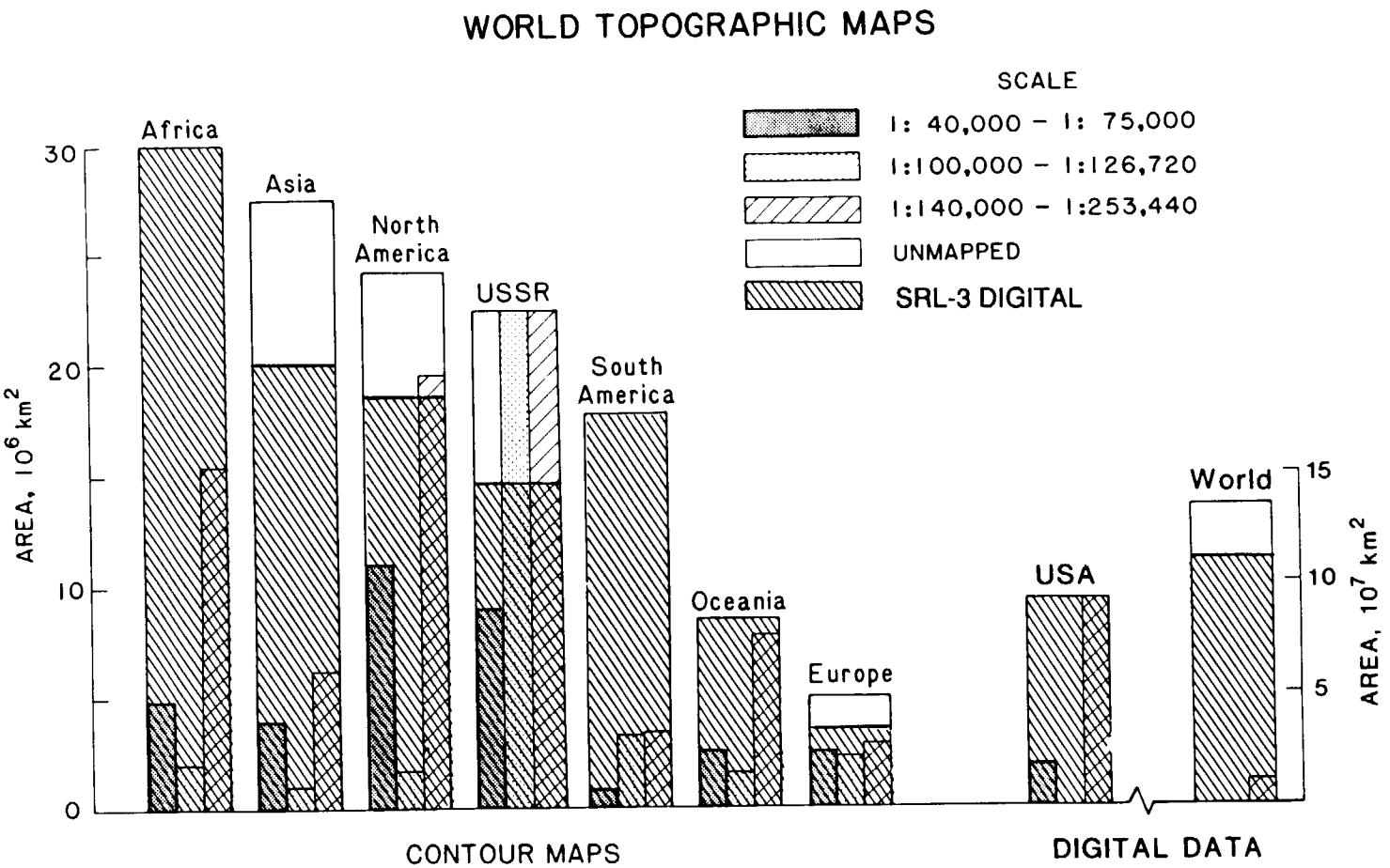

Figure 6-12 b). Availability of topographic data at various scales in both contour map and digital form. Source: United Nations Development Project (from Burke and Dixon, 1988).

7—SAR System Technology

INTRODUCTION

To support the scientific applications utilizing spaceborne imaging radar systems, a set of radar technologies has been identified which can dramatically lower the weight, volume, power and data rates of the radar systems. These smaller and lighter SAR systems can be readily accommodated in small spacecraft and launch vehicles enabling significantly reduced total mission costs. To prioritize the technology needs, a strawman mission scenario is adopted. It includes global topography mapping missions using interferometric SARs and dual frequency, polarimetric SAR mapping missions that will be flown starting in 2000. Specific areas of radar technology include the antenna, RF electronics, digital electronics and data processing. A core radar technology development plan is recommended to develop and demonstrate these technologies and integrate them into the radar missions in a timely manner. It is envisioned that these technology advances can revolutionize the approach to SAR missions leading to higher performance systems at significantly reduced mission costs.

NASA has flown several spaceborne imaging radar missions for Earth observation, starting with the pioneering L-band SAR system that flew on the SEASAT mission in 1978 (Jordan, 1980). This series of spaceborne SARs has provided an increasing level of system capability, culminating in the SIR-C/X-SAR system (IEEE, 1991). This latest system is the first multi-frequency, polarimetric SAR system designed for Earth observations from space. It flew successfully on two shuttle missions in April and October of 1994. An extensive data set was collected over numerous experiment sites around the globe. The multi-frequency, polarimetric radar measurements will be used to address scientific investigations in the areas of geology, hydrology, ecology, oceanography and other disciplines.

Figure 7-1 summarizes the key features of the series of four spaceborne SAR systems developed and flown by NASA for Earth observations. It also summarizes the key radar system technology features, such as frequency, polarization, transmitter/receiver approach and beam steering capability. In addition to these NASA systems, several other spaceborne SAR missions are being conducted by the international community. Examples of three such systems developed by ESA, Japan, and Canada are shown in Figure 7-2a. The key system technology features of these international SAR systems are shown in Figure 7-2b (IEEE, 1991). The potential applications of measurements from all these radar missions in a wide range of Earth science disciplines are given in previous segments of this report.

In support of the spaceborne SAR missions throughout the past two decades, NASA has also been conducting airborne SAR experiments to develop geophysical algorithms to convert the radar measurements to quantitative geophysical parameters. The airborne SAR system was also used to demonstrate advanced radar system concepts such as the interferometric SAR technique (Zebker et al., 1986). The feasibility of obtaining high resolution digital topography data using this technique has been thoroughly demonstrated on numerous airborne experiments. Furthermore, this technique has recently been extended to measure minute topography changes by the differences in the interferometric SAR measurements obtained in multiple passes over the experiment sites (Gabriel et al., 1989). The error sources associated with these techniques are now well characterized, and a logical next step is to apply them to global measurements from space (Zebker et al., 1994).

To assist the planning of the next phase of activities for spaceborne SARs, especially in view of the fact that there are several other SAR programs that are ongoing in the international

community, NASA has requested the National Research Council to conduct a review of the future SAR program direction. A key concern for any future SAR mission is that the mission complexity and cost are often driven by the mass, power, volume and data rate requirements of the radars. Typically, these radars demand large resources from the spacecraft as well as the launch vehicles, leading to high mission costs. An aggressive program to develop key radar technologies for smaller, lighter SAR systems that are more readily accommodated in small spacecraft/launch vehicles can lead to significantly reduced total mission costs. This portion of the review report addresses the specific questions concerning SAR technology and a plan for technology development for SAR program needs. An ad hoc SAR Technology Working Group to support this review was formed. The specific question that this segment of the report addresses is: "What are the priorities in SAR technology development which are critical not only to NASA's maintaining leadership in spaceborne SAR technology but to providing societally relevant geophysical parameters?" This segment summarizes the findings of the SAR Technology Working Group and recommends specific, prioritized technology steps for the NASA SAR program.

SCIENCE PANEL NEEDS SUMMARY

The scientific application drivers for SAR measurements have been described in detail in previous segments of this report and are summarized below:

(1) **Geology:** topography and topographic changes; hazard assessment such as flood potential, volcanoes, earthquakes, etc.

(2) **Oceanography:** ocean currents, winds, ocean surface features, sea ice thickness and coastal processes;

(3) **Hydrology:** soil moisture and snow water equivalence;

(4) **Ecology:** land cover classification, inundation mapping and biomass measurements;

(5) **Ice sheets:** snow facies, seasonal melt, icebergs, surface morphology, ice velocity and surface topography.

In each of these areas, the contributions of SAR data to the geophysical measurements are also addressed by other segments in this report. In some cases, the SAR systems provide a unique capability for the measurements of the geophysical parameters. In other cases, the radar results are combined with other sensor data for the geophysical studies. All the review panels recommend the collection of a long-term, calibrated time series of SAR data for studies of environmental changes. The next section focuses on translating these science drivers and their associated requirements of the SAR systems into a strawman mission scenario. Based on these SAR system requirements and mission needs, recommendations on a technology program are given in the Radar System Technology Discussions sub-section below.

STRAWMAN SAR MISSION SCENARIO

In order to focus the science application drivers summarized in the Science Panel Needs Summary section into SAR system requirements, we have constructed a strawman spaceborne SAR mission scenario. This strawman scenario addresses the key scientific needs, as advocated in the science panel reports, and the data to address those needs which are not presently available from the planned international radar programs. The scenario

includes a global topography mapping mission and a dual frequency, multi-polarization global mapping SAR mission. The global topography mission utilizes the interferometric SAR technique for high resolution, digital topography mapping. The dual-frequency, polarimetric SAR mission focuses on medium-resolution mapping of geophysical parameters such as biomass and soil moisture, and provides high resolution regional-scale measurements for selected experiment studies. Data from this mission scenario, together with data from other international SARs, will provide the comprehensive, long-term data set that is required to address all the science application issues discussed above. This strawman scenario clearly identifies the NASA contribution to the international SAR programs and provides key measurements that will otherwise be unavailable. It is recognized that the mission scenario described is, indeed, a strawman. Significant interactions with the science community, the international SAR mission program planners and NASA are required to properly define the mission scenario. However, for the purpose of this report, this strawman scenario and an assumed schedule for the execution of this scenario will serve as guides for the identification of radar technology needs.

Figure 7-3 shows a schematic drawing of a strawman concept for the global topography mapping mission. This concept utilizes two L-band SAR spacecraft that fly in formation. The formation flying will generate the required interferometric baseline separation between the two SAR antennas. The physical separation of the interferometric baseline needs to be measured to an accuracy of a few mm; the strawman approach is to utilize differential GPS signals. The performance characteristics of the SAR is also shown in Figure 7-3. Radar echoes obtained from the two systems will be processed into SAR imagery. The imagery will then be coherently combined and the interferometric phase measurements will be extracted. These phase measurements are then converted into digital topography information based on the baseline knowledge and other geometric parameters. Data from multiple orbits will be mosaicked to form a global topography model. It is expected that this global digital elevation model will have horizontal posting of about 30 m and vertical height accuracy of 2 to 5 m. This global data set will represent a major improvement in resolution beyond topography information that is currently available. It should be noted that this mission concept can be readily extended to perform measurements of topography changes using multiple passes over selected regions with nearly repeat ground tracks. As mentioned above, this technique has been demonstrated before using similar data sets (Zebker et al., 1994). It is envisioned that topography change detection and measurements need to be conducted on a continuing basis for assessment of hazards and related environmental changes. The key technology driver for a set of low-cost topography mapping missions is to develop a small, light SAR system that can be accommodated in small spacecraft and launch vehicles.

Figure 7-4 shows a schematic drawing for a dual-frequency, polarimetric strawman SAR mission for global vegetation and soil moisture studies. An L-band SAR with quad-linear polarization, together with an X-band SAR with dual polarization, is assumed for this mission. The focus of this mission is on obtaining medium resolution (200 to 300 m) global maps at the L- and X-bands for ecological and hydrological system studies. The specific geophysical measurements include biomass estimates, vegetation classification, plus soil and snow moisture. The mission goal is to provide a global map of these measurements once every several days for assessments of changes in these geophysical quantities. It is also envisioned that the SAR systems can support observations at higher resolution (less than 20 m) over selected areas for regional-scale experiment studies. This system employs advanced on-board SAR signal processing to generate the medium-resolution, accurately calibrated polarimetric SAR imagery over the global land mass. This technology will reduce the on-board data storage and downlink requirements. In addition, a small, lightweight power-efficient SAR system is also required.

A recent interesting SAR technique development is the use of an along-track interferometric SAR system for measurements of ocean phenomena, especially ocean currents. We note that a possible mission concept for along-track interferometric SAR ocean studies is similar to Figure 7-3, except that, instead of flying side-by-side, the spacecraft will fly along-track relative to each other. This approach does not require significant technology changes relative to the strawman mission scenario.

As a basis for planning and prioritizing the SAR technology development, we have arbitrarily selected an assumed schedule for the two missions mentioned. We have assumed that the global topography mapping mission will be developed in the 1997 to 2000 time frame with a launch in 2000 and the dual-frequency, polarimetric SAR mission for global mapping will be developed in the 2000 to 2003 time frame with a launch in 2003. Of course, this schedule needs to be reexamined in the future, but it will serve to set the requirements for the technology development.

RADAR SYSTEM TECHNOLOGY DISCUSSIONS

In this section, the state of the art in spaceborne SAR system technology, as well as the technology needed to address future potential missions are discussed. The five main areas of discussions are: antenna, RF electronics, digital electronics, data processors and system-level technology concepts. For each of these areas, the projected technology needs and their impact on the SAR missions are described. As discussed in the Recommended SAR Technology Program Approach section below, an advanced radar test-bed should be developed. Each of the technology items discussed should be fully tested in a modular fashion within this test-bed.

Antenna Technology Discussions

It is recognized that a key technology challenge in SAR systems is the antenna system. Due to the desire to limit the level of azimuth and range ambiguities in the SAR signal, the physical size of the antenna used cannot be smaller than certain prescribed limits. A typical size for a spaceborne L-band SAR antenna is 10 x 2 m. An antenna of similar size will be required for the strawman missions. Table 7-1 summarizes the size and weight of the antenna systems used in the SAR systems on SEASAT, ERS-1, JERS-1, RADARSAT and SIR-C (Gibbons, et al., 1994; Jordan, 1980). Although the physical size requirements do change with frequency, orbit altitude, swath width and required antenna gain, the antennas listed in Table 7-1 are all large and represent challenges in accommodation for the spacecraft and launch vehicle. These antenna systems also use different technology approaches. The SIR-C/X-SAR system utilizes a distributed phased array antenna at the L- and C-bands, and a slotted waveguide antenna at the X-band (Figure 7-5). The L- and C-band phased arrays employ multiple transmit/receive (T/R) modules that are distributed across the physical apertures of the antennas. These distributed T/R modules also provide electronic beam-steering capability. The ERS-1 and RADARSAT SAR systems utilize slotted waveguide antennas at the C-band, and the JERS-1 SAR system utilizes a microstrip planar array at the L-band. For the strawman mission scenario described in the Strawman SAR Mission Scenario section above, the key technology challenges for the antennas required are: reduction in the antenna weight, accommodation of a large antenna within the envelope of the launch vehicle shroud, reliability of the deployment mechanism, and reduction in the loss through the antenna feed network.

For the mission to be launched in 2000, a lightweight antenna with a minimal stowed volume to fit within a small launch vehicle shroud is required. The use of light weight composite

material to reduce the antenna weight and maintain the required surface flatness is a key technology. Compact deployable antenna structures, with highly reliable deployment mechanisms, need further development and demonstration. Improvements in low loss feed network material technology are desired. As a target for this phase, a passive, L-band planar antenna system with a size of 12 x 2 m that is suitable for the global topography mapping mission should weigh less than 70 kg. In addition, it is also possible to consider using the antenna structure in the SAR system as an additional resource for the spacecraft. For example, the antenna structure can serve as an integral part of the spacecraft structure, which can be used for the mounting of other spacecraft subsystems. This aspect should be investigated in the detailed mission design.

For the missions to be launched in 2003 and beyond, the use of inflatable antenna technology, in the form of planar phased arrays or other suitable reflector shapes in SAR antennas, must be developed. This technology can provide significant advantages in reducing the volume of the stowed antenna at launch, which will allow SAR systems to fly in smaller launch vehicles. It can also reduce the mass of the antenna as well (Freeland et al., 1992). Figure 7-6 shows an example of such an inflatable reflector that is under development for a technology demonstration flight on the Space Shuttle. However, several key technological challenges must be addressed before this approach can be readily adopted for SAR applications: (1) an appropriate antenna feed approach (if the radiative elements are on the inflated antenna surface), (2) the design concept to provide electronic beam-steering, (3) lifetime of the material used, (4) mechanical control of the antenna, and (5) total system reliability. In particular, the incorporation of electronic beam-steering capability with the required fast beam switching time and low side-lobe level, into an inflatable structure must be demonstrated. Another key concern for the global SAR mapping mission is that the inflatable antenna has to support dual-frequency operation and polarimetric measurements.

RF Electronics Technology Discussions

The RF subsystems of spaceborne SARs generate high power microwave transmitter pulses and amplify the radar echoes received through the antenna for digitization and processing. A key technology is the high peak power transmitter that is required. The SIR-C system utilizes distributed T/R modules, whereas the X-SAR utilizes a central transmitter/receiver system. In the multiple T/R module approach, the total peak transmit power is shared among all the modules, and each one only needs to transmit at a relatively lower peak power. Furthermore, the overall system reliability is improved because the multiple modules provide inherent redundancy. Figure 7-7 shows an L-band T/R module used on SIR-C. The key technology issues for the RF electronic subsystems for future SAR missions are substantial reduction in their weight and volumes, and significant improvement in their power efficiency. The power efficiency improvement can lead to reduction in the requirements on the spacecraft power subsystem with corresponding savings in mission cost. Another concern is to improve the reliability of these high-power RF components to reduce the risk of sensor failure. It is also important that the RF electronics operate with stable system gains to allow accurate calibration of the radar results.

Specifically, for the global topography mission at 2000, lightweight, highly efficient solid-state transmitters at the L-band, with peak power in excess of 300 W, are required. Silicon bipolar transistors at this power level presently exist for L-band operation, but their power efficiency should be improved beyond 60%. In addition to the high-power transmitters, the low-power portions of the RF subsystems, such as the exciters and receivers, should be miniaturized by the appropriate use of MMIC technology (see schematic diagram in Figure 7-8). This can lead to drastic reduction of system mass and volume.

For the radar missions through 2010, there are several emerging technologies that should be incorporated. Gallium arsenide MESFET and derivatives, such as heterostructure FETs and pseudomorphic HEMTs, should deliver several tens of watts at C-band and perhaps X-band (Figure 7-9 shows the present assessment of the available peak power per single device in various frequencies). Another example is the microwave power module. This is a blending of solid-state and vacuum electronics with performance benefits not attainable by either technology alone. It combines a wideband MMIC driver, an efficient miniaturized vacuum power booster, and integrated power conditioning, into a compact, lightweight package capable of average powers from several tens to several hundreds of watts. It is suitable for operation at frequencies up to the K-band (where solid-state devices are not as efficient as they are at lower frequencies; see Figure 7-10 for an engineering model example). It should also be noted that continuing improvement in high-power electronics tubes are useful for SAR operations at higher frequencies. Again, in all cases, further reductions in weight and improvements in power efficiency are key issues. For the missions beyond 2000, the technology of performing direct synthesis of RF drive signal from clock signals, avoiding any frequency synthesis process, should be pursued. By delivering the required RF drive signals by direct synthesis, significant portions of the exciter electronics will be eliminated, with a corresponding reduction in mass and volume.

An important challenge in the development of miniaturized RF electronics is the mechanical packaging technology. The small size in the circuitry presents significant challenges in minimizing design time, eliminating undesired RF coupling, and allowing for proper thermal dissipation. Furthermore, the small-scale circuitry will present problems in electrical and performance testing. New methodologies for testing by non-intrusive probing techniques should be developed and applied.

Digital Electronics Technology Discussions

A significant cost driver for SAR systems is that they typically generate large volumes of data at high rates. For example, the SIR-C/X-SAR system has five radar channels that operate at 45 Mb/s. For SIR-C, the digital data handling subsystem was 145 kg in weight and consumed about 800 W of power. Specific technology needs in the digital electronics for future SAR systems include substantial reduction in weight and power consumption, and increased automation of system operation.

For the global topography mapping mission in 2000, ASIC or FPGA technology needs to be adopted to reduce the digital electronics system size and weight. Examples of modules that need to be miniaturized include the digital chirp generator, data digitizer, the formatter, and the timing and control modules. Operating at clock rates of 50 to 100 MHz, their power consumption needs to be reduced by a factor of 10. Fortunately, the performance of digital synthesizers, analog-to-digital converters, floating point multipliers and accumulators, and high speed memories is benefiting from technology improvements that will lower power consumption and raise clock frequencies. In particular, heterojunction bipolar technology can lead to power consumption reduction by a factor of 5 and can more than double the operation speeds. For example, the sampling rate of 12-bit ADCs are projected to grow from 10 MS/s to over 50 MS/s, and that of 8-bit ADCs from 100 MS/s to 1 GS/s. At the same time, scaled CMOS and complementary gallium arsenide heterostructure FET technology are reducing both the access time and power consumption of SRAMs for high speed applications. In addition to these technology items, use of the multi-chip module packaging approach should also be adopted to improve the packaging volume efficiency and system reliability. To reduce the cost of post-launch mission operation, the radar command and operation functions should be highly automated. The radar system controller must perform the function of detailed system parameter setup; this may vary as a function of the orbital

location (e.g., PRF and data window position) as well as the gain setup of the RF and IF portions of the radars in an automated fashion to avoid excessive ground commanding. Onboard selection of proper RF/IF gain based on the radar echo strength, or the use of adaptive data quantization schemes such as a block floating point quantizer is required. These system automation issues will allow significant reduction in mission operation costs.

For the radar missions through 2010, the key digital technology item is on-board SAR processors for missions such as the global vegetation and soil moisture mapping mission. Unfortunately, current programs to develop radiation-hardened processors and memories are lagging behind the commercially available products. A radiation-hardened, 32-bit, 20-Mips processor is not yet available, and the current radiation-hardened SRAM technology is 256K. The onboard SAR data processor should be small, light and consume relatively low power (<50 to 100W). Technology advances in digital signal processing elements should be explored to develop a compact system architecture that is capable of the high throughput rate required(>4 GFLOPS at a sustained rate). This onboard processing technology can lead to dramatic decreases in downlink requirements and subsequent ground data handling. For the radar missions in this time period, the technology of very-high-speed ADC to perform direct data digitization at RFs from 1 to 10 GHz, followed by high-speed digital filters, should be developed. This approach will eliminate portions of the traditional RF subsystem and can potentially lead to more stable system calibration with improved system dynamic range.

Data Processing Systems

At present, nearly all the spaceborne SAR missions utilize ground data processing systems to convert the raw radar data into imagery. The ground processors also perform radiometric calibration, geometric rectification, further processing of the imagery into level 2 products, and the data archive and distribution. There are three major hardware approaches to the development of SAR processing systems: general commercial off-the-shelf (COTS) CPUs that can provide multi-GFLOPS level of computation rate; general COTS CPU augmented by special-purpose, high-computation-rate signal processing boards; and custom-designed, special-purpose SAR processing hardware.

For the radar mission in 2000, the present technology trend is to continue to capitalize on the advancement in COTS hardware that the computer industry is providing, and to utilize highly transportable SAR processing software to reduce the system implementation cost. A key technology driver continues to be the front-end interface to the radar data storage input. Significant investments to increase the throughput, reliability and transportability of this front-end I/O interface are required. Other important technology developments should occur in high-throughput geophysical product generation systems. These systems perform geophysical parameter retrieval based on the SAR imagery and generate higher-level data products. Although the geophysical inversion algorithms are maturing, the use of high-speed computation systems to analyze large data volumes of SAR need to be demonstrated. Significant advances have already been made in the polar ice geophysical processing, and these system approaches need to be extended to other application areas. An issue that should also be addressed is the incorporation of these SAR data sets, both at the imagery level and higher level data products, into the EOS data systems, so that they can be readily accessed by the science community.

For the SAR missions through 2010, as mentioned in the Digital electronics technology discussions above, the use of onboard processors should allow the generation of SAR imagery on the spacecraft. Continuing improvements of onboard processors should be pursued by including the radiometric and geometric calibration functions that require engineering information provided with the radar sensor. In addition to the continuing

improvements in the onboard processor systems, further improvements in the higher level product generation system technology and the development of efficient data product verification processes need to be performed.

Other SAR System Technology Considerations

In the discussions on the science application drivers and the strawman mission scenario, the radar resolution is typically envisioned to be in the range of tens to hundreds of meters. Indeed, the global mapping of vegetation and soil moisture will be conducted with a resolution of 200 to 300 m. However, for certain applications, a high resolution data set, say, at 2 m, can provide significant advantages. For example, once an area of interest is mapped at low resolution, selected segments of that area can be mapped at higher resolution for more detailed studies. These high-resolution data may have commercial and other civilian and military applications beyond the scientific studies discussed here. The high resolution mapping would not be global in nature, but would focus on selected regions for detailed studies. This type of high resolution mapping should be considered for the global topography mapping mission, as well as for the dual-frequency, polarimetric SAR mapping mission. Continuing improvements in the radar sensor technology, especially in high peak transmit power, large system operation bandwidth and high resolution onboard signal processors, would be required.

Although many of the scientific studies have been using radar measurements obtained over distinct frequencies that are widely separated, a tradeoff on the use of a single wide-band radar system, operating over, say, 40% of the bandwidth for some of the applications, should be examined. This wide-band approach can be readily accommodated in most antenna and RF system technologies. It eliminates the use of multiple hardware sets for the distinct frequencies. Of course, the penalty is that the frequency separation is only 40% or so of the RF frequency, but that may be sufficient for certain applications. The utility of such a system concept should be explored.

RECOMMENDED SAR TECHNOLOGY PROGRAM APPROACH

It is recommended that an aggressive radar technology development program be incorporated as part of the core NASA radar program activities. Its primary purpose is to reduce the mass, power, volume and data rate of the radar systems in order to reduce the total mission cost. In addition, prudent adoption of these technologies in developing the radar instrument and data processing systems can improve the system performance, increase its reliability, and lower the radar system development cost. This section summarizes the technology development discussions in the Radar System Technology Discussions section into a specific SAR technology program that is designed to address the needs for the radar missions envisioned for the 2000s.

For the radar mission in 2000, an aggressive technology demonstration program is recommended to ensure that the technologies listed in the Radar System Technology Discussions section above are ready and suitable for incorporation into the radar mission. The crucial technology demonstration studies are:

(1) **Antenna:** a technology demonstration model that includes the use of lightweight composite material for the antenna subarrays, a compact deployable antenna structure with the associated deployment mechanism, and a low loss antenna feed network using low loss material;

(2) **RF subsystem:** development of high efficiency solid-state L-band transmitter module and MMIC-based lightweight exciter and receiver modules;

(3) **Digital electronics:** development of miniaturized digital chirp generator, timing and control module, data digitization and handling unit using ASIC or FPGA technology and appropriate multi-chip module packaging approach;

(4) **Data processing systems:** demonstration of high-throughput, front-end interfaces for the ingestion of radar data into state-of-the-art COTS hardware system for SAR processing.

Table 7-2 shows the projected mass breakdown of such an advanced SAR system for the global topography mission. It is envisioned that the SAR system should weigh less than 100 kg, which represents a factor of 3 or more reduction relative to current, similar systems. A systematic approach to this technology demonstration process is a radar test-bed in which an advanced technology radar system is built up from all technology demonstration items. After each technology item is tested, it will be integrated into the test-bed for an end-to-end system-level test. It should be noted that many of the electronics modules listed above are applicable to radars at different frequencies, and therefore can be used in radar systems beyond the first strawman mission in 2000.

For the radar missions in 2003 and beyond, the technology program should include continuing improvements in the above areas and the following major enabling technology items:

(1) **Antenna:** technology development for an inflatable antenna system that can support electronic beam-steering and multi-frequency, polarimetric SAR observations;

(2) **RF electronics:** technology demonstration of microwave power modules for X-band transmitters and advanced solid-state transmitters for L- and C-band SAR systems and development of direct RF synthesis scheme to further reduce the size, weight and power consumption of the RF subsystem;

(3) **Digital electronics:** technology demonstration for onboard SAR processor to convert the raw SAR data into SAR imagery and development of direct data digitization at RF with high speed ADCs

(4) **Data processing system:** development of a high-throughput processing system for higher-level data product generation.

All these developments should be an integral part of the core radar technology program. The development schedule should ensure that they are ready to support the missions in the first decade of the 2000s. Again, these technology items should be integrated into the radar test-bed to provide full functional demonstration in an end-to-end fashion. With these advances, radar missions should be sufficiently light and small to be launched in Pegasus or other launch vehicles of similar capabilities. These technology advances will fundamentally revolutionize the approach to SAR missions, leading to higher-performance systems at significantly reduced mission costs.

Table 7-1. Summary of approximate mass of civilian spaceborne imaging radars.

	SEASAT 1978	ERS-1 1991	JERS-1 1992	SIR-C 1994	RADARSAT 1995
SYSTEM DESCRIPTION	L-BAND	C-BAND	L-BAND	L-/C-BAND DISTRIBUTED PHASED ARRAY	C-BAND ELECTRONIC BEAM STEERING
ANTENNA MASS (KG)	~103	~85	~130	~450 (ELECTRONICS AND PANELS ONLY)	~680
RADAR SENSOR ELECTRONICS MASS (KG)	~120	AMI SHARED BETWEEN SAR/ SCATTERO-METER	~90	~450 (4 RADAR CHANNELS)	~240

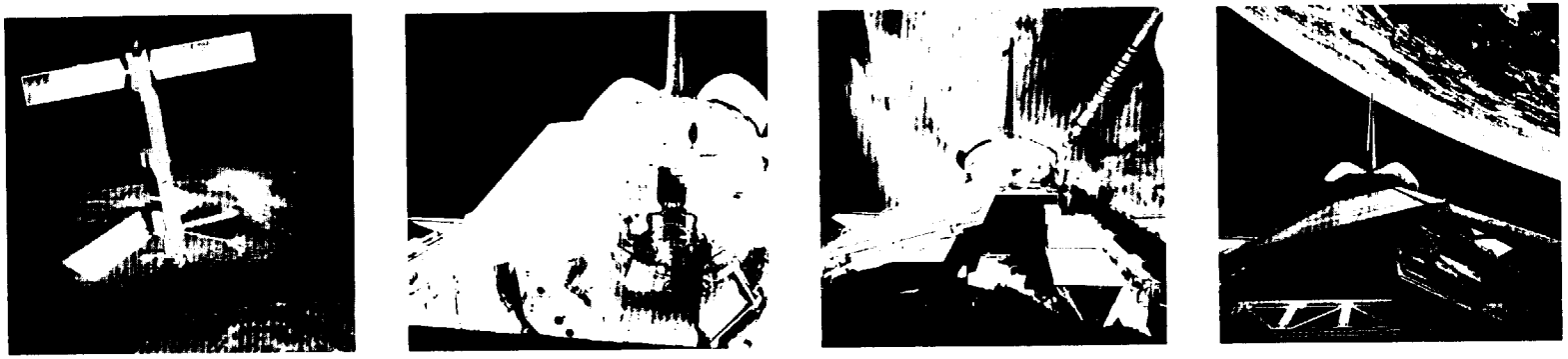

	SEASAT ('78)	SIR-A ('81)	SIR-B ('84)	SIR-C ('94)
FREQUENCY (GHz)	1	1	1	1, 5
POLARIZATION	HH	HH	HH	HH, HV, VH, VV
LOOK ANGLE	20°	50°	20° - 60°	20° - 60°
	ANALOG DATA	ANALOG DATA	DIGITAL DATA	DIGITAL DATA
	CENTRAL TRANSMITTER/RECEIVER	CENTRAL TRANSMITTER/RECEIVER	CENTRAL TRANSMITTER/RECEIVER	DISTRIBUTED T/R MODULES
	FIXED ANTENNA BEAM	FIXED ANTENNA BEAM	MECHANICAL BEAM STEERING	ELECTRONIC BEAM STEERING

Figure 7-1. NASA spaceborne SARs for the earth observations system technology evolution.

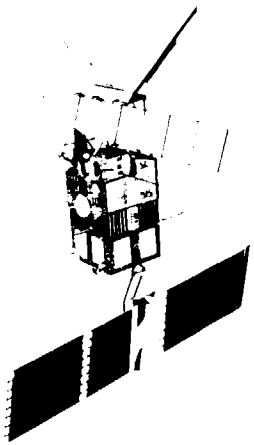

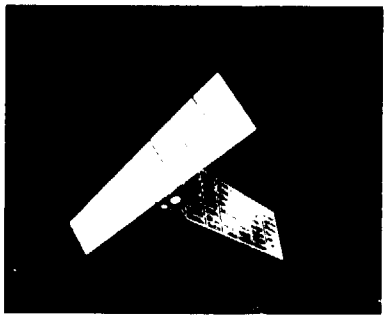

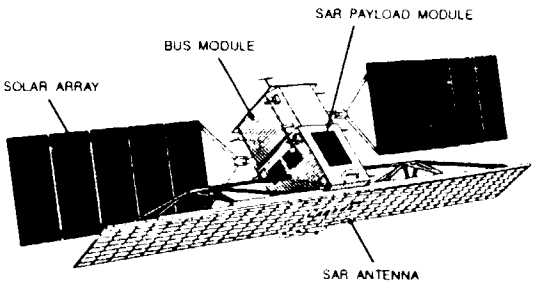

	ERS-1 ('91)	JERS-1 ('92)	RADARSAT
FREQUENCY (GHz)	5	1	5
POLARIZATION	VV	HH	HH
LOOK ANGLE	20°	35°	20° - 60°

Figure 7-2. a) International spaceborne SARs for Earth observation.

- INTERNATIONAL SPACEBORNE SAR PROGRAMS

• EUROPE (ESA)	– ERS-1	: C-BAND, SINGLE POLARIZATION, DIGITAL DATA SYSTEM, CENTRAL TRANSMITTER/RECEIVER, FIXED BEAM
	– ERS-2	: IDENTICAL TO ERS-1
	– ENVISAT	: C-BAND, POLARIZATION MEASUREMENTS
• GERMANY/ITALY	– X-SAR	: X-BAND, SINGLE POLARIZATION, DIGITAL DATA SYSTEM, CENTRAL TRANSMITTER RECEIVER, MECHANICAL BEAM STEERING
• JAPAN	– JERS-1	: L-BAND, SINGLE POLARIZATION, DIGITAL DATA SYSTEM, CENTRAL, TRANSMITTER/RECEIVER, FIXED BEAM
• CANADA	– RADARSAT	: C-BAND, SINGLE POLARIZATION, DIGITAL DATA SYSTEM, DISTRIBUTED T/R; ELECTRONIC BEAM STEERING
• RUSSIA	– ALMAZ I/II	: S-BAND, SINGLE POLARIZATION, DIGITAL DATA SYSTEM, MECHANICAL BEAM-STEERING

Figure 7-2. b) System technology evolution for international SAR programs.

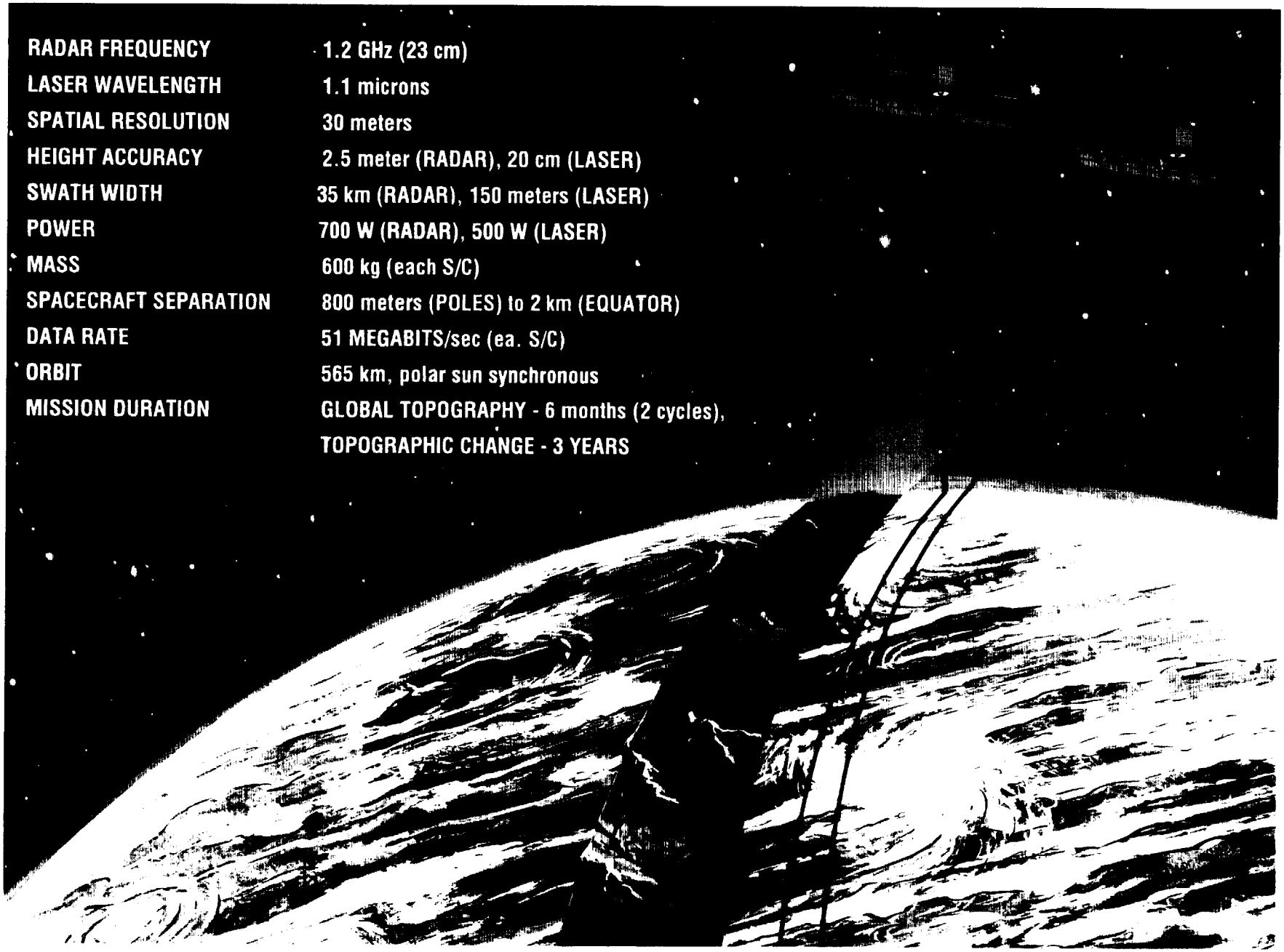

Figure 7-3. Global topography mapping mission concept.

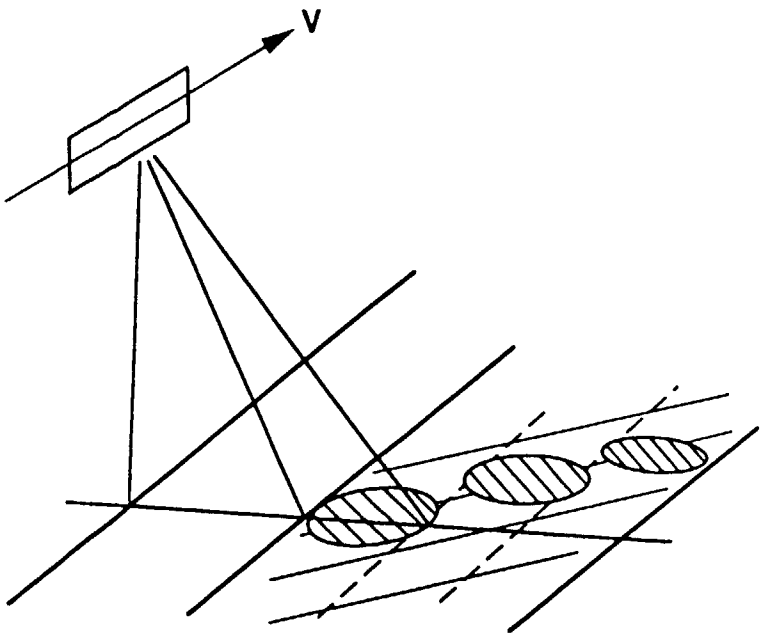

STRAWMAN SAR SYSTEM*

ORBITAL ALTITUDE	560 km
FREQUENCY	L-BAND + X- (OR C-) BAND
POLARIZATION	FULLY POLARIMETRIC L-BAND DUAL POLARIZATION X-BAND
IMAGE RESOLUTION	~300 m
SWATH WIDTH	~500 km
NUMBER OF LOOKS	≳30
PROCESSING	ON-BOARD
DATA RATE	<1 Mb/s

*SYSTEM CAPABLE OF HIGH RESOLUTION FOR REGIONAL-SCALE STUDIES

Figure 7-4. Global SAR mapping mission, medium resolution global mapping with dual-frequency, polarimetric SAR.

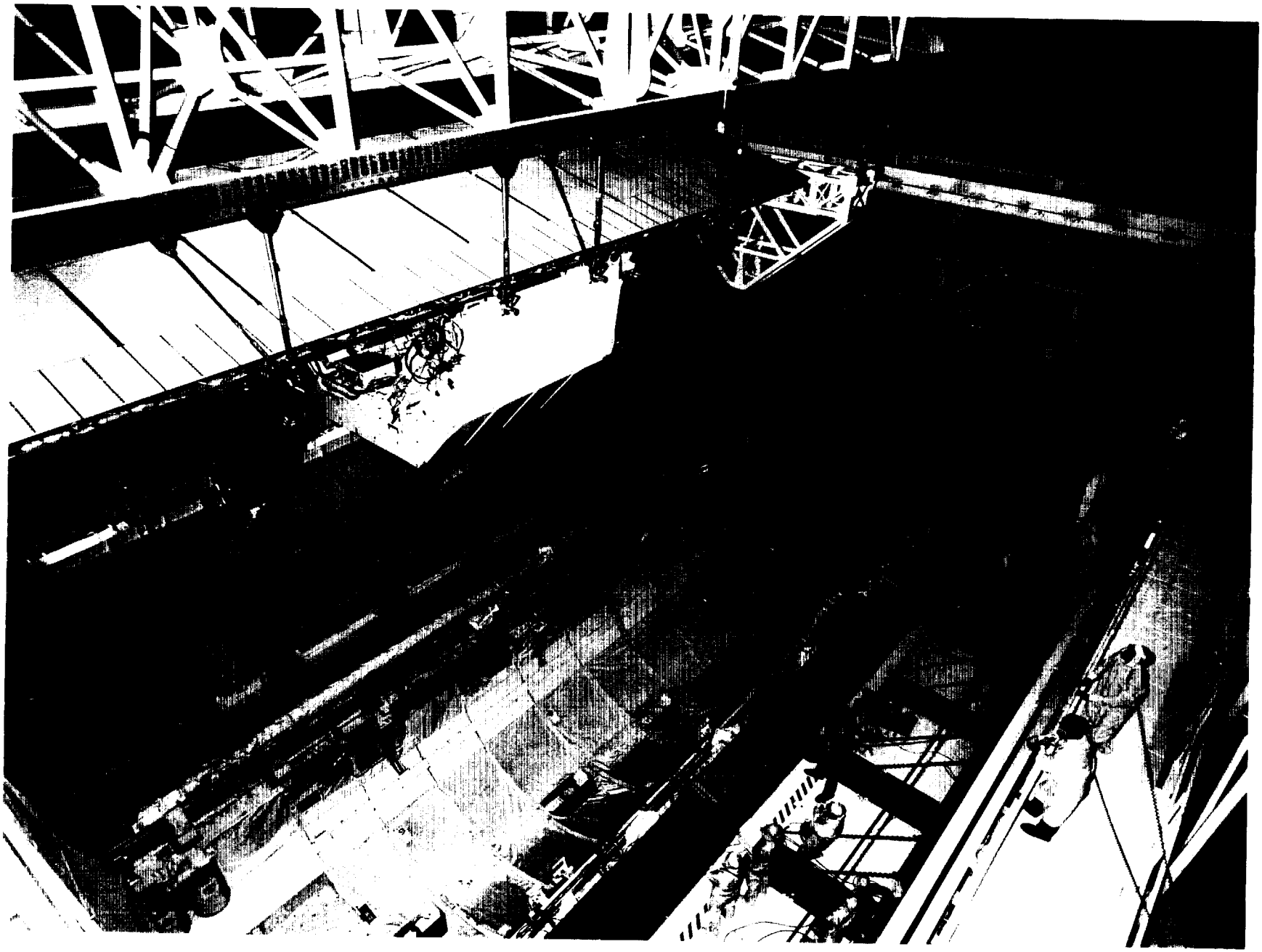

Figure 7-5. SIR-C/X-SAR being lowered into the cargo bay.

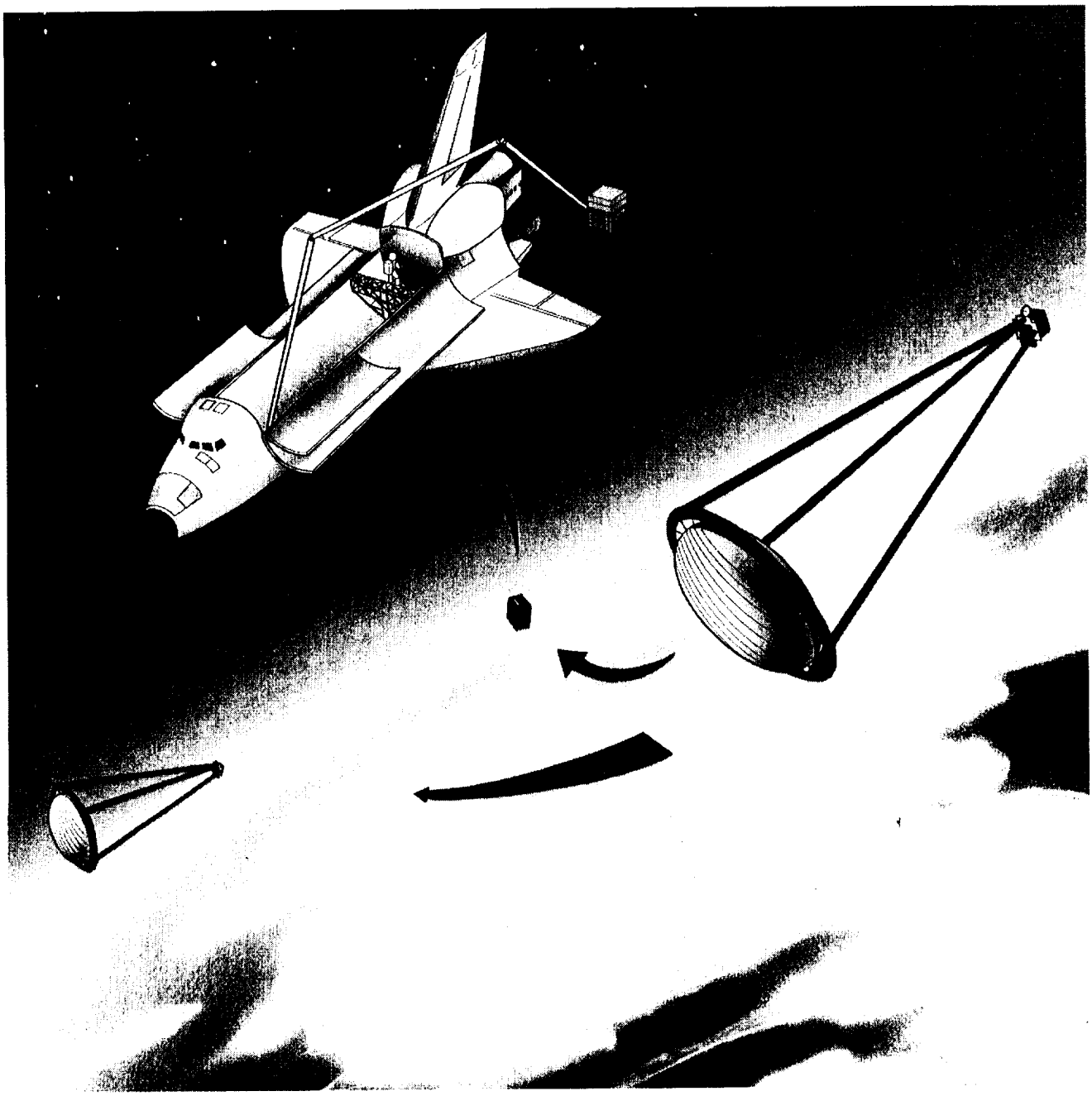

Figure 7-6. In-step inflatable antenna experiment.

Figure 7-7. SIR-C L-band T/R module.

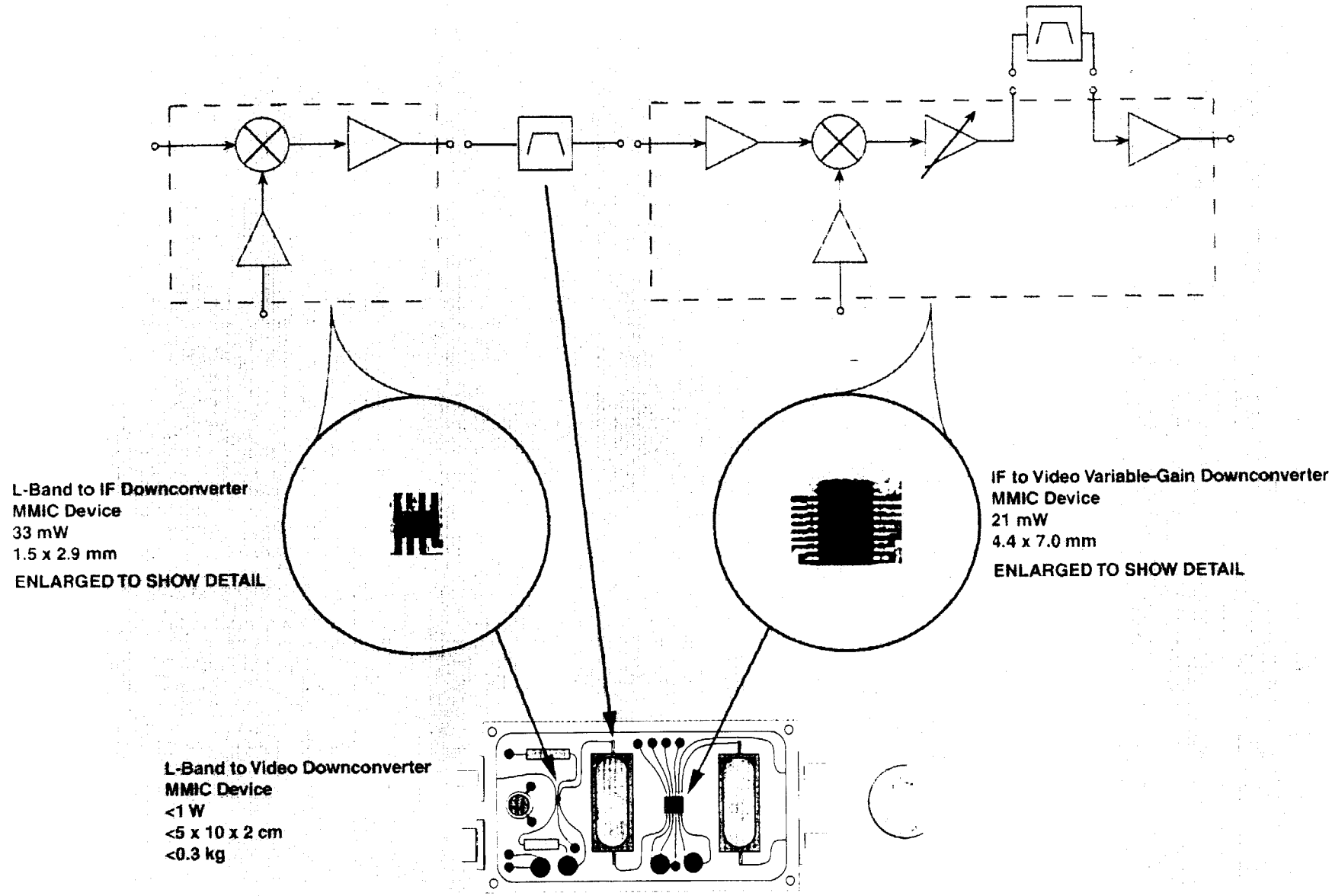

Figure 7-8. Schematic diagram on low-power RF subsystem with MMIC.

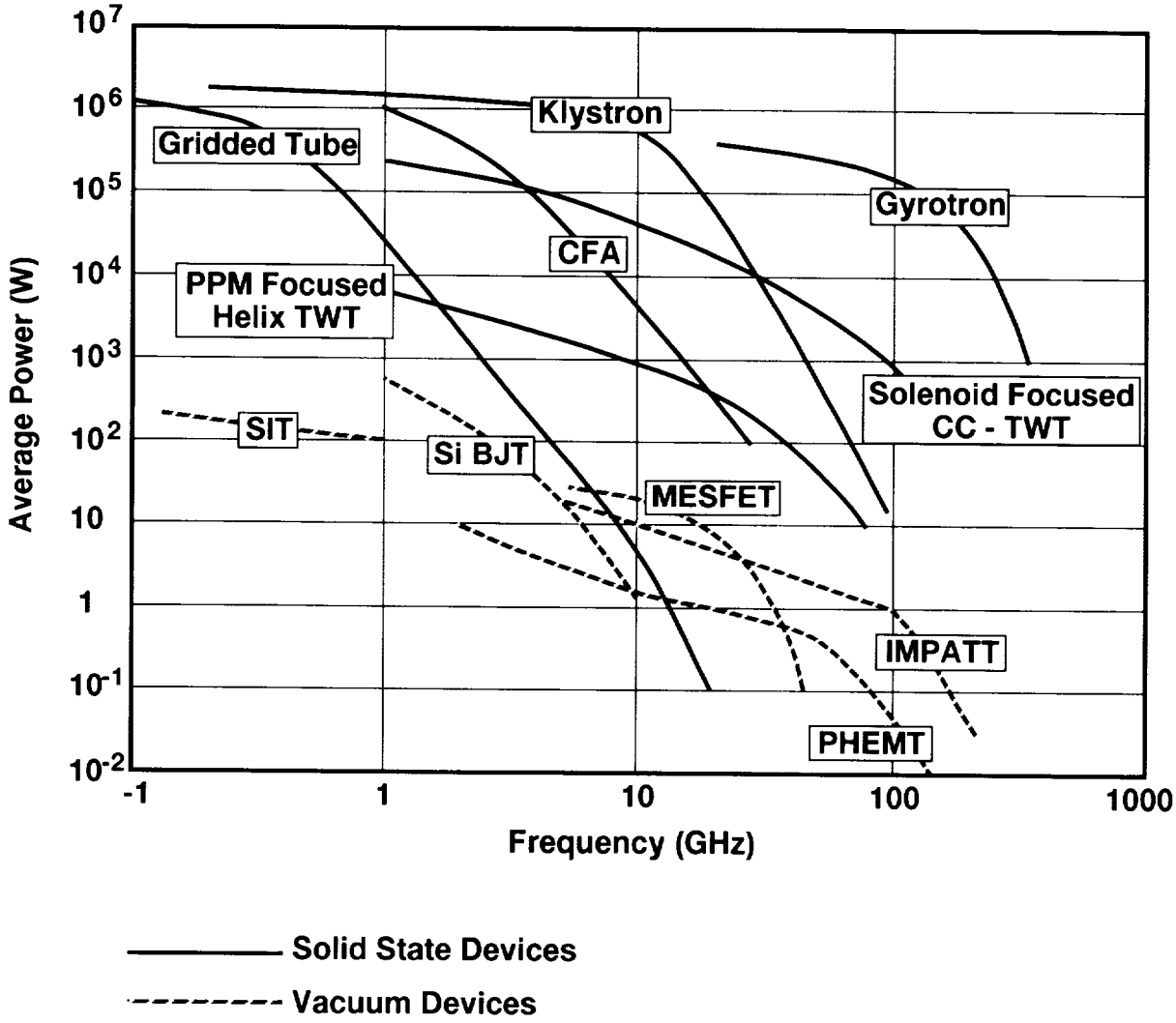

Figure 7-9. Peak transmit power for RF sources vs frequency, circa 1993.

Wideband TWTA and MPM

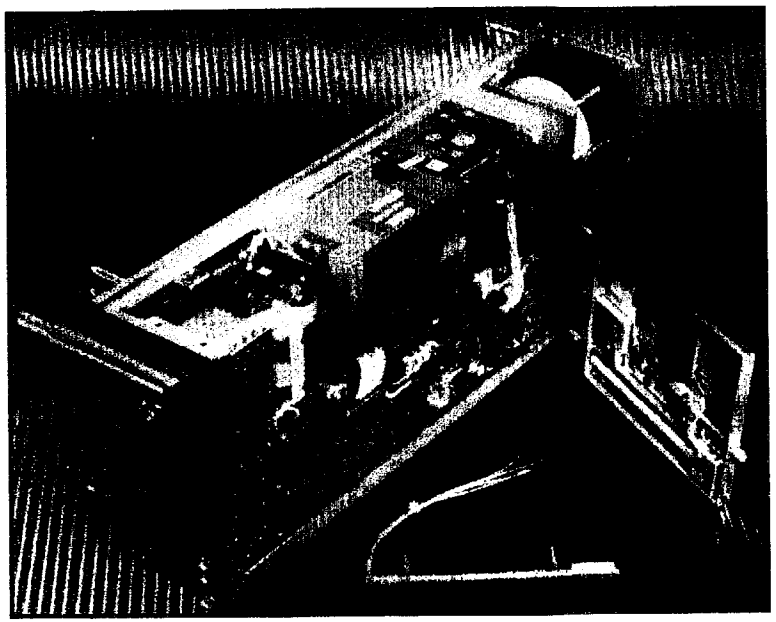

Power: TWTA -- 40 W; MPM -- 100 W
Power Density:
TWTA - 0.029 W/cm^3
MPM - 0.82 W/cm^3

Microwave Power Module

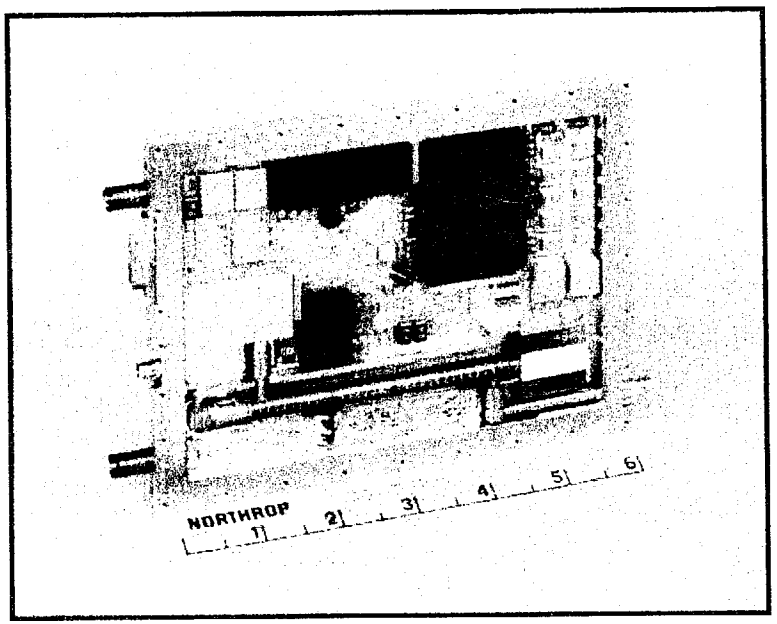

Power: 100 W (CW)
Frequency: 6 to 18 GHz
Size: 122 cm^3
Weight: 0.36 kgm

Figure 7-10. Example of Microwave Power Module and comparison of its characteristics with conventional TWTA.

Table 7-2. Projection of high technology SAR systems for global topography mapping missions in 2000.

SYSTEM	MASS, kg	VOLUME, L x W x H	POWER, W
ANTENNA TOTAL	76		260
ANTENNA PANELS (8)	29	10 m x 3.5 m	0
FRONT-END ELECTRONICS (8)	16	18 x 13 x 4 cm EACH	260
RF FEED NETWORK (3)	6		0
ANTENNA STRUCTURE	25		0
RADAR ELECTRONICS TOTAL	14	22 x 26 x 22 cm VME 6U CHASSIS	180
RF ELECTRONICS SUBSYSTEM	5	18 x 26 x 7.5 cm	49
UPCONVERTER/DRIVER	1	18 x 13 x 2.5 cm	10
RECEIVER BANK-END	1	18 x 13 x 2.5 cm	10
CALIBRATOR	1	18 x 13 x 2.5 cm	2
STALO/FREQUENCY	1	18 x 13 x 2.5 cm	2
CROSS-LINK TRANSMITTER/RECEIVER	1	18 x 13 x 2.2 cm	25
DIGITAL ELECTRONICS SUBSYSTEM	9	22 x 26 x 14.5 cm	95
CMD/TMG/TLM ELECTRONICS	2	22 x 26 x 2 cm	15
DIGITAL CHIRP GENERATOR	1	18 x 13 x 2.5 cm	15
ADC/BUFFER	1	22 x 26 x 2 cm	20
DATA COMPRESSION/FORMATTER	1	22 x 26 x 2 cm	10
ON-BOARD RANGE-ONLY PROC (MEMORY)	1	22 x 26 x 2 cm	10
ON-BOARD RANGE-ONLY PROC (SIGNAL PROCESSOR)	1	22 x 26 x 2 cm	25
POWER DISTRIBUTION	2	22 x 26 x 4.5 cm	0
MISCELLANEOUS	6		36
POWER/CONTROL/DATA CABLES	4		0
HOUSING	2		0
POWER CONVERSION (80% EFF)			36
INSTRUMENT TOTAL	96		440

8—References

2—Ecology

Ahern, F. J., D. G. Leckie, and J. A. Drieman (1993). Seasonal changes in relative C-band backscatter of northern forest cover types. *IEEE Trans. Geosci. Rem. Sens.*, vol. 31, pp. 668–680.

Aselmann, I. and P. J. Crutzen (1989). Global distribution of natural freshwater wetlands and rice paddies, their net primary productivity, seasonality, and possible methane emissions. *J. Atmos. Chem.*, vol. 8, pp. 307–358.

Bacastow, R. B., C. D. Keeling, and T. P. Whorf (1985). Seasonal amplitude increase in atmospheric CO_2 concentration at Mauna Loa, Hawaii, 1959–1982. *J. Geophys. Res.*, vol. 90, pp. 10,529–10,540.

Bartlett, K. B. and R. C. Harriss (1993). Review and assessment of methane emissions from wetlands. *Chemosphere*, vol. 26, pp. 261–320.

Beaudoin, A., T. LeToan, S. Goze, E. Nezry, A. Lopes, E. Mougin, C. C. Hsu, H. C. Han, J. A. Kong, and R. T. Shin (1994). Retrieval of forest biomass from SAR data. *Int. J. Rem. Sens.*, vol. 15, pp. 2777–2796.

Bonan, G. B. (1991a). Atmosphere-biosphere exchange of carbon dioxide in boreal forests. *J. Geophys. Res.*, vol. 96, pp. 7301–7312.

Bonan, G. B. (1991b). Seasonal and annual carbon fluxes in a boreal forest landscape. *J. Geophys. Res.*, vol. 96, pp. 17329–17338.

Bonan, G. B. and H. H. Shugart (1989). Environmental factors and ecological processes in boreal forests. *Ann. Rev. Ecol. Syst.*, vol. 20, pp. 1–28.

Chauhan, N. R., R. H. Lang, and K. J. Ranson (1991). Radar modeling of a boreal forest. *IEEE Trans. Geosci. Rem. Sens.*, vol. 29, pp. 627–638.

D'Arrigo, R., G. C. Jacoby, and I. Y. Fung (1987). Boreal forests and atmosphere biosphere exchange of carbon dioxide. *Nature*, vol. 329, pp. 321–323.

de Grandi, G. F., G. C. Lemoine, H. de Groof, C. Lavalle, and A. J. Sieber (1994). Fully polarimetric classification of the Black Forest MAESTRO 1 AIRSAR data. *Int. J. Rem. Sens.*, vol. 15, pp. 2755–2775.

Dixon, R. K., S. Brown, R. A. Houghton, A. M. Solomon, M. C. Trexler, and J. Wisniewski (1994). Carbon pools and flux of global forest ecosystems. *Science,* vol. 263, pp. 185–190.

Dobson, M. C., L. E. Pierce, K. Sarabandi, F. T. Ulaby, and T. Sharik (1992a). Preliminary analysis of ERS-1 SAR for forest ecosystem studies. *IEEE Trans. Geosci. Rem. Sens.*, vol. 30, No. 2, pp. 203–211.

Dobson, M. C., F. T. Ulaby, T. Le Toan, A. Beaudoin, E. S. Kasischke, and N. C. Christensen (1992b). Dependence of radar backscatter on conifer forest biomass. *IEEE Trans. Geosci. Rem. Sens.*, vol. 30, pp. 412–415.

Dobson, M. C., F. T. Ulaby, and L. E. Pierce (1995a). Land-cover classification and estimation of terrain attributes using synthetic aperture radar. *Rem. Sens. Environ.*, vol. 51, No. 1, pp. 199-214.

Dobson, M. C., L. E. Pierce, and F. T. Ulaby (1995b). Knowledge-based land-cover classification using ERS-1/JERS-1 SAR composites. *IEEE Trans. Geosci. Rem. Sens.*, (in press).

Dobson, M. C., F. T. Ulaby, L. E. Pierce, K. Bergen, and K. Sarabandi (1995c). Land-cover classification and biomass estimation with SIR-C/X-SAR. *IEEE Trans. Geosci. Rem. Sens.* (in press).

Drieman, J. A. (1994). Forest cover typing and clearcut mapping in Newfoundland with C-band SAR. *Can. J. Rem. Sens.*, vol. 20, pp. 11–16.

Durden, S. L., J. J. Van Zyl, and H. A. Zebker (1989). Modeling and observation of the radar polarization signature of forested areas. *IEEE Trans. Geosci. Rem. Sens.*, vol. 27, pp. 290–301.

Foody, G. M., M. B. McCulloch, and W. B. Yates (1994). Crop classification from C-band polarimetric radar data. *Int. J. Rem. Sens.*, vol. 15, pp. 2871–2885.

Fung, I., J. John, J. Lerner, E. Matthews, M. Prather, L. Steele, and P. J. Fraser (1991). Three-dimensional model synthesis of the global methane cycle. *J. Geophys. Res.*, vol. 96, pp. 13,033–13,065.

Harrell, P., L. L. Bourgeau-Chavez, E. S. Kasischke, N. H. F. French, and N. L. Christensen (1995). Sensitivity of ERS-1 and JERS-1 radar data to biomass and stand structure in Alaskan boreal forest. *Rem. Sens. Environ.* (in press).

Hess, L. L. and J. M. Melack (1994). Mapping wetland hydrology with synthetic aperture radar. *Int. J. Ecol. Environ. Sci.*, vol. 20, pp. 74–81.

Hess, L. L., J. M. Melack, and D.S. Simonett (1990). Radar detection of flooding beneath the forest canopy: a review. *Int. J. Rem. Sens.*, vol. 5, pp. 1313–1325.

Hess, L. L., J. M. Melack, S. Filoso, and Y. Wang (1995). Delineation of inundated area and vegetation along the Amazon floodplain with the SIR-C synthetic aperture radar. *IEEE Trans. Geosci. Rem. Sens.* (in press).

Houghton, R. A. (1987). Biotic changes consistent with the increased seasonal amplitude of atmospheric CO_2 concentration. *J. Geophys. Res.*, vol. 92, pp. 4223–4230.

Houghton, R. A., R. D. Boone, J. M. Melillo, C. A. Palm, G. M. Woodwell, N. Myers, B. Moore, and D. L. Skole (1985). Net flux of carbon dioxide from tropical forests in 1980. *Nature*, vol. 316, pp. 617–620.

Hsu, C. C., H. C. Han, R. T. Shin, J. A. Kong, A. Beaudoin, and T. LeToan (1994). Radiative transfer theory for polarimetric remote sensing of pine forest at P band. *Int. J. Rem. Sens.*, vol. 15, pp. 2943–2954.

Hussin, Y. A., R. M. Reich, and R. M. Hoffer (1991). Estimating slash pine biomass using radar backscatter. *IEEE Trans. Geosci. Rem. Sens.*, vol. 29, pp. 427–431.

Kasischke, E. S. and N. H. F. French (1994). Locating and estimating the areal extent of wildfires in Alaskan boreal forests using multiple season AVHRR NDVI composite data. *Rem. Sens. Environ.*, vol. 50 (in press).

Kasischke, E. S., L. L. Bourgeau-Chavez, N. H. F. French, P. Harrell, and N. L. Christensen, Jr. (1992). Initial observations on the use of SAR imagery to monitor wildfires in boreal forests. *Intern. J. Rem. Sens.*, vol. 13, pp. 3495–3501.

Kasischke, E. S., N. L. Christensen, Jr., and L. L. Bourgeau-Chavez (1994a). Correlating radar backscatter with components of biomass in loblolly pine forests. *IEEE Trans. Geosci. Rem. Sens.*, vol. 32 (in press).

Kasischke, E. S., N. L. Christensen, Jr., E. Haney, and L. L. Bourgeau-Chavez (1994b). Observations on the sensitivity of ERS-1 SAR image intensity to changes in aboveground biomass in young loblolly pine forests. *Int. J. Rem. Sens.*, vol. 15, pp. 3–16.

Kasischke, E. S., L. L. Bourgeau-Chavez, and N. H. F. French (1994c). Observations of variations in ERS-1 SAR image intensity associated with forest fires in Alaska. *IEEE Trans. Geosci. Rem. Sens.*, vol. 32, pp. 206–210.

Kasischke, E. S., L. Morrissey, J. B. Way, N. H. F. French, L. L. Bourgeau-Chavez, E. Rignot, J. A. Stearn, and G. P. Livingston (1995a). Monitoring seasonal variations in boreal ecosystems using multi-temporal spaceborne SAR data. *Can. J. Rem. Sens.* (in press).

Kasischke, E. S., N. L. Christensen, Jr., and B. J. Stocks (1995b). Fire, global warming and the mass balance of carbon in boreal forests. *Ecol. Appl.* (in press).

Kuga, Y., M. W. Whitt, K. C. McDonald, and F. T. Ulaby (1990). Scattering models for distributed targets, in *Radar Polarimetry for Geoscience Application* (F. T. Ulaby and C. Elachi, eds.), Artech, Dedham, MA.

Kwok, R., E. Rignot, J. B. Way, A. Freeman, and J. Holt (1994). Polarization signatures of frozen and thawed forests of varying environmental state. *IEEE Trans. Geosci. Rem. Sens.*, vol. 32, pp. 371–381.

Lang, R. H., N. S. Chauhan, J. K. Ranson, and O. Kilic (1994). Modeling P-band SAR returns from a red pine stand. *Rem. Sens. Environ.*, vol. 47, pp. 132–141.

Lemoine, G. G., G. F. de Grandi, and A. J. Sieber (1994). Polarimetric contrast classification of agricultural fields using MAESTRO 1 AIRSAR data. *Int. J. Rem. Sens.*, vol. 15, pp. 2851–2869.

Lopes, A., E. Nezry, R. Touzi, and H. Laur (1993). Structure detection and statistical adaptive filtering in SAR images. *Int. J. Rem. Sens.*, vol. 14, pp. 1735–1758.

Lozano-Garcia, D. F. and R. M. Hoffer (1993). Synergistic effects of combined Landsat-TM and SIR-B data for forest resources assessment. *Int. J. Rem. Sens.*, vol. 14, p. 2677.

Luvall, J. C. and H. R. Holbo (1989). Measurements of short-term thermal responses of coniferous forest canopies using thermal scanner data. *Rem. Sens. Environ.*, vol. 27, pp. 1–10.

McDonald, K. C., M. C. Dobson, and F. T. Ulaby (1990). Using MIMICS to model L-band multiangle and multitemporal backscatter for a walnut orchard. *IEEE Trans. Geosci. Rem. Sens.*, vol. 28, pp. 477–491.

McDonald, K.C., M. C. Dobson, and F. T. Ulaby (1991). Modeling multifrequency diurnal backscatter from a walnut orchard. *IEEE Trans. Geosci. Rem. Sens.*, vol. 29, pp. 852–863.

McDonald, K. C. and F. T. Ulaby (1993). Radiative transfer modeling of discontinuous tree canopies at microwave frequencies. *Int. J. Rem. Sens.*, vol. 14, No. 11, pp. 2097-2128.

McFarlane, N. A., G. J. Boer, J.-P. Blanchet, and M. Lazare (1992). The Canadian Climate Center second generation general circulation model and its equilibrium climate. *Journal of Climate*, vol. 5, pp. 1013–1044.

Melack, J. M., L. L. Hess, and S. Sippel (1994). Remote sensing of lakes and floodplains in the Amazon Basin. *Rem. Sens. Rev.*, vol. 10, pp. 127–142.

Moghaddan, M., S. Durden, and H. Zebker (1994). Radar measurements of forested areas during OTTER. *Rem. Sens. Environ.*, vol. 47, pp. 154–166.

Morrissey, L. A., G. P. Livingston, and S. L. Durden (1994). Use of SAR in regional methane exchange studies. *Int. J. Rem. Sens.*, vol. 15, pp. 1337–1342.

Morrissey, L. A., S. L. Durden, G. P. Livingston, J. A. Stearn, and L. S. Guild (1995). Differentiating methane source areas with multitemporal ERS-1 SAR data within arctic environments. *IEEE Trans. Geosci. Rem. Sens.* (in press).

Ormsby, J. P., B. Blanchard, and A. J. Blanchard (1985). Detection of lowland flooding using microwave systems. *Photo. Eng. Rem. Sens.*, vol. 51, pp. 317–328.

Pierce, L. E., F. T. Ulaby, K. Sarabandi, and M. C. Dobson (1994). Knowledge-based classification of polarimetric SAR images. *IEEE Trans. Geosci. Rem. Sens.*, vol. 31, pp. 1081–1086.

Pope, K. O., E. J. Sheffner, K. J. Linthicum, C. L. Bailey, T. M. Logan, E. S. Kasischke, K. Birney, A. R. Njogu, and C. R. Roberts (1992). Identification of Central Kenyan Rift Valley fever virus vector habitats with Landsat TM and evaluation of their flooding status with airborne imaging radar. *Rem. Sens. Environ.*, vol. 40, pp. 185–196.

Pope, K. O., J. M. Rey-Benayas, and J. F. Paris (1994). Radar remote sensing of forest and wetland ecosystems in the Central American tropics. *Rem. Sens. Environ.*, vol. 48, pp. 205–219.

Post, W. M. (1993). Uncertainties in the terrestrial carbon cycle, in *Vegetation Dynamics and Global Change*. (A. M. Solomon and H. H. Shugart, eds). Chapman and Hall, London, pp. 116–132.

Ranson, J. K. and G. Sun (1994). Northern forest classification using temporal multifrequency and multipolarimetric SAR images. *Rem. Sens. Environ.*, vol. 47, pp. 142–153.

Ranson, K. J. and G. Sun (1994). Mapping biomass of a northern forest using multifrequency SAR data. *IEEE Trans. Geosci. Rem. Sens.*, vol. 32, pp. 388–396.

Ranson, K.J., S. Saatchi, and G. Sun. Boreal forest ecosystem characterization with SIR-C/X-SAR. *IEEE Trans. Geosci. Rem. Sens.* (in press).

Rejmankova, E., D. R. Roberts, R. E. Harbach, J. Pecor, E. L. Peyton, S. Manguin, R. Krieg, J. Polanco, and L. Legters (1993). Environmental and regional determinants of anopheles larval distribution in northern Belize. *Environ. Entomology*, vol. 22, pp. 978–992.

Rejmankova, E., K. O. Pope, M. D. Pohl, and J. M. Rey-Benayas (1995). Freshwater wetland plant communities of northern Belize: Implications for paleoecological studies of Maya wetland agriculture. *Biotropica* (in press).

Richards, J. A., G-Q. Sun, and D. S. Simonett (1987). L-band radar backscatter modeling of forest stands. *IEEE Trans. Geosci. Rem. Sens.*, vol. 25, pp. 487–498.

Rignot, E. and J. B. Way (1994). Monitoring freeze-thaw cycles along north-south Alaskan transects using ERS-1 SAR. *Rem. Sens. Environ.*, vol. 49, pp. 131–137.

Rignot, E., J. B. Way, K. McDonald, L. Viereck, C. Williams, P. Adams, C. Payne, W. Wood, and J. Shi (1994a). Monitoring of environmental conditions in taiga forests using ERS-1 SAR. *Rem. Sens. Environ.*, vol. 49, pp. 145–154.

Rignot, E., J. B. Way, C. Williams, and L. Viereck (1994b). Radar estimates of aboveground biomass in boreal forests of interior Alaska. *IEEE Trans. Geosci. Rem. Sens.*, vol. 32, pp. 1117–1124.

Rignot, E., C. Williams, J. B. Way, and L. Viereck (1994c). Mapping of forest types in Alaskan boreal forests using SAR imagery. *IEEE Trans. Geosci. Rem. Sens.*, vol. 32, pp. 1051–1059.

Schlentner, R. E. and K. Van Cleve (1985). Relationships between CO_2 evolution from soil, substrate temperature and substrate moisture in four mature forest types in interior Alaska. *Can. J. For. Res.*, vol. 15, pp. 97–106.

Schlesinger, M. E. and J. F. B. Mitchell (1987). Climate model simulations of the equilibrium climatic response to increased carbon dioxide. *Reviews of Geophysics*, vol. 25, pp. 760–798.

Smith, T. M., W. P. Cramer, R. K. Dixon, R. Leemans, R. P. Neilson, and A. M. Solomon (1993). The global terrestrial carbon cycle. *Water, Air, Soil Pol.*, vol. 70, pp. 19–37.

Solomon, A. M. and W. Cramer (1993). Biospheric implications of global environmental change, in *Vegetation Dynamics and Global Change*. A. M. Solomon and H. H. Shugart, eds.), Chapman and Hall, London, pp. 25–52.

Sun, G. and D. S. Simonett (1988). Simulation of L-band HH microwave backscattering from coniferous forest stands: a comparison with SIR-B data. *Int. J. Rem. Sens.*, vol. 9, pp. 907–925.

Sun, G., D. S. Simonett, and A. H. Strahler (1991). A radar backscatter model for discontinuous forest canopies. *IEEE Trans. Geosci. Rem. Sens.*, vol. 29, pp. 639–650.

Sun, G. and K. J. Ranson (1995). A three-dimensional radar backscatter model for forest canopies. *IEEE Trans. Geosci. Rem. Sens.* (in press).

Tans, P. P., I. Y. Fung, and T. Takahashi (1990). Observational constraints on the global atmospheric CO_2 budget. *Science*, vol. 247, pp. 1431–1438.

Ulaby, F. T., B. Brisco, and M. C. Dobson (1983). Improved spatial mapping of rainfall events with spaceborne SAR imagery. *IEEE Trans. Rem. Sens.*, vol. 21, pp. 118–121.

Ulaby, F. T., K. Sarabandi, K. McDonald, M. Whitt, and M. C. Dobson (1990). Michigan microwave canopy scattering model. *Int. J. Rem. Sens.*, vol. 11, pp. 1223–1253.

Ulaby, F. T., F. Kouyate, B. Brisco, and T. H. L. Williams (1986). Textural information in SAR images. *IEEE Trans. Geosci. Rem. Sens.*, vol. 24, pp. 232–245.

van Zyl, J. J. (1989). Unsupervised classification of scattering behavior using radar polarimetry data. *IEEE Trans. Geosci. Rem. Sens.*, vol. 27, pp. 36–45.

van Zyl, J. J. and C. F. Burnette (1992). Baysian classification of polarimetric SAR images using adaptive a priori probabilities. *Int. J. Rem. Sens.*, vol. 13, pp. 835–840.

Viereck, L. A. (1983). The effects of fire in black spruce ecosystems of Alaska and northern Canada in *The Role of Fire in Northern Circumpolar Ecosystems (Scope 18)* (R. W. Wein and D. A. MacLean, eds.), John Wiley and Sons, Chichester, England, pp. 201–220.

Wang, Y., F. W. Davis, and J. M. Melack (1993a). Simulated and observed backscatter at P-, L-, and C-bands from ponderosa pine stands. *IEEE Trans. Geosci. Rem. Sens.*, vol. 31, No. 4, pp. 871–879.

Wang, Y., J. L. Day, F. W. Davis, and J. M. Melack (1993b). Modeling L-band radar backscatter from Alaskan boreal forest. *IEEE Trans. Geosci. Rem. Sens.*, vol. 31, pp. 1146–1154.

Wang, Y., F. W. Davis, J. M. Melack, E. S. Kasischke, and N. L. Christensen, Jr. (1994a). The effects of changes in forest biomass on radar backscatter from tree canopies. *Int. J. Rem. Sens.* (in press).

Wang, Y., E. S. Kasischke, F. W. Davis, J. M. Melack, and N. L. Christensen, Jr. (1994b). The effects of changes in loblolly pine biomass and soil moisture variations on ERS-1 SAR backscatter—a comparison of observations with theory. *Rem. Sens. Environ.*, vol. 49, No. 1, pp. 25–31.

Wang, Y., L. L. Hess, S. Filoso, and J. M. Melack (1995). Canopy penetration studies: modeled radar backscatter from Amazon floodplain forests at C-, L-, and P-band. *Rem. Sens. Environ.* (in press).

Waring, R. H., J. B. Way, R. Hunt, Jr., L. Morrisey, K. J. Ranson, J. Weishampel, R. Oren, and S. E. Franklin. Remote sensing with synthetic aperture radar in ecosystem studies. *Bioscience* (in press).

Way, J. B., J. Paris, E. Kasischke, C. Slaughter, L. Viereck, N. Christensen, M. C. Dobson, F. T. Ulaby, J. Richards, A. Milne, A. Sieber, F. J. Ahern, D. Simonett, R. Hoffer, M. Imhoff, and J. Weber (1990). The effect of changing environmental conditions on microwave signatures of forest ecosystems: preliminary results of the March 1988 Alaskan aircraft SAR experiment. *Int. J. Rem. Sens.*, vol. 11, pp. 1119–1144.

Way, J.B. and E.A. Smith (1991). The Evolution of Synthetic Aperture Radar Systems and their progression to the Eos SAR. *IEEE Trans. on Geosci. and Rem. Sens*, vol. 29, pp. 962–985.

Way, J. B., E. J. M. Rignot, K. C. McDonald, R. Oren, R. Kwok, G. Bonan, M. C. Dobson, L. A. Viereck, and J. A. Roth (1994). Evaluating the type and state of Alaska taiga forests with imaging radar for use in ecosystem models. *IEEE Trans. Geosci. Rem. Sens.*, vol. 32, pp. 353–370.

Weishampel, J. F., G. Sun, J. K. Ranson, D. LeJune, and H. H. Shugart (1994). Forest textural properties from simulated microwave backscatter: the influence of spatial resolution. *Rem. Sens. Environ.*, vol. 47, pp. 120–131.

Yueh, S. H., J. A. Kong, J. K. Jao, R. T. Shin, and T. LeToan (1992). Branching model for vegetation. *IEEE Trans. Geosci. Rem. Sens.*, vol. 30, pp. 390–402.

3—Hydrology

Basharinov, A.Y. and A.M Shutko (1975). *Simulation Studies of the SHF Radiation Characteristics of Soils Under Moist Conditions.* NASA Tech. Trans. TTF-16, Greenbelt, MD.

Bell, K. R., B. J. Blanchard, T. J. Schmugge, and M. W. Witczak (1980). Analysis of surface moisture variations within large-field sites. *Water Resources Research,* vol. 16, No. 4, pp. 796–81.

Betts, A. K., J. H Ball, A. C. Baljaars, M. J. Miller and P. Viterbo (1994). Coupling between land surface, boundary layer parametrizations and rainfall on local and regional scales: Lessons from the wet summer of 1993. Fifth Conference on Global Change Studies: *American Meteor. Soc.*, 74th Annual Meeting, Nashville, Tenn., Jan 23-28.

Chang, A. T. C., S. G. Atwater, V. V. Salomonson, J. E. Estes, D. S. Simonett, and M. L. Bryan (1980). L-band radar sensing of soil moisture. *IEEE Trans. Geosci. Rem. Sens.*, vol. 18, No. 4, pp. 303–310.

Chang, J. T. and P. J. Wetzel (1991). Effects of spatial variations of soil moisture and vegetation on the evolution of a prestorm environment: a numerical case study. *Mon. Weather Rev.,* vol. 119, No. 6, pp. 1368-1390.

Delworth, T. L. and S. Manabe (1988). The influence of potential evaporation on the variabilities of the simulated soil wetness and climate. *J. Climate,* vol. 1, pp. 523-547.

Dobson, M. C., and F. T. Ulaby (1986). Preliminary evaluation of the SIR-B response to soil moisture, surface roughness and crop canopy cover. *IEEE Trans. Geosci. Rem. Sens.*, vol. 24, No. 4, pp. 517–526.

Dubois, P.C., J. J. van Zyl, and E. T. Engman (1995). Measuring soil moisture with imaging radars, *IEEE Trans. Geosci. Rem. Sens.* (in press).

Entekhabi, D., H. Nakamura, and E. G. Njoku (1994). Solving the inverse problem for soil moisture and temperature profiles by sequential assimilation of multifrequency remotely sensed observations. *IEEE Trans. Geosci. Rem. Sens.*, vol. 32, No. 2, pp. 438–448.

Fast, J. D. and M. D. McCorcle (1991). The effect of heterogeneous soil moisture on a summer baroclinic circulation in the central United States. *Mon.Weather Rev.*, vol. 119, No. 9, pp. 2140-2167.

Fung, A. K., Z. Li, K.S. Chen (1992). Backscattering from a randomly rough dielectric surface. *IEEE Trans. Geo. Rem. Sens.*, vol. 30, pp. 356-369.

Hawley, M. E., R. H. McCuen, and T. J. Jackson (1982). Volume-accuracy relationship in soil moisture sampling. *J. of the Irrigation and Drainage Div. of ASCE*, 108(IR1):IR1-IR11.

Jackson, T. J. (1980). Profile soil moisture from surface measurements. *J. of the Irrigation and Drainage Div. of ASCE*, 106(IR2):IR81-IR92.

Jackson, T. J., A. Chang, and T. J. Schmugge (1981). Active microwave measurements for estimating soil moisture in Oklahoma. *Photgram. Eng. Rem. Sens.*, vol. 4, pp. 801–805.

Jackson, T. J., M. E. Hawley, and P. E. O'Neill (1987). Preplanting soil moisture using passive microwave sensors. *Water Resources Bulletin*, vol. 23, No. 1, pp. 281–296.

Jackson, T. J., D. M. Le Vine, A. J. Griffis, D. C. Goodrich, T. J. Schmugge, C. T. Swift, and P. E. O'Neill (1993). Soil moisture and rainfall estimation over a semiarid environment with the ESTAR radiometer. *IEEE Trans. Geosci. Rem. Sens.*, vol. 31, No. 4, pp. 836–841.

Jackson, T.J., T.J. Schmugge and J.R. Wang (1982). Passive microwave remote sensing of soil moisture under vegetation canopies. *Water Resour. Res.*, vol. 18, pp. 1137–1142.

Jackson, T.J. and T.J. Schmugge (1991). Correction for effects of vegetation on the microwave emission of soils, *IEEE Int. Geosci. Rem Sen. Symp. Digest,* pp. 753–756.

Kostov, K. G. (1993). Passive microwave remote sensing of soil moisture--experimental and modelling results. *Advances in Space Research,* vol. 13, No. 5, pp. 105–114.

Lanicci, J. M, T. N. Carlson, and T. T. Warner (1987). Sensitivity of the Great Plains severe-storm environment to soil moisture distribution. *MontWeather Rev.*, vol. 115, No. 11, pp. 2660-2673.

Lin D. S., E. F. Wood, K. Beven and S. Saatchi (1994a). Soil moisture estimation over grass-covered areas using AIRSAR. *Int. J. Rem. Sens.*, vol. 15, No. 11, pp. 2323-2343.

Lin D. S., E. F. Wood, P. Troch, M. Mancini, T. Jackson (1994b). Comparisons of remotely sensed and model-simulated soil moisture over a Heterogeneous Watershed. *Rem. Sens. Environ.*, vol. 48, pp 159-171.

Manabe, S., J. Smagorinsky, and R.J. Strickle (1965). Simulated climatology of a general circulation model with a hydrologic cycle, *Mon. Weather Rev.*, vol. 93, pp. 769–798.

Manabe, S. (1969). Climate and ocean circulation, I, The atmospheric circulation and the hydrology of the Earth's surface, *Mon. Weather Rev.*, vol. 97, pp. 739–774.

Oh, Y., K. Sarabandi, and F. T. Ulaby (1992). An empirical model and an inversion technique for radar scattering from bare soil surfaces. *IEEE Trans. Geosci. Rem. Sens.*, vol. 30, No. 2, pp. 370–381.

Reutov, E. A. and A. M. Shutko, (1986). Prior-knowledge-based soil moisture determination by microwave radiometry. *Soviet J. Rem. Sens.*, vol. 5, No. 1, pp. 100–125.

Reutov, E. A. and A. M. Shutko (1990). Microwave spectroradiometry of water content of nonuniformly moistened soil with a surface transition layer. *Soviet J. Rem. Sens.*, vol. 6, No. 1, pp. 72–79.

Rind, D. (1982). The influence of ground moisture conditions in North America on summer climate as modelled in the GISS GCM. *Mon. Weather Rev.*, vol. 110, pp. 1487–1494.

Rogowski, A.S. (1972). Watershed Physics: Soil Variability Criteria. *Water Resour. Res.*, vol. 8, No. 4, pp. 1015-1023.

Rowntree, P.R. and J.R. Bolton (1983). Simulation of the atmospheric response to soil moisture anomalies over Europe. *Q. J. R. Meteorol. Soc.*, vol. 109, pp. 501–526.

Saatchi, S. S., J. J. van Zyl, and G. Asrar (1994). Estimation of canopy water content in Konza Prairie grasslands using SAR measurments during FIFE. *Rem. Sens. Environ.* (in press).

Shi, J. and J. Dozier (1995). Inferring snow wetness using SIR-C's C-band polarimetric synthetic aperture radar. *IEEE Trans. on Geosci. and Rem. Sens.* (paper accepted).

Shukla, J. and Y. Mintz (1982). The influence of land-surface evapotranspiration on Earth's climate, *Science*, vol. 215, pp. 1498–1501.

Ulaby, F. T and P. P. Batlivala (1976). Optimum radar parameters for mapping soil moisture. *IEEE Trans. on Geosci. Electron.*, vol. 14, No. 2, pp. 81–93.

Ulaby, F. T., P. P. Batlivala, and M. C. Dobson (1978). Microwave backscatter dependence on surface roughness, soil moisture and soil texture: Part I—bare soil. *IEEE Trans. on Geosci. Electron.*, vol. 16, pp. 286–295.

Vinnikov, K.Y. and I.B. Yeserkepova (1991). Soil Moisture: Empirical data and model results, *J. Climate*, vol. 4, pp. 66–79.

Walker, J. M and P. R. Rowntree (1977). The effect of soil moisture on circulation and rainfall in a tropical model. *Q. J. Meteorol. Soc.*, vol. 103, pp.29-46.

Wang, J. R., E. T. Engman, J. C. Shiue, M. Rusek, C. Steinmeier (1986). The SIR-B observations of microwave backscatter dependence on soil moisture, surface roughness and vegetation covers. *IEEE Trans. Geosci. Rem. Sens.*, vol. 24, No. 4, pp. 510–516.

4—Marine Science and Applications

Aagaard, K. and E. Carmack (1994). The Arctic Ocean and climate: a perspective, in *The Polar Oceans and Their Role in Shaping the Global Environment* (Johannessen, et al. eds.) AGU, Washington DC, pp. 5–20.

Apel, J. R. (1994). An improved model of the ocean surface wave vector spectrum and its effects on radar backscatter. *J. Geophys. Res.*, vol. 99, No. CB, pp. 16, 269–16, 291.

Alpers, W., and B. Brümmer (1994). Atmospheric boundary layer rolls observed by the synthetic-aperture radar aboard the ERS-1 satellite, *J. Geophys. Res.*, vol. 99, pp. 12,613–12,621.

Bakun, A., and R. H. Parrish (1982). Turbulence, transport and pelagic fish in the California and Peru Current systems, *CalCOFI Report 23*, pp. 99–112.

Beal, R. C., D. G. Tilley, and F. M. Monaldo (1983). Large and small scale spatial evolution of digitally processed ocean wave spectra from Seasat synthetic aperture radar. *J. Geophys. Res.*, vol. 88, pp. 1761–1778.

Beal, R. C., F. M. Monaldo, D. G. Tilley, D. E. Irvine, E. J. Walsh, F. C. Jackson, D. W. Hancock, III, D. E. Hines, R. N. Swift, F. I. Gonzalez and L. F. Zambresky (1986). A comparison of SIR-B directional ocean wave spectra and aircraft scanning radar spectra. *Science*, vol. 232, pp. 1531–1535.

Bourke, R. H. and A. McLaren (1992). Contour mapping of Arctic basin ice draft and roughness parameters. *J. Geophys. Res.*, vol. 97, No. C11, pp. 17,715–17,728.

Burns, J. J., L. H. Shapiro, and F. H. Fay (1981). Ice as marine mammal habitat in the Bering Sea. *The Eastern Bering Sea Shelf: Oceanography and Resources.* (D. W. Hood and J. A. Calder, eds.) vol. 2, pp. 781–797, Univ. of Washington Press, Seattle.

Carsey, F. and R. Garwood. Identification of modeled ocean plumes in Greenland gyre ERS-1 SAR data. *Geophys. Res. Lett.*, vol. 20, pp. 2207–2210.

Carsey, F. and A. Roach (1994). Oceanic convection in the Greenland Sea Odden region as interpreted in satellite data in *The Role of the Polar Oceans in Shaping the Global Environmentt* (O. Johannessen, ed.). AGU Monograph, vol. 85, pp. 211–222.

Cox, G. F. N. and W. F. Weeks (1988). Numerical simulations of the profile properties of undeformed first-year sea ice during the growth season. *J. Geophys. Res.*, vol. 93, pp. 12,449–12,460.

Drinkwater, M., R. Kwok, E. Rignot, H. Israelsson, R. Onstott, and D. Winebrenner (1992). Potential applications of polarimetry to the classification of sea ice, in *Microwave Remote Sensing of Sea Ice* (F. Carsey, ed.). Geophysical Monograph 68, AGU, Washington, D.C., pp. 419–430.

Fetterer, F. M., D. Gineris, and R. Kwok (1994). Sea-ice type maps from Alaska Synthetic Aperture Radar Facility, imagery: an assessment of Arctic multi-year ice coverage estimated through Alaska SAR Facility data analysis. *J. Geophys. Res.*, vol. 99, No. C11, pp. 22,443–22,458.

Fiedler, P. C., G. B. Smith, R. M. Laurs (1984). Fisheries applications of satellite data in the eastern North Pacific. *Marine Fisheries Review*, vol. 46, No. 3, pp. 1-13.

Flemming, N. C. (1995). Making the case for GOOS. *Sea Technology,* Jan., pp. 44–49.

Fu, L., and B. Holt (1982). *SEASAT Views Oceans and Sea Ice with Synthetic Aperture Radar.* Publication 81–120, NASA, Jet Propulsion Laboratory, California Institute of Technology, Pasadena, CA.

Gabriel, A. K. and R. M. Goldstein (1988). Crossed orbit interferometry: theory and experimental results from SIR-B. *Int. J. of Remote Sensing*, vol. 9, pp. 857–872.

Grabak, O., J. A. Johannessen, H. E. Krogstad (1994). Characterization of wind fronts in SAR images. *Int. Geoscience Rem. Sensing Symp.,* Aug. 8-12, Pasadena, CA, p. 543.

Griffin, O. M., R. D. Peltzer, A. M. Reeo (1992). Remote sensing of surface ship wakes. *Naval Engineers Journal*, vol.104, pp. 245–258.

Holt, B., D. A. Rothrock, and R. Kwok (1992). Determination of sea ice motion from satellite images. *Microwave Remote Sensing of Sea Ice* (F. D. Carsey, ed.). Geophysical Monograph 68, pp. 344–354, American Geophysical Union, Washington, D.C.

Keller, W. C., V. Wismann, and W. Alpers (1989). Tower-based measurements of the C-Band radar backscatter crossection. *J. Geophys. Res.*, vol. 94, pp. 924–930.

Kwok, R., E. Rignot, B. Holt, and R. Onstott (1992). Identification of sea ice types in spaceborne synthetic aperture radar. *J. Geophys. Res.*, vol. 97, C2, pp. 2391–2402.

Kwok, R., D. A. Rothrock, H. Stern, and G. Cunningham (1995). Determination of ice age from Lagrangian observations of ice motion. *IEEE Trans. Geoscience and Remote Sensing*, vol. 33, No. 2, pp. 392-400.

Li, F. K. and R. M. Goldstein (1990). Studies of multi-baseline spaceborne interferometric synthetic aperture radars. *IEEE Trans. on Geoscience and Remote Sensing*, vol. 28, No. 1, pp. 88–97.

Liu, A. K., S. Hakkinen, and C. Y. Peng (1993). Wave effects on ocean-ice interaction in the marginal ice zone. *J. Geophys. Res.*, vol. 98, pp. 10,025–10,036.

Liu, A. K., C. Y. Peng, and J. D. Schumacher (1994a). Wave-current interaction study in the Gulf of Alaska for detection of eddies by SAR. *J. Geophys. Res.*, vol. 99, pp. 10,075–10,085.

Liu, A. K., C. Y. Peng, and T. J. Weingartner (1994a). Ocean-ice interaction in the marginal ice zone using SAR. *J. Geophys. Res.*, vol. 99, pp. 22,391–22,400.

MacArthur, J. L. (1987). Spectrasat system design using maximum heritage. *Johns Hopkins APL Tech Digest,* vol. 8 (1), pp. 128–132.

Maykut, G. A. (1986). The surface heat and mass flux. *The Geophysics of Sea Ice,* N. Untersteiner, editor, *NATO ASI Series B: Physics,* vol. 146, Plenum Press, New York, pp. 395–464.

Monaldo, F. M. and R. C. Beal (1994). Real time observations of southern ocean wave fields from the shuttle imaging radar. *Trans. Geoscience and Remote Sensing* (in press).

Ocean Studies Board (OSB) (1992). *Oceanography in the Next Decade.* NAS/NRC.

Onstott, R. (1992). SAR and scatterometer signatures of sea ice. In *Microwave Remote Sensing of Sea Ice* (F. Carsey, ed.), Geophysical Monograph 68, AGU, Washington, D.C., pp. 73–104.

Pierson, W. J. (1965). Wind waves and swell. In *Woods Hole Oceanography Institute Proc. on Oceanography from Space*, Ref. No. 65–10, pp. 393–402.

Rufenach, C. L., L. S. Fedor, J. R. Apel, and F. I. Gonzalez (1985). *Surface and Internal Ocean Wave Observations in Satellite Oceanic Remote Sensing*. (B. Saltzmann, ed.), Academic Press, vol. 27, p. 141.

Schumacher, J. D., W. E. Barber, B. Holt and A. K. Liu (1991). *Satellite observations of mesoscale features in Lower Cook Inlet and Shelikof Strait, Gulf of Alaska*. NOAA Tech. Rep. ERL 445-PMEL 40, p. 18, Pac. Mar. Environ. Lab., Seattle, Wash.

Schweiger, A. J., and D. A. Rothrock (1994). Monitoring sea ice flux through Fram Strait. Proc. Second ERS-1 SAR Symp., Hamburg, 1993, ESA SP-361, pp. 277–279.

Stern, H., D. Rothrock, R. Kwok, and B. Holt (1994). The geophysical processor system: automated analysis of ERS-1 SAR imagery. *Proc. of the Second ERS-1 SAR Symp., Space at the Service of Our Environment,* 1993, Hamburg, pp. 281–286.

Steffen, K. and J. Heinrichs (1994). Feasibility of sea ice typing with synthetic aperture radar: merging of Landsat Thematic Mapper and ERS-1 SAR satellite imagery. *J. Geophys. Res.,* vol. 99, No. C11, pp. 22,413–22,424.

Stern, H., D. A. Rothrock, and R. Kwok (1994). Open water production in the Arctic Sea ice cover: satellite measurements and model parameterization. *J. Geophys. Res.,* (in press).

Stouffer, R., S. Manabe, and K. Bryan (1989). Interhemispheric asymmetry in climate response to a gradual increase of atmospheric CO_2. *Nature*, vol. 342, pp. 660–682.

Thompson, D. R. and J. R. Jensen (1993). Synthetic aperture radar interferometry applied to ship-generated internal waves in the 1989 Loch Linnhe experiment. *J. Geophys. Res.*, vol. 98, No. C6, pp. 10,259–10,269.

Thompson, D. R., H. C. Graber, and R. E. Carande (1994). Measurements of ocean currents with SAR interferometry and HF radar. *Int. Geoscience and Remote Sensing Symp.,* Aug. 8-12, 1994, Pasadena, CA.

True, M., et al. (1994). Thickness characterization of oil spills using active microwave sensors. Presented at the European Symp. on Satellite Remote Sensing, Sept. 26-30, 1994, Rome, Italy.

Vachon, P., O. Johannessen, and J. Johannessen (1994). An ERS-1 SAR image of atmospheric lee waves. *J. Geophys. Res.*, vol. 99, pp. 22,483–22,490.

Wackerman, C., R. Shuchman, and F. Fetterer (1994). Estimation of wind speed and wind direction from ERS-1 imagery. *IGARSS '94 Surface and Atmospheric Remote Sensing: Technologies, Data, Analysis and Interpretation*, Pasadena, Aug. 8-12, 1994, *IEEE,* vol. II, pp. 1222–1224.

Wadhams, P. and B. Holt (1991). Waves in frazil and pancake ice and their detection in Seasat synthetic aperture radar imagery. *J. Geophys. Res.,* vol. 96, pp. 8835–8852.

Wahl, T., K. Eldhusat, and A. Skoelv (1993). Ship traffic monitoring using the ERS-1 SAR. *Proc. of the First ERS-1 Symp.*, ESA SP-359.

Weissman, D. E., K. L. Davidson, R. A. Brown, C. A. Friehe, and F. Li (1994). The relationship between the microwave radar cross section and both wind speed and stress: model function studies using frontal air-sea interaction experiment data. *J. Geophys. Res.*, vol. 99, No. C5, pp. 10,087–10,108.

Williams, R. S., Jr., D. K. Hall, and C. S. Benson (1991). Analysis of glacier facies using satellite techniques. *J. Glaciology,* vol. 37, No. 125, pp. 120–128.

Winebrenner, D., D. Farmer, and I. Joughin (1994). On the response of polarimteric SAR signatures at 24-cm wavelength to sea ice thickness in Arctic leads. *Radio Science*, vol. 30, No. 2, pp. 373-402.

5—Ice Sheets and Glaciers

Alley, R. B., D. A. Meese, C. A. Shuman, A.J. Gow, K.C. Taylor, P.M. Grootes, J.W.C. White, M. Ram, E.D. Waddington, P.A. Mayewski, and G.A. Zielinski (1993). Abrupt increase in Greenland snow accumulation at the end of the Younger Dryas event. *Nature,* vol. 362, pp. 527–529.

Bader, H., 1961. In *Cold Regions Science and Engineering* (F. J. Sanger, ed.). CRREL, Hanover, NH, Part 1, Sec. B2, pp. 1–18.

Bentley, C. R. and M. B. Giovinetto (1991). Mass balance and sea-level change. *Proc. of the International Conference on the Role of the Polar Regions in Global Change.* June 11-15, 1990, Fairbanks, Alaska, University of Alaska, pp. 481–488.

Bindschadler, R. A., K. C. Jezek, and J. Crawford (1987). Glaciological investigations using the Synthetic Aperture Radar imaging system. *Annals of Glaciology*, vol. 9, pp. 11–19.

Bindschadler, R. A. and T. A. Scambos (1991). Satellite-image-derived velocity field of an Antarctic ice stream. *Science*, vol. 252, pp. 242–246.

Broecker, W. S. and G. H. Denton (1989). The role of ocean-atmosphere reorganizations in glacial cycle. *Geochimica et Cosmoschimica Acta*, vol. 53, No. 10, pp. 2465–2501.

Dawson, A. G. (1992). *Ice Age Earth, Late Quaternary Geology and Climate*, Routledge, London.

Denton, G. H. and T. J. Hughes (1981). *The Last Great Ice Sheets*, John Wiley and Sons.

Drewry, D., S. R. Jordan, and E. Jankowski (1982). Measured properties of the Antarctic ice sheet: Surface configuration, ice thickness, volume and bedrock characteristics. *Annals of Glaciology*, vol. 3, pp. 83–91.

Fahnestock, M.A., R.A. Bindschadler, R. Kwok, and K.C. Jezek (1993). Greenland ice sheet surface properties and ice flow from ERS-1 SAR Imagery. *Science*, vol. 262, pp. 1530–1534.

Fairbanks, R.G. (1989). A 17,000-year glacio-eustatic sea level record: influence of glacial melting rates on the Younger Dryas event and deep-ocean circulation. *Nature*, vol. 342, p. 637–642.

Fatland, D.R. and C.S. Lingle (1994). The surface velocity field on Bagley Ice Field, Alaska, before and during the 1993-94 surge of Bering Glacier. *ERS-1 SAR interferometry, Eos, Fall Meeting Supplement,* vol. 75, No. 44, p. 62.

Forster, R.R. and B.L. Isacks (1994). The Patagonian icefields revealed by space shuttle synthetic aperture radar (SIR-C/X-SAR). *Eos, Fall Meeting Supplement*, vol. 75, No. 44, p. 226.

Goldstein, R.M., H. Englehardt, B. Kamb and R.M. Frolich (1993). Satellite radar interferometry for monitoring ice sheet motion: Application to an Antarctic ice stream. *Science*, vol. 262, pp. 1525–1530.

Hartl, P., K.-H. Thiel, X. Wu, C.S.M. Doake, and J. Sievers (1994). Application of SAR interferometry with ERS-1 in the Antarctic. *Earth Observation Quarterly*, vol. 43, ESA, pp. 1–4.

Heinrich, H. (1989). Origin and consequences of cyclic rafting in the northeast Atlantic Ocean during the past 130,000 years. *Quaternary Research*, vol. 29, pp. 142–152.

Jezek, K. and E. Rignot (1994). Katabatic wind processes on the Greenland ice sheet. *Eos, Trans. Geosci. Rem. Sens.*, vol. 75, No. 44, p. 212.

Jezek, K.C. (1993). Spatial patterns in backscatter strength across the Greenland ice sheet. *Proc. of the First ERS-1 Symposium–Space at the Service of our Environment*, Cannes, France, Nov. 4-6, 1992, ESA SP-359, pp. 269–272.

Jezek, K., M.R. Drinkwater, J.P. Crawford, R. Bindschadler, and R. Kwok (1993). Analysis of synthetic aperture radar data collected over the southwestern Greenland ice sheet. *Journal of Glaciology,* vol. 39, No. 131, pp. 119–132.

Joughin I., D. P. Winebrenner and M.A. Fahnestock (1995). Observations of complex ice sheet motion in Greenland using satellite radar interferometry. *Geophysical Res. Letters,* vol. 22, No. 5, pp. 571-574.

Joughin I., D.P. Winebrenner and M.A. Fahnestock (1994). Satellite radar interferometry observations of ice-sheet motion in Greenland. *Eos, Fall Meeting Supplement,* vol. 75, No. 44, p. 223.

Kwok, R. and M.A. Fahnestock (1995). Observations of complex ice sheet motion in Greenland using satellite radar interferometry (in press).

Meier, M.F. (1993). Ice, climate, and sea level; do we know what is happening? In *Ice in the Climate System,* (W. R. Peltier, ed.), NATO ASI Series, vol. I 12, Springer-Verlag, Berlin and Heidelberg, Federal Republic of Germany, pp. 141–160.

Ohmura, A. and N. Reeh (1991). New precipitation and accumulation maps for Greenland. *Journal of Glaciology*, vol. 37, No. 125, pp. 140–148.

Pfeffer, W.T., M.F. Meier, and T.H. Illangasekare (1991). Retention of Greenland runoff by refreezing: implications for projected future sea level change. *Journal of Geophysical Res.*, vol. 96, No. C12, pp. 22,117–22,124.

Rignot, E., K.C. Jezek, and H. Sohn (1995). Ice flow dynamics of the Greenland ice sheet from SAR interferometry. *Geophysical Res. Letters* (in press).

Scambos, T.A., M. J. Dutkiewicz, J. C. Wilson, and R. A. Bindschadler (1992). Application of image cross-correlation to the measurement of glacier velocity using satellite image data. *Remote Sensing of Environment,* vol. 42, pp. 177–186.

Shackleton, N.J. (1987). Oxygen isotopes, ice volume and sea level, *Quaternary Science Reviews,* vol. 6, pp. 183–190.

Vaughan, D.G., R.M. Frolich, and C.S.M. Doake (1994). ERS-1 SAR: Stress indicator for Antarctic ice streams. *Proc. of the Second ERS-1 Symposium*, ESA SP-361, pp. 183–186.

Williams, R.S. Jr., D.K. Hall, and C.S. Benson (1991). Analysis of glacier facies using satellite techniques. *J. of Glaciol.*, vol. 37, No. 125, pp. 120–128.

6—Solid Earth Sciences

Arvidson, R. E., R. Becker, A. Shanabrook, W. Luo, N. Sturchio, M. Sultan, Z. Lotfy, A. M. Mahmood, and Z. El Alfy (1994). Climatic eustatic and tectonic controls on Quaternary deposits and landforms, Red Sea coast, Eqypt. *J. Geophys. Res.*, vol. 99, pp. 12,175–12,190.

Blumberg, D. G. and R. Greeley (1993). Field studies of aerodynamic roughness length. *J. Arid Environ.*, vol. 25, pp. 39–48.

Brakenridge, G. R., J. C. Knox, E. D. Paylor, and F. J. Magilligan (1994). Radar remote sensing aids study of the Great Flood of 1993. *Eos,* vol. 75, pp. 521, 526–527.

Burke, K. and Dixon, T.H. (1988). *Topographic Science Working Group Report to the Land Processes Branch, Earth Science and Applications Division,* NASA Headquarters, Lunar and Planetary Inst., Houston, Texas, pp. 35–39.

Elachi, C. (1987). *Introduction to the Physics and Techniques of Remote Sensing*, Wiley, New York, p. 413.

Evans, D. L., T. G. Farr, and J. J. van Zyl (1992). Estimates of surface roughness derived from synthetic aperture radar (SAR) data. *IEEE Trans Geosci. Rem. Sens.*, vol. 30, pp. 382–389.

Greeley, R., L. Gaddis, N. Lancaster, A. Dobrovolskis, J. Iversen, K. Rasmussen, S. Saunders, J. van Zyl, S. Wall, H. Zebker, and B. White (1991). Assessment of aerodynamic roughness via radar observations. *Acta Mechanica*, suppl. 2, pp. 77–88.

Greeley, R., N. Lancaster, R. J. Sullivan, R. S. Saunders, E. Theileg, S. Wall, A. Dubrovolskis, B. R. White, and J. D. Iversen (1988). A relationship between radar backscatter and aerodynamic roughness. *Geophys. Res. Lttrs.*, vol. 15, pp. 565–568.

Kierein-Young, K. S. (1993). Comparison of inversion models using AIRSAR data for Death Valley, California. In *Summaries of the Fourth Annual JPL Airborne Geoscience Workshop,* JPL Pub. 93-26, vol. 3, Jet Propulsion Laboratory, California Inst. of Technology, Pasadena, CA, pp. 25–28.

Kierein-Young, K. S. and F. A. Kruse (1992). Extraction of quantitative surface characteristics from AIRSAR data from Death Valley, California. In *Summaries of the Third*

Annual JPL Airborne Geoscience Workshop, JPL Publication 92-14, vol. 3, Jet Propulsion Laboratory, California Inst. of Technology, Pasadena, CA, pp. 46–48.

Massonnet, D., K. Feigl, M. Rossi, and F. Adragna (1994). Radar interferometric mapping of deformation in the year after the Landers earthquake. *Nature*, vol. 369, pp. 227–230.

Massonnet, D., M. Rossi, C. Carmona, F. Adragna, G. Peltzer, K. Feigl, and T. Rabaute (1993). The displacement field of the Landers earthquake mapped by radar interferometry. *Nature*, vol. 364, pp. 138–142.

McCauley, J. F., G. G. Schaber, C. S. Breed, M. J. Grolier, C. V. Haynes, B. Issawi, C. Elachi, and R. Blom (1982). Subsurface valleys and geoarcheology of the eastern Sahara revealed by Shuttle radar. *Science*, vol. 218, pp. 1004–1020.

Mouginis-Mark, P. J. (1994). Mitigating volcanic hazards through radar interferometry. *Geotimes*, pp. 11–13, July 1994.

Rowland, S. K., G. A. Smith, and P. J. Mouginis-Mark (1994). Preliminary ERS-1 observations of Alaskan and Aleutian volcanoes. *Remote Sens. Environ.*, vol. 48, pp. 358–369.

Sud, Y. C., J. Shukla, and Y. Mintz (1988). Influence of land surface roughness on atmospheric circulation and precipitation: a sensitivity study with a general circulation model. *J. Applied Meteorol.*, vol. 27, pp. 1036–1054.

Topographic Science Working Group (1988). *Topographic Science Working Group Report to the Land Processes Branch, Earth Science and Applications Division.* NASA Headquarters. Lunar and Planetary Institute, Houston.

van Zyl, J. J. (1989). Unsupervised classification of scattering behavior using radar polarimetry data. *IEEE Trans. Geosci. Rem. Sens.*, vol. 27, pp. 36–45.

van Zyl, J. J., C. F. Burnette, and T. G. Farr (1991). Inference of surface power spectra from inversion of multifrequency polarimetric radar data. *Geophys. Res. Lttrs.*, vol. 18, No. 9, pp. 1787–1790.

Zebker, H. A., C. L. Werner, P. Rosen, and S. Hensley (1994). Accuracy of topographic maps derived from ERS-1 radar interferometry. *IEEE Trans. Geosci. Rem. Sens.*, vol. 32, pp. 823–836.

Zebker, H. A., P. Rosen, R. M. Goldstein, A. Gabriel, and C. L. Werner (1994). On the derivation of coseismic displacement fields using differential radar interferometry: the Landers earthquake. *J. Geophys. Res.*, vol. 99, pp. 19,617–19,634.

7—SAR System Technology

Freeland, R. E., and G. Bilyeu (1992). IN-STEP inflatable antenna experiment. 43rd Congress of the International Astronautical Federation, Washington, D.C., Aug. 28–Sept. 5, 1992, p. 98.

Gabriel, A., R. M. Goldstein, and H. A. Zebker (1989). Mapping small elevation changes over large areas: differential radar interferometry. *J. Geophys. Res.*, vol. 94, No. B7, pp. 9183–9191.

Gibbons, M. D., T. G. Edom, C. J. Bushell, and S. J. Udall (1994). The advance of spaceborne SAR–the ENVISAT ASAR antenna. IAF Paper 94-087, 45th Congress of the International Astronautical Federation, Jerusalem, Israel, Oct 9–14, 1994.

Jordan, R. (1980). The SEASAT-A Synthetic Aperture Radar System. *IEEE J. Ocean Eng.*, vol. OE-5, No. 2, pp. 154–164.

Special section on spaceborne radars for earth and planetary observations, Proc. of the *IEEE*, June 1991.

Zebker, H. and R. Goldstein (1986). Topography mapping from interferometric SAR observations. *J. Geophys. Res.*, vol. 91, No. B5, pp. 4993–4999.

Zebker, H., T. Farr, R. Salazar, and T. Dixon (1994). Mapping the world's topography using radar interferometry: the TOPSAT mission. *Proc. of the IEEE,* vol. 82, No. 12, pp. 1774–1786.

Appendix A

Contributors

Werner Alpers
Institut fur Meereskunde
University of Hamburg
Troplowitzstrassa 7
D-22529 Hamburg 54
GERMANY

Phone: 49-40-4123-5432/-5450
FAX: 49-40-4123-5713
email: alpers@ifm.uni-hamburg.de

John Apel
The Johns Hopkins University
Applied Physics Laboratory
Johns Hopkins Road
Laurel, MD 20707-6099

Phone: 301-953-5038
FAX: 301-953-1093
email: japel@aplcomm.jhuapl.edu

Jim Armitage
Westinghouse Electronic Systems
P.O. Box 1693
Mail Stop A455
Baltimore, Maryland 21203

Phone: (410) 765-8088
FAX:
email: none available

Raymond Arvidson
Washington University
Department of Earth and Planetary Sciences
St. Louis, MO 63031

Phone: (314) 935-5609
FAX: (314) 935-4998
email: arvidson@wunder.wustl.edu

Miriam Baltuck
NASA Headquarters
Code YSG
Washington DC 20546

Phone: (202) 358-0273
FAX: (202) 755-2552
email: mbaltuck@mtpe.hq.nasa.gov

Robert Beal
The Johns Hopkins University
Johns Hopkins Road
Laurel, MD 20707-6099

Phone: (301) 953-5009
FAX: (301) 953-5548/1093
email: r.beal@spacemail.jhuapl.edu

Appendix A

Contributors

Michael Bevis
University of Hawaii
Institute of Geophysics
2525 Correa Road
Honolulu, Hawaii 96822

Phone: (808) 956-8760
FAX: (808) 956-3188
email: bevis@soest.hawaii.edu

Robert Bindschadler
NASA-GSFC
Code 971
Oceans and Ice Branch
Greenbelt Road
Greenbelt, MD 20771

Phone: (301) 286-7611
FAX: (301) 286-0240
email: bob@laural.gsfc.nasa.gov

Dan Blumberg
Arizona State University
Dept of Geology
Tempe, AZ 85287-1404

Phone: (602) 965-7029
FAX:
email: blumberg@asuip2.dnet.nasa.gov

Robert Brakenridge
Dartmouth College
Geography HB 6017
Hanover, New Hamphshire 03755

Phone: (603) 646-2870
FAX: (603) 646-1601
email: brakenridge@dartmouth.edu

Frank Carsey
M/S 300-323
Jet Propulsion Laboratory
4800 Oak Grove
Pasadena, CA 91109

Phone: 818-354-8163
FAX: 818-393-6720
email: frank.d.carsey@jpl.nasa.gov

Alfred T. C. Chang
NASA/Goddard Space Flight Center
Code 974
Greenbelt, MD 20771

Phone: 301-286-8997
FAX: 301-286-1758
email: achang@rainfall.gsfc.nasa.gov

Appendix A

Contributors

Malcom Davidson
University Bonn
Institut for Agriculture
Katzenburgweg 5
D-53115 Bonn
Germany

Phone: 49-228-73-3186
FAX: 49-228-73-3708
email: none available

Frank Davis
University of California
Department of Geography
Santa Barbara, CA 93106

Phone: (805) 893-3438
FAX: (805) 893-3146
email: fd@geog.ucsb.edu

Timothy Dixon
University of Miami
RSMAS
4600 Rickenbacker Causeway
Miami, FL 33149

Phone: 305-361-4660
FAX: 305-361-4632
email: tim@corsica.rsmas.miami.edu

Craig Dobson
University of Michigan
Department of EECS
EECS Building
1301 Beal
Room 3228
Ann Arbor, MI 48109-2122

Phone: (313) 764-0501or (h)663-7535
FAX: (313) 747-2106
email: dobson@umich.edu

Jeff Dozier
University of California-Santa Barbara
School of Environmental Science and Management
Santa Barbara, CA 93106

Phone: (805) 893-7363
FAX: (805) 893-7612
email: dozier@icess.ucsb.edu

Ted Engman
Goddard Space Flight Center
Hydrological Sciences Branch
Code 974
Greenbelt, MD 20771

Phone: (301) 286-5355
FAX: (301) 286-1758
email: tengman@nasamail.nasa.gov

Appendix A
Contributors

Diane Evans
Jet Propulsion Laboratory
Mail Stop 180-703
4800 Oak Grove Drive
Pasadena, CA 91109

Phone: (818) 354-2418
FAX: (818) 354-8333
email: evans@berlin.jpl.nasa.gov

Mark Fahnestock
Joint Center for Earth Systems Science
Department of Meteorology
University of Maryland
College Park, Maryland 20742

Phone: (301) 405-5384
FAX:
email: mark@atmos.umd.edu

Pierre Flament
University of Hawaii at Manoa
Hawaii Institute of Geophysics
1000 Pope Road
Honolulu, HI 96822

Phone: (808) 956-6663/-6418
FAX: (808) 956-9225
email: pierre@mael.soest.hawaii.edu

Samuel Gasster
The Aerospace Corporation
P.O. Box 92957
Los Angeles, CA 90009-2957

Phone: (310) 336-6005
FAX: (310) 336-5581
email: gasster@courier6.aero.org

Prasad Gogineni
University of Kansas
Remote Sensing Lab
2291 Irving Rd. Hill
Lawrence, KS 66045

Phone: (913) 864-7734
FAX:
email: gogineni@eecf.ukans.edu

Ron Greeley
Arizona State University
Department of Geology
Tempe, AZ 85287-1404

Phone: (602) 965-7045
FAX: (602) 965-8102
email: greeley@asu.edu

Appendix A

Contributors

Dorothy Hall
NASA-GSFC
Greenbelt Road
Greenbelt, MD 20771

Phone: (301) 286-6892
FAX:
email: dhall@glacier.gsfc.nasa.gov

Catherine Hanks
University of Alaska
Geophysical Institute
PO Box 757320
Fairbanks, Alaska 99775-7320

Phone: (907) 474-5562
FAX: (907) 474-7290
email: chanks@dino.gi.alaska.edu

Phil Hartl
University of Stuttgart
Kepler Strasse II
700 Stuttgart 1
West Germany

Phone: 49-0711-121-3400
FAX:
email: none available

Dan Held
Westinghouse/ Nordin
Norden Place
P.O.Box 5300
Norwalk, CT 06856

Phone: (203) 852-7890
FAX: (203) 852-7423
email: held@norden.com

Laura Hess
University of California Santa Barbara
Department of Geology
Santa Barbara, CA 93106

Phone: (805) 893-8339
FAX: (805) 893-2578
email: lola@icess.ucsb.edu

Ben Holt
Jet Propulsion Laboratory
Mail Stop 300-323
4800 Oak Grove Drive
Pasadena, CA 91109

Phone: (818) 354-5473
FAX: (818) 393-6720
email: ben@pacific.jpl.nasa.gov

Appendix A

Contributors

John Hurrell
The Aerospace Corportation
P.O. Box 92957
Los Angeles, CA 90009-2957

Phone: (310) 336-6508
FAX: (310) 336-1636
email: john_hurrell@qmail2.aero.org

Bryan Isacks
Cornell University
Dept of Geological Sciences
3110 Snee Hall
INSTOC
Ithaca, NY 14853

Phone: (607) 255-2307
FAX: (607) 254-4780
email: bli1@cornell.edu

Thomas Jackson
USDA-ARS Hydrology Lab
Room 104, Bldg. 007
BARC-West
10300 Baltimore Ave.
Beltsville, MD 20705-2350

Phone: (301) 504-8511
FAX: (301) 504-8931
email: no email

Kenneth Jezek
Byrd Polar Research Center
108 Scott Hall
1090 Carmack Rd.
Columbus, OH 43210

Phone: (614) 292-6531
FAX: (614) 292-4697
email: jezek@iceberg.mps.ohio-state.edu

Eric Kasischke
School of the Enviroment
Duke University
Levine Science Research Building
Research Drive
P.O.Box 90328
Duham, North Carolina 27708

Phone: (919) 613-8039
FAX: (919) 684-8741
email: erick@env.duke.edu.

Fred Kruse
University of Colorado
CIRES/CSES
Campus Box 216
Boulder, CO 80309-0216

Phone: (303) 492-6880
FAX: (303) 492-5070
email: kruse@cses.colorado.edu

Appendix A

Contributors

Dr. W. Kübauch
University Bonn
Institut for Agriculture
Katzenburgweg 5
D-53115 Bonn
Germany

Phone:
FAX:
email:

Ron Kwok
M/S 300-235
Jet Propulsion Laboratory
4800 Oak Grove
Pasadena, CA 91109

Phone: (818) 354-5614
FAX:
email: kwok@kahuna.jpl.nasa.gov

Marv Levenson
Naval Research Laboratory
Code 8231
Washington DC 20375

Phone: (202) 767-0694
FAX: (202) 767-6429
email: levenson@nrlfs1.nrl.navy.mil

Fuk Li
Jet Propulsion Laboratory
Mail Stop 300-227
4800 Oak Grove Drive
Pasadena, CA 91109

Phone: (818) 354-2849/2658;
FAX: (818) 393-6943
email: fuk_li@radar-email.jpl.nasa.gov

Craig Lingle
Alaska SAR Facility
University of Alaska
Geophysical Institute
PO Box 757320
Fairbanks, AK 99775-7320

Phone: (907) 474-7679
FAX: (907) 474-7290
email: clingle@iias.images.alaska.edu

Antony A. Liu
NASA/Goddard Space Flight Center
Code 971
Greenbelt, MD 20771

Phone: (301) 286-8534
FAX: (301) 286-0240
email: liu@neptune.gsfc.nasa.gov

Appendix A
Contributors

Jon Maley
NOAA/NESDIS
Room 2069
Federal Building 4
Washington DC 20233

Phone: (301) 763-7190
FAX: (301) 763-4011
email: rfeden@esdim.noaa.gov

Wolfram Mauser
Institue for Geography
University of Munich
Luisenstr. 37
D-München Germany

Phone: 49-89-5203-320
FAX: 49-89-5203-286
email:

John McCauley
University of Northern Arizona
189 Wilson Canyon Road
Sedona, AZ 86336

Phone: (602) 282-6058 (same as fax @
FAX: (602) 527-7014 (USGS)
email: jmccauley@Iflag2.wr.usgs.mil

Murray McDonald
ERIM
Enviromental Research Institute of Michigan
Suite 1100
1101 Wilson Blvd.
Arlington, VA 22209-2248

Phone: 703/528-5250 x4142
FAX: 703/524-3527
email: mmcdonal@wopia.wo.erim.org

Lyn McNutt
Chief Scientist
Alaska SAR Facility
University of Alaska
903 Koyukuk Drive, PO Box 757320
Fairbanks, AK 93775-7320

Phone: (907) 474-6077
FAX:
email: lyn@dino.gi.alaska.edu

John Melack
University of California-Santa Barbara
Department of Biological Sciences
Santa Barbara, CA 93106

Phone: (805) 893-3879 or -4339
FAX: (805) 893-8016
email: melack@artemia.ucsb.edu

Appendix A

Contributors

Anthony Milne
University of New South Wales
Centre for Remote Sensing
P.O.Box 1
Kensington NSW 2033
Australia

Phone: 61-02-697-4964
FAX: 61-02-662-2087
email: t.milne@unsw.edu.au

Leslie Morrissey
NASA ARC
Mail Stop 242-4
MASA Ames Research Center
Moffett Field, CA 94035-1000

Phone: (415)604-3617
FAX: (415)604-4680
email: leslie@gaia.arc.nasa

Peter Mouginis-Mark
Chair University of Hawaii
Planetary Geosciences Division
Hawaii Institute of Geophysics
2525 Correa Road
Honolulu, HI 96822

Phone: (808) 956-3147
FAX: (808) 956-6322
email: pmm@kahana.pgd.hawaii.edu

Chris Newhall
USGS, Department of Geological Sciences
University of Washington
AJ-20
Seattle, WA 98195

Phone: (206) 553-6986
FAX: (206) 543-3836
email: cnewhall@geophys.washington.edu

Earnest Paylor
NASA Headquarters
Code YS
Washington DC 20546

Phone: (202) 544-6483
FAX: (202) 755-2552
email: mbaltuck@mtpe.hq.nasa.gov

Jeff Plaut
Jet Propulsion Laboratory
4800 Oak Grove
Mail Stop 300-331
Pasadena, CA 91109-8099

Phone: (818) 393-3799
FAX: (818) 393-0046
email: plaut@berlin.jpl.nasa.gov

Appendix A

Contributors

Kevin Pope
GeoEcoArc Research
2222 Foothill Blvd
Suite E-272
La Canada, CA 91011

Phone: (818) 240-6365
FAX: (818) 240-6365
email: none availble at this time

Eric Rignot
M/S 300-243
Jet Propulsion Laboratory
4800 Oak Grove
Pasadena, CA 91109

Phone: (818) 354-1640
FAX:
email: eric@blacks.jpl.nasa.gov

Helmut Rott
Institute for Meteorology and Geophysics
Innrain 52
A-6020 Innsbruck
AUSTRIA

Phone: 43-512-507-2171; 2173
FAX: 43-512-507-2170
email: helmut.rott@uibk.ac.at

David Rutledge
California Institute of Technology
Dept. of Electrical Engineering
211 Steele
Pasadena, CA 91125

Phone: (818) 395-4806
FAX:
email: rutledge@systems.caltech.edu

Sasan Saatchi
Hydrology, Soils, and Ecology Group
Jet Propulsion Laboratory
4800 Oak Grove Dr.
Pasadena, CA 91109

Phone: (818) 354-1051
FAX: (818) 354-9476
email: saatchi@bachhus.jpl.nasa.gov

Gary Salisbury
Ball Aerospace - Systems Division
Mail Stop BE-12
P O Box 1062
Boulder, CO 80306

Phone: (303) 460-2820
FAX: (303) 460-5833
email: gsalisbury@ball.com

Appendix A

Contributors

Gerald Schaber
U.S. Geological Survey
Branch of Astrogeology
2255 North Gemini Drive
Flagstaff, AZ 86001

Phone: (602) 556-7485
FAX: (602) 556-7014 or 7169
email: gschaber@iflag2.wr.usgs.gov

J. C. Shi
Center for Remote Sensing and
Environmental Optics
Ellison Hall, Room 6709
University of California
Santa Barbara, CA 93106

Phone: 805-893-8116 (w),
FAX: (805) 893-2578
email: Internet: shi%crseo@hub.ucsb.edu

Merrill Skolnik
Naval Research Laboratory
Code 5300
Washington DC 20375

Phone: (202) 767-2936
FAX: (202) 767-3658
email: skolnik@radar.nrl.navy.mail

Peter Smith
Jet Propulsion Laboratory
4800 Oak Grove Drive
Mail Stop 302-306
Pasadena, CA 91109-8099

Phone: (818) 354-4424
FAX: (818) 393-4540
email: r.peter.smith@jpl.nasa.gov

Robert Thomas
NASA-HQ
Code YSG
Washington DC 20546-0001

Phone: (202) 358-1154
FAX: (2020 358-2771
email: bthomas@mtpe.hq.nasa.gov

Fawwaz Ulaby
University of Michigan
Dept of EECS
EECS Building
1301 Beal Room 3228
Ann Arbor, MI 48109-2122

Phone: (313) 764-0501 or -0500
FAX: (313) 763-1503
email: ulaby@eecs.umich.edu

Appendix A

Contributors

Jakob van Zyl
Jet Propulsion Laboratory
Mail Stop 300-241
4800 Oak Grove Drive
Pasadena, CA 91109

Phone: (818) 354-1365
FAX: (818) 354-9476
email: jacobv@blacks.jpl.nasa.gov

JoBea Way
Jet Propulsion Laboratory
Mail Stop 300-233
4800 Oak Grove Drive
Pasadena, CA 91109

Phone: (818) 354-8225
FAX: (818) 354-9476
email: jo.bea.way@jpl.nasa.gov

Frederick P. Weber
Forest Service
U.S. Department of Agriculture
2222 W. 2300 South
Salt Lake City, UT 84119

Phone: (801) 975-3660
FAX: (801) 975-3478
email: fswa/s=p.weber/ou=w03a@mps.attmail.com

Ming-Ying Wei
Code YSC
NASA Headquarters
Washington DC 20546-0001

Phone: (202) 358-0274
FAX: (202) 358-2771
email: mwei@mtpe.hq.nasa.gov

Diane Wickland
NASA Headquarters
Code YSE
300 E. Street SW
Washington DC 20546

Phone: (202) 358-0272
FAX: (202) 358-2771
email: dwickland@mtpe.hq.nasa.gov

Cynthia L. Williams
USDA Forest Service
Institute of Northern Forestry
308 Tanana Drive
Fairbanks, AK 99775

Phone: (907) 474-3325 and 8163
FAX: (907) 474-3350
email: cwilliams@spruce.lter.alaska.edu

Appendix A

Contributors

Howard Zebker
Jet Propulsion Laboratory
Mail Stop 300-227
4800 Oak Grove Drive
Pasadena, CA 91109

Phone: (818) 354-8780
FAX: (818) 393-6943
email: zebker@jakey.jpl.nasa.gov

Eric F. Wood
Princeton University
Princeton, New Jersey 08544

Phone: (609) 258-4655
FAX: (609) 258-1270
email: efwood@pucc.princeton.edu

Dr. W. Kübauch
University Bonn
Institut for Agriculture
Katzenburgweg 5
D-53115 Bonn
Germany

Phone:
FAX:
email:

Laura Hess
University of California Santa Barbara
Department of Geology
Santa Barbara, CA 93106

Phone: (805) 893-8339
FAX: (805) 893-2578
email: lola@icess.ucsb.edu

Wolfram Mauser
Institute for Geography
University of Munich
Luisenstr. 37
D-München
Germany

Phone: 49-89-5203-320
FAX: 49-89-5203-286
email:

Manfred Zink
Institut fur Hochfrequenztechnik
P. O. Box 1116
Wessling D-82230
Germany

Phone: 49-8153-28-2386
FAX: 49-8153-28-1449
email: zink@ohf015.hf.op.dlr.de

Appendix B -- Comparison of SAR Systems and Frequencies Used

Table B-1. Comparison of SAR Systems

PARAMETER	AIRSAR	ERS-1	ERS-2	SIR-C	X-SAR (flown with SIR-C)	RADARSAT	ENVISAT (ASAR)	JERS-1	ALOS	Mir-Priroda	ALMAZ-1
RADAR BAND	P,L,C	C	C	C,L	X	C	C	L-Band	L-Band	L,S-Band	S-Band
POLARIZATION	ALL	VV	VV	ALL	VV	HH	HH/VV/HV	HH	HH	*	HH
INCIDENCE ANGLE (DEG)	17-60	24	24	17-60	17-60	17-50	20-45	35	*	35	30-60
RESOLUTION (m)	5	25	25	25	25	10-100	30	18	*	*	15
SWATH WIDTH (km)	10-15	100	100	15 -100	15-40	50-170 (500 km in scansar)	50-400	75	*	120	20-45
SYSTEM SENSITIVITY (dB)	-40	-25	-25	-50	-22	-23	*	-20	*	*	*
ALTITUDE (km)	7.3	790	785	225	225	790	800	568	700	394	300
SIMULTANEOUS FREQUENCIES	3	1	1	3	3	1	1	1	*	2	1
SIMULTANEOUS POLARIZATIONS	4	1	1	4	4	1	2	1	*	*	1
ORBIT INCLINATION (deg)	aircraft	97.7	97.7	57	57	98.6	100	97.7	98.2	51.6	72.7
BANDWIDTH (MHz)	20, 40	13.5	13.5	10, 20	10, 20	12-30	14	50	*	*	*
DATA RATE (Mbps)	256	165	165	90 or 46/channel	45	110	100	74	*	*	*
LAUNCH DATE	1988 - Present	July 1991	*spring 1995*	April/October 1994	April/October 1994	*fall 1995*	*late 1998*	February 1992	*Jan/Feb 2000*	*1995*	March 1991
LIFETIME (years)	-	3	3	11 days	11 days	5	5	2	3-5	2 minimum	2.5

* Information is unavailable at this time

Table B-2. Microwave Bands Available for SAR.

Name	wavelength (cm)	Frequency (GHz)
Ka	1.13-0.75	26.5–40
K	1.67-0.75	18–26.5
Ku	2.40-1.67	12.5–18
X	3.75-2.40	8–12.5
C	7.5-3.75	4–8
S	15-7.5	2–4
L	30-15	1–2
P	130-30	0.230–1

Appendix C
ACRONYMS

4DDA	4-D Data Assimilation
ADC	Analog to Digital Converter
AIRSAR	Airborne Synthetic Aperture Radar
ASAR	Advanced Synthetic Aperture Radar
ASF	Alaska Synthetic Aperture Radar Facility
ASIC	Application Specific Integrated Circuit
ASTER	Advanced Spaceborne Thermal Emission and Reflection Radiometer
ATISAR	Along-Track Interferometric Synthetic Aperture Radar
AVHRR	Advanced Very High Resolution Radiometer
AVIRIS	Airborne Visible/Infrared Imaging Spectrometer
C	C-band, as in CHH or CVV
CES	Committee on Earth Studies
CMOS	Complementary Metal-Oxide Semiconductor
COTS CPU	Commercial Off-The-Shelf CPU
CPU	Central Processing Unit
CV	Coefficient of Variation
DAAC	Distributed Active Archive Center
DC-8	Douglas Commercial aircraft cargo - model 8
DEM	Digital Elevation Map
DMSP	Defense Meteorological Satellite Program
EEZ	Exclusive Economic Zone
ENSO	El Niño, Southern Oscillation
ENVISAT	Enviromental Satellite
EOS	Earth Observing System
EPA	Environmental Protection Agency
ERS-1, ERS-2	European Remote Sensing Satellite
ESA	European Space Agency
ESTAR	Electronically Steered Thinned Array Radiometer
FET	Field Effect Transistor
4DDA	4-D Data Assimilation
FPGA	Field Programmable Gate Array
GCMs	General Circulation Models
GCRP	Global Change Research Program
GFLOP	Giga (=Billion) Floating Point Operations per second
GPS	Geophysical Processor System, or Global Positioning System
GOM	Geometrical Optics Model
HAPEX-MOBILHY	Hydrologic Atmospheric Pilot Experiment andModelisation du Bilan Hydrique
HEMT	High-Electron Mobility Transistor
hf	high frequency
HH	Horizontal polarized transmission, Horizontally polarized reception
HIROS	High-Resolution Infrared Sounder
HV	Horizontal polarized transmission, Vertically polarized reception
I/O	Input and Output
IEM	Integral Equation Method
IF	Intermediate Frequency

Appendix C
ACRONYMS

(continued)

INPA	Instituto de Pesquisas Amazonas
IF	Intermediate Frequency
INPA	Instituto de Pesquisas Amazonas
ISLSCP	International Satellite Land Surface Climatology Project
ITU	International Telecommunications Union
JERS-1	Japanese Earth Remote-Sensing Satellite
JPL	Jet Propulsion Laboratory
L	L-band, as in LHH or LVV
MESFET	Metal-Semiconductor Field-Effect Transistor
MLE	Maximum Likelihood Estimator
MMIC	Millimeter/Microwave Integrated Circuit
MPM	Manipulator Positioning Mechanism or Manufacture Procedure Manual
MTPE	Mission to Planet Earth
NASA	National Aeronautics and Space Administration
NDVI	Normalized Difference Vegetation Index
NESDIS	National Environment Satellite Data and Information Services
NOAA	National Oceanic and Atmospheric Administration
OMTPE	Office of Mission to Planet Earth
ONR	Office of Naval Research
OSB	Ocean Studies Board
POM	Physical Optics Model
PRF	Pulse Repetition Frequency
RADAM	Brazilian Airborne Mapping of the Amazon
RADAR	RAdio Detection And Ranging
RADARSAT	Radar Satellite
RAR	Real-Aperture Radar
RF	Radio Frequency
RGB	Red, Green, and Blue
RGPS	*Radarsat* Geophysical Processor System
SAR	Synthetic Aperture Radar
SCANSAR	Scanning Synthetic Aperture Radar
SIR-A, SIR-B	Shuttle Imaging Radar-A , -B
SIR-C/X-SAR	Spaceborne Imaging Radar-C, X-Band Synthetic Aperture Radar
SPM	Small Perturbation Model
SPOT	Systeme Probatoire d'Observation de la Terre
SRAM	Static Random Access Memory
SRL-1, SRL-2	Space Radar Laboratory
SSB	Space Studies Board
STS 59 and STS 68	Space Transport System
TDR	Time Domain Reflectivity
TM	Thematic Mapper

(continued)

TOGA/COARE	Tropical Ocean Global Atmosphere/Coupled Ocean-Atmosphere Response Experiment
TOPEX/POSEIDON	Ocean Topography Experiment
TOPSAR	TOPographic Synthetic Aperture Radar
T/R modules	Transmit/Receive
TSS	Tug Structural Support
TWT	Traveling Wave Tube
USCB	University of California at Santa Barbara
U.S.S.R.	Union of Soviet Socialist Republics
U.S.	United States
USGS	United States Geological Survey
VH	Vertically polarized transmission, Horizontally polarized reception
VLBI	Very Long Baseline Interferometery
VV	Vertically polarized transmission, Vertically polarized reception
W	Watts
WAM	Wave Analysis Model

REPORT DOCUMENTATION PAGE

Form Approved
OMB No. 0704-0188

1. AGENCY USE ONLY (Leave blank)	2. REPORT DATE	3. REPORT TYPE AND DATES COVERED
	April 1995	April '94 - Feb. '95

4. TITLE AND SUBTITLE

Spaceborne Synthetic Aperture Radar: Current Status and Future Directions -- A Report to the Committee on Earth Sciences

5. FUNDING NUMBERS

6. AUTHOR(S)

D. Evans, E. Kasischke, J. Melack, J. Dozier, J. van Zyl, J. Apel, F. Carsey, R. Bindschadler, K. Jezek, R. Arvidson, B. Minster, P. Mougionis-Mark, F. Li, M. Skolnik

7. PERFORMING ORGANIZATION NAME(S) AND ADDRESS(ES)

Jet Propulsion Laboratory
4800 Oak Grove Drive
Pasadena, CA 91109

8. PERFORMING ORGANIZATION REPORT NUMBER

NASA TM-4679

9. SPONSORING/MONITORING AGENCY NAME(S) AND ADDRESS(ES)

National Aeronautics and Space Administration
Washington, DC 20546-0001

10. SPONSORING/MONITORING AGENCY REPORT NUMBER

TM-4679

11. SUPPLEMENTARY NOTES

12a. DISTRIBUTION/AVAILABILITY STATEMENT

Subject Category 32

12b. DISTRIBUTION CODE

13. ABSTRACT *(Maximum 200 words)*

This report provides a context in which questions put forth by NASA's Office of Mission to Planet Earth (OMPTE) regarding the next steps in spaceborne synthetic aperture radar (SAR) science and technology can be addressed. It summarizes the state-of-the-art in theory, experimental design, technology, data analysis, and utilization of SAR data for studies of the Earth, and describes potential new applications. The report is divided into five science chapters and a technology assessment.

The chapters summarize the value of existing SAR data and currently planned SAR systems, and identify gaps in observational capabilities needing to be filled to address the scientific questions. Cases where SAR provides complementary data to other (non-SAR) measurement techniques are also described.

The chapter on technology assessment outlines SAR technology development which is critical not only to NASA's providing societally relevant geophysical parameters but to maintaining competitiveness in SAR technology, and promoting economic development.

14. SUBJECT TERMS

Synthetic Aperture Radar; Earth Sciences

15. NUMBER OF PAGES

171

16. PRICE CODE

17. SECURITY CLASSIFICATION OF REPORT	18. SECURITY CLASSIFICATION OF THIS PAGE	19. SECURITY CLASSIFICATION OF ABSTRACT	20. LIMITATION OF ABSTRACT
Unclassified	Unclassified	Unclassified	Unlimited